Volatile and fluid-mobile element systematics of mantle xenoliths from selected Kamchatka arc volcanoes

Ľubomíra Tomaníková

Submitted in accordance with the requirements for the degree of
Doctor of Philosophy

The University of Leeds
School of Earth and Environment

October 2019

The candidate confirms that the work submitted is her own, except where work which has formed part of jointly-authored publications has been included. The contribution of the candidate and the other authors to this work has been explicitly indicated below. The candidate confirms that appropriate credit has been given within the thesis where reference has been made to the work of others.

The majority of work in Chapter 5 of this thesis has appeared in the following publication:

Tomanikova, L., Savov, I.P., Harvey, J., de Hoog, J.C.M., Churikova, T.G., Gordeychik, B. and Yogodzinski, G.M. 2019. A limited role for metasomatized subarc mantle in the generation of boron isotope signatures of arc volcanic rocks. *Geology*. **47**(6), pp.517–521, doi.org/10.1130/G46092.1.

The authors contributed to the manuscript as following: **L. Tomanikova**, supervised by I. Savov and J. Harvey, collected Avachinsky and Shiveluch mantle xenoliths in Kamchatka, carried out mineral major, minor and trace element analyses, wrote research proposals to analyze vein mineral B abundances and $\delta^{11}B$, generated B isotope mixing model and was in charge of collating the manuscript, J.C.M. de Hoog assisted with B and $\delta^{11}B$ analyses, T. Churikova and B. Gordeychik assisted with fieldwork in Kamchatka and G. Yogodzinski collected Shiveluch mantle xenoliths. All authors were involved in data interpretation discussions.

Acknowledgements

First of all, I would like to thank Ivan Savov and Jason Harvey for their supervision throughout the course of my PhD studies. Thanks to Ivan for always starting our supervision meetings with a chat about my wellbeing and his enthusiasm for my new scientific discoveries and Jason for his help with structuring and proof-reading my many pieces of writing. I would like to acknowledge their support and encouragement while writing my first manuscript and later, my thesis.

Thank you to Tatiana Churikova and Boris Gordeychik for organizing fieldwork in Kamchatka, assistance with sample collection and exportation from Russia and many productive discussions. To Rosie Jones, Steve Turner, Mikhail Yarin, N. Egorova and Yu. M. Puzankov for their assistance in the field.

The help of John 'Harri' Wyn Williams with sample preparation is greatly appreciated as is the guidance of Richard Walshaw and Duncan Hedges while training and assisting me on the SEM and EPMA. I am grateful to Cees-Jan de Hoog for his assistance with SIMS analyses and many boron discussions during conferences and research visits to Edinburgh and to Frances Jenner and Sam Hammond for their assistance with LA-ICP-MS analyses.

Thank you to Alex Iveson and Madeleine Humphreys for insightful discussions and permission to use their yet unpublished datasets (sample *SH11* and Shiveluch, Avachinsky and Bakening high-Mg# olivine-hosted melt inclusions).

I would like to thank all my friends and colleagues for their support and making my PhD experience less stressful. I appreciate the help of Eduardo Morgado, my hermano querido, with the many mineral composition and P-T spreadsheets. Special thanks to Faraz who was there for me to celebrate my successes and comfort me

during my failures. Without you, my PhD experience would have been much more difficult.

Finally, I would like to thank my family for supporting my ambitions to study abroad and pursue my chosen career path. Thank you for your unconditional care and love. I could not have asked for a better family.

Abstract

Contrary to the studies of arc volcanic rocks, mantle xenoliths offer a direct means to study mantle processes above subduction zones. The Kamchatka arc comprises a unique group of volcanoes that erupt veined (metasomatized) mantle xenoliths. The wide spatial distribution of mantle xenolith-bearing volcanoes spanning from the volcanic front (Avachinsky and Shiveluch, this study) to the rear-arc (Bakening, this study) makes Kamchatka the perfect place to investigate metasomatic subarc processes.

A combined study of major and trace element compositions with B contents and $\delta^{11}B$ of metasomatic minerals in Avachinsky and Shiveluch mantle xenoliths is used to constrain the composition and source of fluids and melts responsible for melt-rock reactions occurring in the subarc and rear-arc mantle. A close inspection of Bakening mantle xenoliths revealed that they do not contain any hydrous metasomatic minerals suitable for B and $\delta^{11}B$ analyses. Thus, the study of metasomatic reactions in the rear-arc mantle at Bakening is limited here to major and trace element mineral compositions.

Multiple pulses of compositionally diverse fluids and melts derived from progressively deeper portions of the subducting slab percolate through the subarc mantle. The low B contents and negative $\delta^{11}B$ of vein minerals in Avachinsky and Shiveluch xenoliths indicate that they are products of fluids and melts released from subducted and already dehydrated altered oceanic crust and, to a lesser extent, from serpentinite. Avachinsky and Shiveluch mantle xenoliths, however, were later overprinted by evolved melts in the upper crust prior to the eruption. Vein amphibole major and trace element compositions indicate their equilibration with

evolved melts similar to amphibole- and plagioclase-hosted melt inclusions in Shiveluch volcanic rocks (Humphreys et al., 2008). Contrastingly, Bakening xenoliths lack any evidence of extensive fluid-fluxing of the rear-arc mantle, which was instead fluxed by pyroxenite melt mixed with a small amount of carbonatite component.

Table of Contents

List of Figures

List of Tables

List of Abbreviations

List of acronyms

AOC	Altered oceanic crust
BSE	Back-scattered electrons
CF	Composite fluid
CKD	Central Kamchatka depression
DM	Depleted mantle
DMM	Depleted MORB mantle
EIMF	Edinburgh ion microprobe facility
EPMA	Electron probe micro-analyzer
Eq	Equilibrium
EVF	Eastern volcanic front
FME	Fluid-mobile elements
FMQ	Fayalite-magnetite-quartz buffer
HFSE	High field strength elements
HREE	Heavy rare earth elements
LA-ICP-MS	Laser-ablation inductively-coupled plasma mass spectrometry
LILE	Large-ion lithophile elements
LREE	Light rare earth elements
Lit	Literature
m.a.s.l.	Metres above sea level
MORB	Mid-ocean ridge basalt
REE	Rare earth elements
RSD	Relative standard deviation
SCLM	Sub-continental lithospheric mantle
SEM	Scanning electron microscope
SIMS	Secondary ion mass spectrometry
SR	Sredinny range
Std	Standard

List of mineral abbreviations

am	Amphibole
chl	Chlorite
cpx	Clinopyroxene
Fo_x	Olivine with X % Magnesium
ol	Olivine
opx	Orthopyroxene
phl	Phlogopite
pl	Plagioclase
spl	Spinel

List of mineral chemical formulae

Mg_2SiO_4	Forsterite (olivine)
$MgSiO_3$	Enstatite (orthopyroxene)
$MgCaSi_2O_6$	Diopside (clinopyroxene)
$NaCa_2(Mg_4Al)(Si_6Al_2)O_{22}(OH)_2$	Pargasite (amphibole)
$Ca_2(Mg_4Al)(Si_7Al)O_{22}(OH)_2$	Magnesio-hornblende (amphibole)
$KMg_3AlSi_3O_{10}(OH)_2$	Phlogopite
$NaAlSi_3O_8$	Albite (plagioclase)
$Mg_5Al(AlSi_3O_{10})(OH)_8$	Clinochlore (chlorite)

Chapter 1

Introduction

1.1 Characteristic features of subduction zones

Much of the volcanic activity on Earth occurs at subduction zones. Subduction zones are located at plate margins where the subducting (typically oceanic) plates descend into the mantle (Figure 1). Generation of arc volcanic rocks is attributed to contribution of volatiles from the hydrated subducting plate (Tatsumi, 1989). The top of the subducting oceanic plate consisting of sediment and altered oceanic crust (AOC) is hydrated by seawater that may percolate even deeper to reach the deep gabbroic and/or lithospheric mantle portion of the slabs through fracture zones (Manea et al., 2014; McCaig et al., 2019). With ongoing subduction and increasing pressure and temperature, the subducting slab dehydrates and liberates volatiles that percolate into the overlying depleted subarc mantle. The high solidus temperature of dry mantle peridotite (T ~ 1460 °C at 3 GPa; Hirschmann, 2000) is dramatically suppressed via the addition of volatiles (T ~ 900 to 800 °C at 1.5 to 3 GPa, respectively; Grove et al., 2006), which facilitate melting of otherwise highly depleted and colder mantle wedge.

Studies of the composition of arc volcanic rocks demonstrate that the liberated slab components comprise a combination of sediment melt, AOC-derived fluid, residual AOC melt and serpentinite fluid (e.g. Tatsumi, 1989; Elliott, 2004; Savov et al., 2007). Elevated contents of rare earth elements (REE), Th, Be and radiogenic Pb

and Sr in arc volcanic rocks are attributed to sediment melt component (Morris et al., 1990; Hawkesworth et al., 1997; Elliott, 2004), whereas elevated contents of large ion lithophile elements (LILE) and heavy ^{11}B are attributed to AOC- and serpentinite-derived fluids, respectively (e.g. Elliott, 2004; DeHoog and Savov, 2018 and references therein).

Slab-derived fluid and melt flow that connects the slab dehydration or melting site with the mantle melting region occurs either via interconnected vein network (John et al., 2012; Pirard and Hermann, 2015; Plümper et al., 2016) or via diapiric rise of buoyant serpentine-dominated mélanges (Nielsen and Marschall, 2017) or a combination of both (Figure 1).

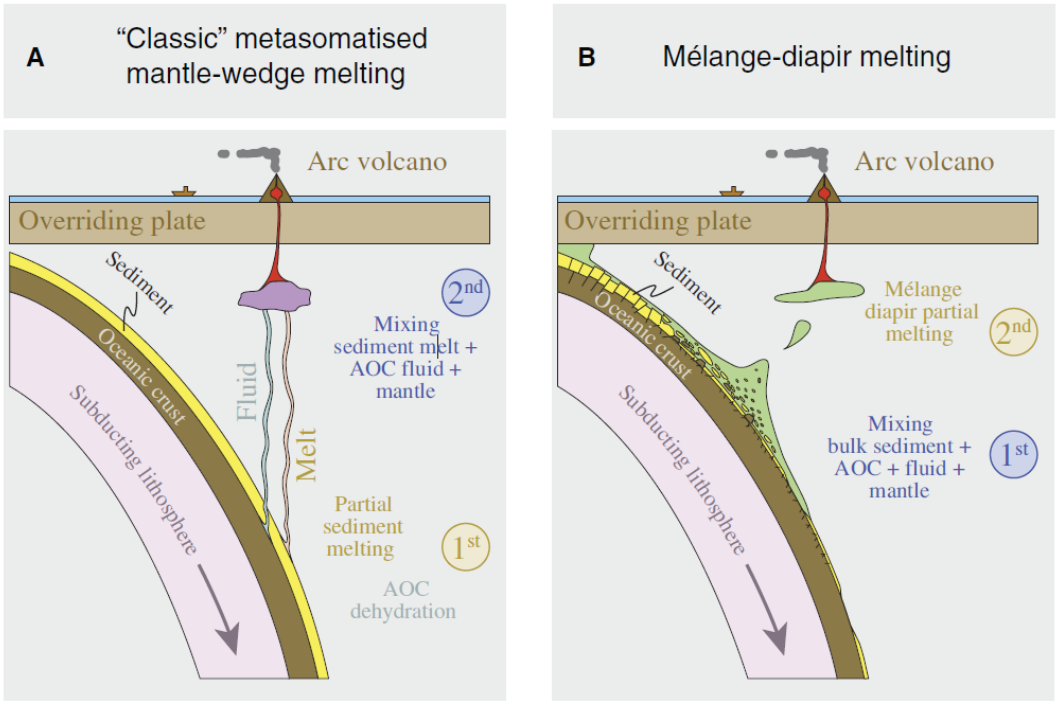

Figure 1. *Models of slab material transport in subduction zones. In A), slab-derived fluids and melts are transported to the mantle melting region via veins (John et al., 2012; Pirard and Hermann, 2015; Plümper et al., 2016) and in B), mélange diapirs made up of a mix of slab-derived material rise to the mantle melting region. Figure is from Nielsen and Marschall (2017).*

1.2 Kamchatka subduction zone

1.2.1. Regional geology

The Kamchatka arc (Far East Russia) is part of the active Kuril-Kamchatka subduction zone located in the north-western Pacific (Figure *2*). It is situated on the continental margin of the Eurasian plate overlying the ~ 80 Ma old (Cretaceous) Pacific plate subducting at ~ 7.5 to 8.3 cm/yr (Avdeiko et al., 2007). The Kamchatka arc comprises three volcanic belts: the Eastern volcanic front (EVF), the Central Kamchatka depression (CKD) and the Sredinny range (SR; e.g. Churikova et al., 2001; Portnyagin and Manea, 2008). The Central Kamchatka depression arc volcanoes are shifted westward relative to those of the EVF due to shallowing of slab dip from the EVF (~55 °) in the south of the peninsula to the CKD (~35 °) in the north of the peninsula (Gorbatov et al., 1997). The Kurile-Kamchatka trench terminates at the junction with the Aleutian transform fault (Figure 2).

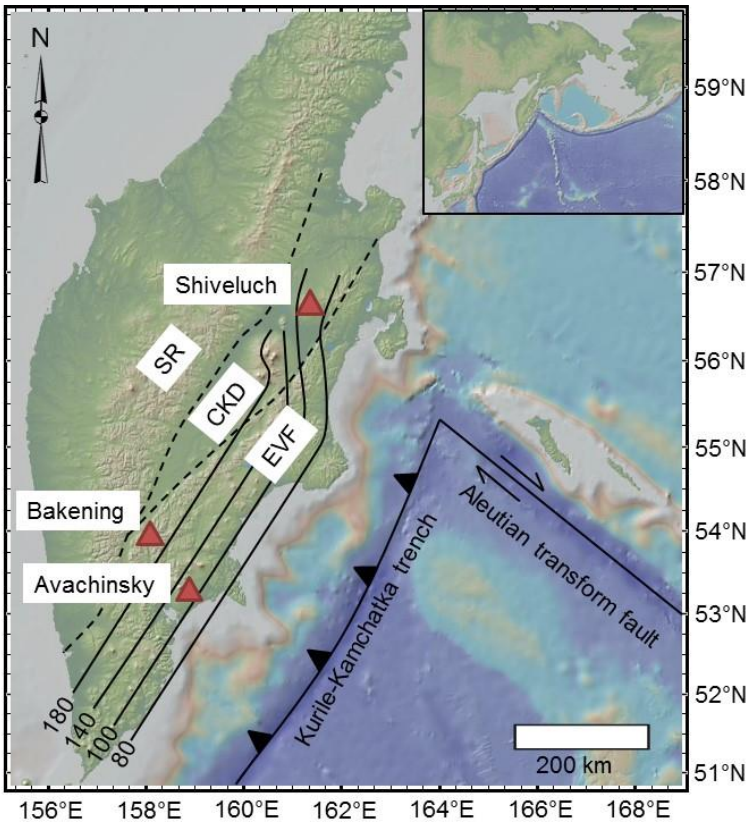

Figure 2. *Location of the Kamchatka peninsula in the north-western Pacific (inset) and Avachinsky, Bakening and Shiveluch volcanoes in the Kamchatka peninsula. The Eastern volcanic front (EVF), the Central Kamchatka depression (CKD) and the Sredinny range (SR) are outlined by dashed lines. Solid lines outline depth-to-slab contours in km (Gorbatov et al., 1997). Modified from GeoMapApp (http://www.geomapapp.org/; Ryan et al., 2009).*

The modern Kamchatka peninsula is formed by three volcanic arc trench systems arranged in an en echelon manner from northeast to southwest (Figure 3):

- West Kamchatka (active in the Eocene)
- Mid-Kamchatka-Kurile (active in the Late Oligocene-Miocene)
- Kurile-Kamchatka (active from 5 Ma ago; Avdeiko et al., 2007).

The trench and the volcanic front moved progressively eastward to its present position due to collisions with Shipunski, Kronotski and Kamchatski blocks of the inactive Kronotski volcanic arc 10-2 Ma ago (Figure 3). Each of the respective

collisions caused closure of a segment of the old trench system and the formation of a new segment eastward. The southern boundary of the collision events is marked by the Avacha, also known as Malki-Petropavlovsk transverse fault zone, dividing the peninsula into the northern and southern segments (Lander and Shapiro, 2007). The SR represents an ancient volcanic front of the Mid-Kamchatka-Kurile subduction zone that has been active since the Miocene (Figure 4; Avdeiko et al., 2007; Lander and Shapiro, 2007).

The Kamchatka arc uniquely portrays the initial and final stages in the life cycle of a subduction zone. The SR represents the waning stage of the older (Miocene) Mid-Kamchatka volcanic arc, while the EVF represents the initiation stage (Figure 4; Avdeiko et al., 2007; Lander and Shapiro, 2007). The different stages are reflected in different mantle composition under the EVF and SR. The composition of mantle under the EVF and CKD is similar to that of depleted N-MORB whereas mantle composition under the SR resembles that of OIB (Churikova et al., 2001; Churikova et al., 2007; Volynets et al., 2010). The depleted mantle composition in the rear-arc of the EVF is either variably enriched with a slab component or an OIB-like mantle (Dorendorf et al., 2000).

Kamchatka arc volcanoes are among those otherwise very rare and sporadic cases, where the erupted volcanic rocks include fragments of metasomatized mantle xenoliths (Kepezhinskas et al., 1995; Kepezhinskas and Defant, 1996; Arai et al., 2003; Arai et al., 2007; Ishimaru et al., 2007; Bryant et al., 2007; Halama et al., 2009; Ionov, 2010; Ionov et al., 2011; Bénard and Ionov, 2012; Ionov et al., 2013; Bénard and Ionov, 2013; Bénard et al., 2017; Siegrist et al., 2019). Studies of these mantle xenoliths have been central to investigating across-arc metasomatic processes in the subarc mantle. For this study, I collected mantle xenoliths from

Avachinsky, Bakening and Shiveluch volcanoes (Figure 2), in addition to revisiting the Shiveluch mantle xenolith suite studied by Bryant et al. (2007).

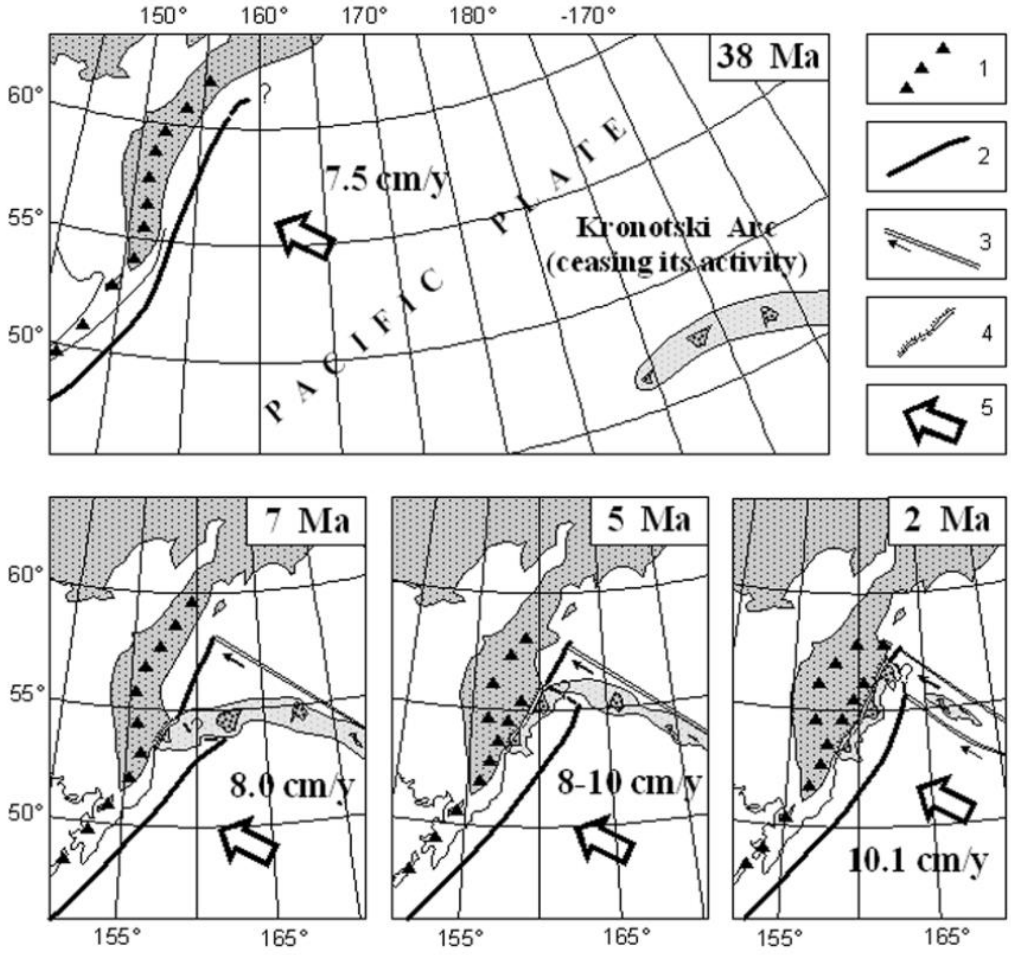

Figure 3. *Geodynamic reconstructions of the post-Eocene Kamchatka subduction zone history. Legend numbers: 1 = volcanic belt, 2 = trench, 3 = transform fault, 4 = Grechishkin thrust suture, 5 = Pacific plate velocity vector relative to Eurasia. Figure is from Lander and Shapiro (2007).*

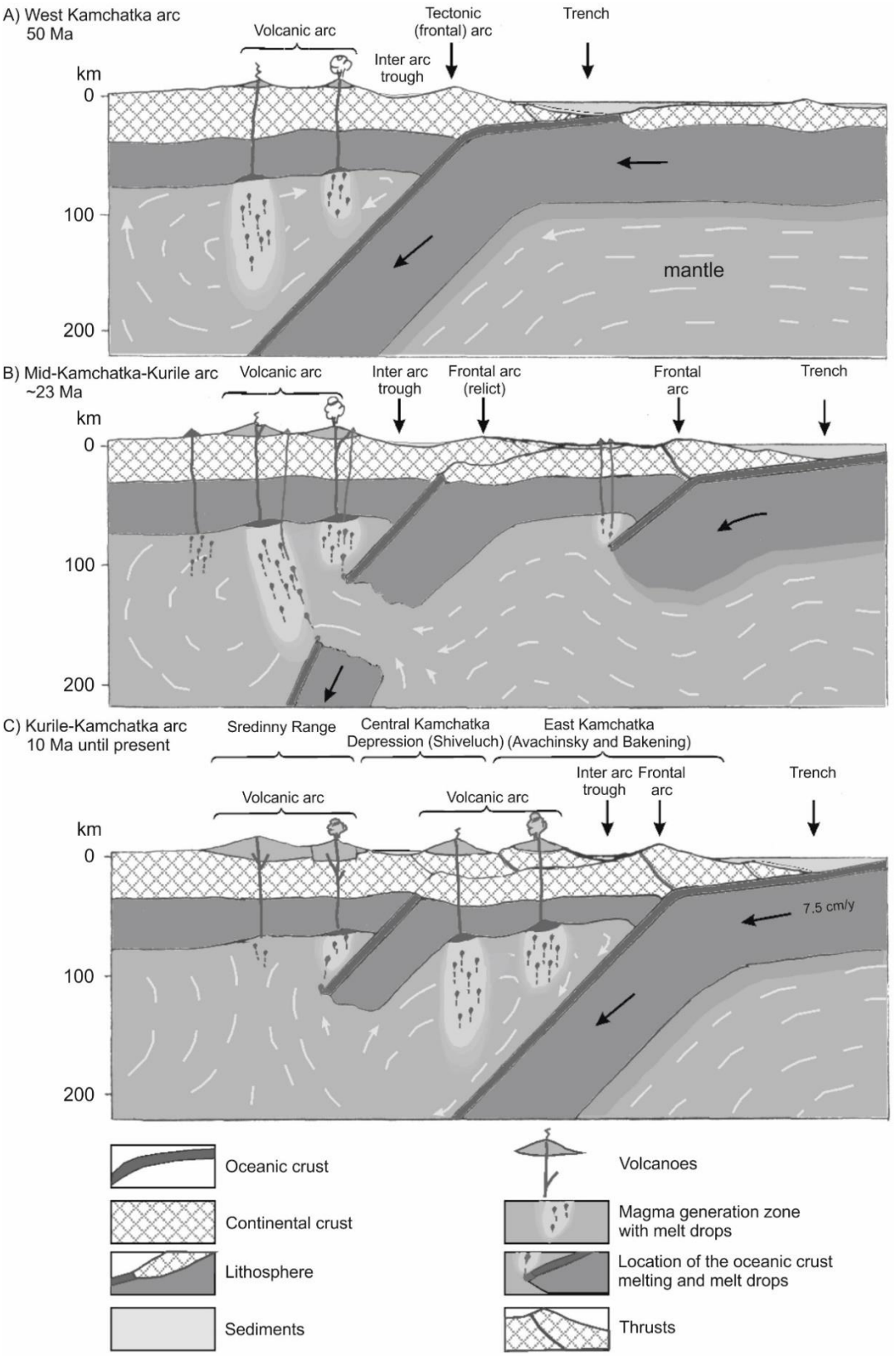

Figure 4. *Evolution history of the modern Kamchatka arc system. Figure is adapted from Avdeiko et al. (2007).*

1.2.2. Avachinsky volcano

Avachinsky volcano (Figure 5A) is located in the EVF at a depth-to-slab of ~ 120 km (Figure 2; Gorbatov et al., 1997). The characteristic volcanic rocks erupted at Avachinsky comprise low-K andesites to basaltic andesites (Braitseva et al., 1995; Braitseva et al., 1998) that have the highest B contents and $\delta^{11}B$ of all studied Kamchatka volcanoes (36.3 µg g^{-1} and + 5.58 ‰; Ishikawa et al., 2001). Metasomatized mantle xenoliths (Figure 5B), representative of high-degree partial melt residues (estimated degree of partial melting = 28 to 35 %; Ionov, 2010), were recovered from an andesitic pyroclastic flow from the *I Av* stage of volcanic activity (7500-3700 years ago; Braitseva et al., 1998). Avachinsky peridotites have been metasomatized by AOC-derived melts and fluids subsequent to the high degree of mantle melting (Kepezhinskas and Defant, 1996; Arai et al., 2003; Arai et al., 2007; Ishimaru et al., 2007; Ionov and Seitz, 2008; Halama et al., 2009; Ionov, 2010; Soustelle et al., 2010; Ionov et al., 2011; Bénard and Ionov, 2012; Bénard and Ionov, 2013; Bénard et al., 2017).

Figure 5. *A) Summit of Avachinsky volcano located at 2751 m.a.s.l. and B) large block of veined mantle peridotite found in ca. 4000 years old andesitic pyroclastic flow (Braitseva et al., 1998) located at 53°16'36.0''N and 158°46'38.2''E on the western flank of Avachinsky volcano.*

1.2.3. Bakening volcano

Bakening volcano (Figure 6A) is located in the rear-arc of the EVF at a depth-to-slab of ~ 200 km (Figure 2; Gorbatov et al., 1997). Erupted volcanic rocks typically consist of dacites and andesites and numerous basaltic cinder cones are scattered across the Bakening volcanic field (Dorendorf et al., 2000).

Novy Bakening (New Bakening) is one of the largest, youngest and best preserved dacitic cones that is known for the occurrence of mantle xenoliths, ranging from wehrlites (olivine and clinopyroxene) to websterites (orthopyroxene and clinopyroxene) and pyroxenites (Dorendorf et al., 2000). The xenoliths are entrained in plateau basalts (Figure 6B; Dorendorf et al., 2000) and reportedly originate from the plagioclase-spinel transition zone (Koloskov et al., 2017). No comprehensive study of Bakening mantle xenoliths exists to date.

Figure 6. *A) View of Bakening volcano located at 2278 m.a.s.l. from our camp site. Photo courtesy of R. Jones. B) Mantle xenolith-bearing plateau basalts located on the north-eastern flank of the Novy Bakening cone at 53°56‘00.5‘’N and 158°06‘26.4‘’E. Note the person above the snow field for scale.*

1.2.4. Shiveluch volcano

Shiveluch volcano is the northernmost active volcano in the Kamchatka peninsula (Figure 2). It is located in the CKD at a depth-to-slab of ~ 90 km (Figure 2; Gorbatov et al., 1997). The summit of Shiveluch volcano consists of the active Young Shiveluch superimposed on the flanks of the extinct Old Shiveluch volcano (Figure 7; Ponomareva et al., 2007; Gorbach et al., 2013).

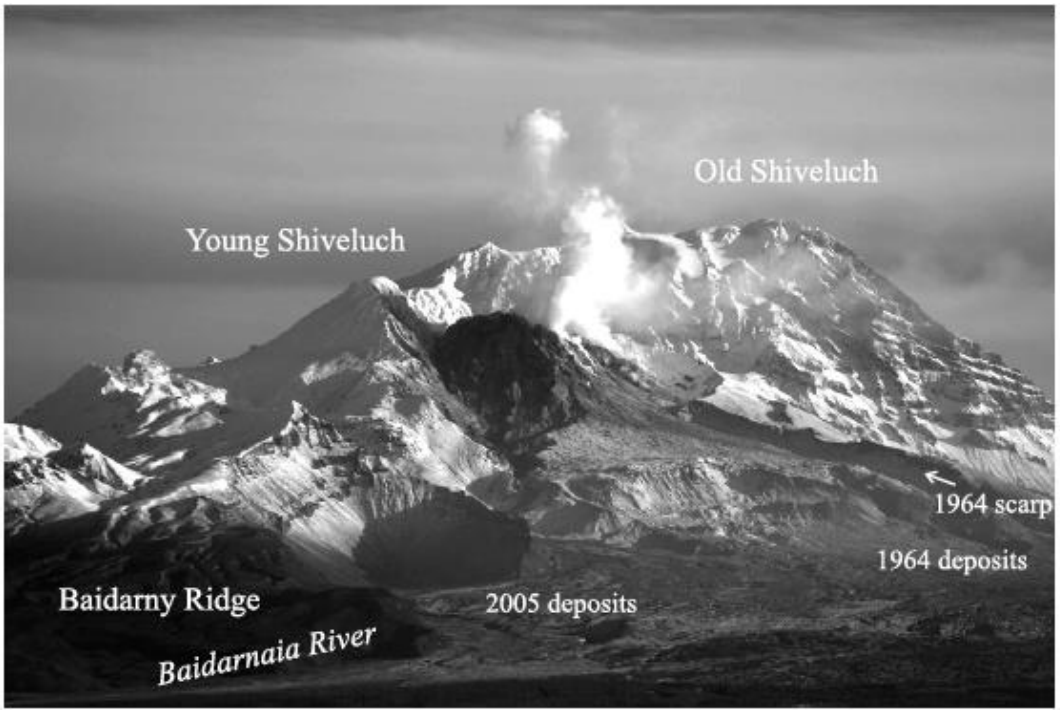

Figure 7. *Photograph of the active Young Shiveluch volcano emitting a gas plume. Extinct Old Shiveluch crater is in the background. The foreground of Young Shiveluch is covered by 1964 and 2005 pyroclastic deposits. Photo is from Ponomareva et al. (2007).*

Typical lavas erupted at Young Shiveluch during the Holocene are medium-K andesites which contain high-Mg# olivine (Mg# = 75.6 to 92.5) with Cr-spinel inclusions (Ponomareva et al., 2007; Nekrylov et al., 2018). These lavas possess typical geochemical characteristics of adakites, such as high MgO, NiO, Cr_2O_3 and Sr contents and elevated Ni/Co, Cr/V and Sr/Y (Defant and Drummond, 1990) relative to other medium-K andesites in Kamchatka. The origin of adakite-like

volcanic rocks at Young Shiveluch (Kepezhinskas et al., 1997; Yogodzinski et al., 2001; Münker et al., 2004) has been attributed to slab melting at the Kamchatka-Aleutian junction by upwelling of hot asthenospheric mantle (Peyton et al., 2001; Yogodzinski et al., 2001; Levin et al., 2005). The Pacific plate is torn by the Aleutian transform fault creating a slab window through which hot asthenosphere upwells and heats up the subducting plate underneath Shiveluch (Figure 8; Yogodzinski et al., 2001).

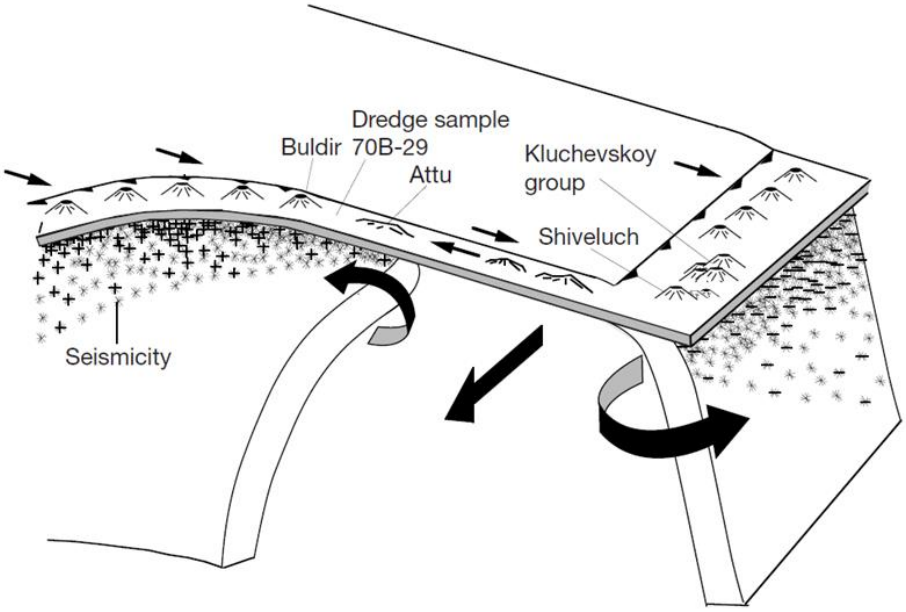

Figure 8. *Asthenospheric mantle flow around the subducting Pacific plate underneath Shiveluch. The Aleutian transform fault zone tears the subducting Pacific plate which is heated up by the upwelling hot asthenospheric mantle. Figure is from Yogodzinski et al. (2001).*

Older erupted volcanic rocks constituting the Old Shiveluch volcanic edifice consist of both andesites and basaltic andesites (Gorbach et al., 2013). The shift in magma chemistry between the Old and Young volcanic centres has been attributed to different source compositions of their parental magmas (a shift from fluid-fluxed to melt-fluxed subarc mantle; Ferlito, 2011).

Like Avachinsky, Shiveluch volcanic rocks also have high concentrations of B and positive $\delta^{11}B$ ratios (24.9 µg g^{-1} and + 3.58 ‰; Ishikawa et al., 2001). However, amphibole- and plagioclase hosted melt inclusions in Shiveluch volcanic rocks typically record higher B contents of 50 to 80 µg g^{-1} and can contain as much as 175 µg g^{-1} of B (Humphreys et al., 2008). The high B and other fluid mobile element (FME) contents were attributed to the subduction of the Aleutian transform fault underneath the CKD (Manea et al., 2014). The transform fault exposes the lower oceanic crust and the upper oceanic lithosphere to seawater that may lead to pervasive seafloor serpentinization of large portions of the subducting oceanic plate including the lithospheric mantle, dehydration of which liberates volatiles and causes mantle melting under the CKD (Figure 9; Konrad-Schmolke and Halama, 2014; Konrad-Schmolke et al., 2016).

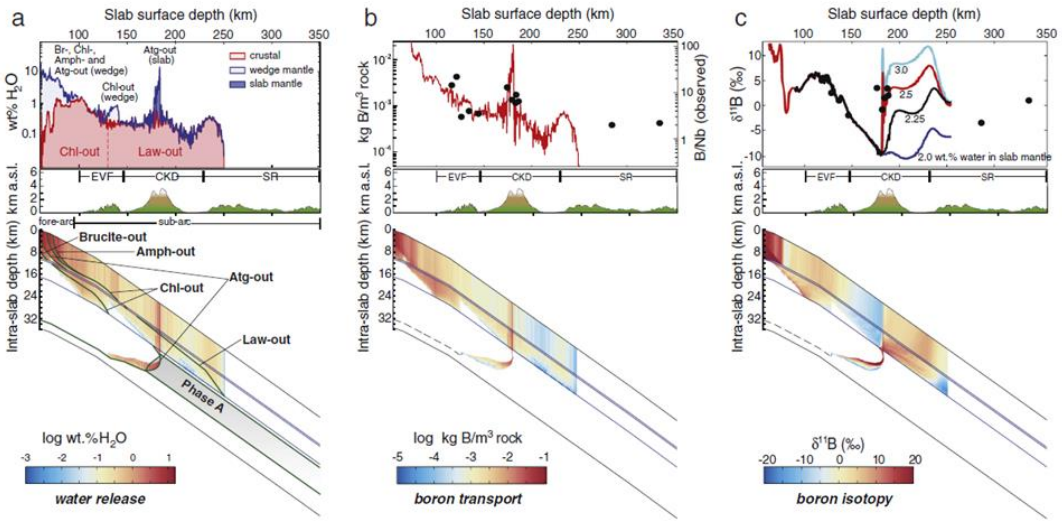

Figure 9. *Modelled slab-derived water (A) and boron (B) release and $\delta^{11}B$ of the released fluids (C) in Kamchatka subduction zone. The Central Kamchatka depression volcanism coincides with high water and B flux of positive $\delta^{11}B$ derived from antigorite dehydration in the slab lithospheric mantle. Figure is from Konrad-Schmolke and Halama (2014).*

Fragments of veined mantle xenoliths were recovered from pyroclastic flow of the 1964 eruption (Figure 10). It has been reported that the anhydrous

orthopyroxene-rich veins cross-cutting the xenoliths record percolation of silica-rich, hydrous fluids and melts through the uppermost subarc mantle whereas the hydrous amphibole- and phlogopite-rich veins record percolation of fluids of late-stage magmatic origin (Bryant et al., 2007).

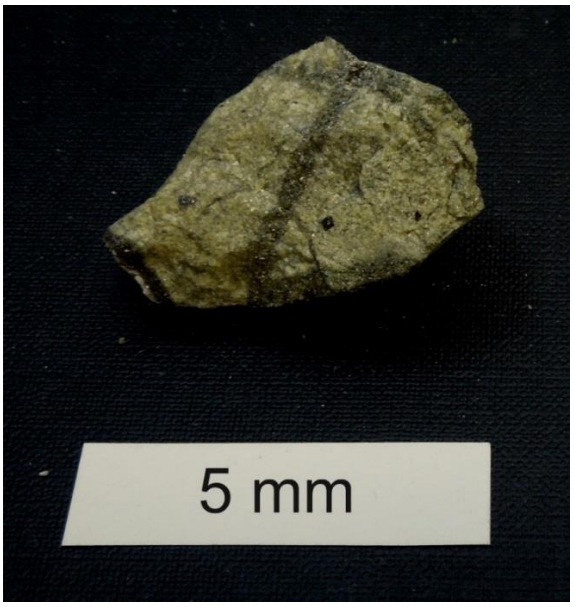

Figure 10. *Photo of Shiveluch harzburgite SH98X-16. Note the mm-scale vein cross-cutting the host xenolith.*

1.3. Rationale and overview of research questions

In contrast to the studies of arc volcanic rocks, mantle xenoliths provide direct insights into the composition and the nature of metasomatic processes occurring in the subarc mantle. Veined ultramafic xenoliths record percolation of compositionally diverse melts through the subarc mantle that carry trace element characteristics and isotopic signatures of their sources.

Metasomatic processes and reactions occurring in Kamchatka subarc mantle are investigated here via the study of volatile, fluid-mobile and trace element systematics of metasomatized ultramafic xenoliths from three Kamchatka arc volcanoes, Shiveluch, Avachinsky and Bakening (Figure 2). These three Kamchatka

arc volcanoes were selected on the basis of the occurrence of veined mantle xenoliths and their spatial distribution across arc representing a transect through Kamchatka subarc mantle. Shiveluch volcano is located in the CKD at a depth-to-slab of ~ 90 km and on the track of a subducting transform fault (Figure 2; Gorbatov et al., 1997), Avachinsky volcano is located in the EVF at a depth-to-slab of ~ 120 km (Figure 2; Gorbatov et al., 1997) and Bakening volcano is located in the rear-arc EVF at a depth-to-slab of ~ 200 km (Figure 2; Gorbatov et al., 1997). The new results presented here are used to challenge the existing models of subduction zone geochemistry (e.g. Konrad-Schmolke and Halama, 2014) and contribute valuable primary data of mantle volatile and FME contents and distribution under arc volcanic fronts.

The aims and objectives of my thesis are:

- to constrain FME and $\delta^{11}B$ systematics of veined mantle xenoliths,
- to determine composition and source of melts and fluids percolating through the Kamchatka subarc mantle,
- to quantify the role of slab-derived melts and fluids on magma genesis at Kamchatka arc volcanoes and
- to construct a transect through Kamchatka subarc mantle spanning from the volcanic front dominantly fluxed with slab-derived fluids at Avachinsky versus slab-derived melts at Shiveluch and to the rear-arc at Bakening.

The thesis is sub-divided into six chapters, including the introductory Chapter 1 and methodology Chapter 2. Chapter 3 presents new major, minor and trace element mineral compositions in Avachinsky and Bakening mantle xenoliths, which are described for the first time. The following research questions are addressed in Chapter 3:

- *What is the composition of the subarc and rear-arc mantle?* It is estimated that higher degrees of mantle melting under the volcanic front produce a refractory mantle residue relative to the lower degrees of mantle melting in the rear-arc.
- *Do metasomatic processes and melt-rock reactions differ between the subarc and rear-arc mantle?* Influx of slab-derived fluids decreases with increasing depth-to-slab (e.g. Rüpke et al., 2004) which affects the degree of mantle melting and the nature of melt-rock reactions occurring in the subarc and rear-arc mantle.
- *What is the composition and origin of the metasomatic agent? Is it identical to that trapped in high-Mg# olivine-hosted melt inclusions?* Experimental mineral-melt trace element partition coefficients are used to constrain the composition of melts in equilibrium with metasomatic minerals.

Chapter 4 presents new major, minor and trace element and halogen (Cl and F) mineral compositions in Shiveluch mantle xenoliths. The following research questions are addressed in Chapter 4:

- *What is the composition and origin of the metasomatic agent? Is it identical to that trapped in high-Mg# olivine-hosted melt inclusions?* In addition to the experimental mineral-melt trace element partition coefficients used in Chapter 3, the composition of melt in equilibrium with vein amphibole is constrained from amphibole major element (Zhang et al., 2017; Humphreys et al., 2019) and halogen (Cl and F) compositions.

Chapter 5 presents new measurements of B contents and $\delta^{11}B$ of vein minerals in Shiveluch and Avachinsky xenoliths. The following research questions are addressed in Chapter 5:

- *What is the B budget of Kamchatka subarc mantle?* A unique investigation of the B cycle in Avachinsky and Shiveluch subarc mantle is carried out via hydrous vein mineral B and $\delta^{11}B$ analyses.
- *Which subducting slab lithology is the source of B in Kamchatka arc?* It has been demonstrated that each subducting slab lithology (i.e. sediment, altered oceanic crust and serpentinite) possesses distinct $\delta^{11}B$, which is widely used as a tracer of slab-derived melts and fluids (e.g. DeHoog and Savov, 2018 and references therein).
- *What is the role of metasomatized subarc mantle on the genesis of Kamchatka arc volcanic rocks?* A popular model of partial melting of metasomatized subarc mantle generating the characteristic FME-rich signature of arc volcanic rocks (e.g. Kepezhinskas et al., 1995; Kepezhinskas and Defant, 1996) is challenged with the new $\delta^{11}B$ of hydrous vein minerals.

Chapter 6 presents discussion and conclusions in which a geochemical transect through the Kamchatka subarc mantle synthesizes results from Chapters 3, 4 and 5 and in which the results are compared to mantle xenoliths from other volcanic arcs.

Chapter 2

Analytical methods

Mineral compositions were measured by *in-situ* analytical techniques described in this chapter. Major and minor element mineral abundances were analyzed via electron probe micro-analyzer, trace element abundances were analyzed via laser-ablation inductively coupled plasma mass-spectrometer and B, $\delta^{11}B$, water and halogen (Cl and F) abundances and isotopic compositions were analyzed via secondary ion mass spectrometer. Equilibration temperature and oxygen fugacity calculations are described at the end of this chapter.

2.1 Electron probe micro-analysis (EPMA)

Mineral major and minor element abundances were obtained on a JEOL JXA8230 electron microprobe at the University of Leeds. Three different sets of operating conditions were used (Table 1) dependent on mineralogy.

Table 1. *EPMA operating conditions*

Mineral	Accelerating voltage (kV)	Beam current (nA)	Count times major elements (s)	Count times minor elements (s)
Olivine, pyroxenes, spinel	20	30	30	30-45
Phlogopite	20	10	10	30 (Ni), 60 (F and Cl)
Amphibole	20	15	15	30 (Cl), 60 (F)

Primary standards almandine (Al), olivine USNM 2566 Springwater (Si, Mg, Fe), diopside (Si, Mg, Ca), rhodonite (Mn), rutile (Ti), Cr_2O_3 (Cr), Ni metal (Ni) and haematite (Fe) were used to calibrate the mafic mineral analyses. Spot size was 1 µm.

For phlogopite and amphibole analyses, the primary standards employed were almandine (Al, Fe), diopside (Si, Mg, Ca), rhodonite (Mn), jadeite (Na), K-feldspar (K), rutile (Ti), Ni metal (Ni), fluorite (F) and halite (Cl). Spot size was 6 µm.

Mineral standards San Carlos olivine (Fo_{90}) USNM 111312/444, chromite USNM 117075, 7308 Geo2 diopside, 7302 almandine, Kakanui hornblende USNM 143965 and 7314 K-spar were run as unknowns in between the mineral point analyses to assess data quality (Figure 11).

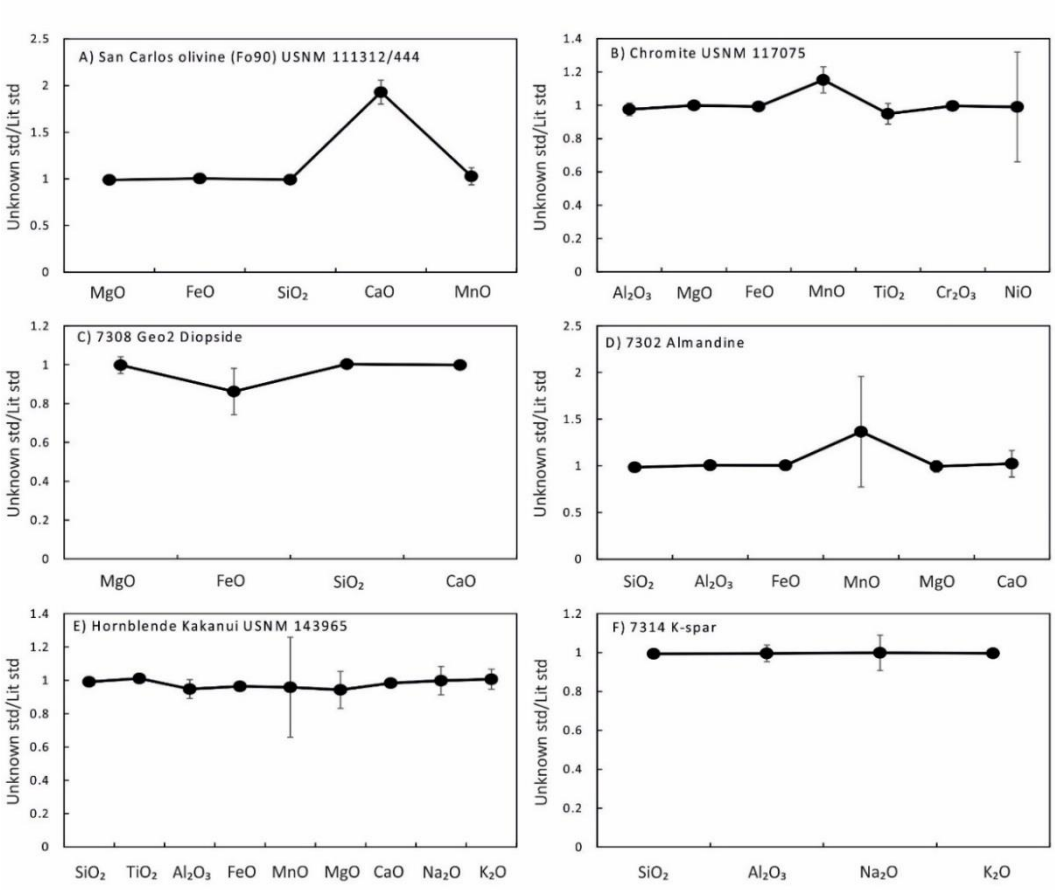

Figure 11. *A) to F) Data quality assessment of EPMA major and minor element mineral analyses. Average standard compositions run as unknowns in between mineral analyses are*

normalized to the reference literature values of each standard. All symbols are larger than the error bars unless shown.

2.2 Laser-ablation inductively-coupled plasma mass spectrometry (LA-ICP-MS)

Mineral trace element concentrations were obtained on inductively coupled plasma mass-spectrometer (ICP-MS) using an Agilent 8800 ICP-MS Triple Quad attached to a laser ablation system Photon Machines Analyte Excimer 193 nm at the Open University. The laser beam diameter was 65 µm and laser repetition rate was 10 Hz. The total acquisition time was 90 s per spot including 30 s laser warm-up time and 30 s wash-out time. Glass standards NIST 610 and NIST 612 were used for calibration and Ca and Si (determined by the EPMA) were used for normalization of data. Glass standard BCR was run as unknown in between the mineral point analyses to assess data quality (Figure 12).

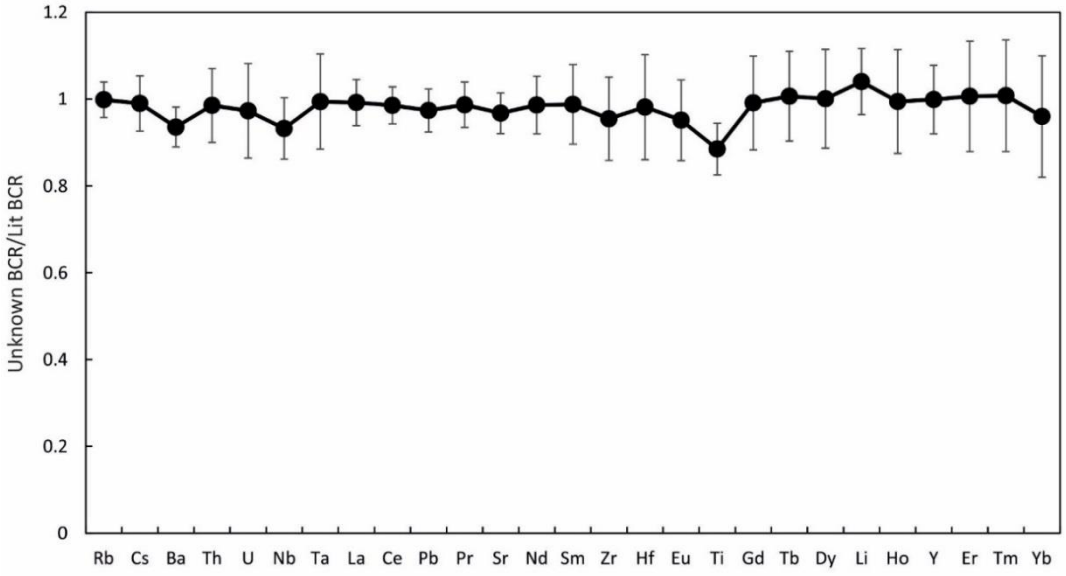

Figure 12. *Data quality assessment of LA-ICP-MS trace element mineral analyses. Average BCR glass standard compositions run as unknowns in between mineral analyses are normalized to the reference literature values of BCR glass standard.*

2.3 Secondary ion mass spectrometry (SIMS)

2.3.1 Boron and $\delta^{11}B$

Boron concentrations and $\delta^{11}B$ were measured *in situ* in phlogopite, amphibole, orthopyroxene, olivine and plagioclase using a Cameca IMS-1270 at the Edinburgh Ion Microprobe Facility (EIMF). Boron isotopic compositions are reported as variations in per mil from the boron isotopic standard NIST 951 (boric acid):

$$\delta^{11}B = \left[\frac{\left(\frac{^{11}B_{Sample}}{^{10}B_{Sample}} \right)}{\left(\frac{^{11}B_{NIST\ 951}}{^{10}B_{NIST\ 951}} \right)} - 1 \right] \times 1000 \qquad \textit{Equation 1}$$

The primary ion beam of $^{16}O_2^-$ was accelerated to 22.5 kV and impacted upon the sample surface. Beam current steadily increased during the analytical session from 16 to 37 nA and beam size diameter ranged from 20 µm to 30 µm. ^{10}B and ^{11}B signals were detected sequentially using a single electron multiplier, with counting times of 8s and 2s, respectively, and 100 cycles per analysis. A mass resolution of 2000 (m/Δm) was used to resolve ^{9}BeH and ^{10}BH interferences. Boron concentrations were estimated from ^{11}B count rates using GSD1-G as a standard (50 ppm B).

Uncertainties of the B concentrations are ~ 20 % RSD. Amphibole 21664 and 21805, mica MVE02-8-5, 80-3 and JJE01-3 (for phlogopite), serpentine Srp 21826 and Srp-geiss1 and basaltic glass GSD1-G, BCR2-G and pyroxene JJE01-X-3 (for olivine and pyroxene) were used as calibration standards for isotope ratios (DeHoog et al., 2017). Significant matrix effects were observed between different hydrous minerals, as already reported by DeHoog et al. (2017), with offsets of -3.1 ‰, -3.5 ‰ and -4.8 ‰ for amphibole, mica and serpentine compared to basaltic glasses and

pyroxene, respectively. Mean relative reproducibility of the $\delta^{11}B$ value for the samples was 1.4 ‰ for phlogopite, 1.6 ‰ for amphibole, 1.5 ‰ for orthopyroxene, 1.7 ‰ for olivine and 1.3 ‰ for plagioclase.

2.3.2 Water and halogens (Cl and F)

Water and halogen (Cl and F) contents were measured *in situ* in Shiveluch phlogopite and amphibole using Cameca IMS-4f at the Edinburgh Ion Microprobe Facility (EIMF). Beam current was steady at 5 nA, decreasing towards the end of the analytical session to 4.4 nA and beam size diameter was 20 μm. The concentrations of ^{1}H, ^{35}Cl and ^{19}F were obtained by using ^{30}Si determined by the previous EPMA analysis. Amphibole Lac-Kip, Kipawa, Grenada and Kakanui, hornblende Norway, N 610 and biotite NBS 30, UNIL B2 and UNIL B4 were used as calibration standards.

Water contents were re-analysed at a different analytical session in the same amphibole and phlogopite grains to monitor repeatability of my previous analysis (Figure 13). Significant matrix effects were observed in amphibole due to Na_2O and Mg# and between phlogopite and biotite. Amphibole repeat analyses were re-calibrated using low-Na_2O amphibole Kipawa, Grenada, Kakanui and Norway. However, no matching amphibole standard has such high Mg# as the analysed Shiveluch amphibole. Significantly lower water contents of Shiveluch amphibole were obtained during the repeat analysis whereas those of Shiveluch phlogopite are consistently high (Figure 13).

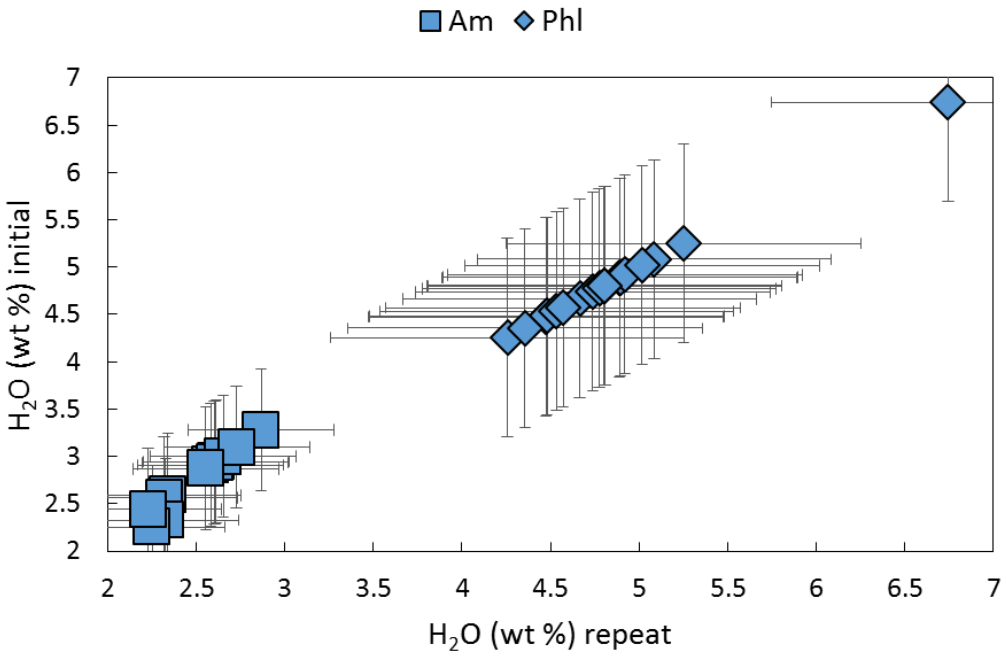

***Figure 13**. Water contents of Shiveluch amphibole and phlogopite analysed during the initial and repeat SIMS sessions.Error bars represent 2σ.*

2.4 Temperature-oxygen fugacity calculations

Equilibration temperature of peridotites was calculated using the olivine-spinel geothermometer of O'Neill and Wall (1987):

$$T = \frac{6530+28P+(5000+10.8P)(X_{Mg}^{ol}-X_{Fe}^{ol})-1960\left(1+X_{Ti}^{spl}\right)\left(X_{Mg}^{spl}-X_{Fe^{2+}}^{spl}\right)+18620X_{Cr}^{spl}+25150(X_{Fe^{3+}}^{spl}+X_{Ti}^{spl})}{RlnK_D+4.705}$$

Equation 2

where mole fractions of Mg, Fe, Ti, Cr and Fe^{3+} in olivine, spinel and orthopyroxene are:

$$X_{Mg}^{ol} = \frac{Mg}{(Mg + Fe)}$$

Equation 3

$$X_{Mg}^{spl\ and\ px} = \frac{Mg}{(Mg + Fe^{2+})}$$

Equation 4

$$X_{Fe}^{ol} = \frac{Fe}{(Fe + Mg)}$$ ***Equation 5***

$$X_{Fe}^{spl\ and\ px} = \frac{Fe^{2+}}{(Fe^{2+} + Mg)}$$ ***Equation 6***

$$X_{Ti}^{spl} = \frac{Ti}{(Ti + Fe^{3+} + Cr)}$$ ***Equation 7***

$$X_{Cr}^{spl} = \frac{Cr}{(Ti + Fe^{3+} + Cr)}$$ ***Equation 8***

$$X_{Fe^{3+}}^{spl} = \frac{Fe^{3+}}{(Ti + Fe^{3+} + Cr)}$$ ***Equation 9***

$$K_D = \frac{\frac{X_{Mg}^{ol}}{X_{Fe^{2+}}^{spl}}}{\frac{X_{Fe}^{ol}}{X_{Mg}^{spl}}}$$ ***Equation 10***

and R is 8.31441 (J $K^{-1}mol^{-1}$), pressure is in kilobars and temperature is in degrees Kelvin.

Equilibration temperature of pyroxenites was calculated using the two-pyroxene geothermometer of Brey and Köhler (1990):

$$T_{BKN} = \frac{23664 + \left(24.9 + 126.3X_{Fe}^{cpx}\right)P}{13.38 + (lnK_{D^*})^2 + 11.59X_{Fe}^{opx}}$$ ***Equation 11***

where

$$K_{D^*} = \frac{(1 - Ca^*)^{cpx}}{(1 - Ca^*)^{opx}}$$ ***Equation 12***

$$Ca^{*} = \frac{Ca^{M2}}{(1 - Na^{M2})} \qquad \textbf{\textit{Equation 13}}$$

and pressure is in kilobars and the calculated temperature is in degrees Kelvin.

Error of the two-pyroxene geothermometer was estimated to be ± 50 °C (Putirka, 2008). Pressure was assumed to be 1.5 GPa in the equilibration temperature calculations because of the absence of a reliable geobarometer for spinel peridotites independent of temperature. In contrast to geobarometers, geothermometers applicable to spinel peridotites are independent of pressure. Pressure shift of 1 GPa in olivine-spinel geothermometer (O'Neill and Wall, 1987) changes the calculated temperature only by 14 °C.

Ferric iron (Fe^{3+}) in spinel and orthopyroxene was estimated via the general equation of Droop (1987):

$$F = 2X(1 - \frac{T}{S}) \qquad \textbf{\textit{Equation 14}}$$

where F is the number of Fe^{3+} ions per X oxygens, T is the ideal number of cations per formula unit and S is the observed cation total per X oxygens calculated assuming all iron to be Fe^{2+}. The equation assumes that no element has variable valency other than Fe and that oxygen is the only anion. The equation is applicable to ferromagnesian oxide and silicate minerals.

Oxygen fugacity (fo_2) was calculated after Wood et al. (1990) and is reported in log units relative to fayalite-magnetite-quartz buffer (FMQ; Mattioli and Wood, 1988):

$$\log(fo_2)_{P,T} = logfo_2(FMQ)_{P,T} + \frac{220}{T} + 0.35 - \frac{0.0369P}{T} - 12logX_{Fe}^{ol} - \frac{2620}{T}X_{Mg}^{ol\ 2} + 3log(X_{Fe}^{M1} \cdot X_{Fe}^{M2})^{opx} + 2log\ a_{Fe_3O_4}^{spl}$$ ***Equation 15***

where

$$X_{Fe}^{M1} = \frac{Fe^{2+} + Fe^{3+}}{Sum\ M1}$$ ***Equation 16***

$$X_{Fe}^{M2} = \frac{Fe^{2+}}{Sum\ M2}$$ ***Equation 17***

$$\log a_{Fe_3O_4}^{spl} = \log\left[\frac{(Fe^{2+}) \cdot (Fe^{3+})^2}{4}\right] + \frac{1}{T}[406(Al)^2 + 653(Mg)(Al) + 299(Cr)^2 + 199(Al)(Cr) + 346(Mg)(Cr)]$$ ***Equation 18***

and pressure is in bars and temperature is in degrees Kelvin.

Chapter 3

A transect through Kamchatka subarc mantle via the study of metasomatized mantle xenoliths from Avachinsky and Bakening volcanoes

3.1 Introduction

Shifts in composition of arc volcanic rocks across-arc have been reported in several Kamchatka studies (Hochstaedter et al., 1996; Churikova et al., 2001; Duggen et al., 2007). It has been demonstrated that subarc mantle composition exerts the main control on the systematic compositional shift from volcanic front to rear-arc volcanic rocks. Kamchatka arc front volcanic rocks are more depleted than their fertile rear-arc counterparts (Hochstaedter et al., 1996; Churikova et al., 2001) and can contain trace amounts of sediment melt in their source (Duggen et al., 2007). Hochstaedter et al. (1996) proposed that the fertile rear-arc mantle becomes depleted by the time it reaches volcanic front. In their 'dynamic mantle wedge' model, rear-arc mantle flows towards the trench. Trace amounts of sediment melt component in arc front volcanic rocks from Mutnovsky volcano have also been attributed to the trench-ward flow of moderately depleted rear-arc mantle (Duggen et al., 2007). However, radiogenic isotope studies indicated that mantle is compositionally homogeneous underneath most Kamchatka arc volcanoes, resembling that of Pacific MORB, with only a limited amount of sediment melt

component (< 1 %; Kersting and Arculus, 1995; Turner et al., 1998; Churikova et al., 2001).

In Kamchatka, subarc mantle processes can be studied directly via mantle xenoliths recovered from volcanoes situated across-arc. As demonstrated via the study of arc volcanic rocks, systematic differences between subarc and rear-arc mantle composition exist in Kamchatka (Duggen et al., 2007). Here, I investigate metasomatic processes occurring in the subarc and rear-arc mantle via the study of metasomatized mantle xenoliths. In this study, Avachinsky represents a volcanic front volcano located in the eastern volcanic front (EVF) and Bakening represents the counter-part rear-arc volcano (Figure 2). These two volcanoes were selected based on their spatial distribution and the occurrence of metasomatized mantle xenoliths.

This chapter provides petrological descriptions of Avachinsky and Bakening mantle xenoliths (section 3.2) and major (section 3.3) and trace element (section 3.4) composition of their constituent minerals and the calculated composition of melts with which they are in equilibrium (3.5.4). The trace element composition of melts in equilibrium with amphibole and clinopyroxene in Avachinsky and Bakening xenoliths is used to constrain the composition of the mantle melting source under the volcanic arc and rear-arc, respectively (section 3.5.4).

3.2 Petrological descriptions

3.2.1 Avachinsky xenoliths

Avachinsky mantle xenoliths consist of large blocks (up to 15 cm in length; Figure 5B) of mantle peridotite comprised of olivine, orthopyroxene and spinel

(classified as harzburgites; Figure 14 and Table 2; Streckeisen, 1979). Only one Avachinsky xenolith consists of clinopyroxene, olivine and interstitial amphibole and is classified as pyroxenite (Figure 14 and Table 2; Streckeisen, 1979).

Avachinsky peridotites display protogranular and porphyroclastic textures that are characteristic of mantle xenoliths (Figure 15 and Table 2; Mercier and Nicolas, 1975). Olivine grain size gradually decreases from protogranular to porphyroclastic. Protogranular texture is characterized by mosaic-shaped crystals with straight-lined boundaries whereas porphyroclastic texture is characterized by two olivine populations, large elongate strained crystals called porphyroclasts and small polygonal strain-free crystals called neoblasts (Figure 15; Mercier and Nicolas, 1975). Avachinsky pyroxenite displays coarse texture.

Detailed petrographic study has revealed a thin hornblende selvage between harzburgites and the host andesite (Figure 16A) and numerous melt-rock reaction textures such as dunite veins (Figure 16B and C), orthopyroxene replacement by secondary clinopyroxene (Figure 16D) and a network of cross-cutting hydrous (Figure 16E) and anhydrous veins (Figure 16F). Hydrous veins are composed of amphibole, orthopyroxene, clinopyroxene and occasionally relict phlogopite (Figure 16E). Anhydrous veins are dominantly composed of orthopyroxene and clinopyroxene, with only occasional amphibole (Figure 16F). Both vein types are observed in *AVX-16-03-10* whereby an anhydrous vein is cross-cut by a hydrous vein (Figure 17B). The hydrous vein branches into two (Figure 17A). One of the two hydrous veins (vein 1) is produced at the expense of primary harzburgite minerals, olivine and orthopyroxene, whereas the other hydrous vein (vein 2) replaces a former orthopyroxenite vein.

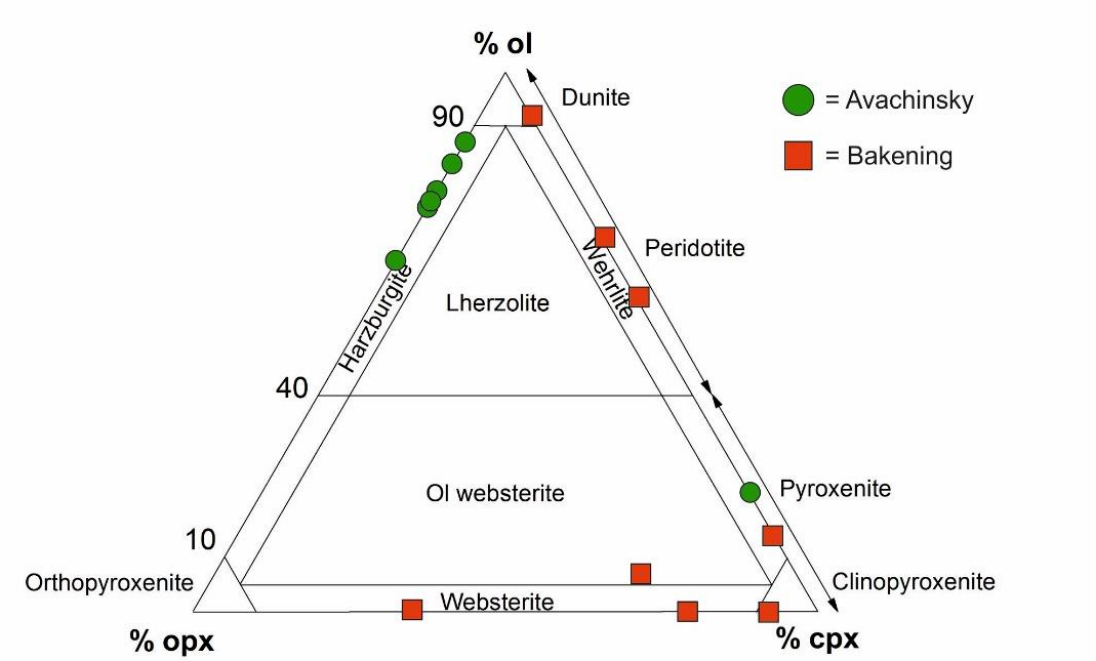

Figure 14. *Classification diagram of mantle xenoliths from Avachinsky and Bakening volcanoes (diagram after Streckeisen, 1979).*

Table 2. *Classification of Avachinsky and Bakening mantle xenoliths*

Volcanic centre	Sample	Rock type	Group	% ol	% opx	% cpx	Texture
Avachinsky	AVX-16-03-01	Pyroxenite	Wehrlite	22		78	Coarse
	AVX-16-03-02	Peridotite	Harzburgite	78	22		Porphyroclastic
	AVX-16-03-07	Peridotite	Harzburgite	87	13		Protogranular
	AVX-16-03-09	Peridotite	Harzburgite	87	13		Porphyroclastic
	AVX-16-03-10	Peridotite	Harzburgite	76	24		Protogranular
	AVX-16-03-20	Peridotite	Harzburgite	75	25		Protogranular
	AVX-16-03-23	Peridotite	Harzburgite	83	17		Protogranular
	AVX-16-03-24	Peridotite	Harzburgite	65	35		Protogranular
Bakening	BAK-16-22-01A	Pyroxenite	Olivine websterite	7	25	68	Coarse
	BAK-16-22-01B	Peridotite	Wehrlite	58		42	Protogranular
	BAK-16-22-03	Peridotite	Wehrlite	69		31	Protogranular
	BAK-16-22-04	Peridotite	Dunite	92		8	Protogranular
	BAK-16-22-05	Pyroxenite	Clinopyroxenite		8	92	Coarse
	BAK-16-22-09	Pyroxenite	Wehrlite	14		86	Coarse
	BAK-16-22-32	Pyroxenite	Websterite		65	35	Coarse
	BAK-16-22-42	Pyroxenite	Websterite		21	79	Coarse

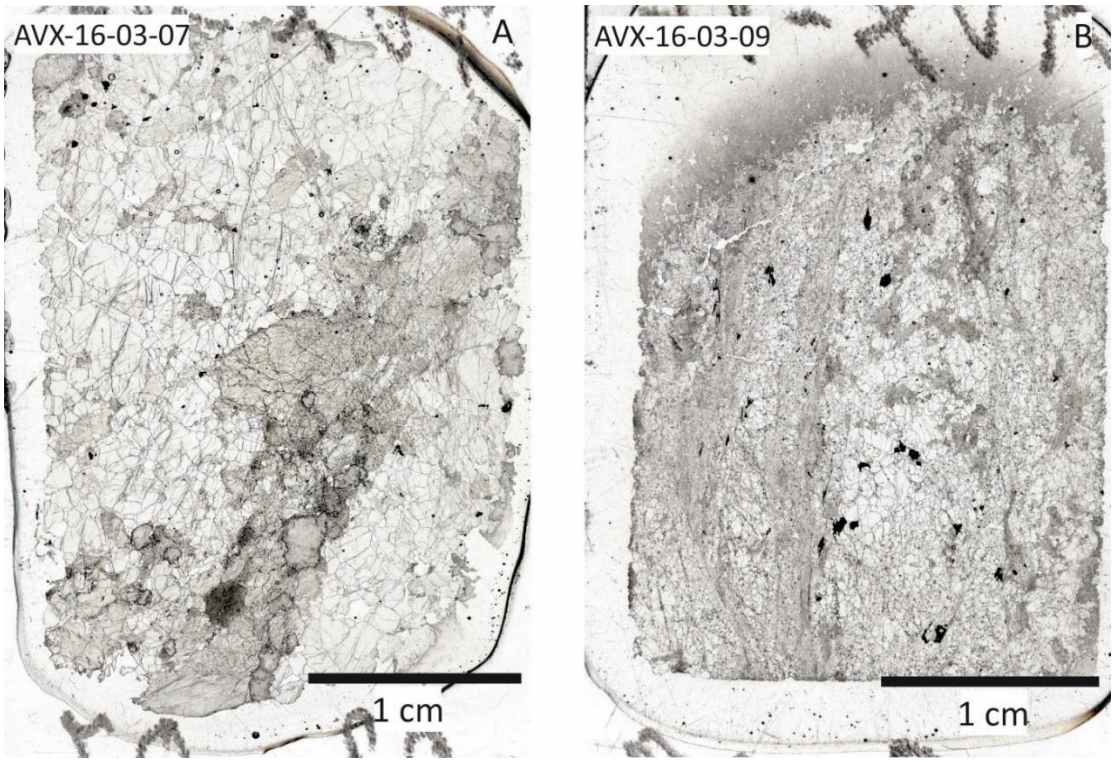

Figure 15. *Thin section scanned images showing A) protogranular texture in harzburgite AVX-16-03-07 and B) porphyroclastic texture in harzburgite AVX-16-03-09.*

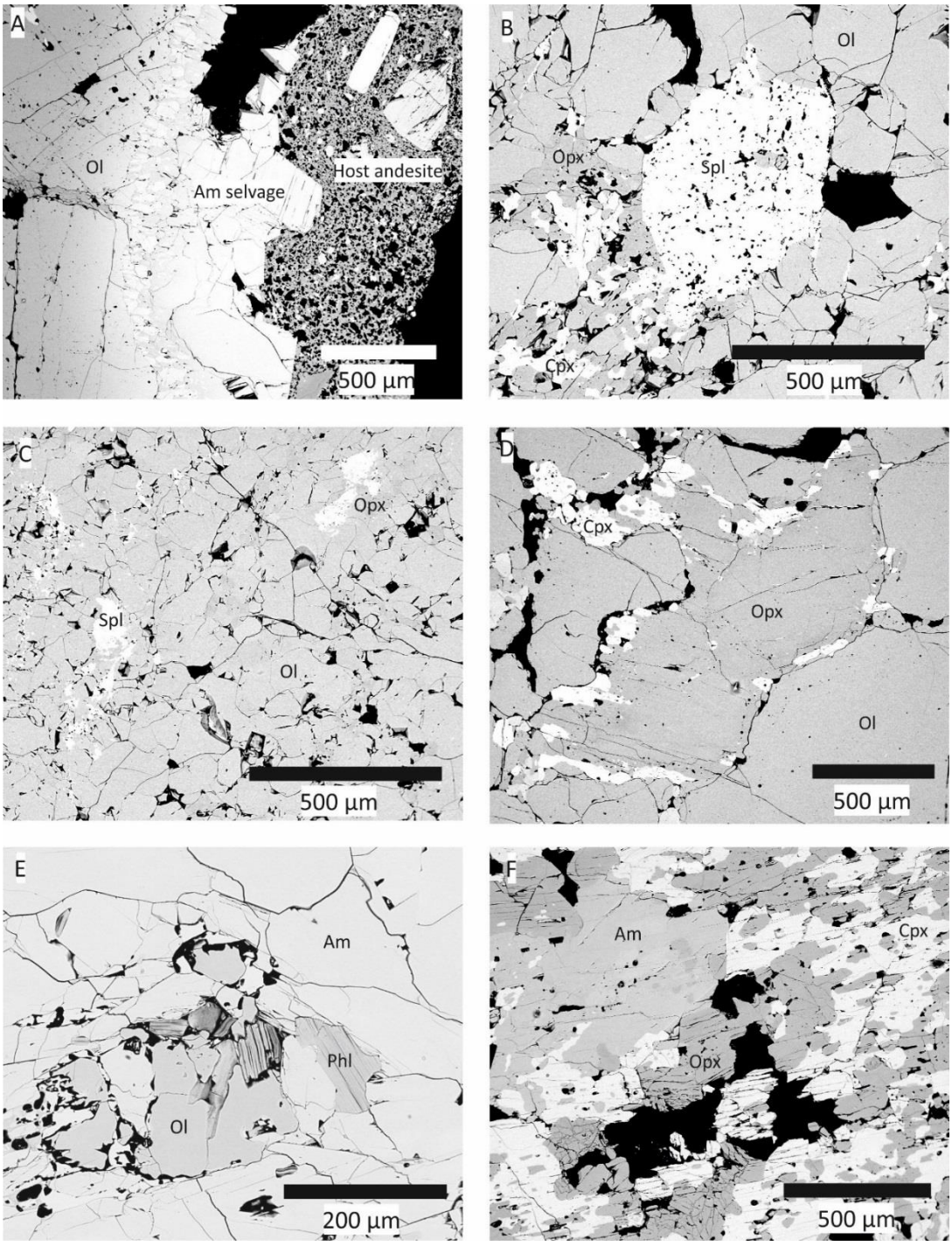

Figure 16. *Melt-rock reaction textures recorded in Avachinsky mantle xenoliths. A) Amphibole selvage formed between harzburgite AVX-16-03-20 and the host andesite. B) Melt inclusions in spinel and C) olivine neoblasts in dunite vein in AVX-16-03-09. D) Clinopyroxene overgrowing coarse orthopyroxene around the edges in AVX-16-03-02. E) Rare cluster of phlogopite grains inside hydrous vein cross-cutting AVX-16-03-24. F) Orthopyroxene overgrown by amphibole and clinopyroxene in anhydrous vein cross-cutting AVX-16-03-23. Abbreviations: Am = amphibole, Cpx = clinopyroxene, Ol = olivine, Opx = orthopyroxene, Phl = phlogopite and Spl = spinel.*

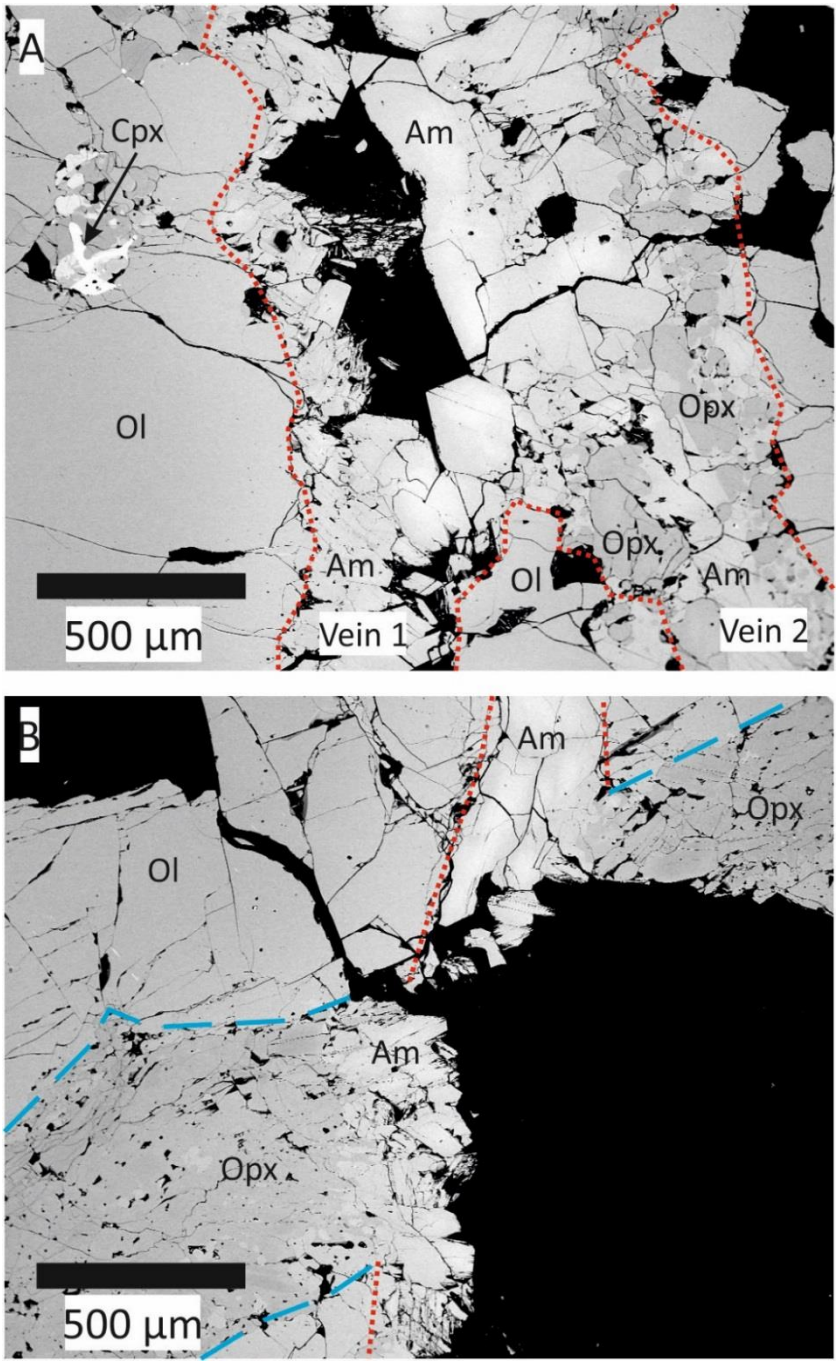

Figure 17. *Vein types in AVX-16-03-10. A) Amphibole-rich hydrous vein branches into two (vein 1 and 2). B) Hydrous vein (outlined by red dotted line) cross-cuts orthopyroxenite vein (outlined by blue dotted line). Abbreviations are the same as in Figure 16.*

3.2.2 Bakening xenoliths

Bakening mantle xenoliths are smaller than Avachinsky xenoliths, their dimensions range from 1 to 4 cm in length. Their composition varies from pyroxene-

dominated websterite (n = 2), clinopyroxenite (n = 1), wehrlite (n = 1) and olivine websterite (n = 1) to olivine-dominated wehrlite (n = 2) and dunite (n = 1; Figure 14 and Table 2). Similar to Avachinsky peridotites, Bakening peridotites display protogranular texture (Mercier and Nicolas, 1975) and Bakening pyroxenites display coarse texture.

Bakening pyroxenites and peridotites record several melt-rock reaction textures such as mineral zoning (Figure 18A) and dissolution (Figure 18B) in the host basalt, poikilitic overgrowths of clinopyroxene (oikocrysts) on orthopyroxene and olivine (chadacrysts; Figure 18C and D) and rapidly quenched symplectite consisting of olivine and glass (Figure 18F). Exsolution lamellae of orthopyroxene and spinel occur in some coarse clinopyroxene grains but comparatively few orthopyroxene grains contain clinopyroxene exsolution lamellae (Figure 18C and E).

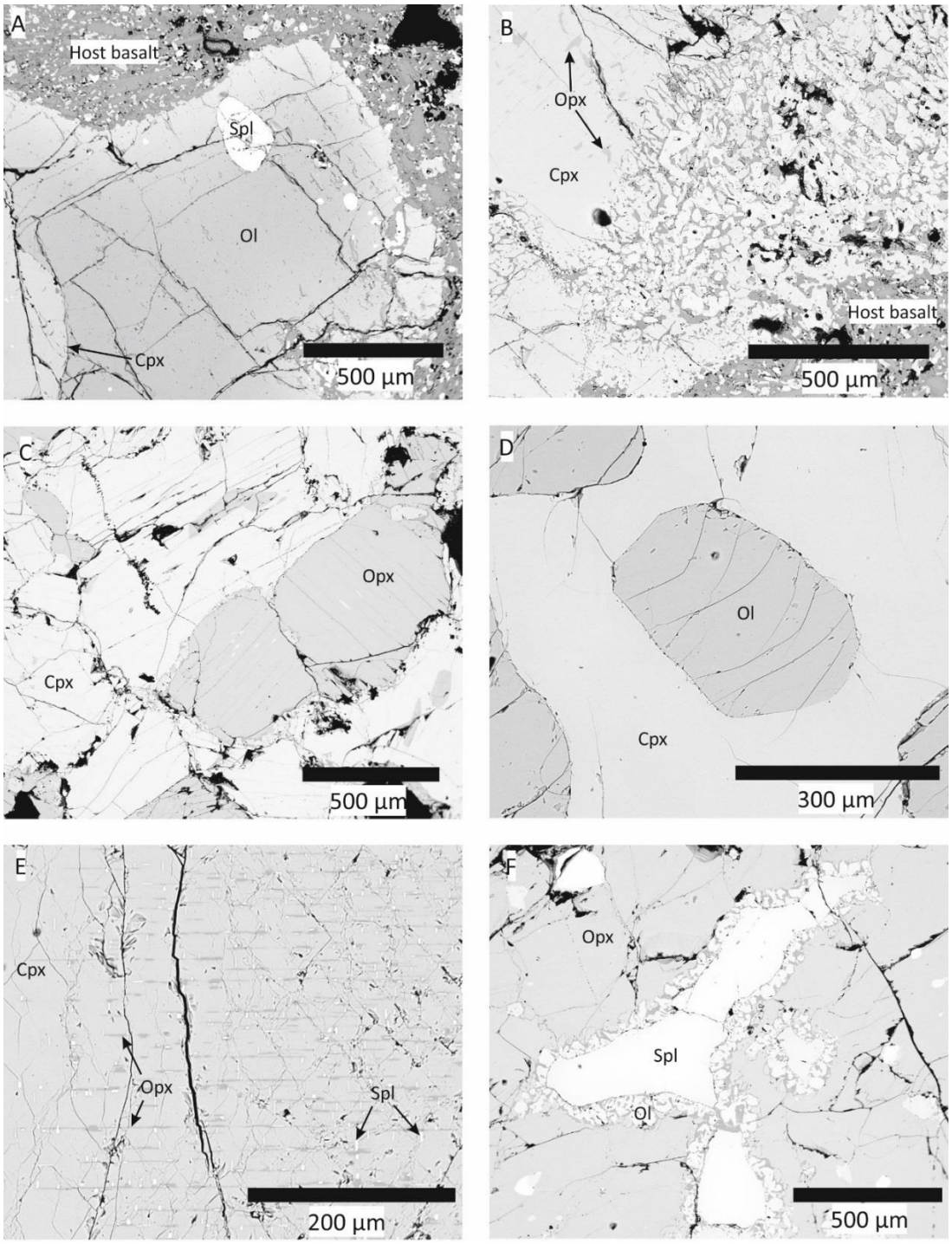

Figure 18. *Melt-rock reaction textures recorded in Bakening mantle xenoliths. A) Zoned olivine grain adjacent to the host basalt in wehrlite BAK-16-22-01B. B) Dissolution of clinopyroxene at the contact with the host basalt in olivine websterite BAK-16-22-01A. C) Crystallization of clinopyroxene at the expense of orthopyroxene in websterite BAK-16-22-42. D) Poikilitic clinopyroxene enclosing an olivine grain in wehrlite BAK-16-22-01B. E) Exsolution lamellae of orthopyroxene and spinel in coarse clinopyroxene in wehrlite BAK-16-22-01B. Note that the exsolution lamellae are at right angle to each other. F)*

Symplectite around spinel in websterite BAK-16-22-32. Abbreviations are the same as in Figure 16.

3.3 Major element mineral chemistry

Mineral major element abundances (average values in Table 3 and Table 4 and all data in Table A16, Table A17, Table A18, Table A19, Table A20 and Table A21 in Appendix A) were measured by electron probe micro analyser (EPMA) using a JEOL JXA8230 instrument at the University of Leeds (for analytical conditions see section 2.1).

3.3.1 Olivine

The composition of olivine in Avachinsky mantle xenoliths varies in forsterite component from Fo_{82} to Fo_{92} and in Bakening mantle xenoliths from Fo_{76} to Fo_{87} (Figure 19, Table 3 and Table 4). Silica content increases with higher olivine Fo component in all xenoliths except for *BAK-16-22-04* in which silica content varies from 39.3 wt % to 40.8 wt % at a constant Fo component (~ 86.8; Figure 19A). Nickel content of Avachinsky olivine ranges from 0.33 to 0.45 wt % (average NiO = 0.39 wt %) and extends to higher concentrations than that of Bakening, ranging from 0.04 to 0.35 wt % (average NiO = 0.23 wt %; Figure 19B). Bakening olivine NiO content decreases with increasing MnO ranging from 0.17 to 0.34 wt % (average MnO = 0.27 wt %) and is higher than that of Avachinsky ranging from 0.12 to 0.16 wt % (average MnO = 0.14 wt %) except for a group of high-MnO olivine (average MnO = 0.45 wt %) in harzburgite *AVX-16-03-20*.

In Avachinsky xenoliths, the low Fo and high MnO olivine is located next to hydrous vein and in Bakening xenoliths the low Fo, low NiO and high MnO olivine

is adjacent to the host basalt except for websterite *BAK-16-22-32*. Olivine in websterite *BAK-16-22-32* is a quenched mineral phase intergrown with glass that formed around clinopyroxene, orthopyroxene and spinel grains (Figure 18).

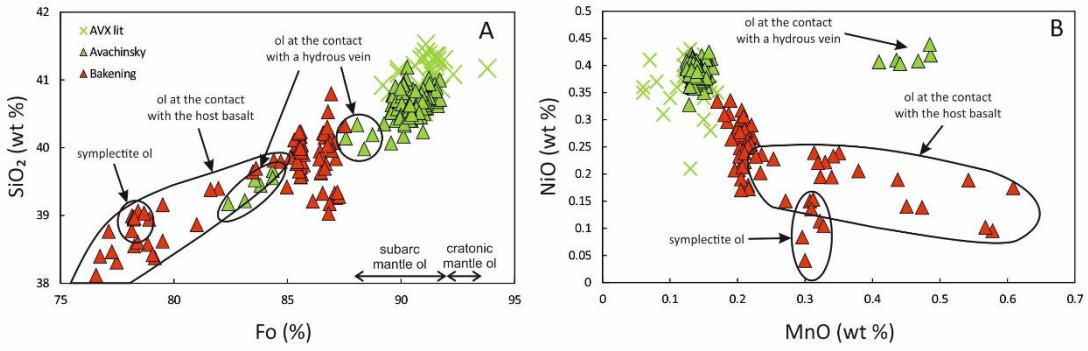

Figure 19. *A) and B) Co-variation plots of major elements in olivine in Avachinsky and Bakening mantle xenoliths. Avachinsky olivine has higher Fo component and NiO content and lower MnO content than that of Bakening. Note that olivine in websterite BAK-16-22-32 is a quench mineral phase related to the host basalt. Data is compared to Avachinsky olivine literature values from Arai et al. (2003), Ishimaru et al. (2007), Ionov (2010) and Bénard and Ionov (2013).*

3.3.2 Spinel

Spinel in Avachinsky xenoliths is Cr-rich with Cr# [Cr# = Cr/(Cr + Al)] ranging from 47 to 75 whereas spinel in Bakening xenoliths is Al-rich with Cr# ranging from 1.5 to 30 (Figure 20, Table 3 and Table 4). The refractory mantle origin of Avachinsky harzburgites is demonstrated by the high Cr# and Mg# [Mg# = Mg/(Mg + Fe^{3+})] of spinel that are similar to spinel from other depleted subarc mantle peridotites (Figure 20A) and by their high Fo component in olivine (Figure 20B). Spinel exsolved as thin lamellae in Bakening clinopyroxene possesses higher CaO (from 0.55 to 0.83 wt %) and SiO_2 (from 0.04 to 0.57 wt %) contents than the discrete spinel grains.

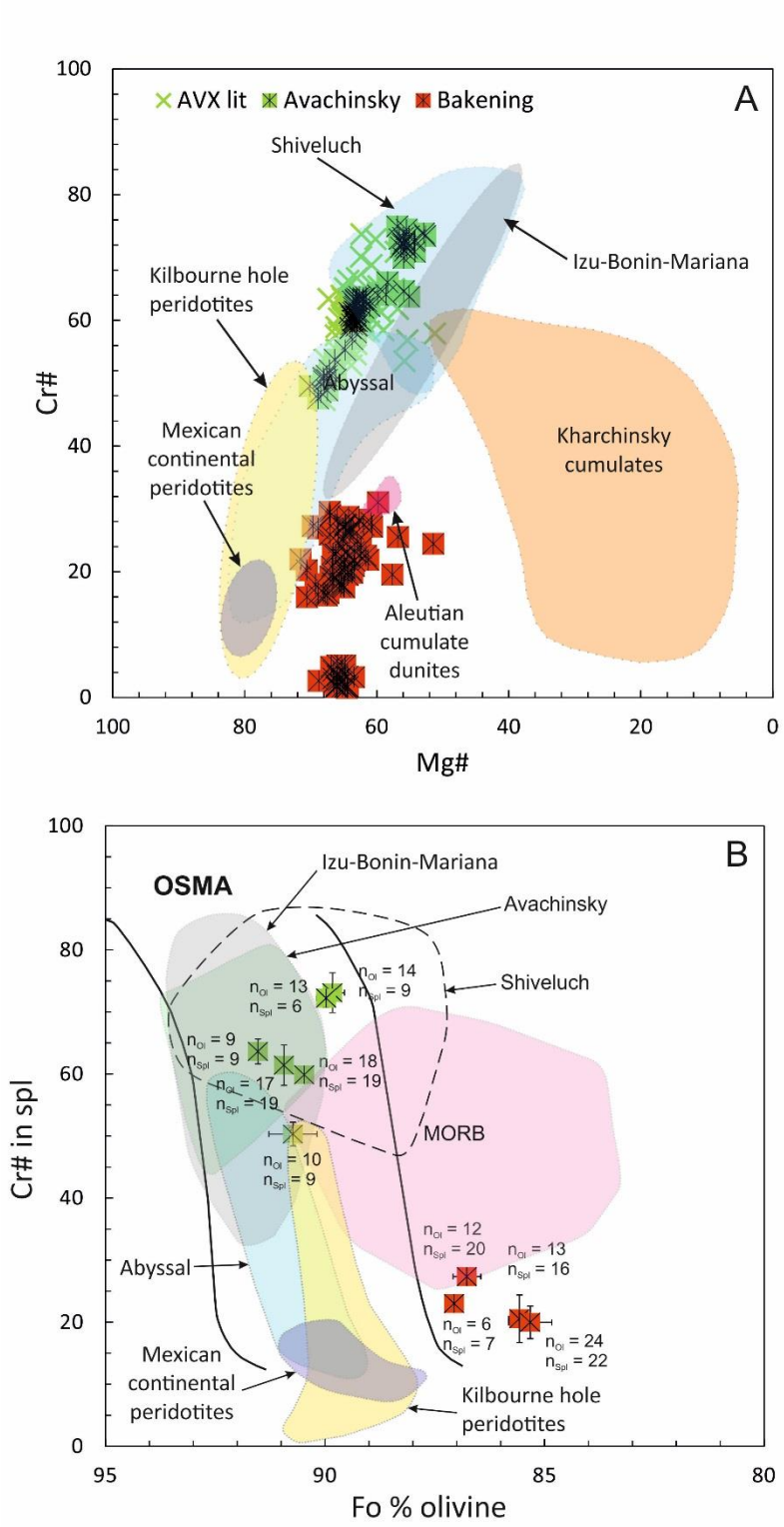

Figure 20. *A) Spinel Cr# versus Mg# and B) average spinel Cr# versus average olivine Fo component in Avachinsky and Bakening mantle xenoliths. Avachinsky data falls within the olivine-spinel mantle array (OSMA; Arai, 1994) whereas Bakening data lies outside OSMA. Figure was modified after Bryant et al. (2007), Shiveluch field was constrained from Bryant et al. (2007) and my data presented in Chapter 2, Avachinsky field was constrained from Kepezhinskas and Defant (1996), Arai et al. (2003), Ishimaru et al. (2007), Halama et al.*

(2009) and Ionov (2010), Kilbourne hole peridotite field was constrained from Harvey et al. (2012) and MORB field was constrained from Arai (1992). Concentration of Fe^{3+} was calculated after Droop (1987).

3.3.3 Orthopyroxene

Orthopyroxene is classified as Mg-rich enstatite (Figure 21) with Mg# ranging from 83 to 93 in Avachinsky xenoliths and from 79 to 88 in Bakening xenoliths (Figure 22, Table 3 and Table 4). Silica content increases from 53.3 to 57.9 wt %, average of 56.6 wt % in Avachinsky xenoliths and from 51.8 to 54.6 wt %, average of 53.2 wt % in Bakening xenoliths (Figure 22A) whereas MnO and TiO_2 contents decrease with increasing Mg# (Figure 22B and C). No systematic trends exist for NiO, CaO and Cr_2O_3 contents with increasing Mg# (Figure 22D, E and F).

In Avachinsky harzburgites, no systematic difference in major element composition exists between primary interstitial and vein orthopyroxene except for *AVX-16-03-20*. Vein orthopyroxene in *AVX-16-03-20* has lower Mg# (from 83.5 to 85.2), SiO_2 (from 54.4 to 55.6 wt %) and Cr_2O_3 (below detection limit to 0.3 wt %) and higher MnO (from 0.41 to 0.55 wt %) than vein and primary orthopyroxene in the other Avachinsky harzburgites.

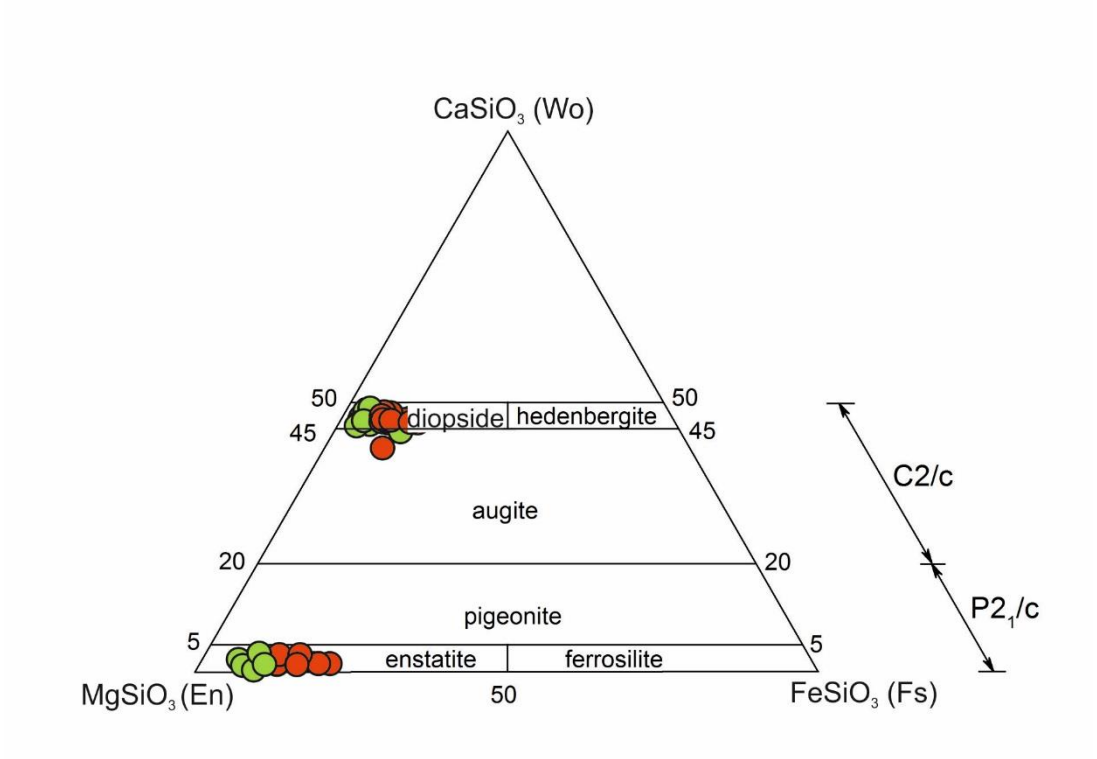

Figure 21. *Classification of Avachinsky (green circles) and Bakening (red circles) orthopyroxene (enstatite) and clinopyroxene (diopside and augite) after Morimoto (1988).*

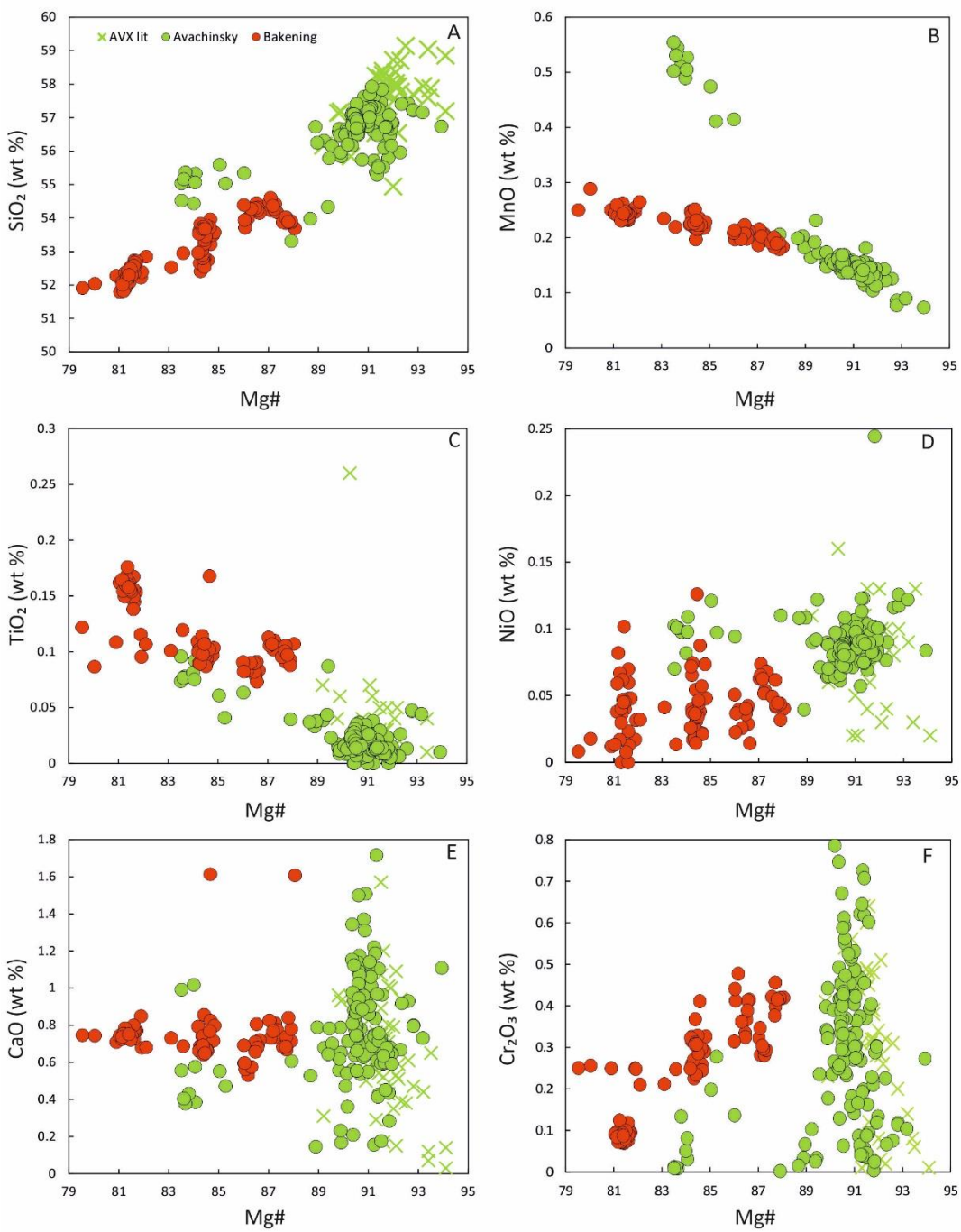

Figure 22. *A) to F) Co-variation plots of major elements in Avachinsky and Bakening orthopyroxene. Avachinsky orthopyroxene has higher SiO_2, NiO, CaO, Cr_2O_3 and Mg# and lower MnO and TiO_2 contents than that of Bakening. No distinction between vein and primary interstitial orthopyroxene in Avachinsky xenoliths was made in this plot because of their similar major element composition. Data is compared to Avachinsky orthopyroxene literature values from Arai et al. (2003); Ishimaru et al. (2007); Ishimaru and Arai (2008); Ionov (2010); Ishimaru and Arai (2011); Bénard and Ionov (2012); Bénard and Ionov (2013).*

3.3.4 Clinopyroxene

Clinopyroxene is classified as diopside and augite (Figure 21) with Mg# ranging from 80.3 to 94.8 in Avachinsky xenoliths and from 77 to 88.8 in Bakening xenoliths (Figure 23, Table 3 and Table 4).

Silica and CaO contents increase from 53.3 to 57.9 wt %, average of 56.6 wt % and from 21.8 to 25.2 wt %, average of 23.9 wt %, respectively in Avachinsky xenoliths and from 51.8 to 54.6 wt %, average of 53.2 wt % and from 19.5 to 23.3 wt %, average of 22.2 wt %, respectively in Bakening xenoliths (Figure 23A and E). Their MnO, TiO_2 and Na_2O contents decrease with increasing Mg#. No systematic trend exists for NiO content with increasing Mg#. Instead, a wide range of NiO content exists at constant clinopyroxene Mg# (Figure 23D). Both, exsolution-free and exsolution-bearing clinopyroxenes in Bakening xenoliths are compositionally identical.

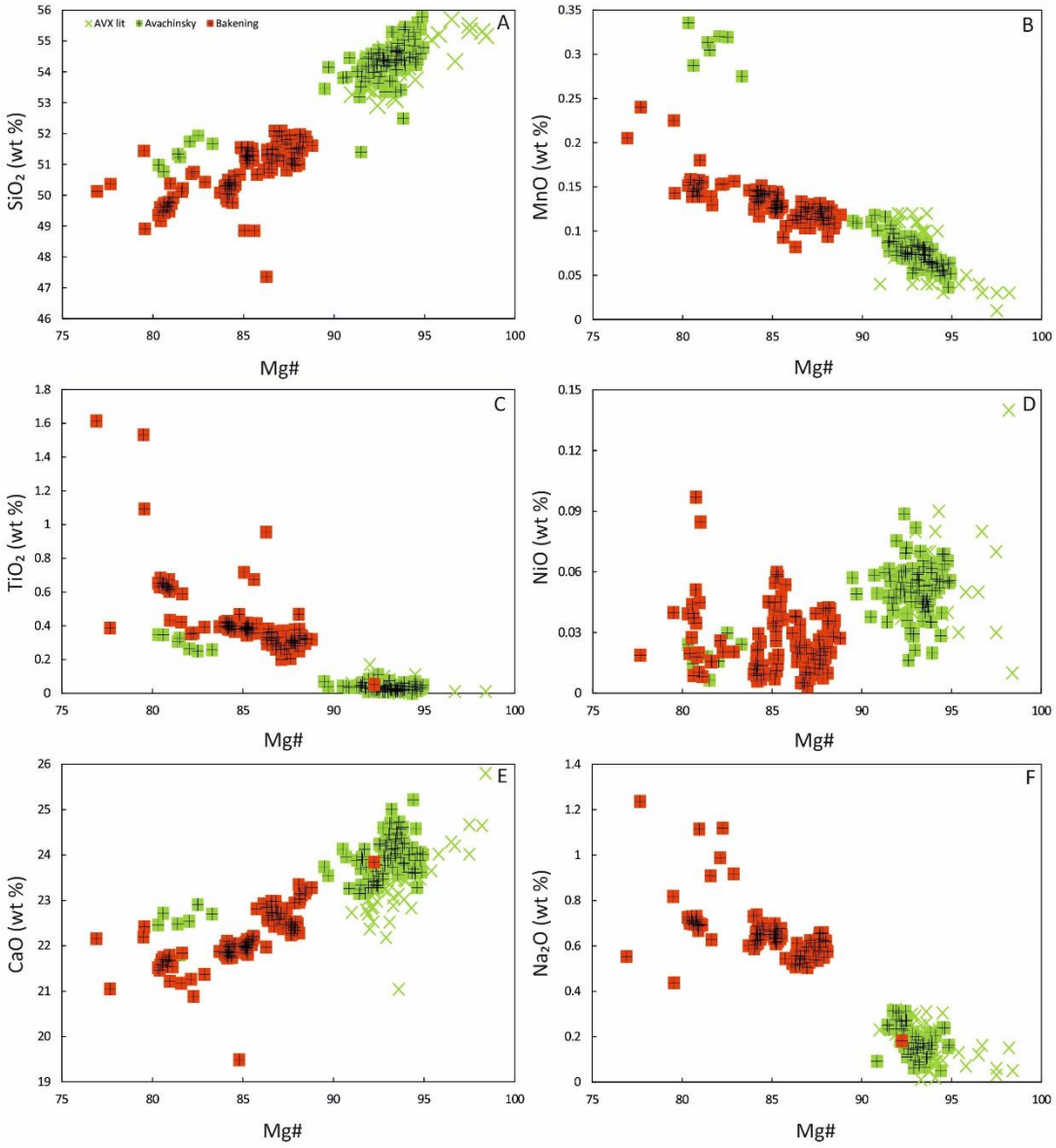

***Figure 23**. A) to F) Co-variation plots of major elements in Avachinsky and Bakening clinopyroxene. Avachinsky clinopyroxene has higher SiO_2, NiO, CaO and Mg # and lower MnO, TiO_2 and Na_2O contents than that of Bakening. Data is compared to Avachinsky clinopyroxene literature values from Arai et al. (2003); Ishimaru et al. (2007); Ishimaru and Arai (2008); Ionov (2010); Ishimaru and Arai (2011); Bénard and Ionov (2012); Bénard and Ionov (2013).*

3.3.5 Amphibole

Vein amphibole in Avachinsky xenoliths displays a large variation in Mg# (from 70 to 94; Figure 24 and Table 3). Their MnO and TiO_2 contents decrease with increasing Mg# (Figure 24A and B) and range from 0.04 to 0.35 wt % (average

MnO = 0.15 wt %) and from 0.02 to 1.34 wt % (average TiO_2 = 0.62 wt %), respectively. In *AVX-16-03-10* and *AVX-16-03-20*, vein amphibole NiO content increases with increasing Mg# and ranges from 0.03 to 0.15 wt % whereas no NiO trend is displayed in amphibole in *AVX-16-03-*24 (Figure 24C). Amphibole in *AVX-16-03-10* and *AVX-16-03-20* possesses higher TiO_2 (from 0.6 to 1.4 wt %) and Na_2O contents (from 1.75 to 2.6 wt %) than that of *AVX-16-03-24* (from 0.01 to 0.3 wt % and from 0.6 to 2 wt %, respectively; Figure 24B and D). Na_2O content of vein amphibole in *AVX-16-03-20* and *AVX-16-03-24* decreases with increasing Mg# whereas that of *AVX-16-03-10* stays at a constant average value of 2.37 wt % with increasing Mg# (Figure 24D).

Avachinsky vein amphibole is calcic and predominantly falls into two categories, magnesiohornblende and pargasite (Figure 25; Leake et al., 1997).

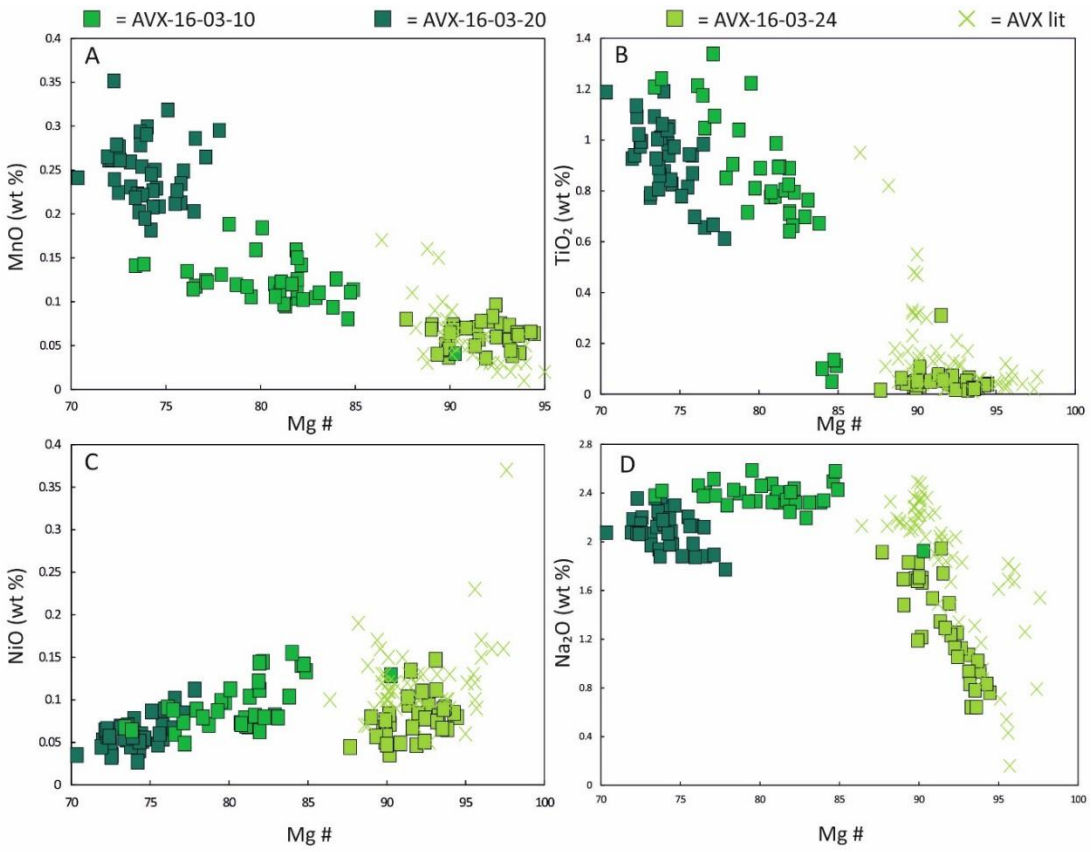

Figure 24*. A) to D) Co-variation plots of major elements in Avachinsky amphibole. Data is compared to Avachinsky amphibole literature values from Arai et al. (2003); Ishimaru et al. (2007); Ishimaru and Arai (2008); Ionov (2010); Ishimaru and Arai (2011); Bénard and Ionov (2012); Bénard and Ionov (2013).*

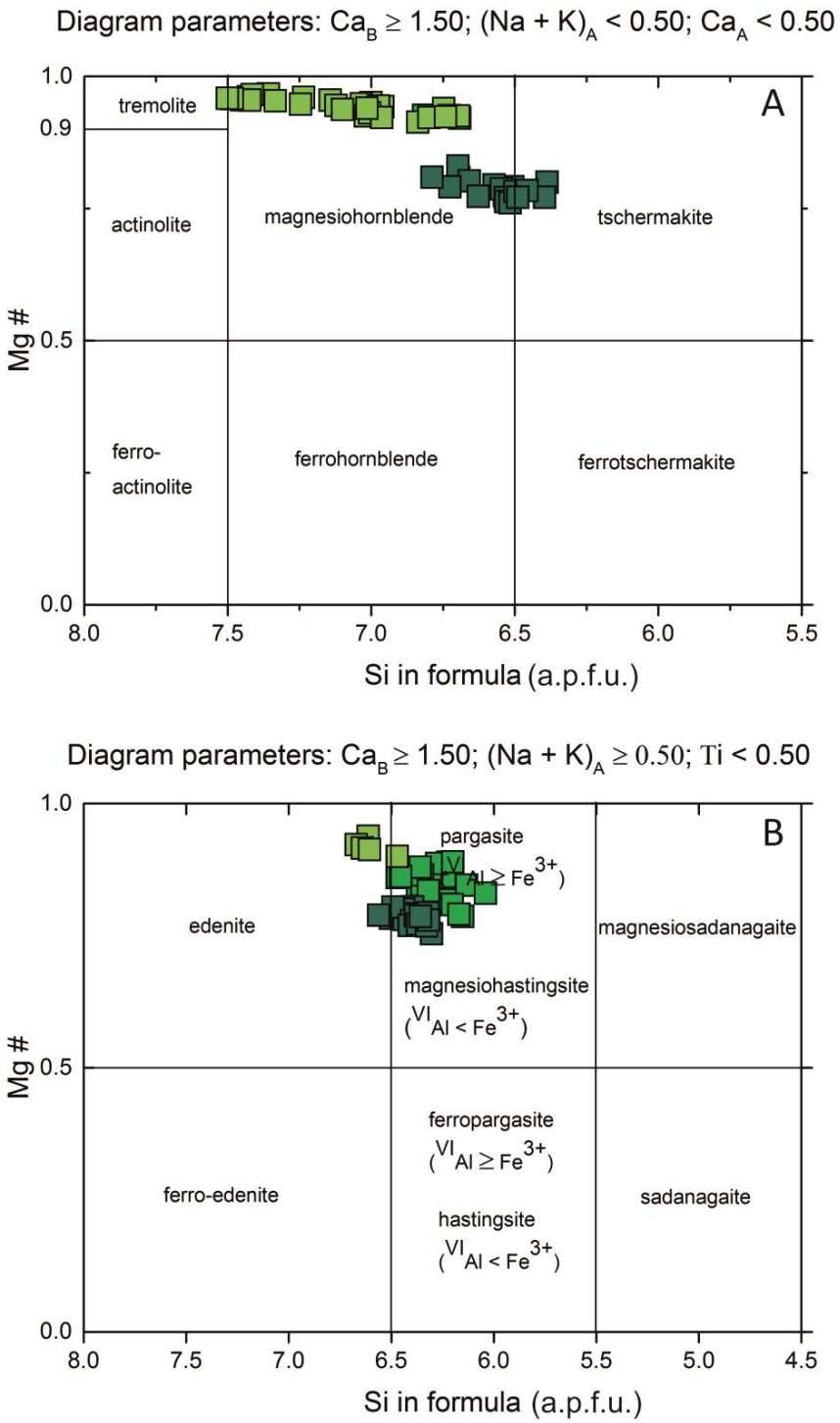

***Figure 25**. Classification of Avachinsky vein amphibole after Leake et al. (1997). Two groups of compositionally distinct amphibole occur in Avachinsky veins. A) Amphibole with lower $(Na + K)_A$ is classified as magnesiohornblende and tschermakite and B) amphibole with higher $(Na + K)_A$ is classified as pargasite, magnesiohastingsite and edenite. Legend is the same as in Figure 24.*

Table 3. *Average mineral major and minor element data of Avachinsky mantle xenoliths*

Sample	AVX-16-03-02				AVX-16-03-07				AVX-16-03-10				
Mineral	Ol	Opx	Cpx	Spl	Ol	Opx	Cpx	Spl	Ol	Opx	Cpx	Spl	Am
	n = 17	n = 24	n = 27	n = 19	n = 18	n = 29	n = 23	n = 19	n = 15	n = 18	n = 6	n = 8	n = 36
SiO_2	40.68	57.26	54.79	bdl	40.50	56.89	54.22	bdl	40.44	55.75	53.07	bdl	44.10
TiO_2	bdl	0.02	0.03	0.05	bdl	0.02	0.04	0.05	nd	0.02	0.02	0.08	0.79
Al_2O_3	nd	1.12	1.17	18.61	nd	1.41	1.70	19.72	nd	1.86	1.76	25.27	13.36
Cr_2O_3	0.05	0.33	0.52	44.15	0.02	0.43	0.60	43.86	0.02	0.33	0.57	38.13	nd
FeO	8.89	5.97	2.37	19.86	9.34	6.32	2.46	19.00	9.78	6.23	2.37	19.06	7.21
NiO	0.40	0.09	0.06	0.14	0.38	0.08	0.05	0.12	0.39	0.09	0.05	0.17	0.09
MnO	0.13	0.15	0.07	0.24	0.14	0.15	0.07	0.24	nd	0.15	0.08	0.20	0.12
MgO	50.04	34.22	18.14	13.15	49.74	33.98	17.69	13.19	49.21	34.90	18.20	14.91	16.94
CaO	0.04	1.06	23.92	0.01	0.03	0.90	23.98	bdl	0.11	0.71	24.25	0.12	11.38
Na_2O	bdl	0.01	0.19	bdl	bdl	0.01	0.17	bdl	nd	nd	nd	nd	2.37
K_2O	nd	nd	nd	nd	nd	nd	nd	nd	nd	nd	nd	nd	0.16
Cl	nd	nd	nd	nd	nd	nd	nd	nd	nd	nd	nd	nd	0.01
F	nd	nd	nd	nd	nd	nd	nd	nd	nd	nd	nd	nd	0.02
Total	100.22	100.22	101.26	96.23	100.14	100.19	100.99	96.20	99.95	100.03	100.36	97.94	96.56
Mg #	90.94	91.09	93.16	63.33	90.47	90.55	92.77	63.28	89.95	94.80	93.18	67.97	85.27
Cr #	na	na	na	61.42	na	na	na	59.87	na	na	na	50.32	na

Abbreviations: Ol = olivine, Opx = orthopyroxene, Cpx = clinopyroxene, Spl = spinel, Am = amphibole, bdl = below detection limit, nd = not determined, na = not applicable.

***Table 3**. Continued*

Sample	AVX-16-03-20					AVX-16-03-23				AVX-16-03-24					
Mineral	Ol	Opx	Cpx	Spl	Am	Ol	Opx	Cpx	Spl	Ol	Opx	Cpx	Spl	Am	Phl
	n = 9	n = 12	n = 6	n = 10	n = 39	n = 13	n = 22	n = 16	n = 6	n = 14	n = 11	n = 14	n = 12	n = 33	n = 3
SiO_2	40.84	55.34	51.67	bdl	44.86	40.87	56.76	54.46	bdl	40.58	56.77	54.11	bdl	50.41	40.09
TiO_2	bdl	0.06	0.26	0.06	0.90	bdl	0.02	0.04	0.07	bdl	0.01	0.03	0.06	0.05	0.03
Al_2O_3	bdl	1.20	2.69	17.34	11.53	bdl	0.86	0.60	13.66	bdl	0.87	1.04	14.02	8.39	18.16
Cr_2O_3	0.01	0.14	0.10	45.03	nd	bdl	0.14	0.14	53.01	0.01	0.28	0.09	52.36	0.08	0.04
FeO	8.36	9.21	5.69	22.36	9.76	9.80	6.10	2.03	19.46	9.92	6.21	2.81	19.53	3.44	2.60
NiO	0.37	0.09	0.02	0.13	0.06	0.39	0.09	0.06	0.07	0.39	0.08	0.05	0.06	0.07	0.13
MnO	0.14	0.41	0.28	0.34	0.25	0.14	0.14	0.06	0.29	0.15	0.15	0.10	0.31	0.06	0.02
MgO	50.66	31.90	15.92	12.19	15.61	49.36	34.61	18.38	11.40	49.20	34.42	17.62	11.26	21.13	23.69
CaO	0.09	0.59	22.70	bdl	11.51	0.07	0.55	24.01	bdl	0.07	0.63	23.74	bdl	11.79	0.12
Na_2O	nd	nd	nd	nd	2.09	nd	nd	nd	nd	nd	nd	nd	nd	1.31	1.83
K_2O	nd	nd	nd	nd	0.12	nd	nd	nd	nd	nd	nd	nd	nd	0.23	6.27
Cl	nd	nd	nd	nd	0.01	nd	nd	nd	nd	nd	nd	nd	nd	0.01	bdl
F	nd	nd	nd	nd	0.04	nd	nd	nd	nd	nd	nd	nd	nd	0.02	0.01
Total	100.46	98.94	99.32	97.45	96.74	100.63	99.28	99.76	97.97	100.31	99.42	99.58	97.61	97.00	91.86
Mg #	91.53	87.39	86.88	58.54	78.50	89.97	90.99	94.16	55.97	89.83	91.66	92.16	55.42	94.21	94.16
Cr #	na	na	na	63.62	na	na	na	na	72.24	na	na	na	71.50	na	na

Abbreviations: Ol = olivine, Opx = orthopyroxene, Cpx = clinopyroxene, Spl = spinel, Am = amphibole, Phl = phlogopite, bdl = below detection limit, nd = not determined, na = not applicable.

Table 4. *Average mineral major and minor element data of Bakening mantle xenoliths*

Sample	BAK-16-22-01A			BAK-16-22-01B				BAK-16-22-03				
Mineral	Ol	Opx	Cpx	Ol	Opx	Cpx	Spl	Ol	Opx I	Opx II	Cpx	Spl
	n = 6	n = 8	n = 12	n = 13	n = 9	n = 15	n = 16	n = 21	n = 1	n = 1	n = 15	n = 21
SiO_2	38.51	52.31	50.33	39.69	54.18	51.56	bdl	40.01	54.39	53.94	51.17	bdl
TiO_2	0.01	0.10	0.40	0.01	0.08	0.30	0.28	0.01	0.09	0.08	0.37	0.45
Al_2O_3	bdl	4.81	5.94	bdl	3.34	4.27	40.45	bdl	3.22	3.50	4.51	40.71
Cr_2O_3	0.01	0.25	0.38	0.08	0.39	0.83	15.53	0.05	0.31	0.44	0.77	15.08
FeO	19.83	11.28	5.43	13.75	8.80	4.22	23.74	14.05	9.12	9.07	4.47	24.72
NiO	0.22	0.02	0.02	0.28	0.03	0.01	0.20	0.23	0.05	0.02	0.03	0.23
MnO	0.35	0.25	0.15	0.21	0.21	0.12	0.18	0.21	0.21	0.21	0.12	0.18
MgO	40.89	28.92	14.81	45.78	31.43	15.84	15.00	46.02	31.46	31.38	15.53	15.46
CaO	0.05	0.73	21.56	0.04	0.66	22.60	0.01	0.02	0.69	0.60	22.81	0.15
Na_2O	bdl	0.04	0.83	bdl	0.02	0.56	bdl	bdl	0.03	0.01	0.53	bdl
K_2O	bdl	bdl	bdl	bdl	bdl	bdl	bdl	bdl	bdl	bdl	bdl	bdl
Cl	nd	nd	nd	nd	nd	nd	nd	nd	nd	nd	nd	nd
F	nd	nd	nd	nd	nd	nd	nd	nd	nd	nd	nd	nd
Total	99.85	98.71	99.85	99.82	99.13	100.31	95.39	100.58	99.57	99.25	100.30	97.09
Mg #	78.61	82.03	82.92	85.57	86.42	86.99	64.84	85.38	86.01	86.04	86.08	65.48
Cr #	na	na	na	na	na	na	20.55	na	na	na	na	19.97

Abbreviations: Ol = olivine, Opx = orthopyroxene, Cpx = clinopyroxene, Spl = spinel, bdl = below detection limit, nd = not determined, na = not applicable.

Table 4. *Continued*

Sample	BAK-16-22-04				BAK-16-22-05		BAK-16-22-09				BAK-16-22-32				BAK-16-22-42	
Mineral	Ol	Opx	Cpx	Spl	Opx	Cpx	Ol	Opx	Cpx	Spl	Ol	Opx	Cpx	Spl	Opx	Cpx
	n = 20	n = 6	n = 15	n = 14	n = 13	n = 19	n = 6	n = 7	n = 19	n = 7	n = 7	n = 23	n = 19	n = 13	n = 16	n = 30
SiO_2	40.03	54.36	51.00	bdl	52.96	50.23	39.24	53.89	51.13	bdl	38.96	52.29	49.63	bdl	53.60	51.31
TiO_2	nd	0.11	0.43	0.50	0.11	0.40	bdl	0.10	0.37	0.54	0.02	0.16	0.64	0.35	0.10	0.42
Al_2O_3	nd	2.71	3.90	36.57	4.81	5.88	bdl	3.30	4.36	42.27	bdl	5.07	6.22	54.16	4.12	4.89
Cr_2O_3	0.09	0.30	0.66	20.51	0.25	0.37	0.05	0.42	0.81	19.03	0.02	0.09	0.15	2.39	0.32	0.47
FeO	12.76	8.40	4.09	23.28	10.02	5.08	12.43	7.97	4.21	20.46	20.19	11.76	6.13	23.62	10.05	4.83
NiO	0.27	0.06	0.03	0.23	0.03	0.01	0.32	0.04	0.02	0.19	0.11	0.04	0.03	0.23	0.06	0.04
MnO	nd	0.20	0.11	0.18	0.22	0.14	0.19	0.19	0.12	0.21	0.31	0.24	0.15	0.14	0.23	0.13
MgO	46.96	32.03	16.17	14.86	29.94	15.09	46.91	32.18	16.09	15.01	40.88	28.90	14.44	16.24	30.65	15.42
CaO	0.08	0.77	22.74	0.21	0.79	21.87	bdl	0.84	22.37	0.07	0.08	0.75	21.64	0.12	0.69	22.02
Na_2O	nd	nd	nd	nd	0.03	0.66	bdl	0.02	0.61	bdl	bdl	0.02	0.70	bdl	0.03	0.65
K_2O	nd	nd	nd	nd	bdl	bdl	bdl	bdl	bdl	bdl	bdl	bdl	bdl	bdl	bdl	bdl
Cl	nd	nd	nd	nd	nd	nd	nd	nd	nd	nd	nd	nd	nd	nd	nd	nd
F	nd	nd	nd	nd	nd	nd	nd	nd	nd	nd	nd	nd	nd	nd	nd	nd
Total	100.17	98.95	99.13	96.38	99.17	99.73	99.14	98.94	100.08	97.79	100.59	99.33	99.72	97.26	99.85	100.18
Mg #	86.76	89.37	89.93	64.86	84.18	84.12	87.06	87.80	87.21	63.38	78.30	81.40	80.77	65.58	84.46	85.04
Cr #	na	na	na	27.34	na	na	na	na	na	23.22	na	na	na	2.90	na	na

Abbreviations: Ol = olivine, Opx = orthopyroxene, Cpx = clinopyroxene, Spl = spinel, bdl = below detection limit, nd = not determined, na = not applicable.

3.3.6 P-T and fO_2

Avachinsky and Bakening mantle xenoliths equilibrated at temperatures ranging from 760.9 to 811.1 °C ± 50 °C and from 895.6 to 979.3 °C ± 50 °C, respectively (Figure 26 and Table 5). Equilibration temperature of peridotites was calculated using the spinel-olivine geothermometer of O'Neill and Wall (1987) and that of pyroxenites using the two-pyroxene geothermometer of Brey and Köhler (1990). Error was estimated by Putirka (2008). The higher temperature of *AVX-16-03-24* (914.2 °C; Figure 26 and Table 5) was estimated from orthopyroxene-clinopyroxene pair inside the hydrous vein and records temperature of melt percolation through the vein rather than xenolith equilibration in the subarc mantle. Equilibration temperature estimate of clinopyroxene-exsolved orthopyroxene in Bakening xenoliths ranges from 850 to 920 °C ± 50 °C (Brey and Köhler, 1990; Putirka, 2008). Comparatively, the estimated crystallization temperature of pyroxene in Avachinsky basaltic andesite ranges from 950 to 1100 °C (Castellana, 1998) and temperature estimated from spinel-hosted melt inclusions in Avachinsky mantle xenoliths which record magma temperatures are as low as 900 °C (Ionov et al., 2011). No comparison between equilibration temperature of Bakening mantle xenoliths and that of the host basalts can be drawn as their equilibration temperature is not reported.

Equilibration pressure was constrained by the Central Kamchatka depression geotherm defined by continental crust thermal gradient of 23 °C km^{-1} and asthenospheric mantle thermal gradient of 8.5 °C km^{-1} (Portnyagin and Manea, 2008) and ranges from 1.1 to 1.2 GPa in Avachinsky xenoliths and from 1.5 to 1.85 GPa in Bakening xenoliths (Figure 26 and Table 5). The pressure estimates indicate

that Avachinsky mantle xenoliths last equilibrated at 33 to 36 km depth at the crust-mantle interface that in Kamchatka is located at ~ 35 km (Levin et al., 2002) whereas Bakening mantle xenoliths last equilibrated at 45 to 55.5 km depth in the lithospheric mantle. For comparison, the estimated equilibration pressure of Avachinsky central vent lavas falls below 0.2 GPa (Castellana, 1998) which is equivalent to 6 km depth.

Oxygen fugacity (fO_2) was calculated after Wood et al. (1990) and ranges from + 0.45 to + 0.84 log units relative to FMQ (Mattioli and Wood, 1988) in Bakening xenoliths (Table 5). A single fO_2 value of + 1.61 log units relative to FMQ was obtained for harzburgite *AVX-16-03-10* (Table 5) because only a limited number of mantle xenoliths contained olivine, spinel and primary orthopyroxene that are required to calculate fO_2. The highly oxidized conditions at Avachinsky are consistent with fO_2 constrained from high-Mg# olivine-spinel inclusions from Avachinsky volcanic rocks (fO_2 = + 1.35 to + 1.77 log units FMQ) attributed to the influx of AOC-derived components (Nekrylov et al., 2018). However, Bakening fO_2 is lower than that estimated by Nekrylov et al. (2018) ranging from + 1.38 to + 1.74 log units FMQ.

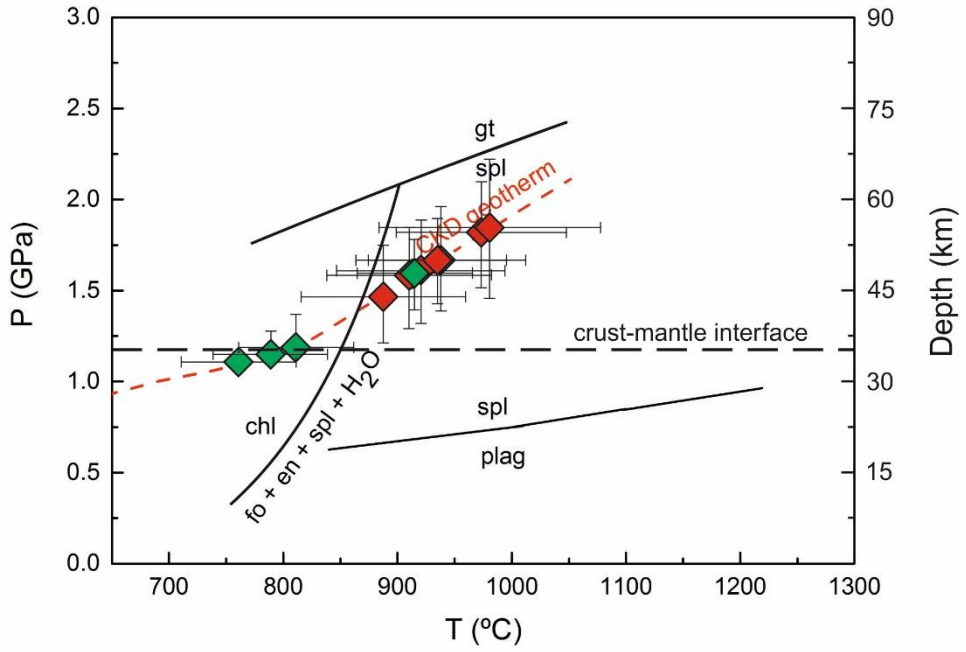

***Figure 26**. Equilibration pressure-temperature conditions of Avachinsky (green diamonds) and Bakening (red diamonds) mantle xenoliths. Equilibration temperatures of peridotites and pyroxenites were calculated via olivine-spinel geothermometer of O'Neill and Wall (1987) and two-pyroxene geothermometer of Brey and Köhler (1990), respectively. Pressures were estimated from the CKD geotherm (Portnyagin and Manea, 2008). Chlorite breakdown reaction and garnet-spinel transition is from Ulmer and Trommsdorff (1999) and spinel-plagioclase transition is from O'Neill (1981). Crust-mantle interface is located at 35 km depth in Kamchatka (Levin et al., 2002).*

***Table 5**. Average equilibration temperature, pressure and oxygen fugacity of Avachinsky and Bakening mantle xenoliths*

Sample	Number of mineral pairs	T (°C)	T 2σ (°C)	P[§] (GPa)	fO_2 (FMQ)
AVX-16-03-02	2	790.8 ± 50*	2.4	1.15 ± 0.1	nd
AVX-16-03-07	1	811.1 ± 50*	na	1.2 ± 0.15	nd
AVX-16-03-10	1	760.9 ± 50*	na	1.1 ± < 0.1	+ 1.61
AVX-16-03-24 (vein)	1	914.2 ± 50†	na	nd	nd
BAK-16-22-01A	2	922 ± 50†	23	1.65 ± 0.3	nd
BAK-16-22-01B	3	973.7 ± 50*	24	1.8 ± 0.3	+ 0.45
BAK-16-22-03	5	979.3 ± 50*	46	1.85 ± 0.35	nd
BAK-16-22-04	5	938 ± 50*	24	1.7 ± 0.25	+ 0.84
BAK-16-22-05	5	913.8 ± 50†	14	1.6 ± 0.25	nd
BAK-16-22-09	4	910.1 ± 50†	22	1.6 ± 0.25	nd
BAK-16-22-32	2	895.6 ± 50†	21	1.5 ± 0.25	nd
BAK-16-22-42	3	935.1 ± 50†	10	1.7 ± 0.2	nd

Abbreviations: na = not applicable, nd = not determined

*Temperature calculated via olivine-spinel geothermometer of O'Neill and Wall (1987)

†Temperature calculated via two-pyroxene geothermometer of Brey and Köhler (1990)

§Pressure constrained from CKD geotherm defined by continental crust thermal gradient of 23 °C km^{-1} and asthenospheric mantle thermal gradient of 8.5 °C km^{-1} (Portnyagin and Manea, 2008). The estimated thickness of Kamchatka continental crust is 35 km (Levin et al., 2002).

3.4 Trace element mineral chemistry

Mineral trace element abundances (average values in Table 6 and Table 7 and all data in Table B22, Table B24 and Table B25 in Appendix B) were measured by inductively coupled plasma mass-spectrometer (ICP-MS) using an Agilent 8800 ICP-MS Triple Quad attached to a laser ablation system Photon Machines Analyte Excimer 193 nm at the Open University (for analytical conditions see section 2.3).

3.4.1 Clinopyroxene

3.4.1.1 Avachinsky xenoliths

Except for Sr and Li, vein clinopyroxene in *AVX-16-03-24* is depleted in all incompatible trace elements relative to primitive mantle (Figure 27A; McDonough and Sun, 1995). Two types of clinopyroxene were recognized in *AVX-16-03-24* based on their distinct primitive mantle-normalized (McDonough and Sun, 1995) REE distribution trends (Figure 27B and C). In *type I clinopyroxene*, LREE decrease in abundance from La (ranges from 0.08 to 0.1 μg g^{-1}) to Nd (ranges from 0.04 to 0.07 μg g^{-1}) whereas HREE increase in abundance from Tb (ranges from 0.13 to 0.18 μg g^{-1}) to Lu (ranges from 0.3 to 0.45). Mid-REE Sm, Eu and Gd are below detection limit (Figure 27B). In *type II clinopyroxene*, REE increase in abundance

from La (average La = 0.12 µg g^{-1}) to Lu (average Lu = 0.56 µg g^{-1}). Negative Eu anomalies occur in two *type II clinopyroxene* grains (Figure 27C).

Vein clinopyroxene in *AVX-16-03-20* is enriched in all incompatible trace elements relative to primitive mantle (McDonough and Sun, 1995) except for La, Pb, Zr and Li (Figure 28A). Light REE increase in abundance from La (La = 0.50 µg g^{-1}) to Sm (Sm = 5.65 µg g^{-1}) and HREE slightly decrease in abundance from Gd (Gd = 5.18 µg g^{-1}) to Lu (Lu = 3.89 µg g^{-1}) with a weak negative Eu anomaly (Figure 28B).

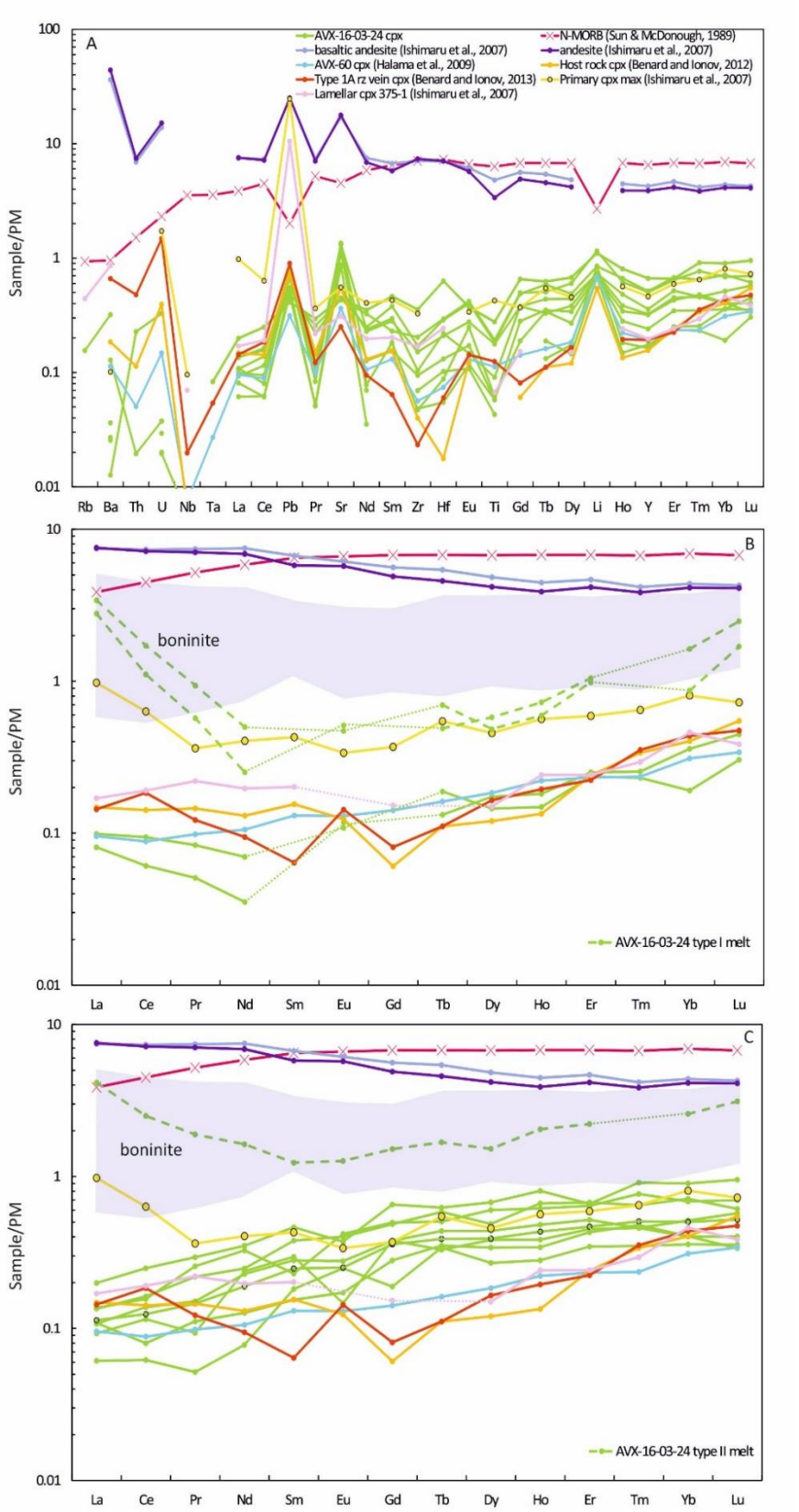

Figure 27. *A) Trace element distribution and B) and C) rare earth element (REE) distribution in AVX-16-03-24 type I and type II clinopyroxene and their respective*

equilibrium melts. Data is normalized to primitive mantle (PM; McDonough and Sun, 1995). N-MORB (Sun and McDonough,1989), typical Avachinsky andesite and basaltic andesite (Ishimaru et al., 2007) and similar Avachinsky clinopyroxene (Ishimaru et al., 2007; Halama et al., 2009; Bénard and Ionov, 2012; Bénard and Ionov, 2013) are shown for comparison. Purple field corresponds to REE composition of boninite (Hickey and Frey, 1982; Pearce et al., 1992; Kelemen et al., 2003). Incompatible trace elements that were not reported in the above studies are inferred by dotted lines.

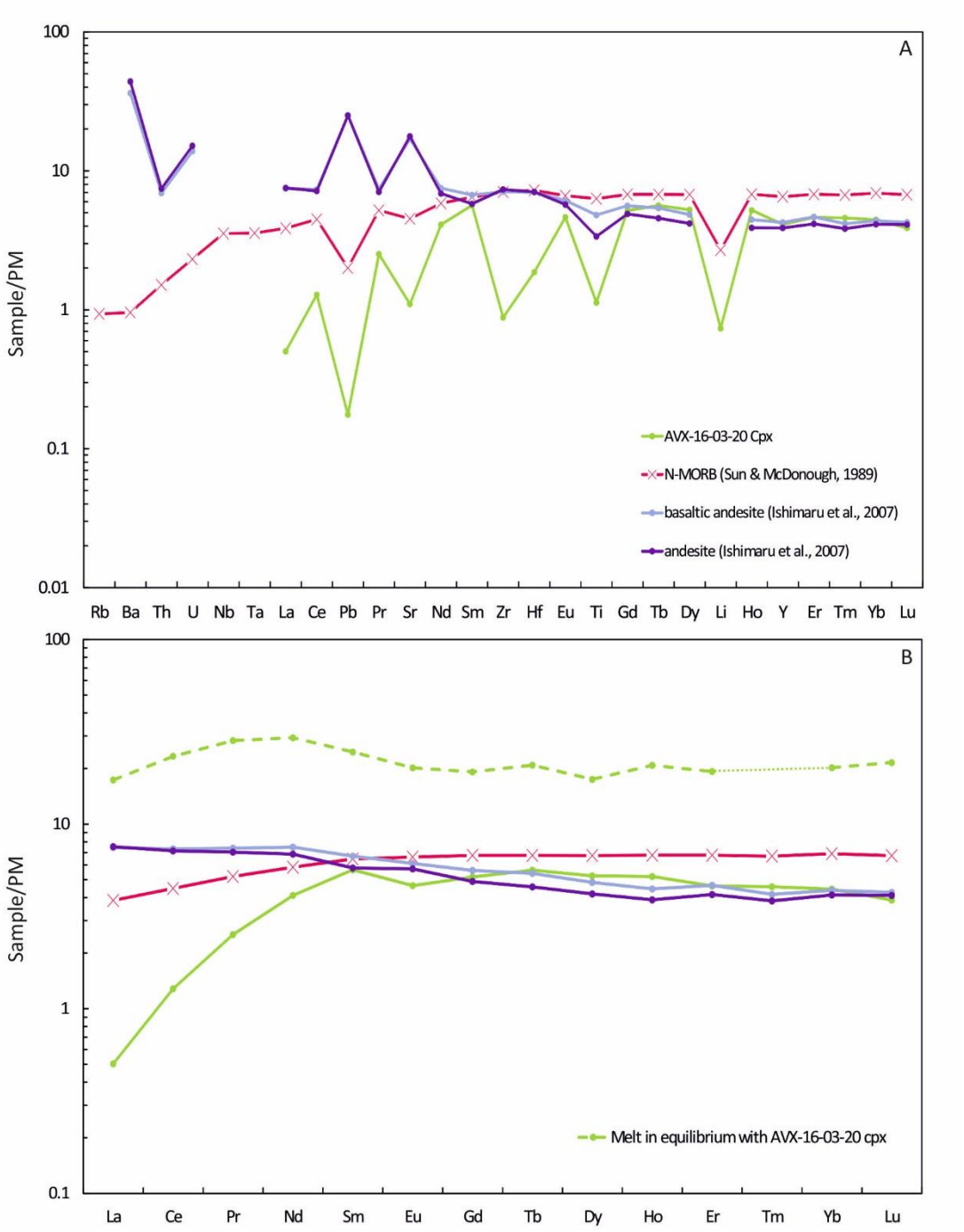

***Figure 28**. A) Trace element distribution and B) rare earth element (REE) distribution in AVX-16-03-20 clinopyroxene and its respective equilibrium melt. Data is normalized to*

primitive mantle (PM; McDonough and Sun, 1995). N-MORB (Sun and McDonough,1989) and typical Avachinsky andesite and basaltic andesite (Ishimaru et al., 2007) are shown for comparison.

3.4.1.2 Bakening xenoliths

All Bakening clinopyroxene is enriched in incompatible trace elements relative to primitive mantle (McDonough and Sun, 1995) except for Rb, Ba, Nb and Ta (Figure 29, Figure 30 and Figure 31) and some Bakening clinopyroxene is also depleted in Th, U, Pb and Zr. Three types of clinopyroxene were recognized in Bakening xenoliths based on their distinct primitive mantle-normalized (McDonough and Sun, 1995) REE distribution trends (Figure 29B, Figure 30B and Figure 31B).

Type I clinopyroxene occurs only in dunite *BAK-16-22-04*. Light REE decrease in abundance from La (average La = 5.58 µg g^{-1}) to Nd (average Nd = 2.62 µg g^{-1}) and HREE are flat (e.g. average Yb = 2.3 µg g^{-1}; Figure 29B). Distribution trend of REE in *type I clinopyroxene* is similar to that of metasomatic clinopyroxene disseminated in Bakening xenoliths (Kepezhinskas and Defant, 1996) and harzburgite clinopyroxene close to lherzolite contact in Lherz xenoliths (LeRoux et al., 2007).

Type II clinopyroxene occurs only in wehrlite *BAK-16-22-03* and displays convex-up LREE trend while HREE decrease in abundance from Gd (average Gd = 3.67 µg g^{-1}) to Lu (average Lu = 2.17 µg g^{-1}; Figure 30B). Its REE abundances and distribution trends are identical to bulk-rock pyroxenite (Koloskov et al., 2017) and lherzolite clinopyroxene close to harzburgite contact in ultramafic xenoliths from the Lherz massif, France (LeRoux et al., 2007).

Type III clinopyroxene is the most common as it occurs in six Bakening xenoliths. Light REE increase in abundance from La (average La ranges from 0.77 µg g^{-1} to 1.95 µg g^{-1}) to Sm (average Sm ranges from 2.08 µg g^{-1} to 4.28 µg g^{-1}) and

HREE slightly decrease in abundance from Sm to Lu (average Lu ranges from 1.76 µg g^{-1} to 2.37 µg g^{-1}) except clinopyroxene in *BAK-16-22-32* whose HREE slightly increase in abundance from Sm to Lu (average Lu = 4.62 µg g^{-1}; Figure 31B). Abundances and distribution trends of REE in *type III clinopyroxene* are identical to primary clinopyroxene from other Bakening xenoliths (Kepezhinskas and Defant, 1996) and lherzolite clinopyroxene in Lherz xenoliths (LeRoux et al., 2007). Furthermore, heavy REE abundances and distribution trends fall within that of bulk-rock Bakening pyroxenite (Koloskov et al., 2017).

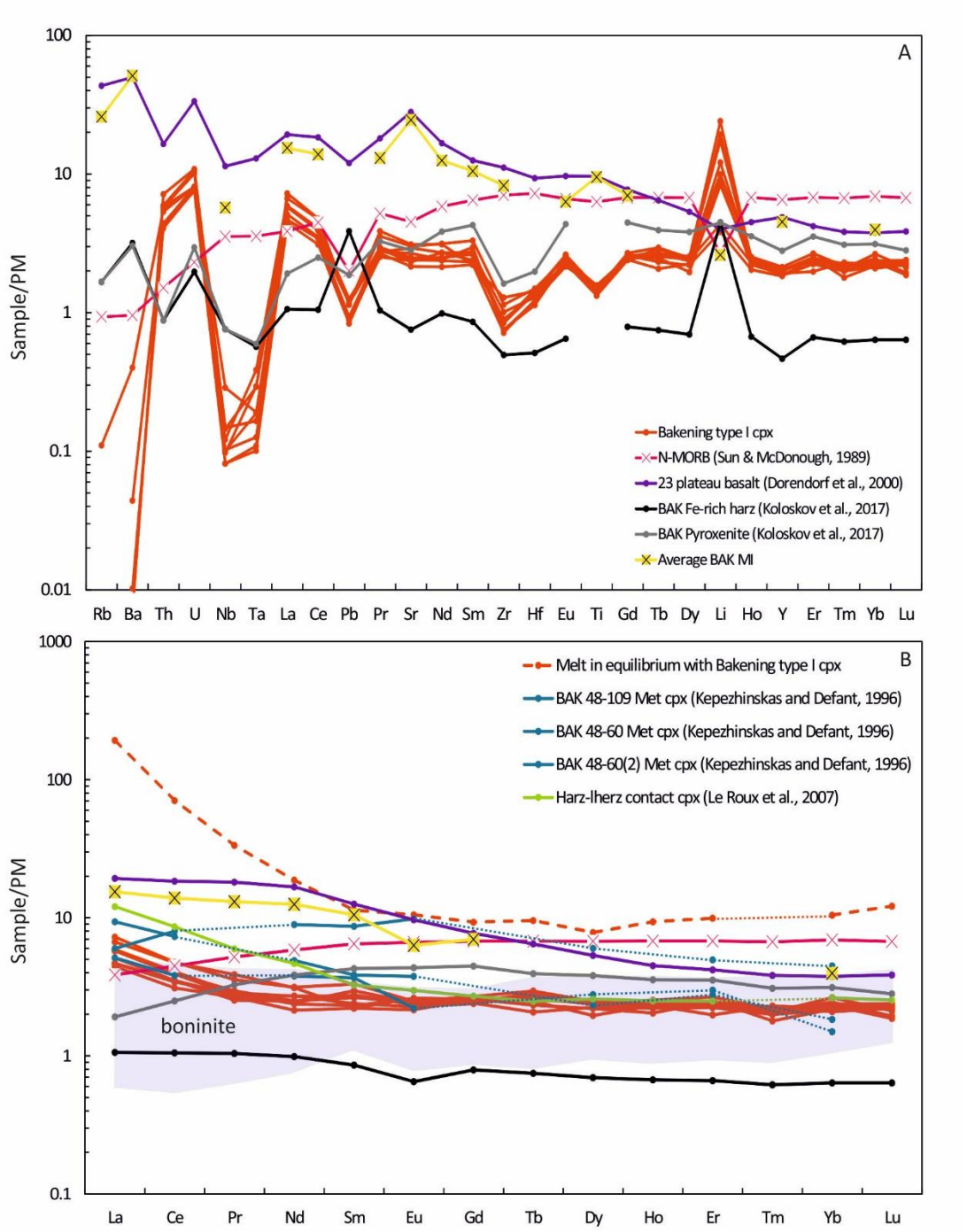

Figure 29. *A) Trace element distribution and B) rare earth element (REE) distribution in Bakening type I clinopyroxene and its respective equilibrium melt calculated from clinopyroxene-melt partition coefficients from Green et al. (2000). Data is normalized to primitive mantle (PM; McDonough and Sun, 1995). N-MORB (Sun and McDonough,1989), bulk-rock host basalt (Dorendorf et al., 2000) and Bakening mantle xenoliths (Koloskov et al., 2017), similar metasomatic Bakening clinopyroxene and Lherz clinopyroxene (Kepezhinskas and Defant, 1996; LeRoux et al., 2007) and high-Mg# olivine-hosted Bakening melt inclusions (Iveson et al., in prep) are shown for comparison. Purple field corresponds to REE composition of boninite (Hickey and Frey, 1982; Pearce et al., 1992;*

Kelemen et al., 2003). Incompatible trace elements that were not reported in the above studies are inferred by dotted lines.

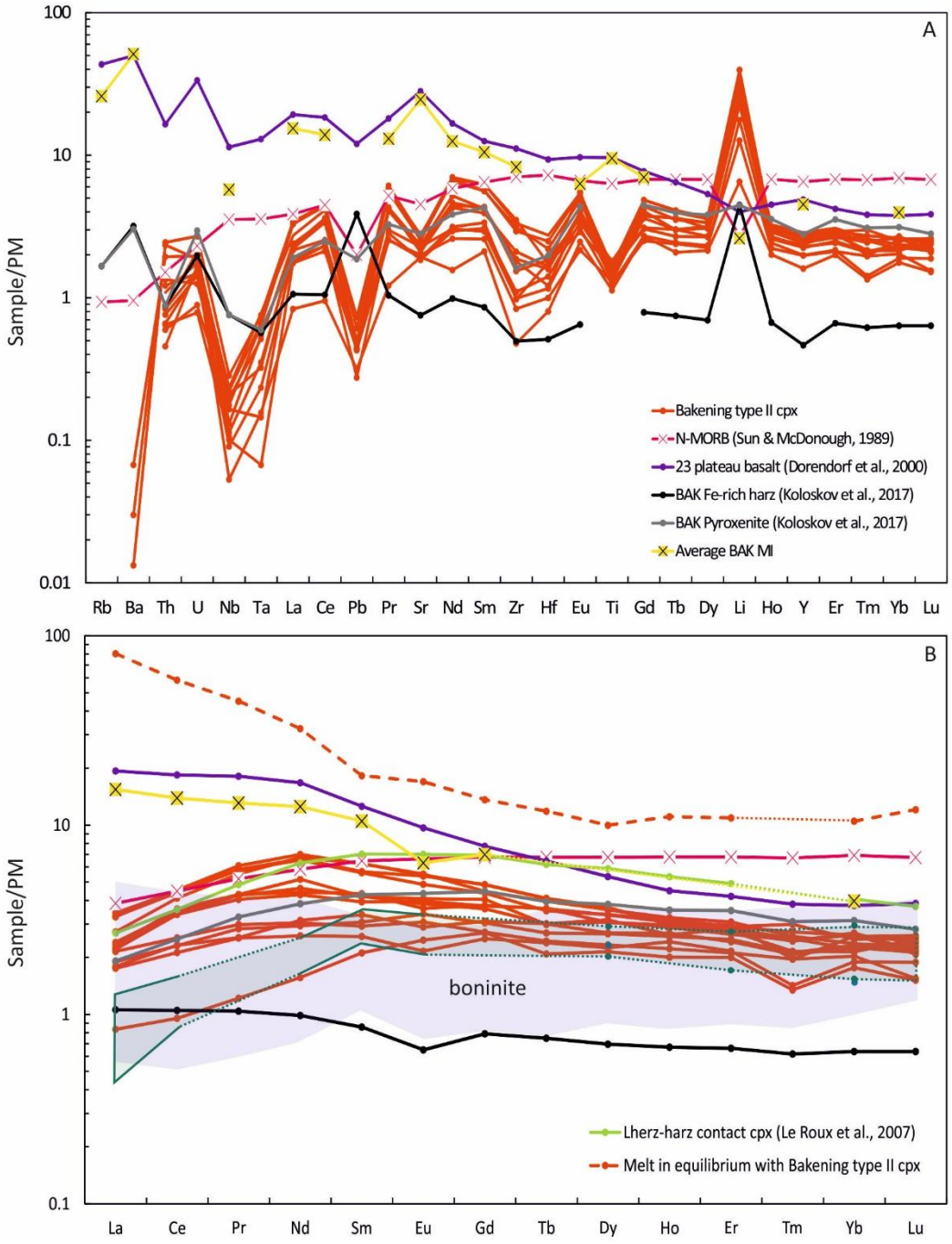

***Figure 30**. A) Trace element distribution and B) rare earth element (REE) distribution in Bakening type II clinopyroxene and its respective equilibrium melt calculated from clinopyroxene-melt partition coefficients from Green et al. (2000). Data is normalized to primitive mantle (PM; McDonough and Sun, 1995). N-MORB (Sun and McDonough,1989), bulk-rock host basalt (Dorendorf et al., 2000) and Bakening mantle xenoliths (Koloskov et al., 2017) and similar primary Bakening clinopyroxene (dark green field) and Lherz clinopyroxene (Kepezhinskas and Defant, 1996; LeRoux et al., 2007) and high-Mg# olivine-*

hosted Bakening melt inclusions (Iveson et al., in prep) are shown for comparison. Purple field corresponds to REE composition of boninite (Hickey and Frey, 1982; Pearce et al., 1992; Kelemen et al., 2003). Incompatible trace elements that were not reported in the above studies are inferred by dotted lines.

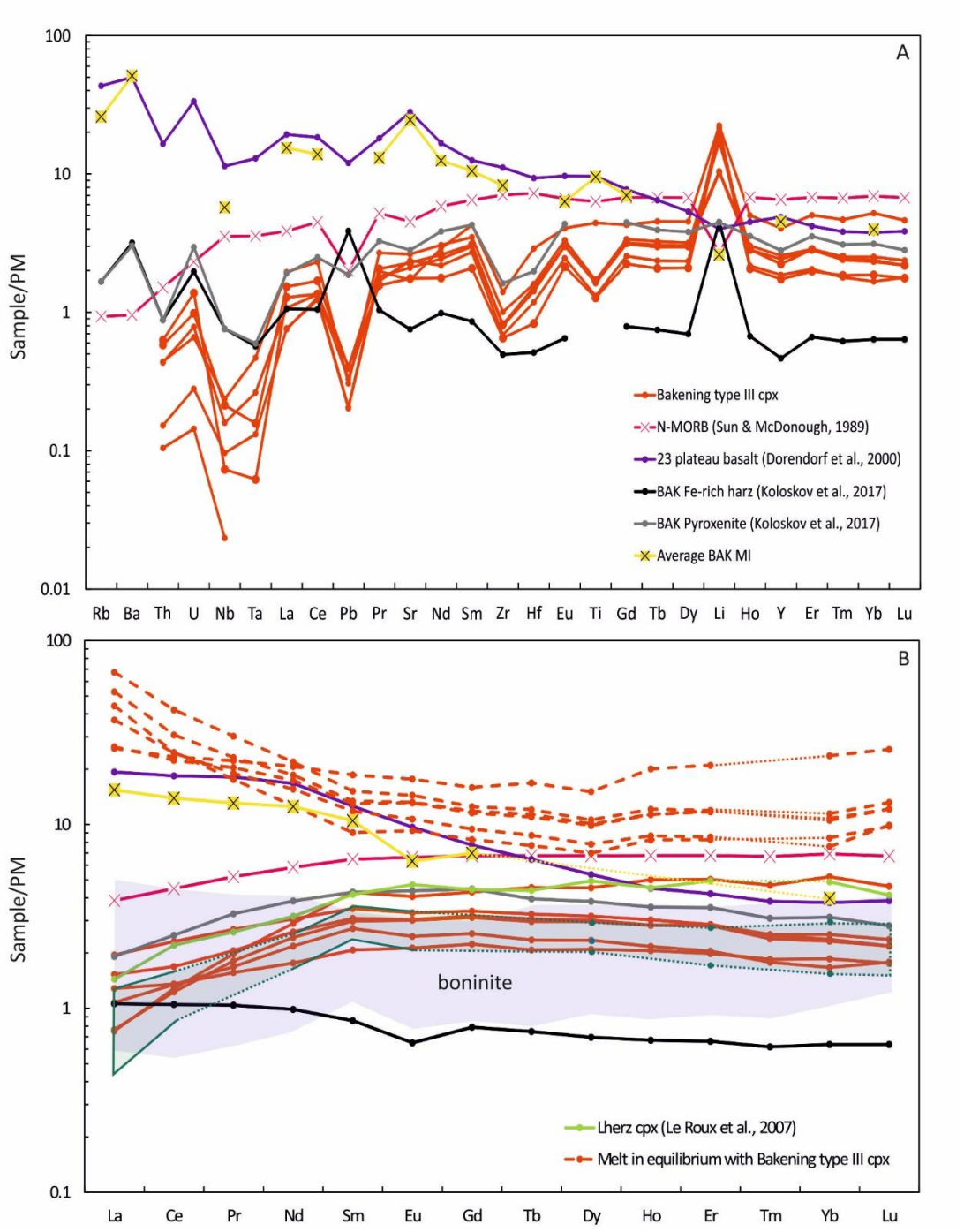

Figure 31. *A) Trace element distribution and B) rare earth element (REE) distribution in Bakening type III clinopyroxene and their respective equilibrium melts calculated from clinopyroxene-melt partition coefficients from Green et al. (2000). Data is normalized to primitive mantle (PM; McDonough and Sun, 1995). N-MORB (Sun and McDonough,1989),*

bulk-rock host basalt (Dorendorf et al., 2000) and Bakening mantle xenoliths (Koloskov et al., 2017) and similar primary Bakening clinopyroxene (dark green field) and Lherz clinopyroxene (Kepezhinskas and Defant, 1996; LeRoux et al., 2007) and high-Mg# olivine-hosted Bakening melt inclusions (Iveson et al., in prep) are shown for comparison. Purple field corresponds to REE composition of boninite (Hickey and Frey, 1982; Pearce et al., 1992; Kelemen et al., 2003). Incompatible trace elements that were not reported in the above studies are inferred by dotted lines.

3.4.2 Amphibole

Primitive mantle-normalized (McDonough and Sun, 1995) incompatible trace element distribution trends of Avachinsky vein amphiboles vary from enriched in *AVX-16-03-10* and *AVX-16-03-20* (Figure 32A and Figure 33A) to depleted in *AVX-16-03-24* (Figure 34A).

In *AVX-16-03-10*, vein amphibole is enriched in all incompatible trace elements relative to primitive mantle except for Rb, Th, Nb, Ta, Li and U (Figure 32A). Light REE increase in abundance from La (average La = 2.07 µg g^{-1}) to Sm (average Sm = 7.03 µg g^{-1}) whereas heavy REE are flat (e.g. average Yb = 4.93 µg g^{-1}) with a small negative Eu anomaly (Figure 32B). Exceptionally, vein amphibole *am 10* displays convex-up LREE trend while HREE display concave-up trend (dot-dashed line in Figure 32B). Distribution trend of REE in vein amphibole *am 10* is similar to those reported in Ishimaru et al. (2007), Ishimaru and Arai (2008) and Bénard and Ionov (2013). The other vein amphiboles possess REE distribution trends similar to calcic amphibole reported in Ishimaru et al. (2007).

Vein amphibole in *AVX-16-03-20* is enriched in most incompatible trace elements relative to primitive mantle except for Rb, Th, U, Ta and Li (Figure 33A). Light REE increase in abundance from La (average La = 0.97 µg g^{-1}) to Sm (average Sm = 5.94 µg g^{-1}) whereas HREE gradually decrease from Gd (average Gd = 7.95 µg g^{-1}) to Lu (average Lu = 0.67 µg g^{-1}) with a pronounced negative Eu anomaly

(Figure 33B). The distribution trend of all incompatible trace elements is identical to selvage-related type 2 amphibole described by Bénard and Ionov (2013).

In *AVX-16-03-24*, vein amphibole is depleted in all incompatible trace elements relative to primitive mantle except for Rb, Ba, Pb and Sr (Figure 34A). Primitive mantle-normalized REE trends display concave-up light REE, pronounced positive Eu anomalies and increase in HREE abundance from Gd (average Gd = 0.51 µg g^{-1}) to Lu (average Lu = 0.67 µg g^{-1}; Figure 34B). The distribution trend of HREE in *AVX-16-03-24* amphibole is similar to Avachinsky amphibole reported by Ishimaru and Arai (2008) and Halama et al. (2009). Two amphibole grains in *AVX-16-03-24* possess different primitive mantle-normalized incompatible trace element trends, whose REE abundances gradually increase from La to Lu with both, negative and positive Eu anomalies (Figure 34B).

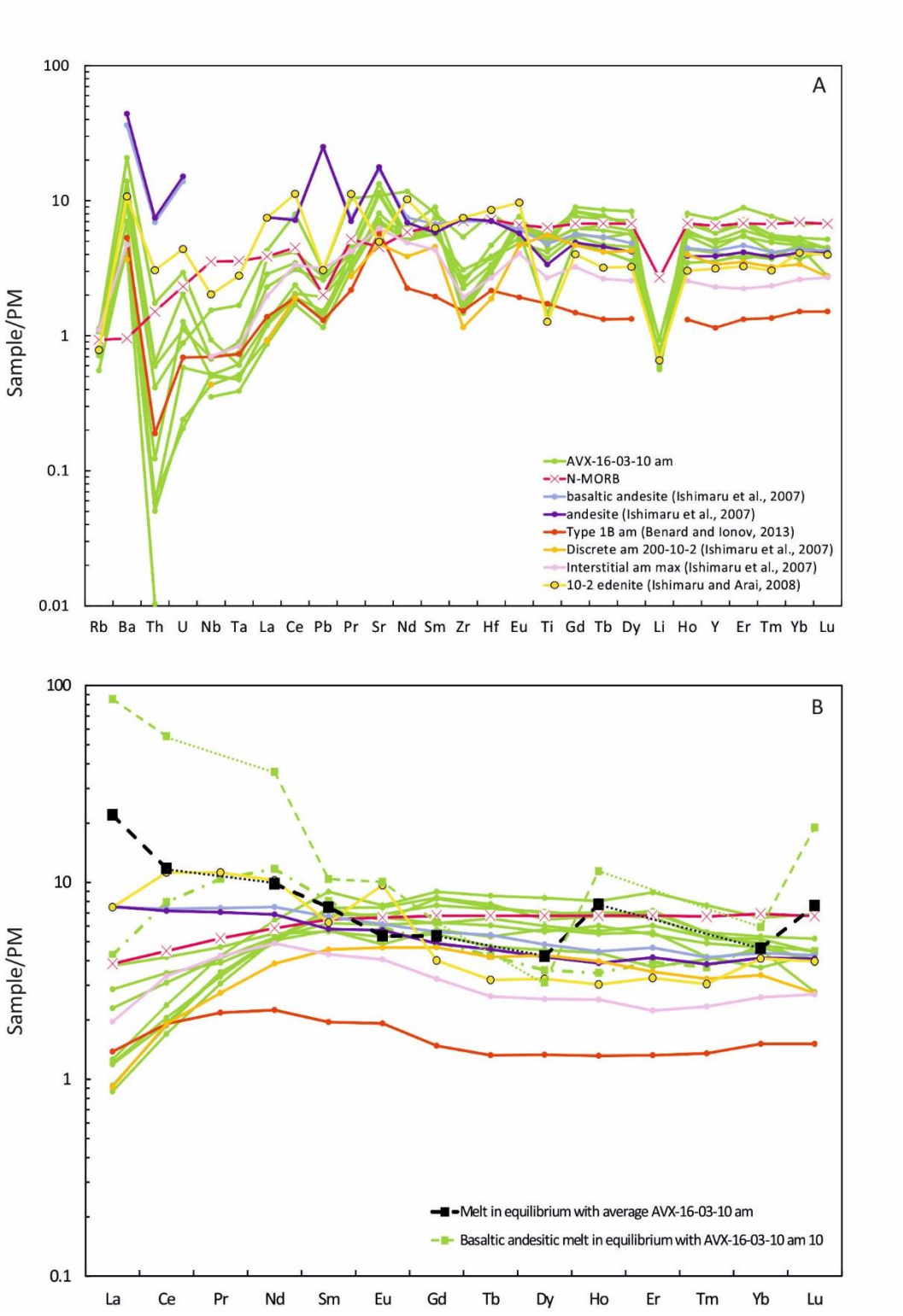

***Figure 32**. A) Trace element distribution and B) rare earth element (REE) distribution in AVX-16-03-10 vein amphibole including am 10 (dot-dashed line) and andesitic and basaltic andesitic equilibrium melts calculated after Humphreys et al. (2019). Data is normalized to primitive mantle (PM; McDonough and Sun, 1995). N-MORB (Sun and McDonough,1989), typical Avachinsky andesite and basaltic andesite (Ishimaru et al., 2007) and similar Avachinsky amphibole (Ishimaru et al., 2007; Ishimaru and Arai, 2008; Bénard and Ionov,*

2013) are shown for comparison. Incompatible trace elements that were not reported in the above studies are inferred by dotted lines.

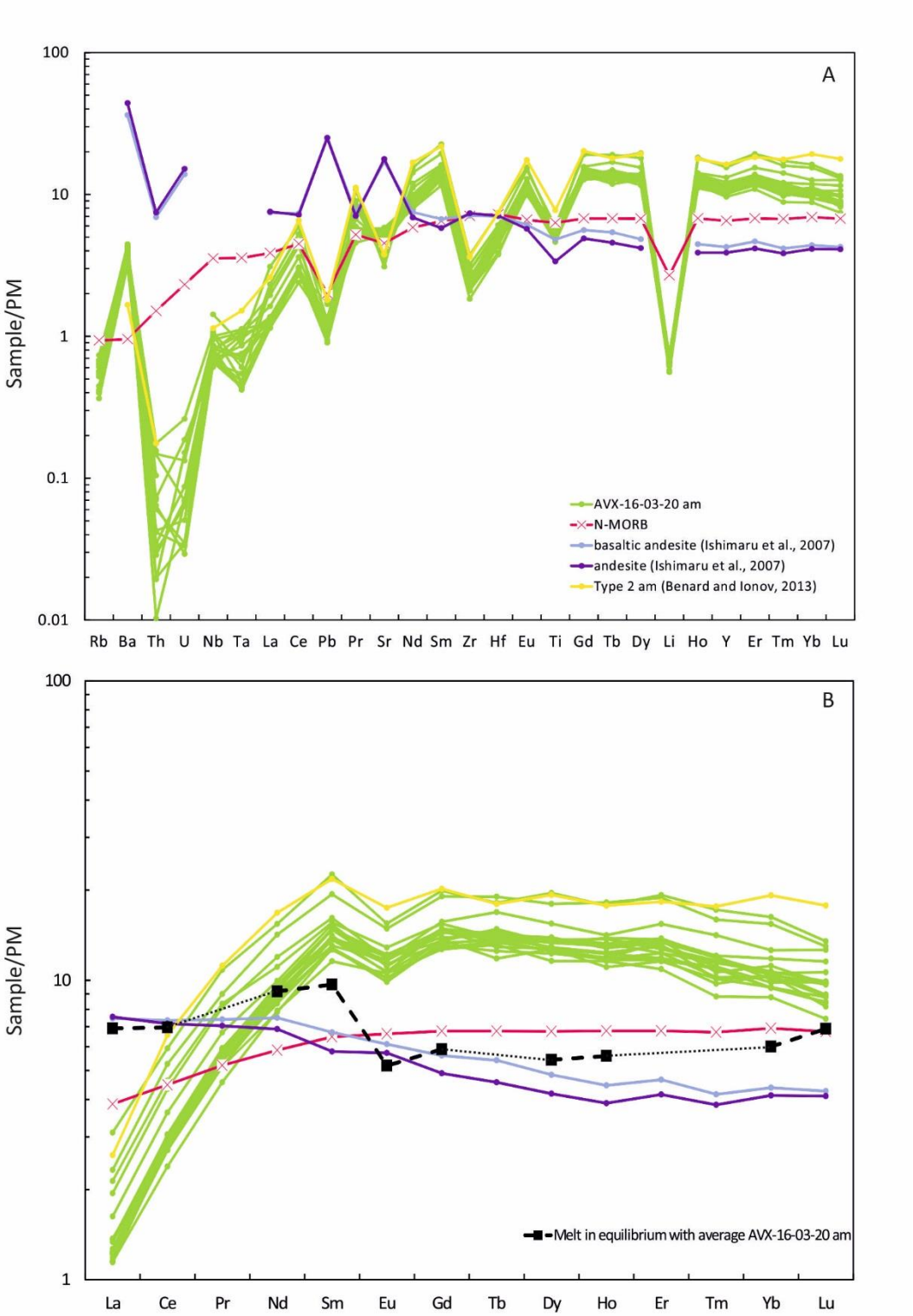

Figure 33*. A) Trace element distribution and B) rare earth element (REE) distribution in AVX-16-03-20 vein amphibole and equilibrium melt calculated after Humphreys et al. (2019). Data is normalized to primitive mantle (PM; McDonough and Sun, 1995). N-MORB (Sun and McDonough,1989), typical Avachinsky andesite and basaltic andesite (Ishimaru et*

al., 2007) and identical Avachinsky amphibole (Bénard and Ionov, 2013) are shown for comparison. Incompatible trace elements that were not reported in the above studies are inferred by dotted lines.

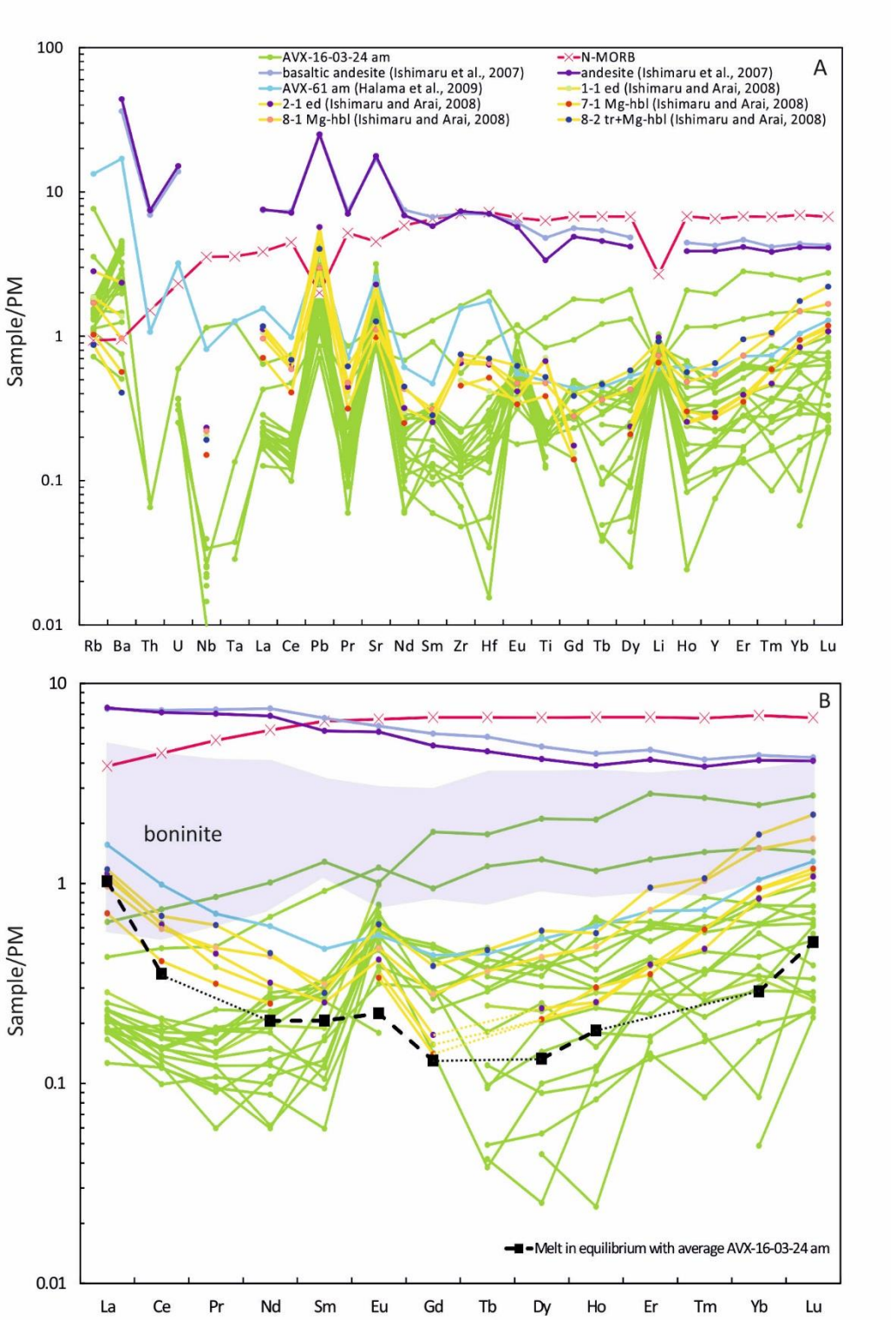

***Figure 34**. A) Trace element distribution and B) rare earth element (REE) distribution in AVX-16-03-24 vein amphibole and equilibrium melt calculated after Humphreys et al. (2019). Data is normalized to primitive mantle (PM; McDonough and Sun, 1995). N-MORB*

(Sun and McDonough,1989), typical Avachinsky andesite and basaltic andesite (Ishimaru et al., 2007) and similar Avachinsky amphibole (Ishimaru and Arai, 2008; Halama et al., 2009) are shown for comparison. Purple field corresponds to REE composition of boninite (Hickey and Frey, 1982; Pearce et al., 1992; Kelemen et al., 2003). Incompatible trace elements that were not reported in the above studies are inferred by dotted lines.

Table 6. *Average vein mineral trace element data in Avachinsky mantle xenoliths*

Sample	AVX-16-03-24		AVX-16-03-20		AVX-16-03-10
Mineral	cpx	am	cpx	am	am
	n = 9	n = 19	n = 1	n = 19	n = 11
Rb (μg g^{-1})	bdl	1.12	bdl	0.34	0.51
Ba	0.46	18.55	bdl	25.06	59.44
Th	bdl	bdl	bdl	0.01	0.03
U	bdl	bdl	bdl	bdl	0.02
Nb	bdl	bdl	bdl	0.55	0.45
Ta	bdl	bdl	bdl	0.03	0.03
La	0.07	0.16	0.33	0.97	1.34
Ce	0.21	0.34	2.19	5.58	5.32
Pb	0.09	0.28	0.03	0.18	0.30
Pr	0.04	0.05	0.65	1.60	1.15
Sr	17.35	34.96	22.59	95.19	181.79
Nd	0.24	0.30	5.10	12.26	7.55
Sm	0.12	0.12	2.32	5.94	2.85
Zr	1.45	2.50	9.45	25.66	25.98
Hf	0.06	0.09	0.52	1.41	1.14
Eu	0.04	0.10	0.74	1.78	0.98
Ti	152.53	346.78	1511.88	6484.04	5322.61
Gd	0.22	bdl	2.81	7.95	3.74
Tb	0.04	bdl	0.54	1.42	0.64
Dy	0.26	0.28	3.57	9.25	4.07
Li	1.33	1.14	1.18	1.04	1.09
Ho	0.06	0.06	0.78	1.97	0.89
Y	1.56	1.77	17.69	49.65	22.34
Er	0.20	0.24	1.98	5.89	2.65
Tm	0.03	bdl	0.30	0.80	0.35
Yb	0.22	0.26	2.04	4.83	2.18
Lu	0.04	0.05	0.27	0.67	0.30

Abbreviations: cpx = clinopyroxene, am = amphibole, bdl = below detection limit.

Table 7. *Average clinopyroxene trace element data in Bakening mantle xenoliths*

Sample Mineral	BAK-16-22-01A cpx n = 6	BAK-16-22-01B cpx n = 8	BAK-16-22-03 cpx n = 13	BAK-16-22-04 cpx n = 9	BAK-16-22-05 cpx n = 14	BAK-16-22-09 cpx n = 20	BAK-16-22-32 cpx n = 10	BAK-16-22-42 cpx n = 17
Rb (µg g^{-1})	bdl	bdl	bdl	bdl	bdl	bdl	bdl	bdl
Ba	bdl	bdl	bdl	bdl	bdl	bdl	bdl	bdl
Th	0.05	0.06	0.09	0.43	0.03	0.03	0.01	0.01
U	0.02	0.03	0.03	0.18	0.01	0.02	bdl	0.01
Nb	0.14	0.05	0.11	0.09	0.16	0.10	0.02	0.06
Ta	0.01	bdl	0.02	0.01	0.02	0.01	bdl	0.01
La	0.99	0.95	1.51	3.62	1.26	0.70	0.49	0.50
Ce	2.83	2.27	5.37	6.50	3.87	2.26	2.15	2.06
Pb	0.06	0.07	0.07	0.16	0.05	0.05	0.03	0.03
Pr	0.52	0.45	1.02	0.76	0.68	0.43	0.56	0.46
Sr	45.38	34.95	44.99	51.79	52.31	47.01	34.03	41.70
Nd	3.25	2.21	5.65	3.28	3.83	2.72	4.02	3.04
Sm	1.25	0.96	1.70	1.06	1.42	1.10	1.93	1.21
Zr	8.57	6.83	19.84	9.63	10.56	7.19	14.74	8.35
Hf	0.43	0.24	0.47	0.38	0.45	0.34	0.82	0.40
Eu	0.47	0.37	0.60	0.37	0.51	0.38	0.69	0.46
Ti	2039.88	1534.65	1748.85	1771.05	2045.41	1580.20	5336.92	1956.11
Gd	1.73	1.39	2.00	1.36	1.84	1.39	2.59	1.70
Tb	0.30	0.21	0.32	0.26	0.32	0.23	0.45	0.29
Dy	2.03	1.41	2.02	1.58	2.14	1.58	3.05	2.00
Li	27.30	30.31	39.80	19.23	16.73	34.11	35.77	16.35
Ho	0.42	0.31	0.41	0.35	0.45	0.32	0.75	0.42
Y	9.58	7.45	10.19	8.46	11.03	8.01	17.41	10.42
Er	1.25	0.87	1.15	1.04	1.25	0.90	2.21	1.23
Tm	0.17	0.13	0.15	0.14	0.17	0.12	0.32	0.16
Yb	1.05	0.82	1.02	1.01	1.11	0.74	2.29	1.02
Lu	0.15	0.12	0.15	0.15	0.16	0.12	0.31	0.15

Abbreviations: cpx = clinopyroxene, bdl = below detection limit.

3.5 Discussion

3.5.1 Textural history of Avachinsky and Bakening xenoliths

3.5.1.1 Avachinsky xenoliths

Harzburgite is a residual mantle lithology to an extensive melt extraction from the subarc mantle whereby clinopyroxene is consumed by mantle melting (e.g. Frey et al., 1985). Consistent with this process, Avachinsky harzburgites do not contain any primary clinopyroxene (Figure 14 and Table 2) indicating high degree of mantle melting (clinopyroxene-out by 29 % wet melting of the subarc mantle; Bizimis et al., 2000). Subsequent to extensive melt extraction, Avachinsky harzburgites were modally metasomatized by melts of various compositions. Firstly, the inclusion of relict phlogopite intergrown with olivine in *AVX-16-03-24* indicates that Avachinsky harzburgites were metasomatized by a K-rich melt (Figure 16E):

$$Mg_2SiO_4 + 3MgSiO_3 + melt\ (\tfrac{1}{2}\ K_2O,\ \tfrac{1}{2}\ Al_2O_3\ and\ H_2O) \rightarrow Mg_2SiO_4 + KMg_3AlSi_3O_{10}(OH)_2 \qquad \textbf{Equation 19}$$

Secondly, Avachinsky harzburgites are cross-cut by dunite and orthopyroxenite veins (Figure 16C and F):

$$Mg_2SiO_4 + MgSiO_3 + melt\ (SiO_2\text{-}undersaturated) \rightarrow Mg_2SiO_4 + melt\ (SiO_2\text{-}saturated) \qquad \textbf{Equation 20}$$

$$Mg_2SiO_4 + MgSiO_3 + melt\ (SiO_2\text{-}saturated) \rightarrow 3MgSiO_3 \qquad \textbf{Equation 21}$$

Major element composition of vein orthopyroxene and its high Mg# identical to primary orthopyroxene (Figure 22) indicate that the anhydrous orthopyroxenite veins must have equilibrated in the lithospheric subarc mantle. Thirdly, the anhydrous orthopyroxenite veins were overgrown by clinopyroxene in *AVX-16-03-02, AVX-16-03-07, AVX-16-03-23* and in *AVX-16-03-24* also by amphibole (Figure 16D and F):

$$MgSiO_3 + melt\ (CaO\ and\ SiO_2) \rightarrow MgCaSi_2O_6 \qquad \textbf{Equation 22}$$

$$9MgSiO_3 + melt\ (5CaO, Na_2O, 3Al_2O_3, SiO_2\ and\ H_2O) \rightarrow MgCaSi_2O_6 + 2NaCa_2(Mg_4Al)(Si_6Al_2)O_{22}(OH)_2 \qquad \textbf{Equation 23}$$

Finally, amphibole-rich hydrous veins genetically related to the selvage cross-cut *AVX-16-03-20* and anhydrous vein in *AVX-16-03-10* (Figure 17B):

$$MgCaSi_2O_6 + NaCa_2(Mg_4Al)(Si_6Al_2)O_{22}(OH)_2 + melt \rightarrow Ca_2(Mg_4Al)(Si_7Al)O_{22}(OH)_2 + plagioclase\ of\ unknown\ composition \qquad \textbf{Equation 24}$$

3.5.1.2 Bakening xenoliths

Bakening peridotites contain abundant clinopyroxene and lack orthopyroxene (Figure 14 and Table 2). It has been demonstrated that clinopyroxene-bearing dunite and often lherzolite, is the product of re-fertilization of refractory mantle peridotite (Rudnick et al., 1993; LeRoux et al., 2007). Similarly, clinopyroxene-bearing dunite *BAK-16-22-04* and wehrlites *BAK-16-22-01B* and *BAK-16-22-03* can represent parts of re-fertilized mantle peridotite.

Bakening peridotites and pyroxenites underwent a series of melt-rock reactions. Firstly, percolation of basaltic melt transformed some Bakening peridotites into dunite by removal of clinopyroxene and orthopyroxene and re-crystallization of olivine (Kelemen, 1990) such as in *BAK-16-22-04* (Equation 20). Secondly, Bakening peridotites and pyroxenites were re-fertilized by another batch of melt that reacted with orthopyroxene to produce clinopyroxene (Equation 22; Figure 18C and D). This melt-rock reaction must have re-fertilized large portions of the lithospheric rear-arc mantle as clinopyroxene enclosing and replacing orthopyroxene and, sometimes olivine, is observed in all Bakening xenoliths. Some clinopyroxene grains exsolved thin lamellae of orthopyroxene and spinel (Figure 18E). Clinopyroxene grains containing exsolution lamellae are identical in major element composition to clinopyroxene free of exsolution lamellae. Equilibration temperature estimate of clinopyroxene-exsolved orthopyroxene ranges from 850 to 920 °C ± 50 °C and falls within equilibration temperature range of Bakening xenoliths (Figure 26 and Table 4). Therefore, it is inferred that the thin orthopyroxene lamellae in clinopyroxene represent relict orthopyroxene overgrown by clinopyroxene formed during re-fertilization of the rear-arc mantle rather than exsolutions produced during cooling. The origin of spinel exsolution lamellae in clinopyroxene remains unresolved despite their reported occurrence in ultramafic and mafic rocks in the Syum-Keu ophiolite massif in the Arctic Urals and Haladala pluton, China, respectively (Savelieva et al., 2016; Zhu et al., 2018). Finally, Bakening xenoliths were intruded by the host basalt along mineral grain boundaries which caused dissolution of clinopyroxene (Figure 18B) and zoning in olivine (Figure 18A) adjacent to the host rock. Rapid transport of Bakening xenoliths to the surface

(estimated 1 to 10 days; Gordeychik et al., 2018) quenched the intruding host basaltic melt and formed symplectite composed of olivine and glass around spinel and clinopyroxene grains (Figure 18F).

3.5.2 Depletion of Avachinsky and Bakening mantle xenoliths

Harzburgite is the most abundant mantle lithology recovered at Avachinsky (Figure 14 and Table 2). The lack of primary clinopyroxene in Avachinsky harzburgites indicates high degree of melt extraction at the volcanic front. The estimated degree of mantle melting at Avachinsky ranges from 17 to 21 % based on high Cr# of spinel (Hellebrand et al., 2001). A consistently high degree of mantle melting exceeding 20 % was estimated via modal mineralogy (Baker and Stolper, 1994) and low trace element abundances in clinopyroxene (Figure 35; Bizimis et al., 2000). However, the degree of mantle melting might be even higher than the above estimates because of the complete consumption of clinopyroxene in Avachinsky harzburgites. Wet melting in excess of 29 % would completely consume clinopyroxene in the subarc mantle (Bizimis et al., 2000).

The high degree of melt extraction in Avachinsky xenoliths coupled with high Cr# of spinel and forsterite component in olivine are characteristic of other subarc peridotites such as those from the Izu-Bonin-Mariana arc (Figure 20B). Vein formation post-dates the extensive mantle melting precluding their origin as fragments of the sub-continental lithospheric mantle (SCLM). The metasomatized mantle xenoliths do not represent inclusions of older mantle veins as palaeogeographic reconstructions of the NW Pacific show a single continuous subduction zone in the region since at least 50 Ma (Hall, 2002). Combined with the lack of evidence for > 50Ma old subducted slabs under Kamchatka (Levin et al.,

2002), all indicates that the current metasomatized mantle xenoliths are representative of subarc metasomatism in the past 50 Ma.

Bakening xenoliths constitute of a range of wehrlites, (olivine) websterites, dunite and clinopyroxenite (Figure 14 and Table 2). Bakening peridotites and pyroxenites are more fertile than Avachinsky peridotites (i.e. higher modal proportion of clinopyroxene). The estimated degree of mantle melting at Bakening ranges from 8 to 11 % based on low Cr# of spinel (Hellebrand et al., 2001). The result is consistent with low degree dry melting of MORB-source mantle (Figure 35; Bizimis et al., 2000). The lower degree of mantle melting at Bakening reflects its greater depth-to-slab (Figure 2; Gorbatov et al., 1997) and lower influx of altered oceanic crust (AOC)-derived fluids than at Avachinsky. Alternatively, the low Cr# spinel and olivine forsterite component in Bakening mantle xenoliths can indicate their origin as fragments of the SCLM (Figure 20B). Bakening xenoliths have been recovered from Novy Bakening plateau basalts whose mantle source is variably depleted and, indeed, similar in composition to that of OIB (Dorendorf et al., 2000).

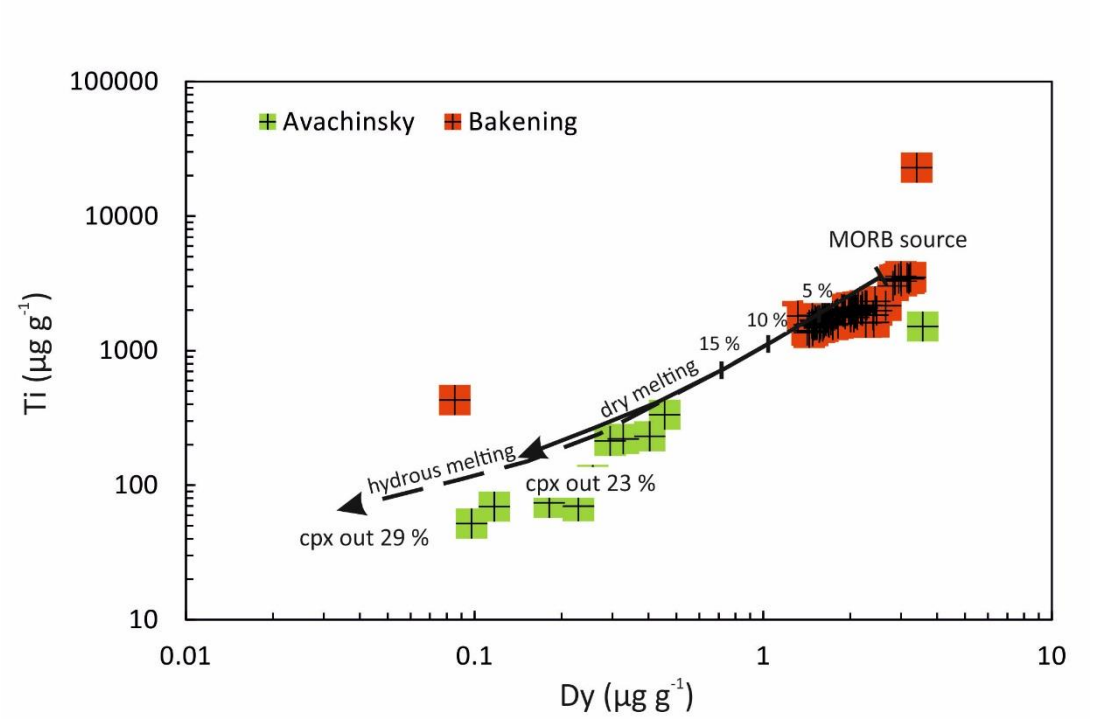

***Figure 35**. Ti versus Dy in Avachinsky and Bakening clinopyroxene. Low degree (< 10 %) of dry partial melting of MORB-source mantle is required to reproduce trace element-rich clinopyroxene compositions in Bakening xenoliths whereas hydrous melting of a depleted MORB-source mantle is required to account for the trace element-poor clinopyroxene compositions in Avachinsky xenoliths. Dry and hydrous melting curves of a MORB-source mantle were calculated by Bizimis et al. (2000) via incremental, non-modal batch melting equations. The starting MORB-source mantle has undergone 9 % dry partial melting in the hydrous melting model. Figure was modified after Bizimis et al. (2000).*

3.5.3 Composition estimate of Avachinsky and Bakening subarc mantle

Until a decade ago, primary mantle melts were considered to have equilibrated with olivine in peridotite rather than pyroxene in pyroxenite (Sobolev et al., 2005 and references therein). Peridotite-derived partial melts have distinctively higher MgO, CaO and MnO contents and lower SiO_2 and NiO contents than partial melts of pyroxenite (Sobolev et al., 2007). The contents of NiO in mantle olivine is an especially useful discriminator between peridotite-derived and pyroxenite-derived melts because Ni is highly compatible in olivine (e.g. Beattie et al., 1991). Nickel content of a peridotite mantle-derived partial melt is controlled by olivine which

tends to incorporate NiO and produce NiO-poor equilibrium melts whereas NiO content of pyroxenite mantle-derived partial melt is controlled by pyroxene which does not incorporate NiO and produces NiO-rich equilibrium melts (Sobolev et al., 2005; Sobolev et al., 2007). Thus, olivine in equilibrium with pyroxenite-derived melt would have higher NiO content than that of peridotite-derived melt.

Avachinsky olivine has intermediate NiO content and high Fo component whereas Bakening olivine has lower NiO content and Fo component (Figure 36). Avachinsky olivine lies mostly within peridotite partial melt field which indicates that it equilibrated with peridotite-derived melts (Straub et al., 2008) whereas Bakening olivine lies along olivine fractionation trend from pyroxenite partial melt. Avachinsky and Bakening olivine low in Fo re-equilibrated with melts percolating through hydrous veins and with the host basaltic melt, respectively. Interaction between olivine and peridotite-derived partial melt sustains high Fo component and constant NiO content of olivine in Avachinsky xenoliths. In Bakening xenoliths, progressive olivine fractionation from pyroxenite partial melt lowers both NiO content and Fo component in olivine. Furthermore, melt derived from partial melting of pyroxenite would form clinopyroxene enriched in Ti and HREE (e.g. Green et al., 2000; Ionov et al., 2002) in contrast to low degree dry MORB-source melting model at Bakening (Figure 35; Bizimis et al., 2000).

The wide range of NiO content at constant Fo in *BAK-16-22-03* and *BAK-16-22-01B* cannot be produced by olivine fractionation from pyroxenite partial melt alone. Instead, it can be attributed to mixing of melts with different NiO content (i.e. mixing of fractionated peridotite partial melt with fractionated pyroxenite partial melt; Figure 36) either in the lithospheric mantle or in magma chamber.

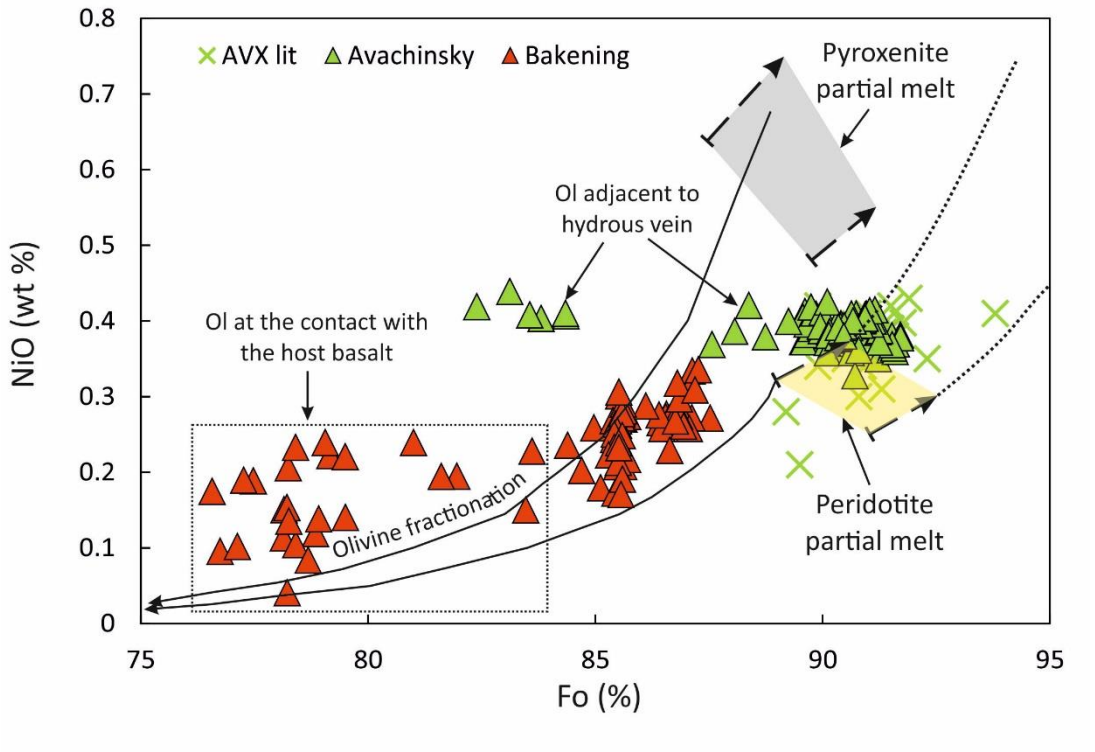

Figure 36. *NiO versus Fo in Avachinsky and Bakening olivine. Peridotite and pyroxenite partial melt compositions produced by serially melting peridotite and pyroxenite, respectively (Straub et al., 2008) are outlined by dashed lines. Dotted line extending from peridotite partial melt composition field represents hypothetical melt composition produced after clinopyroxene exhaustion. The starting bulk-rock composition of peridotite and pyroxenite undergoing melting was constrained by Straub et al. (2008) based on the composition of Mexican arc mantle xenoliths. Low Fo and NiO Bakening olivine located at the contact with the host basalt is outlined by dotted rectangle. Quench symplectite olivine in websterite BAK-16-22-32 falls within the low Fo and low NiO field, too. Figure is modified after Straub et al. (2008).*

3.5.4 Metasomatic processes in Avachinsky and Bakening subarc mantle

3.5.4.1 Melt composition estimate at Avachinsky

Major and trace element composition of melts in equilibrium with vein amphibole were calculated after Zhang et al. (2017) and Humphreys et al. (2019), respectively. A broad range of amphibole equilibrium melt compositions spanning from basalt to dacite was observed in xenolith *AVX-16-03-10* whereas in *AVX-16-03-24* amphibole equilibrium melt compositions span from andesite to rhyolite and

those in *AVX-16-03-20* are dacitic in composition (Figure 37). The 'early-stage' vein amphibole that equilibrated with basalt and basaltic andesite in *AVX-16-03-10* occurs in hydrous vein 2 whereas the 'late-stage' vein amphibole that equilibrated with andesite and dacite occurs in hydrous vein 1 and in anhydrous vein (Figure 17). The two amphibole populations either formed in equilibrium with two genetically unrelated melts where hydrous vein 2 amphibole formed in an earlier melt-rock reaction pre-dating the influx of the host andesite which formed amphibole in hydrous vein 1, or the composition of the intruding andesite shifted to basaltic andesite and basalt via melt-rock interaction with the former vein orthopyroxene and primary olivine outside vein. REE distribution trends of melts in equilibrium with hydrous vein 1 and 2 amphibole in *AVX-16-03-10* differ between basaltic andesite and andesite (Figure 32B). The more primitive basaltic andesite is enriched in LREE relative to the more evolved andesite indicating their different origins. Thus, trace element composition of melt in equilibrium with *AVX-16-03-10* vein amphibole provides evidence for percolation of two compositionally distinct and genetically unrelated melts.

Vein amphibole in *AVX-16-03-20* and *AVX-16-03-24* equilibrated with more evolved rhyolite and dacite, respectively (Figure 37). Vein amphibole that equilibrated with the most evolved melt in each sample is classified as Mg-hornblende whereas vein amphibole that equilibrated with andesite and dacite in *AVX-16-03-24* and *AVX-16-03-20*, respectively, is classified as Mg-hornblende, tschermakite, pargasite, edenite and Mg-hastingsite. This compositional variability indicates that two populations of vein amphibole exist in *AVX-16-03-24* and *AVX-16-03-20*. The early-stage amphibole population, i.e. Mg-hastingsite, pargasite and

edenite, formed in equilibrium with melt of more mafic composition and subsequently re-equilibrated with a later-stage dacite and rhyolite that formed the late-stage amphibole population consisting of Mg-hornblende and tschermakite. Trace element composition of the early-stage vein amphibole population must have been overprinted by later-stage evolved melts as the two amphibole populations in *AVX-16-03-20* and *AVX-16-03-24* possess identical REE distribution trends (Figure 33 and Figure 34).

Vein amphibole in *AVX-16-03-20* (Figure 33B) possesses the same trace element distribution trend and abundances as type 2 amphibole described in Bénard and Ionov (2013). Their study demonstrated that this amphibole type originates from the selvage and thus is related to late-stage magmatic processes occurring during xenolith transport through the plumbing system. Vein amphibole in *AVX-16-03-24* (Figure 34B) compares to Avachinsky amphibole described in Ishimaru and Arai (2008) and Halama et al. (2009). Consistent with Halama et al. (2009), REE distribution trend of melt in equilibrium with *AVX-16-03-24* vein amphibole is similar to boninites (Hickey and Frey, 1982; Pearce et al., 1992; Kelemen et al., 2003). Its REE abundances are lower than those of boninites (Hickey and Frey, 1982) and primitive mantle (McDonough and Sun, 1995) indicating the extremely depleted nature of Avachinsky subarc mantle.

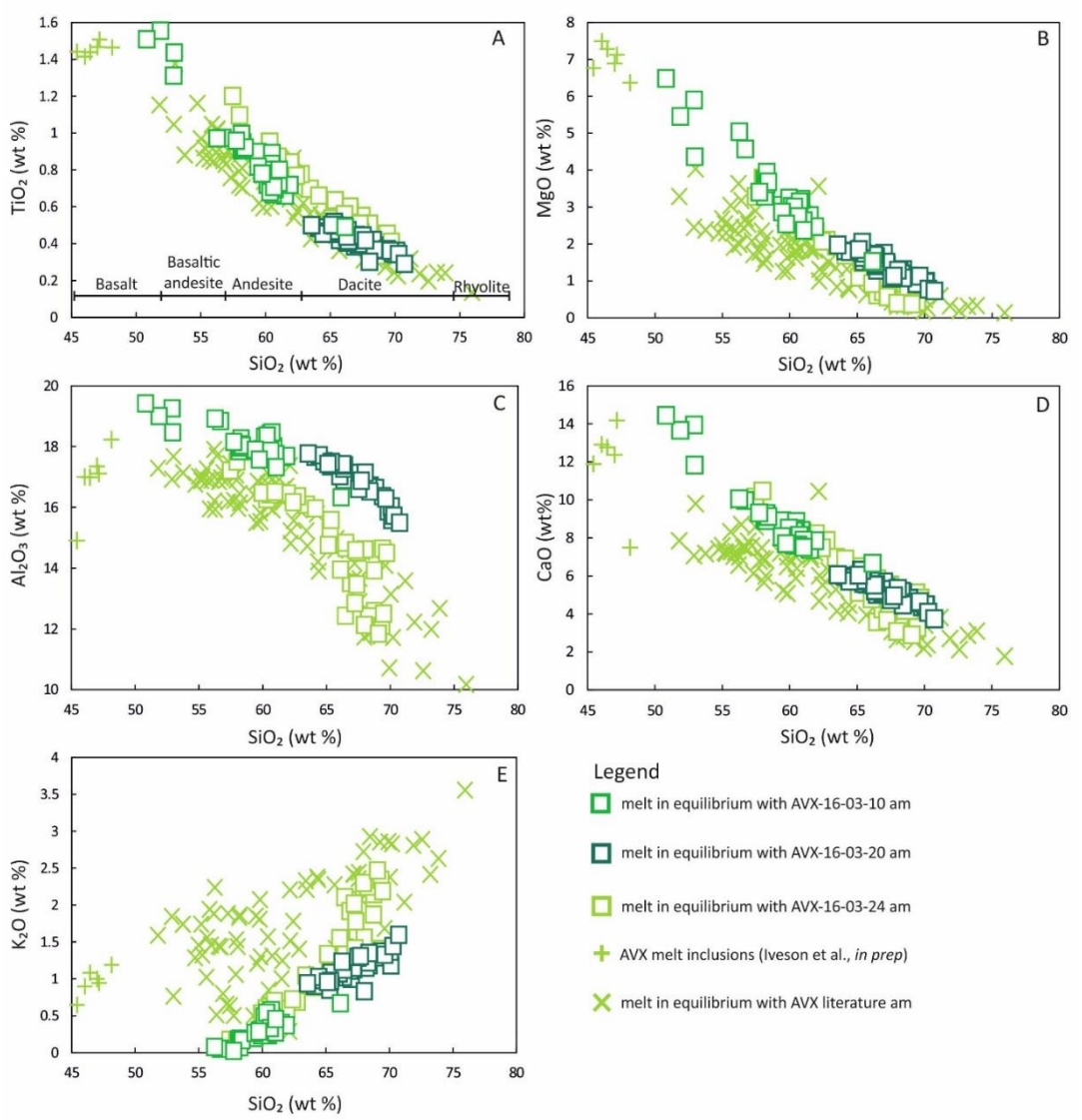

Figure 37. *A) to E) Major element composition and classification of melts in equilibrium with Avachinsky vein amphibole calculated after Zhang et al. (2017) . Melt classification scheme is adopted from Le Bas et al. (1986). Avachinsky melt inclusions are from Iveson et al. (in prep) and amphibole from other Avachinsky mantle xenolith studies (Arai et al., 2003; Ishimaru et al., 2007; Ishimaru and Arai, 2008; Ionov, 2010; Ishimaru and Arai, 2011; Bénard and Ionov, 2012; Bénard and Ionov, 2013; Bénard et al., 2017) is shown for comparison.*

Trace element composition of melts in equilibrium with vein clinopyroxene in harzburgite *AVX-16-03-24* and *AVX-16-03-20* were calculated via clinopyroxene-melt partition coefficients from Green et al. (2000). Compared to other studies of Avachinsky xenoliths, REE distribution trends and abundances of *type I*

clinopyroxene in *AVX-16-03-24* (Figure 27B) resemble those of vein reaction zone clinopyroxene reported in Bénard and Ionov (2013). The reaction zone clinopyroxene overgrowing orthopyroxene in type 1A vein originated from rapidly crystallized hot low-Ca boninitic melt that intruded the peridotite along fractures. This re-fertilization reaction is common in Avachinsky peridotites as anhydrous orthopyroxenite veins overgrown by clinopyroxene were also identified in *AVX-16-03-02, AVX-16-03-07, AVX-16-03-10* and *AVX-16-03-23* (Figure 16 and Figure 17).

REE distribution trend of *type II clinopyroxene* (Figure 27C) is similar to that reported in Halama et al. (2009). The trace element composition of melts in equilibrium with both types of vein clinopyroxene in *AVX-16-03-24* fall within the boninite field (Hickey and Frey, 1982), which is consistent with the composition of melt in equilibrium with vein amphibole (Figure 34B) and the study of Halama et al. (2009). *Type I clinopyroxene*, however, possesses lower MREE abundances relative to boninites (Figure 27B).

Heavy REE abundances of clinopyroxene in harzburgite *AVX-16-03-20* are identical to those of the host andesite (Figure 28B). Although composition of clinopyroxene equilibrium melt is enriched in REE, it displays similar REE distribution trend to that of the host andesite (Figure 28B). Consistent with the REE distribution trend of melt in equilibrium with vein amphibole (Figure 33B), vein clinopyroxene in *AVX-16-03-20* is also related to the selvage.

3.5.4.2 Melt composition estimate at Bakening

Trace element distribution trends of melts in equilibrium with Bakening clinopyroxene are similar to each other (Figure 38) despite the variability in clinopyroxene REE distribution trends (Figure 29, Figure 30 and Figure 31). Melts in equilibrium with Bakening clinopyroxene are enriched in LREE relative to HREE which are generally flat. They possess higher REE abundances than the host basalt (Figure 38).

The presence of carbonatite melt in Bakening xenoliths has been reported by Kepezhinskas and Defant (1996). They identified melt pockets containing apatite, amphibole, phlogopite and glass whose trace element composition resembled that of carbonatite, i.e. high Sr, Nb, Zr and REE contents with large HFSE/REE fractionations such as high La/Yb, Zr/Hf, Sr/Sm and Nb/La and low Ti/Eu and Y/Er (Kepezhinskas and Defant, 1996). Likewise, elevated LREE abundances in Bakening clinopyroxene can be attributed to carbonatite melt (Figure 38). Variable amounts of carbonatite (Moore et al., 2015) was mixed with the primitive mantle (McDonough and Sun, 1995) to estimate percentage of carbonatite component in the source of Bakening clinopyroxene equilibrium melts. The most LREE-rich melt *BAK-16-22-04* requires approximately 1 % carbonatite component in the source but the majority of Bakening melts require less than 0.7 % carbonatite component (Figure 38). Consistent with my result, Rudnick et al. (1993) estimated that mixing of 0.5 % carbonatite into spinel harzburgite accounts for the elevated REE composition of arc mantle xenoliths. At higher melt fractions (up to 5 %), percolating carbonatite melt would react with the mantle peridotite to form clinopyroxene and olivine at the expense of orthopyroxene (Rudnick et al., 1993).

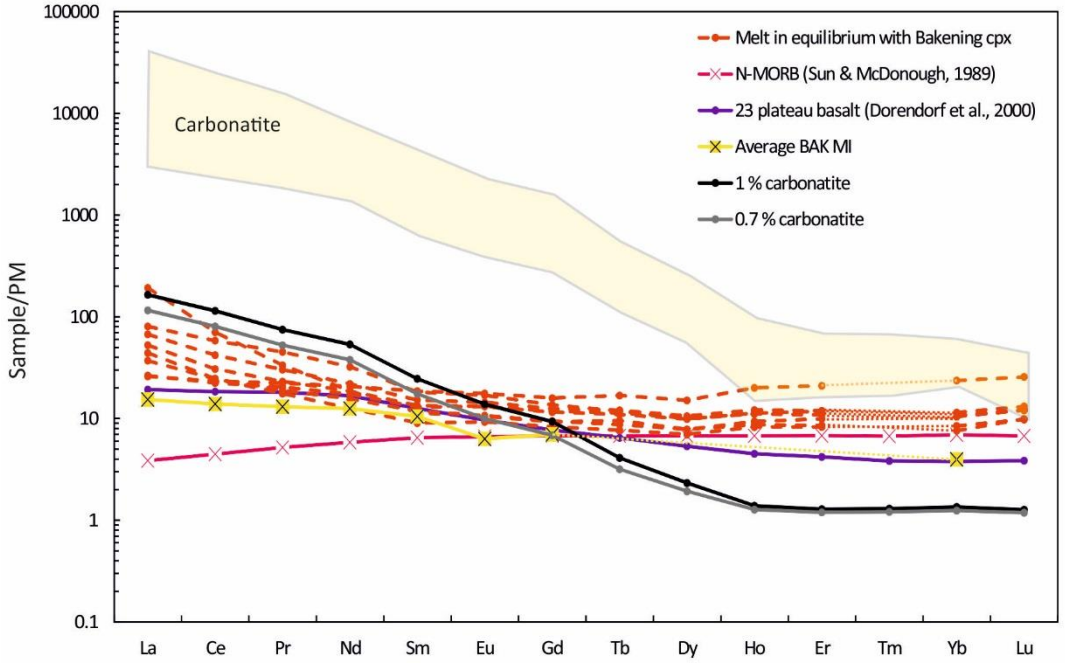

Figure 38*. REE distribution in melts in equilibrium with Bakening clinopyroxene compared to carbonatite (Moore et al., 2015). Only a small percentage of carbonatite (< 1 %) is required to raise LREE abundances of Bakening clinopyroxene equilibrium melts.*

Apart from elevated LREE, Ca/Al (90 to 220) and low Ti/Eu (0.15 to 0.8), melts in equilibrium with Bakening clinopyroxene do not possess any other fractionated HFSE/REE ratios characteristic of carbonatites (e.g. typical carbonatite Ti/Eu = 0.3 to 180, Zr/Hf = 30 to 120, La/Yb = 70 to 3000, Nb/Ta = 70 to 400; Rudnick et al., 1993; Moore et al., 2015). Carbonatite component in Bakening subarc mantle might have been diluted by pyroxenite melt inferred from low Fo component and NiO content of olivine (Figure 36).

At Lherz, France, clinopyroxene-bearing lherzolites and dunite were produced via refertilization of previously depleted mantle peridotite (LeRoux et al., 2007). It was demonstrated that the refertilization melt was similar in composition to aluminous websterite. The origin of the refertilization front was attributed to

upwelling of asthenospheric melts through the lithosphere ahead of a melting front (LeRoux et al., 2007).

Bakening *type I, II and III clinopyroxene* is identical in REE distribution trends and abundances to Lherz clinopyroxene at harzburgite-lherzolite contact and in lherzolites (Figure 29, Figure 30 and Figure 31). Similar to Lherz, the source of Bakening refertilization melt was constrained to be pyroxenite (Figure 36) which is consistent with the high MREE and HREE abundances of melts in equilibrium with Bakening clinopyroxene (Figure 38). Therefore, it is concluded that Bakening clinopyroxene equilibrated with pyroxenite-derived refertilization melt mixed with a small percentage (< 1 %) of carbonatite.

3.6 Conclusions

- Subarc mantle underneath Avachinsky is highly depleted as demonstrated by the low modal abundance of clinopyroxene in Avachinsky harzburgites (Figure 14 and Table 1), high Cr# of spinel (Figure 20) and low HREE abundances in vein clinopyroxene (Figure 27) and amphibole (Figure 34). The estimated degree of melting at Avachinsky exceeds 20 %.
- Rear-arc mantle underneath Bakening is more fertile than that of Avachinsky. Bakening peridotites contain HREE-enriched clinopyroxene (Figure 29, Figure 30 and Figure 31) and low Cr# spinel (Figure 20) consistent with lower estimated degree of melting ranging from 8 to 11 %.
- The high Fo component and intermediate NiO content of olivine in Avachinsky peridotites indicated that partial mantle melts equilibrated with peridotite whereas lower Fo component and NiO content of olivine in

Bakening peridotites indicated that partial mantle melts equilibrated with pyroxenite (Figure 36).

- At Avachinsky, four metasomatic episodes were identified based on textural observations. The first melt-rock reaction formed phlogopite and dunite veins (Figure 16C and E), the second melt-rock reaction produced anhydrous orthopyroxene-rich veins (Figure 16F and Figure 17B), the third melt-rock reaction re-fertilized the anhydrous orthopyroxene-rich veins to form clinopyroxene and amphibole (Figure 16D and F) and the fourth melt-rock reaction formed hydrous amphibole-rich veins (Figure 16E and Figure 17).
- Trace element composition of melt in equilibrium with vein clinopyroxene and amphibole overgrowing orthopyroxene in an anhydrous orthopyroxene-rich vein in harzburgite *AVX-16-03-24* is identical to that of boninite (Figure 27 and Figure 34).
- Vein amphibole in harzburgites *AVX-16-03-10* and *AVX-16-03-20* equilibrated with more evolved andesite and dacite, respectively that are genetically related to the selvage (Figure 32 and Figure 33).
- At Bakening, only two metasomatic episodes were identified based on textural observations, the formation of dunite veins and re-fertilization.
- Composition of melt in equilibrium with Bakening clinopyroxene is enriched in REE relative to primitive mantle, particularly in LREE, and approximates to that of pyroxenite melt mixed with < 1 % carbonatite (Figure 38).

Chapter 4

Compositional diversity of metasomatic fluids and melts recorded in veined mantle xenoliths from Shiveluch volcano, Kamchatka arc

4.1 Introduction

Studies of arc volcanic rocks infer that slab-derived components (sediment melt, altered oceanic crust (AOC)-derived fluid, residual AOC melt and serpentinite fluid) metasomatize depleted subarc mantle and produce the characteristic arc signature of the erupted volcanic rocks (i.e. high abundances of large-ion lithophile elements (LILE) and low abundances of high field strength elements (HFSE); e.g. Tatsumi, 1989). It has been suggested that these slab-derived components percolate through an interconnected vein network to transport slab-derived components to magma storage sites in the uppermost lithospheric mantle (Pirard and Hermann, 2015; Plümper et al., 2016). Evidence of this process is recorded in metasomatized subarc mantle xenoliths recovered from Kamchatka arc volcanoes, which are cross-cut by veins consisting of pyroxene, amphibole and phlogopite whose origins are rarely established except for the well-studied Avachinsky peridotites (Kepezhinskas et al., 1995; Kepezhinskas and Defant, 1996; Arai et al., 2003; Arai et al., 2007; Bryant et al., 2007; Ishimaru et al., 2007; Ishimaru and Arai, 2008; Halama et al., 2009; Bénard and Ionov, 2012; Bénard and Ionov, 2013; Bénard et al., 2017; Tomanikova et al., 2019). In contrast, little is known about the veins that cross-cut harzburgites

and dunites from Shiveluch volcano in Kamchatka. Previous studies proposed that they are deuteric products of the last stages of arc magma crystallization (Bryant et al., 2007). Their low concentrations of B and negative $\delta^{11}B$ have demonstrated an absence of a genetic link between the hydrous veins and the Kamchatka arc magmas (Tomanikova et al., 2019) and thus their origins remain enigmatic.

In this chapter, I investigate metasomatic processes occurring in the subarc mantle at Shiveluch via the study of veined mantle xenoliths. Here, I report major and minor element (section 4.3), trace element (section 4.4) and halogen (Cl and F) compositions of amphibole and phlogopite from veins cross-cutting Shiveluch mantle xenoliths (section 4.5) and bulk-rock compositions of their volcanic host rocks. I present evidence for percolation of compositionally diverse slab-derived fluids and melts and evolved magmatic melts through the veins (section 4.6.2) and constrain halogen (Cl and F) composition of melt that equilibrated with the hydrous vein minerals (section 4.6.4).

4.2 Petrological description of Shiveluch mantle xenoliths

All Shiveluch mantle xenoliths were recovered from the 1964 pyroclastic flow deposit and, with the exception of *SHIV-16-12-06* (Figure 39) and *SH11*, were described by Bryant et al. (2007). The most abundant xenolith type is harzburgite (n = 9), dunite (n = 3), lherzolite (n = 1) and clinopyroxene- and olivine-rich websterites (both n = 1; Figure 40 and Table 8). Shiveluch peridotites display protogranular, porphyroclastic and equigranular textures that are characteristic of mantle xenoliths (Table 8; Mercier and Nicolas, 1975). Olivine grain size gradually decreases from protogranular to porphyroclastic and equigranular and spinel occurs

in between grain boundaries and as inclusions in olivine. Shiveluch pyroxenites display coarse adcumulate texture (Bryant et al., 2007).

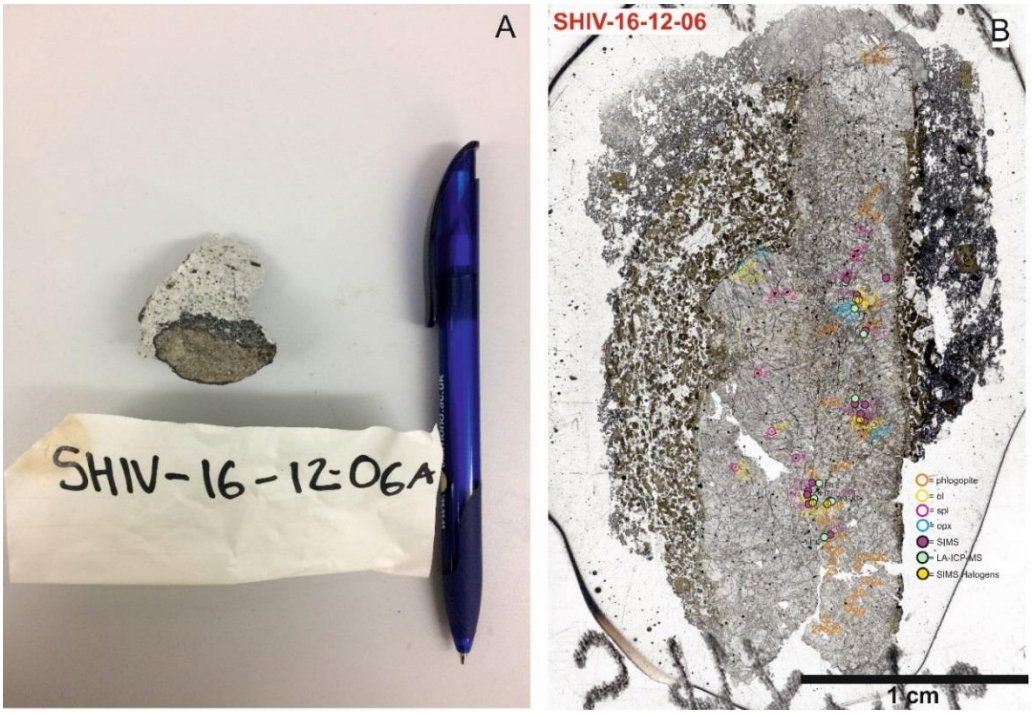

Figure 39. *A) Photograph and B) thin section scan image of dunite SHIV-16-12-06.*

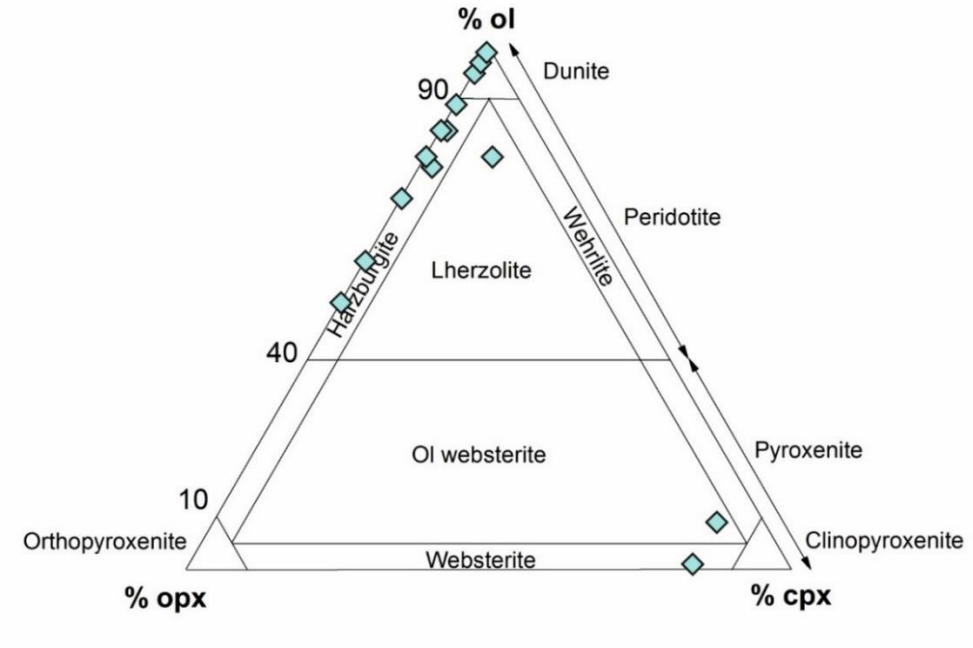

Figure 40*. Classification diagram (Streckeisen, 1979) of Shiveluch mantle xenoliths.*

Table 8. *Classification of Shiveluch mantle xenoliths*

Sample	Rock Type	Group	% ol	% opx	% cpx	Texture
SH98X-01	Lherzolite	Peridotite	79	10	11	Protogranular
SH98X-04	Harzburgite	Peridotite	51	49		Porphyroclastic
SH98X-06	Harzburgite	Peridotite	79*	21		Porphyroclastic
SHX98X-07	Harzburgite	Peridotite	77*	21	2	Porphyroclastic
SHX98-15	Websterite	Pyroxenite	1*	16	83	Coarse
SH98X-16	Harzburgite	Peridotite	84*	15	1	Porphyroclastic
SH98X-18	Harzburgite	Peridotite	71	29		Porphyroclastic
SHX03-01	Harzburgite	Peridotite	59	41		Porphyroclastic
SHX03-04	Dunite	Dunite	97	3		Protogranular
SHX03-17	Harzburgite	Peridotite	84*	16		Protogranular
SHX03-18	Harzburgite	Peridotite	89	11		Equigranular
SHX03-19	Ol Websterite	Pyroxenite	9*	8	83	Coarse
SHX No Nos	Dunite	Dunite	98	2		Equigranular
SHIV-16-12-06	Dunite	Dunite	95	5		Porphyroclastic
SH11	Igneous	Diorite	na	na	na	na

Abbreviations: ol = olivine, opx = orthopyroxene, cpx = clinopyroxene, na = not applicable

* = data from Bryant et al. (2007)

The xenoliths are mantled by amphibole and orthopyroxene selvages inhibiting olivine dissolution in the host andesite during their transport to the surface. Xenolith-hosted olivine immediately adjacent to the selvage is often zoned. Sample *SH11* was intruded by the host andesite with which it reacted to form a broad reaction zone comprised of coarse orthopyroxene, amphibole, plagioclase, phlogopite, oxides and occasionally clinopyroxene and apatite (Humphreys, 2006).

A striking feature of Shiveluch peridotites is the network of hydrous mineral-bearing cross-cutting veins (Figure 41A, B and C). Coarse amphibole, phlogopite and orthopyroxene grow in the centre of the veins and orthopyroxene and minor clinopyroxene typically grow at vein boundaries (Figure 41A, B and C). Plagioclase grows in between the early minerals (Figure 41C). Conspicuous dark lamellae within the phlogopite grains are formed by secondary chlorite that replaces phlogopite along cleavage planes (Figure 41A, B and C and Figure 42A).

The vein minerals crystallized in successive stages. Amphibole inclusions in a phlogopite grain indicated that amphibole was the first hydrous mineral to crystallize in the vein cross-cutting harzburgite *SHX03-17*, followed by phlogopite (Figure 42A), and, finally orthopyroxene (Figure 42B).

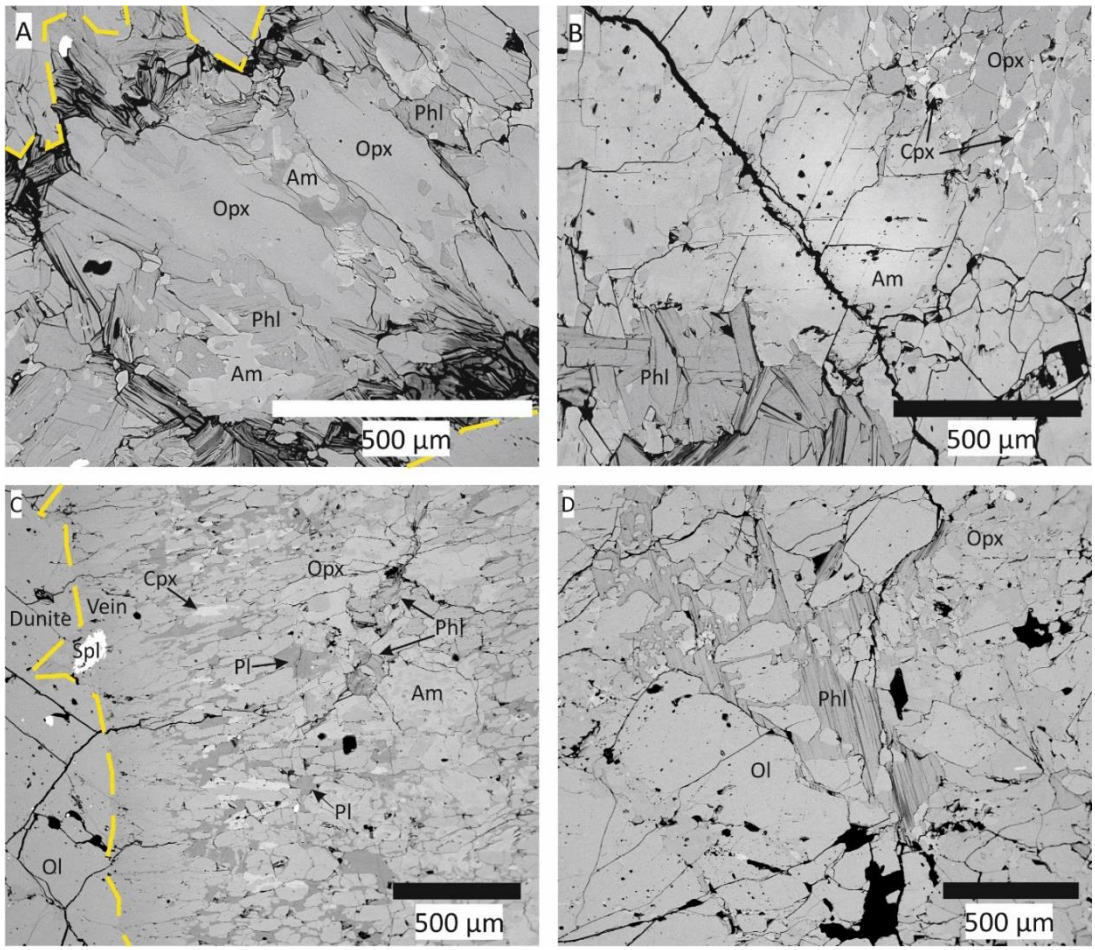

Figure 41. *Melt-rock reaction textures recorded in Shiveluch mantle xenoliths, as seen under back-scatter electron imaging. A) Cross-section through a phlogopite- and orthopyroxene-rich vein in SHX03-17. B) Coarse amphibole and phlogopite in the centre of a vein in SH98X-16. C) Interstitial plagioclase formed by late-stage melt infiltration at the vein edge of SHX03-04. D) An interconnected network of poikilitic phlogopite in SHIV-16-12-06. Dark chlorite lamellae within phlogopite are visible in A), B) and D). Yellow dashed line outlines vein edges. Abbreviations: Am = amphibole, Cpx = clinopyroxene, Ol = olivine, Opx = orthopyroxene, Phl = phlogopite, Pl = plagioclase and Spl = spinel.*

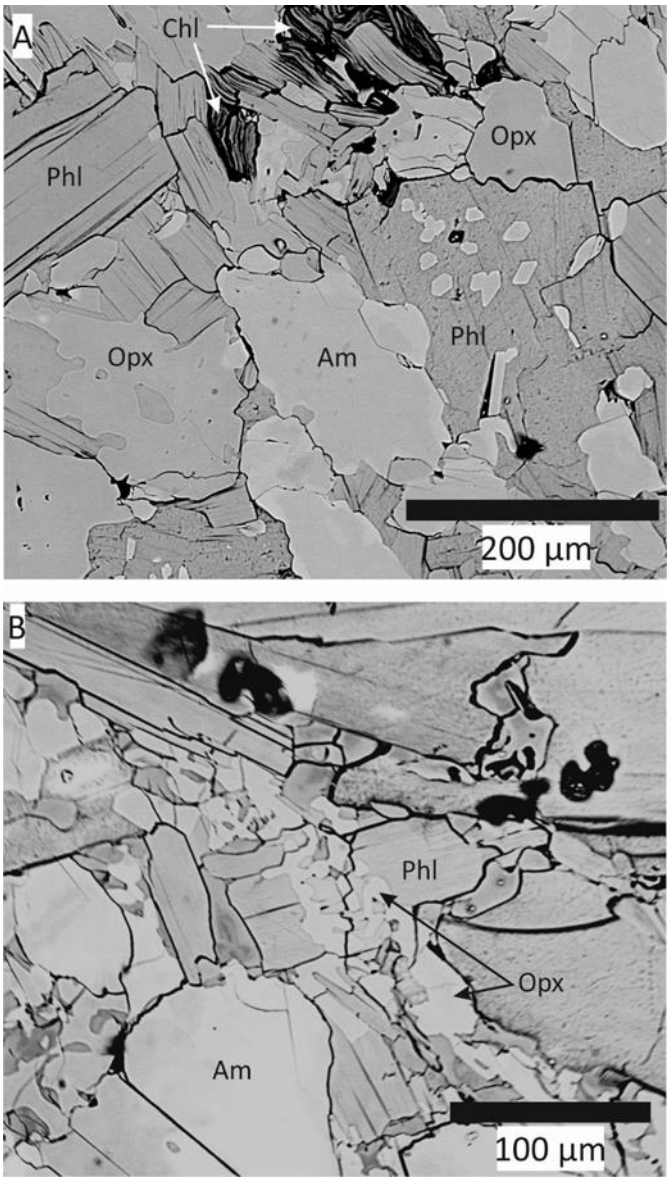

Figure 42*. Relative timing of vein mineral growth. A) Amphibole crystallised first, followed by phlogopite, which contains amphibole inclusions and finally, orthopyroxene that contains phlogopite inclusions in harzburgite SHX03-17. B) Orthopyroxene overgrowing phlogopite in vein cross-cutting SHX03-18. Abbreviations are the same as in Figure 41 and Chl = chlorite.*

4.3 Major element mineral chemistry

Mineral major and minor element abundances (average values in Table 9 and all data in Table A16, Table A17, Table A18, Table A19, Table A20 and Table A21 in Appendix A) were measured by electron probe micro analyser (EPMA) using a

JEOL JXA8230 instrument at the University of Leeds (for analytical conditions see section 2.1).

4.3.1 Olivine

The composition of olivine in Shiveluch mantle xenoliths varies in forsterite component from Fo_{88} to $Fo_{93.7}$ (Figure 43 and Table 9) whereas forsterite component in olivine rim adjacent to the selvage varies from $Fo_{82.8}$ to $Fo_{84.9}$ and rises to $Fo_{89.5}$ in olivine core. Silica content increases with higher olivine forsterite component (Figure 43). Olivine grains in *SHX03-18* that possess high Fo component are in contact with the cross-cutting hydrous vein.

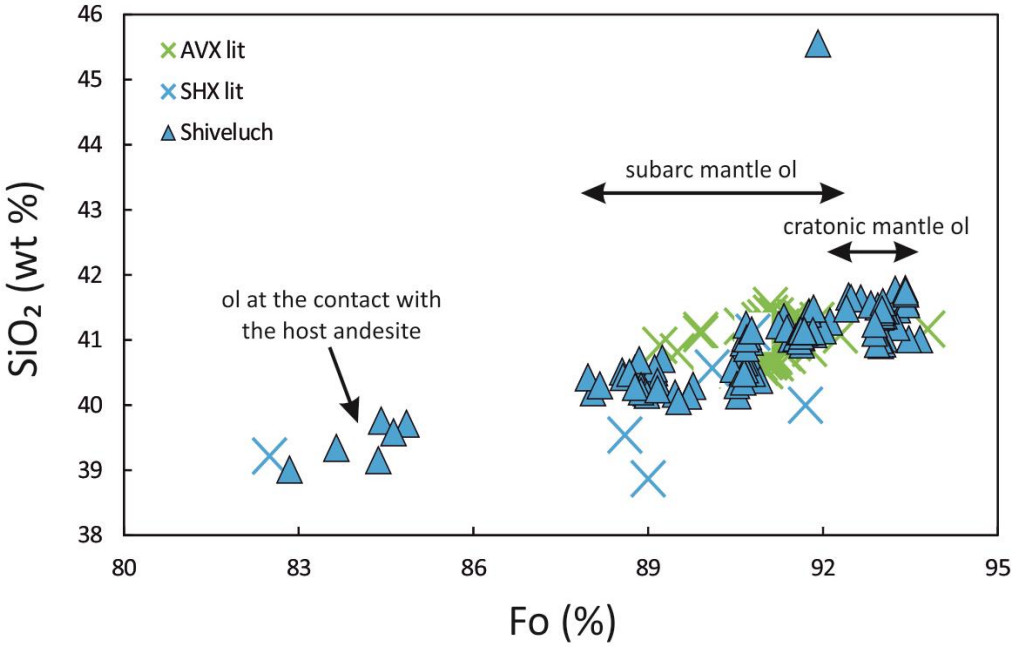

Figure 43. *Co-variation plot of major elements in olivine in Shiveluch mantle xenoliths. Data is compared to Shiveluch olivine from Bryant et al. (2007), Avachinsky olivine from Arai et al. (2003), Ishimaru et al. (2007), Ionov (2010) and Bénard and Ionov (2013) and cratonic olivine from Boyd and Mertzman (1987) and Boyd et al. (1997).*

4.3.2 Spinel

Spinel is Cr-rich, its Cr# [Cr# = Cr/(Cr + Al)] ranges from 51.5 to 81.5 (Figure 44 and Table 9). The high Cr# and Mg# [Mg# = Mg/(Mg + Fe^{3+})] are similar to refractory spinel from depleted subarc mantle peridotites from Avachinsky (Kepezhinskas and Defant, 1996; Arai et al., 2003; Ishimaru et al., 2007; Halama et al., 2009 and Ionov, 2010) and Izu-Bonin-Mariana (Parkinson and Pearce, 1998). Coupled with high Fo component in olivine, Shiveluch spinel falls within the olivine-mantle spinel array (OSMA; Arai, 1994) consistent with spinel in depleted subarc peridotites from Avachinsky and Izu-Bonin-Mariana (Figure 44B).

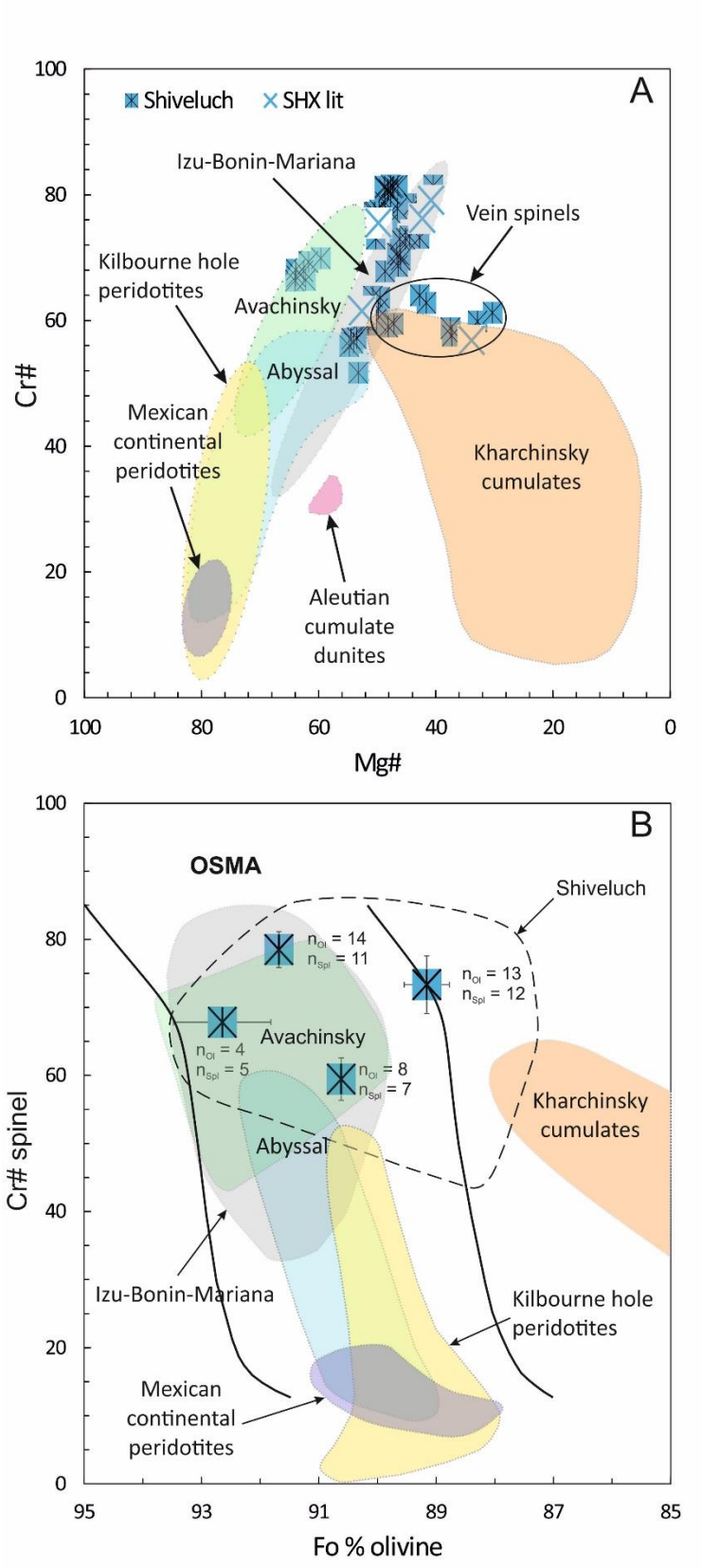

Figure 44*. A) Spinel Cr# versus Mg# in Shiveluch xenoliths and B) average spinel Cr# versus average Fo component in olivine from Shiveluch mantle xenoliths which fall within*

the olivine-spinel mantle array (OSMA; Arai, 1994). Figure was modified after Bryant et al. (2007), Avachinsky field was constrained from Kepezhinskas and Defant (1996), Arai et al. (2003), Ishimaru et al. (2007), Halama et al. (2009) and Ionov (2010) and Kilbourne hole peridotite field was constrained from Harvey et al. (2012). Concentration of Fe^{3+} in spinel was calculated after Droop (1987).

4.3.3 Orthopyroxene

Vein orthopyroxene is classified as Mg-rich enstatite (Figure 45) with Mg# [Mg# = Mg/(Mg + Fe^{3+})] ranging from 75 to 93 (Figure 46A and Table 9). Silica (54.1 to 58.35 wt %, average of 56.36 wt %) content increases with increasing Mg# (Figure 46A). Selvage pyroxene grains have low Mg# (75 to 80) and SiO_2 (54.1 to 54.8 wt %). Reaction zone orthopyroxene in *SH11* is enstatite with Mg# ranging from 70 to 77 (Table 9).

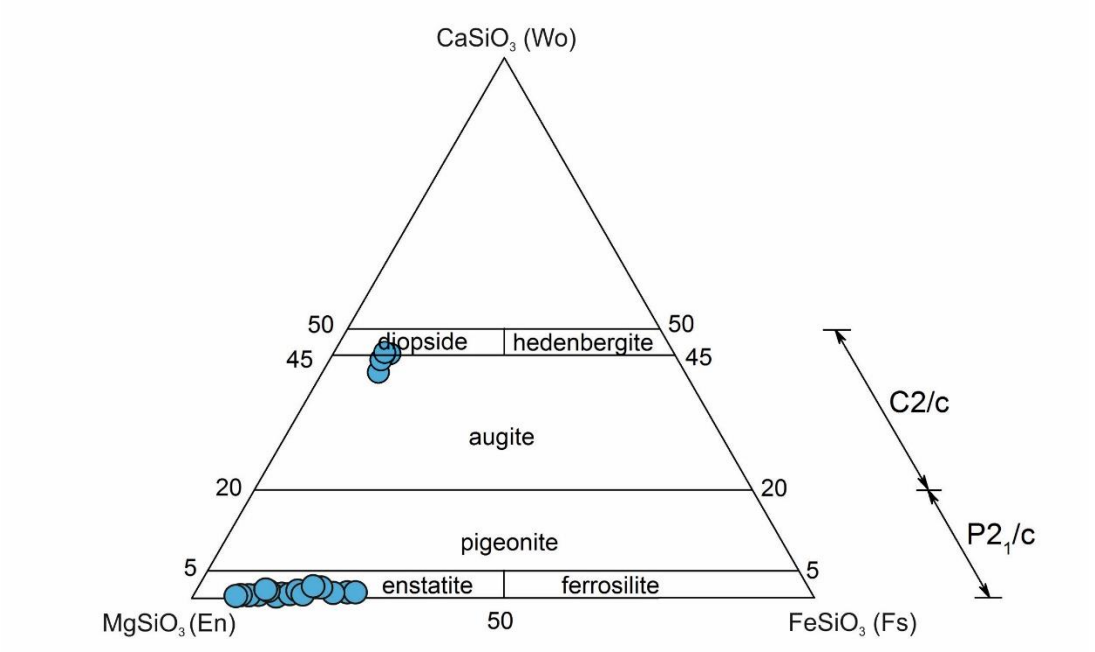

Figure 45. *Classification of Shiveluch orthopyroxene (enstatite) and clinopyroxene (diopside) after Morimoto (1988).*

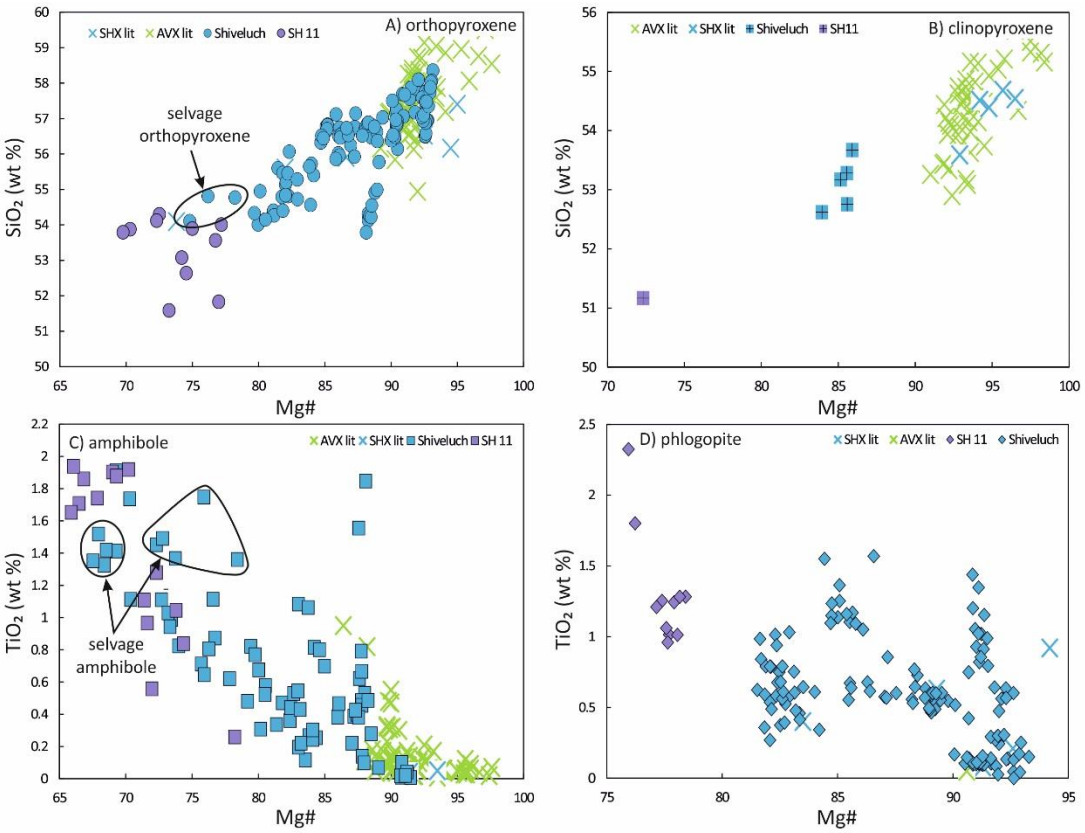

Figure 46. *Co-variation plots of major elements in orthopyroxene in A), clinopyroxene in B), amphibole in C) and phlogopite in D) from Shiveluch mantle xenoliths. Data is compared to Shiveluch literature values from Bryant et al. (2007) and Avachinsky literature values from Arai et al. (2003); Ishimaru et al. (2007); Ishimaru and Arai (2008); Ionov (2010); Ishimaru and Arai (2011); Bénard and Ionov (2012); Bénard and Ionov (2013).*

4.3.4 Clinopyroxene

Vein clinopyroxene is classified as diopside and augite (Figure 45) with Mg# ranging from 84 to 86 (Figure 46B). A few grains of vein clinopyroxene were only found in dunite *SHX03-04* (Table 9) and in harzburgite *SH98X-16* (not analyzed). Silica (52.6 to 53.7 wt %, average of 53.1 wt %) content increases with increasing Mg# (Figure 46B). Shiveluch vein clinopyroxene has lower Mg# and SiO_2 contents than primary clinopyroxene in Shiveluch xenoliths (Bryant et al., 2007) and vein clinopyroxene in Avachinsky xenoliths (Arai et al., 2003; Ishimaru et al., 2007; Ishimaru and Arai, 2008; Ionov, 2010; Ishimaru and Arai, 2011; Bénard and Ionov,

2012; Bénard and Ionov, 2013). A single grain of diopside was identified in *SH11* with Mg# = 72.3 (Figure 46B and Table 9).

4.3.5 Amphibole

Vein amphibole displays a large variation in Mg# (from 73 to 91.5) between samples. Its TiO_2 content generally decreases with increasing Mg# and ranges from 0.01 to 1.8 wt % (average of 0.5 wt %) (Figure 46C). Selvage amphibole in *SH98X-04* and *SHX03-04* is enriched in Ti (TiO_2 = 1.3 to 1.7 wt %) and depleted in Mg (Mg# = 68 to 78) relative to amphibole from the other samples (Figure 46C). Their compositions overlap with reaction zone amphibole in *SH11*. Shiveluch vein amphibole falls predominantly into two categories, magnesiohornblende and pargasite/magnesiohastingsite (Figure 47; cf. Leake et al., 1997). Amphibole in *SH11* is classified as magnesiohornblende (cf. Leake et al., 1997) with Mg# ranging from 66 to 78.

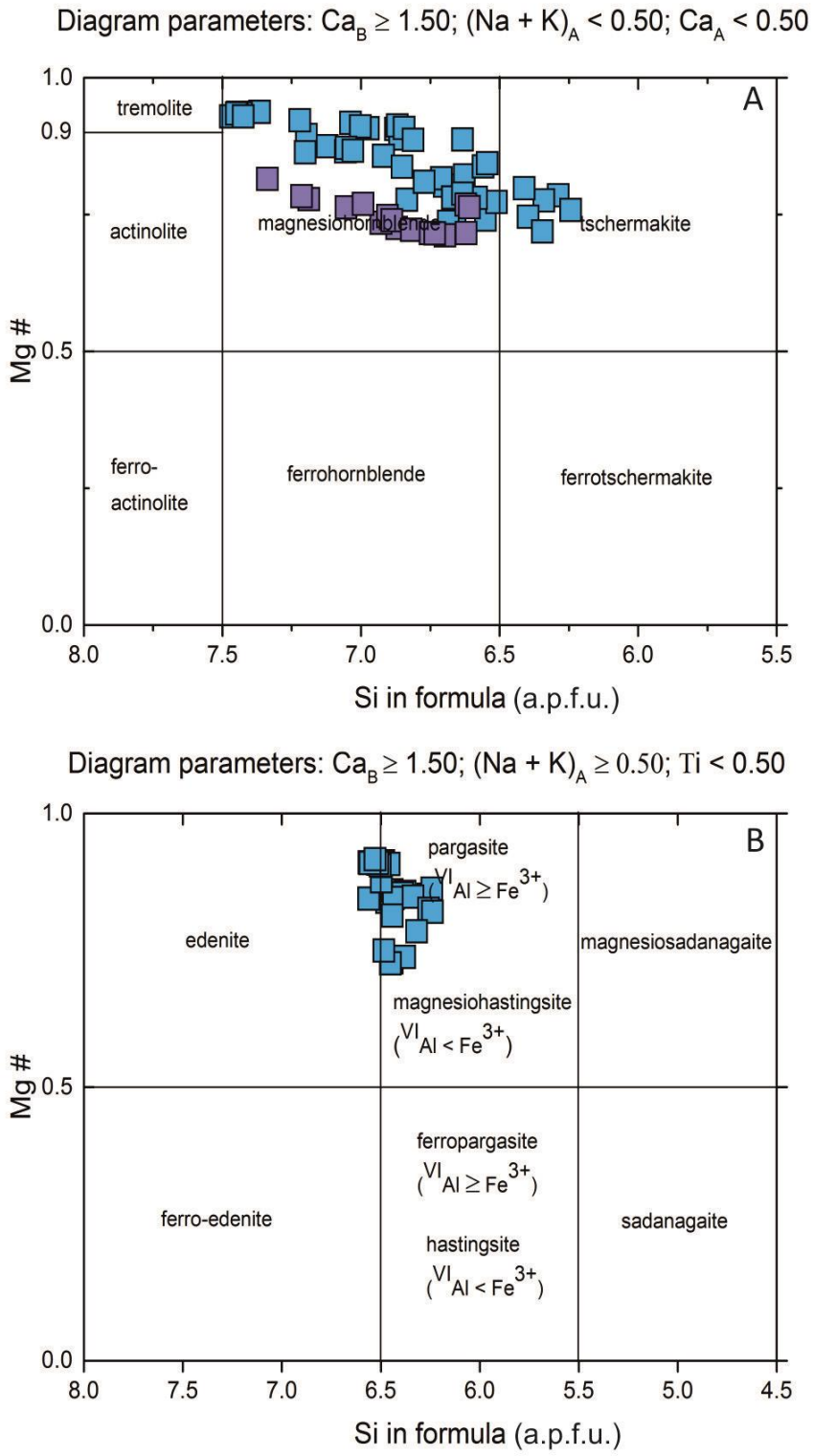

Figure 47. *Classification of Shiveluch vein amphibole after Leake et al. (1997). Two groups of compositionally distinct amphibole occur in Shiveluch veins. A) Amphibole with lower $(Na + K)_A$ is classified as magnesiohornblende and tschermakite and B) amphibole with higher $(Na + K)_A$ is classified as pargasite, magnesiohastingsite and edenite. Legend is the same as in Figure 46C.*

4.3.6 Mica

Mica, classified as phlogopite (Figure 48), displays a narrow range in Mg# within the individual veins cross-cutting Shiveluch mantle xenoliths. Their Mg# span from 81.5 to 93.5 across all xenoliths. They display variable TiO_2 contents at constant Mg#, ranging from 0.03 to 1.57 wt % (average TiO_2 = 0.58 wt %; Figure 46D). Reaction zone phlogopite in *SH11* has a narrow range in Mg# from 76 to 78.5.

In all samples where phlogopite was observed, alteration to chlorite along cleavage planes has occurred, identified as dark lamellae in back-scattered electron images (Figure 41). Chlorite Mg# range from 84 to 88 and their TiO_2 contents range from 0.11 to 0.79 wt % (Table 9).

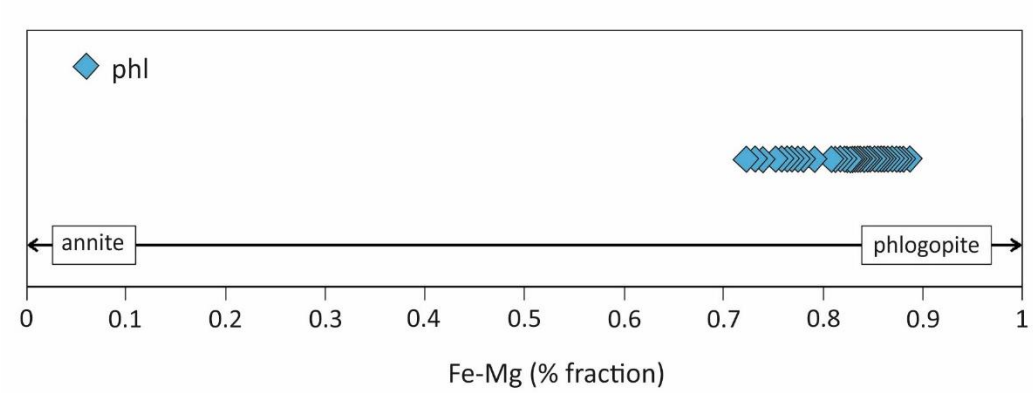

Figure 48. *Classification of Shiveluch vein mica. All mica is classified as phlogopite.*

Table 9. *Average mineral major and minor element data of Shiveluch mantle xenoliths*

Sample	SHX03-01				SHX03-04						SHX03-17					
Mineral	Ol	Opx	Am	Phl	Ol	Spl	Opx	Cpx	Am	Phl	Ol	Spl	Opx	Am	Phl	Chl
	n = 6	n = 9	n = 10	n = 12	n = 8	n = 19	n = 17	n = 5	n = 18	n = 4	n = 9	n = 11	n = 14	n = 5	n = 18	n = 1
SiO_2	41.02	56.82	46.02	38.86	40.49	bdl	54.01	53.10	44.89	39.01	41.14	bdl	56.76	53.70	39.79	38.78
TiO_2	0.01	0.07	0.67	1.02	0.01	0.43	0.04	0.22	0.52	0.60	0.01	0.29	bdl	0.02	0.11	0.11
Al_2O_3	bdl	1.15	11.61	16.20	bdl	15.76	0.90	1.11	11.45	15.37	bdl	7.86	0.82	4.70	15.49	5.13
Cr_2O_3	0.01	0.15	0.53	0.57	0.10	34.25	0.01	0.02	0.10	0.01	0.01	47.24	0.01	0.02	0.09	0.27
FeO	9.22	6.49	4.71	3.99	9.23	35.22	10.77	5.28	7.78	5.20	8.31	31.71	7.74	3.83	4.20	5.45
NiO	0.40	0.09	nd	nd	0.24	0.22	0.11	0.10	0.16	0.41	0.24	0.11	0.07	nd	nd	nd
MnO	0.11	0.13	0.06	0.02	0.18	0.39	0.43	0.22	0.16	0.04	0.18	0.43	0.32	0.14	0.03	0.03
MgO	50.39	34.49	19.03	22.94	50.23	9.82	32.75	17.10	18.05	24.48	51.37	9.52	34.26	21.99	23.95	22.92
CaO	0.02	0.59	11.58	0.04	0.01	0.02	0.43	22.36	11.06	0.26	0.01	bdl	0.19	11.48	0.05	2.83
Na_2O	bdl	bdl	2.31	1.70	bdl	nd	nd	nd	2.11	0.73	nd	nd	nd	0.88	0.98	0.84
K_2O	0.01	0.01	0.46	7.11	0.01	nd	nd	nd	0.37	7.27	nd	nd	nd	0.10	8.16	0.36
Total	101.17	99.94	97.13	92.73	100.41	96.11	99.37	99.51	96.82	93.77	101.26	97.16	100.17	96.98	93.09	87.23
Mg #	90.69	90.45	87.80	91.11	90.65	47.18	85.77	85.23	80.50	89.27	91.68	47.73	88.74	91.09	91.04	88.23
Cr #	na	na	na	na	na	59.46	na	na	na	na	na	80.14	na	na	na	na

Abbreviations: Ol = olivine, Opx = orthopyroxene, Am = amphibole, Phl = phlogopite, Spl = spinel, Cpx = clinopyroxene, Chl = chlorite, bdl = below detection limit, nd = not determined, na = not applicable.

Table 9. *Continued*

Sample	SHX03-18					SHIV-16-12-06				SH98X-04		SH98X-16			
Mineral	Ol	Spl	Opx	Am	Phl	Ol	Spl	Opx	Phl	Am	Phl	Am	Phl	Chl	Chl
	n = 4	n = 6	n = 23	n = 17	n = 15	n = 11	n = 12	n = 8	n = 30	n = 3	n = 7	n = 16	n = 17	n = 1	n = 1
SiO_2	41.20	bdl	56.73	46.47	39.02	40.24	bdl	54.54	37.80	43.96	39.57	49.25	38.54	40.03	38.62
TiO_2	0.01	0.34	0.07	1.03	1.16	nd	0.70	0.04	0.61	1.42	0.57	0.47	0.60	0.79	0.68
Al_2O_3	bdl	15.05	0.41	10.10	15.94	nd	10.52	2.66	16.88	10.93	14.56	7.85	16.01	16.81	16
Cr_2O_3	0.11	47.27	0.01	0.02	0.01	0.05	42.73	0.03	nd	0.07	0.69	0.04	0.27	0.03	0.01
FeO	6.75	21.45	8.85	9.67	6.56	10.60	33.42	7.67	4.51	11.90	5.18	5.62	5.73	6.97	6.75
NiO	0.28	0.10	nd	nd	nd	0.21	0.10	0.05	0.12	nd	nd	nd	nd	nd	nd
MnO	0.13	0.32	0.31	0.19	0.04	nd	0.38	0.20	0.03	0.27	0.02	0.14	0.03	0.07	0.07
MgO	52.56	13.09	32.28	16.49	21.56	48.94	9.01	33.25	21.31	14.54	23.02	19.54	22.63	21.50	20.49
CaO	0.01	bdl	0.56	11.12	0.02	0.21	0.12	0.55	0.04	11.07	0.04	11.90	0.03	3.21	2.14
Na_2O	nd	nd	0.01	1.89	1.57	nd	nd	nd	2.11	2.11	0.91	1.51	0.95	0.19	0.26
K_2O	nd	nd	0.01	0.40	7.07	nd	nd	nd	6.28	0.36	8.32	0.30	8.42	0.36	2.12
Total	101.02	97.61	99.22	97.52	93.25	100.21	96.98	98.99	89.87	96.72	93.00	96.70	93.31	90.13	87.41
Mg #	93.27	62.55	86.65	75.17	85.40	89.16	44.49	88.54	82.54	68.54	88.79	86.07	87.54	84.6	84.4
Cr #	na	67.82	na	na	na	na	73.33	na	na	na	na	na	na	na	na

Abbreviations: Ol = olivine, Spl = spinel, Opx = orthopyroxene, Am = amphibole, Phl = phlogopite, Chl = chlorite, bdl = below detection limit, nd = not determined, na = not applicable.

Table 9. *Continued*

Sample	SH98X-18	SHX-No-No		SH11		
Mineral	Phl	Ol	Opx	Opx	Am	Phl
	n = 25	n = 18	n = 31	n = 11	n = 16	n = 11
SiO_2	39.30	41.25	56.99	53.33	46.95	38.38
TiO_2	0.31	0.01	0.02	0.09	1.42	1.31
Al_2O_3	16.60	bdl	1.04	1.56	7.96	15.65
Cr_2O_3	0.45	0.01	0.03	0.06	0.02	0.45
FeO	3.55	7.09	6.29	15.34	10.93	9.23
NiO	nd	0.34	0.09	nd	nd	nd
MnO	0.02	0.15	0.21	0.74	0.28	0.05
MgO	23.61	51.97	34.79	24.37	14.48	17.83
CaO	0.05	0.01	0.19	0.64	11.34	0.03
Na_2O	1.48	bdl	bdl	0.02	1.42	0.84
K_2O	7.49	0.01	bdl	0.02	0.32	7.90
Total	93.07	100.81	99.65	96.17	95.13	91.67
Mg #	92.22	92.89	90.69	73.89	70.18	77.48
Cr #	na	na	na	na	na	na

Abbreviations: Phl = phlogopite, Ol = olivine, Opx = orthopyroxene, Am = amphibole, bdl = below detection limit, nd = not determined, na = not applicable.

4.3.7 Calculated temperature, pressure and oxygen fugacity conditions

Shiveluch mantle xenoliths equilibrated at temperatures ranging from 715 to 903 °C ± 50 °C (Figure 49). The temperatures were calculated using the spinel-olivine geothermometer of O'Neill and Wall (1987) and error was estimated by Putirka (2008). The absence of primary orthopyroxene-clinopyroxene mineral pairs in equilibrium with each other precluded the use of other geothermometers calibrated for natural peridotites (e.g. the two-pyroxene geothermometer of Brey and Köhler, 1990). Comparatively, the pre-eruptive temperature of Shiveluch andesite erupted during the most recent volcanic period (2001-2004) is ~ 840 °C based on hornblende-plagioclase thermometry (Humphreys et al., 2006)

Equilibration pressure was constrained by Central Kamchatka depression geotherm defined by continental crust thermal gradient of 23 °C km^{-1} and asthenospheric mantle thermal gradient of 8.5 °C km^{-1} (Portnyagin and Manea, 2008) and ranges from 1 to 1.5 GPa (Figure 49 and Table 10). The pressure estimates indicate that Shiveluch mantle xenoliths last equilibrated at 30 to 45 km depth in the lithospheric mantle, close to the crust-mantle interface located at ~ 35 km in Kamchatka (Levin et al., 2002). For comparison, the maximum magma pressure estimated from maximum H_2O content of amphibole- and plagioclase-hosted melt inclusions in Shiveluch volcanic rocks is ~ 0.16 GPa (Humphreys et al., 2006), which is equivalent to 4.8 km depth.

Oxygen fugacities (fo_2) were calculated after Wood et al. (1990) and range from + 2.4 to + 2.6 log units relative to FMQ (Mattioli and Wood, 1988; Table 10). Only a limited number of mantle xenoliths contained olivine, spinel and primary orthopyroxene that are required to calculate fo_2. It has been reported that Shiveluch

subarc mantle is highly oxidized with fO_2 ranging from + 1.3 to + 3.7 log units relative to FMQ (Nekrylov et al., 2018). The high fO_2 of the Central Kamchatka depression subarc mantle was attributed to the influx of AOC-derived components. Additionally, coexisting sulfide and sulfate mineral phases might buffer subarc mantle oxidation state under the northern part of the Central Kamchatka depression via oxidation of mantle sulfides or reduction of sulfate ion (Bénard et al., 2018).

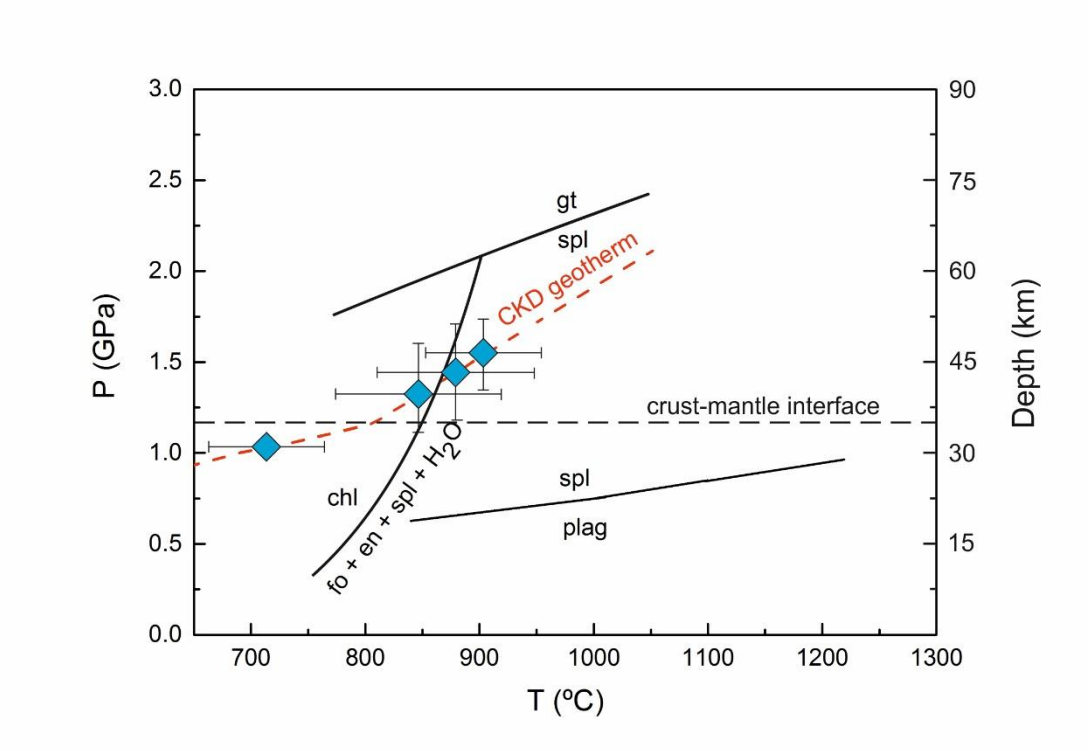

Figure 49. *Equilibration pressure-temperature conditions of Shiveluch mantle xenoliths. Temperatures were calculated using the olivine-spinel geothermometer of O'Neill and Wall (1987). Pressures were estimated from the Central Kamchatka depression geotherm (Portnyagin and Manea, 2008). Chlorite breakdown reaction and garnet-spinel transition is from Ulmer and Trommsdorff (1999) and spinel-plagioclase transition is from O'Neill (1981). Crust-mantle interface is located at 35 km depth in Kamchatka (Levin et al., 2002).*

***Table 10**. Average equilibration temperature and pressure and oxygen fugacity of Shiveluch mantle xenoliths*

Sample	Number of mineral pairs	T (°C)	T 2σ (°C)	P* (GPa)	fO_2
SHX03-04	5	882 ± 50	19	1.4 ± 0.2	nd
SHX03-17	5	847 ± 50	22	1.3 ± 0.25	+ 2.6
SHX03-18	1	715 ± 50	na	1 ± < 0.1	nd
SHIV-16-12-06	1	903 ± 50	na	1.5 ± 0.2	+ 2.4

Abbreviations: na = not applicable, nd = not determined.

* Pressure constrained from CKD geotherm defined by continental crust thermal gradient of 23 °C km^{-1} and asthenospheric mantle thermal gradient of 8.5 °C km^{-1} (Portnyagin and Manea, 2008). The estimated thickness of Kamchatka continental crust is 35 km (Levin et al., 2002).

4.4 Trace element mineral chemistry

Mineral trace element abundances (average values in Table 11 and all data in Table B22 and Table B23 in Appendix B) were measured by inductively coupled plasma mass-spectrometer (ICP-MS) using an Agilent 8800 ICP-MS Triple Quad attached to a laser ablation system Photon Machines Analyte Excimer 193 nm at the Open University (for analytical conditions see section 2.3).

4.4.1 Amphibole

Shiveluch vein amphiboles are enriched in all incompatible trace elements (Rb, Ba, Th, U, Nb, Ta, La, Ce, Pb, Pr, Sr, Nd, Sm, Zr, Hf, Eu, Ti, Gd, Tb, Dy, Li, Ho, Y, Er, Tm, Yb and Lu) relative to primitive mantle (Figure 50A and Table 11; McDonough and Sun, 1995). Primitive mantle-normalized amphibole trends display convex-up LREE while HREE gradually decrease in abundance from Gd to Lu (Figure 50B).

4.4.2 Phlogopite

Relative to primitive mantle abundances the phlogopite is enriched in LILE, but depleted in REE (often below detection limit; Figure 51A and Table 11). Their REE trends are concave-up with positive Eu anomalies and HREE close to the detection limit in primitive mantle-normalized phlogopite plots (Figure 51B). The abundances of REE in chlorite-bearing phlogopite are elevated in harzburgites *SHX03-18* and *SH98X-16* relative to those of chlorite-free phlogopite (Figure 52).

Table 11. *Average hydrous vein mineral trace element data of Shiveluch mantle xenoliths and bulk-rock data of their volcanic host rocks*

Sample	SHX03-04	SHX03-17	SHX03-18			SHIV-16-12-06	SH98X-16			SHX 1964 andesite	SHX mica tephra
Mineral	Am	Phl	Am	Phl	Phl*	Phl	Am	Phl	Phl*	Bulk rock	Bulk rock
	n = 3	n = 12	n = 25	n = 7	n = 8	n = 11	n = 19	n = 21	n = 2		
Rb (µg g^{-1})	1.10	172.85	0.76	205.14	190.80	88.74	1.77	205.94	167.32	19.30	23.90
Cs	bdl	1.94	bdl	3.62	3.71	2.32	bdl	8.28	9.44	0.6	0.7
Ba	52.12	1066.43	30.50	2477.32	2277.31	1686.54	13.95	870.22	595.67	351.00	336.00
Th	0.19	0.02	0.21	0.01	0.01	0.02	0.33	0.01	bdl	1.10	1.10
U	0.09	0.03	0.08	0.02	0.01	0.06	0.11	0.02	0.02	0.60	0.50
Nb	1.80	2.57	1.41	2.71	2.61	10.59	0.74	0.55	0.52	1.70	2.70
Ta	0.16	0.23	0.09	0.23	0.21	0.58	0.07	0.05	0.04	0.20	0.10
La	3.28	0.05	5.21	0.24	1.17	0.65	4.30	0.04	0.76	7.80	7.50
Ce	13.33	0.07	21.33	0.58	2.89	0.81	14.47	0.06	1.38	16.90	16.60
Pb	0.50	0.69	0.60	1.78	1.55	6.35	0.50	1.00	2.21	1.10	1.60
Pr	2.65	0.01	3.90	0.09	0.43	0.07	2.30	0.01	0.11	2.53	2.50
Sr	121.45	21.98	68.66	42.05	47.84	121.17	98.83	25.71	39.76	497.00	402.70
Nd	14.08	0.04	21.21	0.45	2.09	0.24	10.78	0.05	0.47	11.10	12.30
Sm	3.98	0.01	6.16	0.07	0.36	0.08	2.69	0.02	0.06	2.62	3.05
Zr	62.00	7.88	45.42	8.30	8.62	26.14	25.64	1.89	1.74	98.50	75.70
Hf	2.70	0.51	2.48	0.38	0.39	0.44	1.54	0.06	0.05	2.60	2.30
Eu	1.42	0.03	1.79	0.06	0.12	0.07	0.87	0.01	0.02	0.83	1.05
Ti	3992.99	514.81	5673.04	7904.15	7281.16	3315.04	2846.87	2388.49	1931.59	5800	7600
Gd	4.01	bdl	6.36	0.11	0.34	bdl	2.63	bdl	0.15	2.60	3.53
Tb	0.62	bdl	1.03	0.01	0.02	0.01	0.43	bdl	bdl	0.36	0.50
Dy	3.77	0.02	6.21	0.03	0.09	0.01	2.52	0.02	0.02	2.23	3.05
Li	3.93	5.83	6.44	9.15	9.54	2.80	4.03	4.64	3.97	nd	nd
Ho	0.73	bdl	1.31	bdl	0.02	bdl	0.56	bdl	bdl	0.45	0.58
Y	20.43	0.11	32.34	0.15	0.44	0.15	14.43	0.08	0.34	13.10	16.20
Er	2.21	0.02	3.76	0.01	0.05	0.01	1.62	0.01	0.01	1.27	1.68
Tm	0.30	bdl	0.52	bdl	0.01	bdl	0.24	bdl	bdl	0.18	0.23
Yb	2.08	0.04	3.27	0.01	0.05	0.03	1.59	0.01	bdl	1.21	1.52
Lu	0.29	0.01	0.50	bdl	0.01	0.01	0.25	bdl	0.01	0.19	0.25

Abbreviations: Am = amphibole, Phl = phlogopite, bdl = below detection limit, nd = not determined. * = phlogopite containing chlorite lamellae

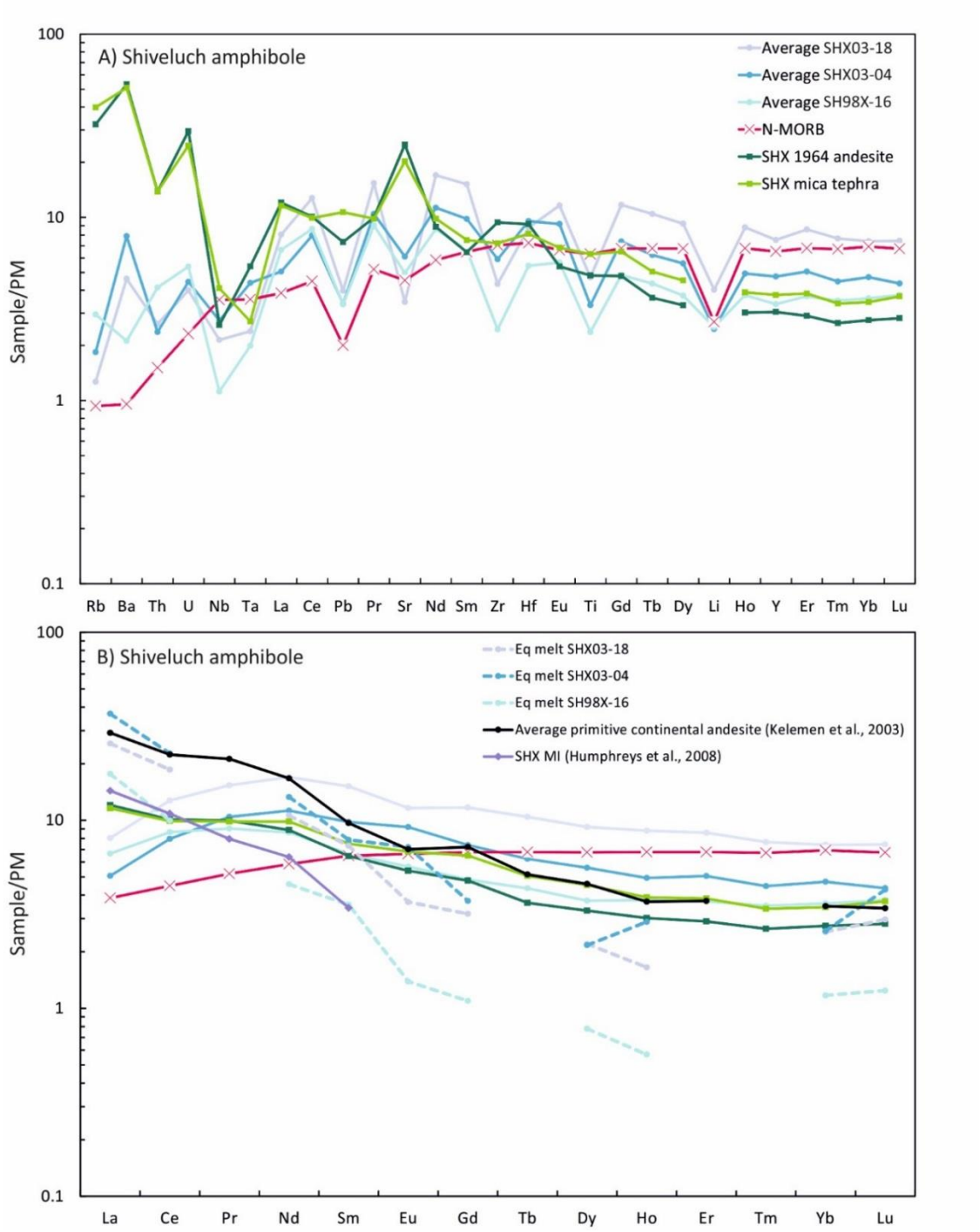

Figure 50. *A) Trace element distribution and B) rare earth element (REE) distribution in Shiveluch vein amphibole, bulk-rock 1964 andesite, mica-bearing basaltic tephra and melt in equilibrium with Shiveluch vein amphibole (eq melt) calculated after Humphreys et al. (2019). Concentrations are normalized to the composition of primitive mantle (PM; McDonough and Sun, 1995). N-MORB (Sun and McDonough,1989), average primitive continental andesite (Kelemen et al., 2003) and evolved amphibole- and plagioclase-hosted melt inclusions from Shiveluch arc volcanic rocks (Humphreys et al., 2008) are shown for comparison.*

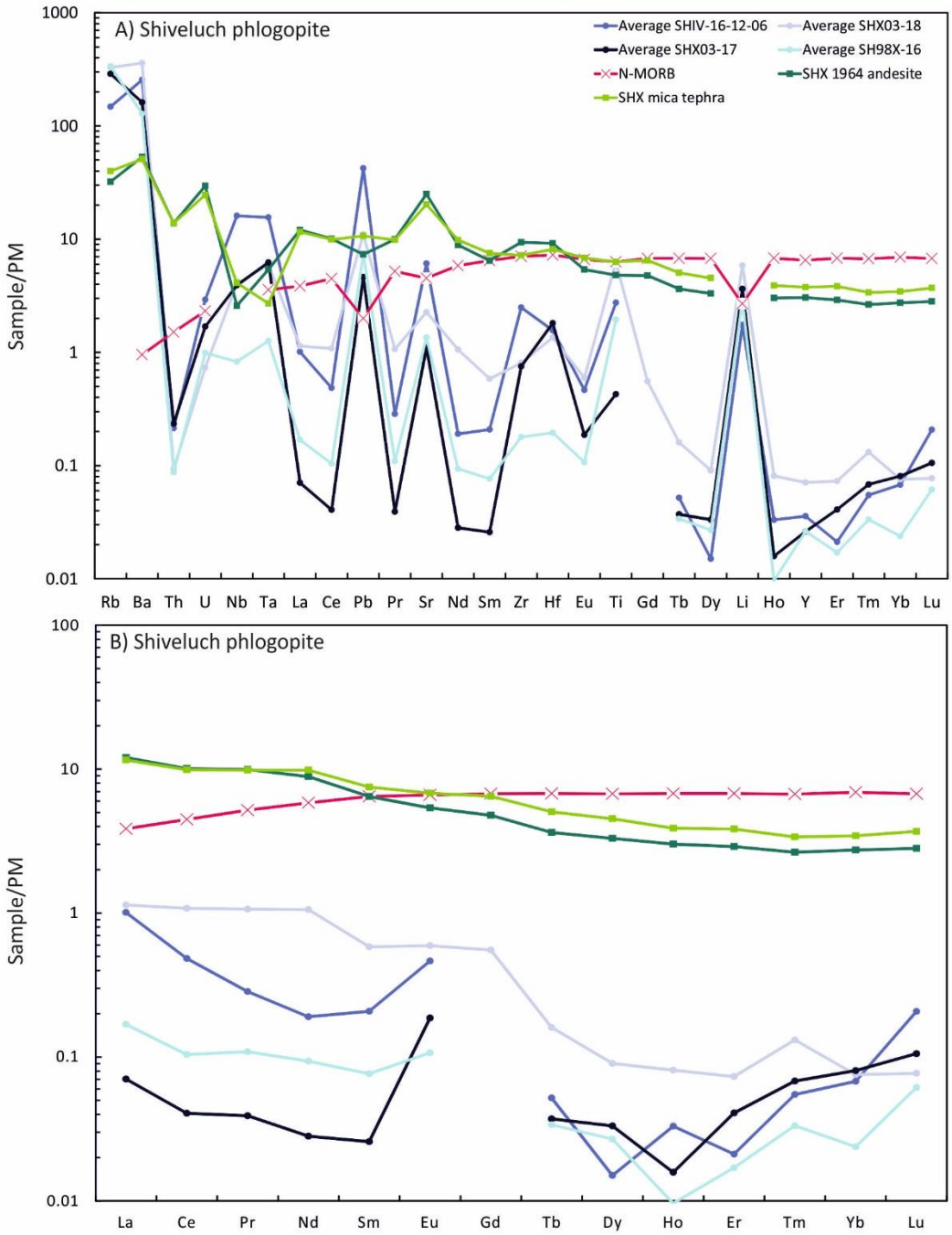

Figure 51. *A) Trace element distribution and b) rare earth element (REE) distribution in Shiveluch phlogopite, bulk-rock 1964 andesite and mica-bearing basaltic tephra. Concentrations are normalized to the composition of primitive mantle (PM; McDonough and Sun, 1995). N-MORB (Sun and McDonough,1989) is shown for comparison.*

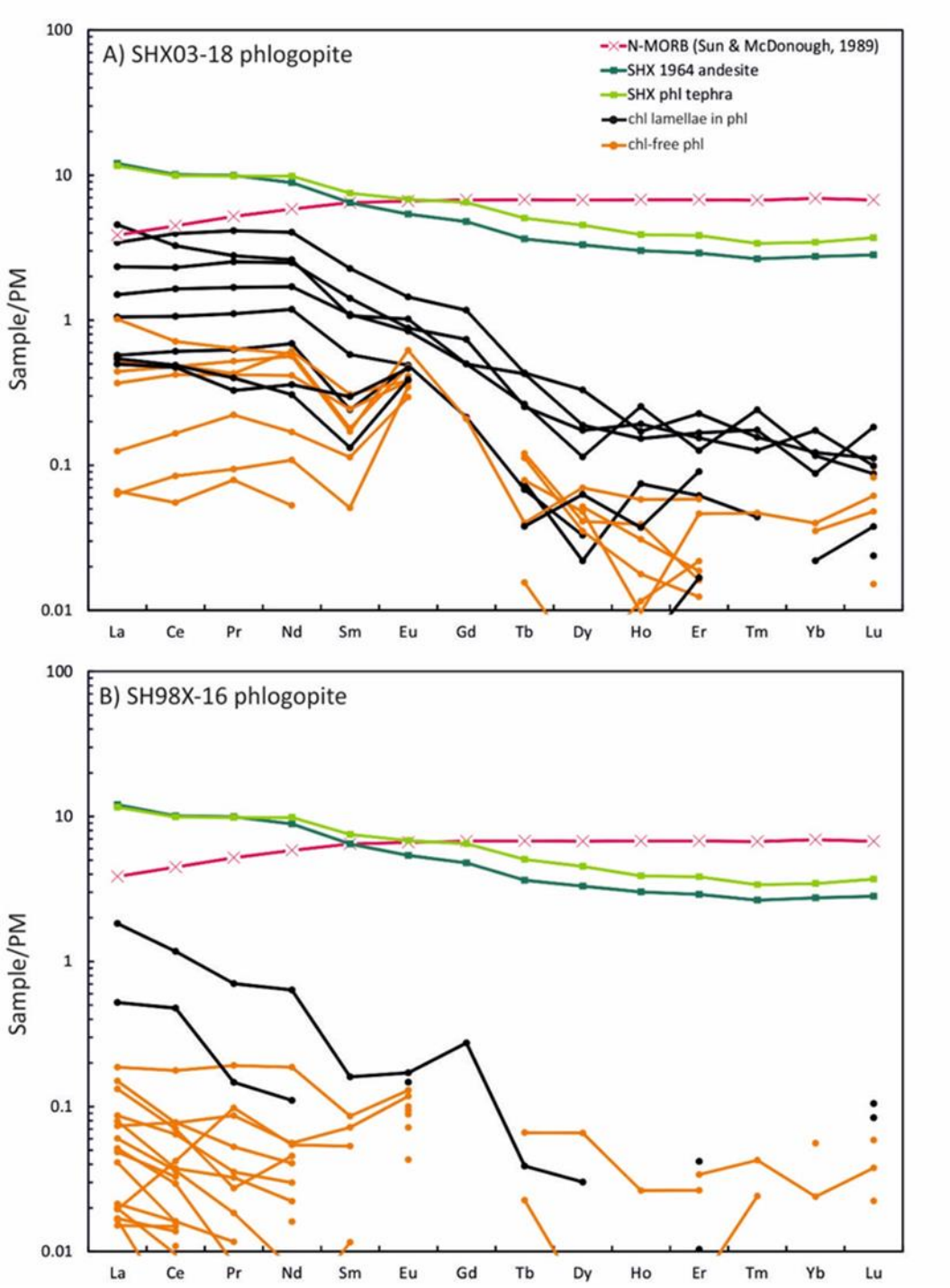

Figure 52. *Rare earth element (REE) distribution in A) SHX03-18 and B) SH98X-16 chlorite-bearing phlogopite (black lines) and chlorite-free phlogopite (orange lines), bulk-rock 1964 andesite and mica-bearing basaltic tephra. Concentrations are normalized to the composition of primitive mantle (PM; McDonough and Sun, 1995). N-MORB (Sun and McDonough,1989) is shown for comparison.*

4.5 Water and halogens (Cl and F)

Mineral halogen (Cl and F) and water contents were analysed using a Cameca IMS-4f at the Edinburgh Ion Microprobe Facility (see section 2.3.2). Mineral water contents were analysed on two separate occasions to monitor data reproducibility (Figure 13).

4.5.1 Water contents

Water contents in amphibole and phlogopite range from 2.23 to 2.87 wt % and from 4.26 to 6.74 wt %, respectively (Table 12). Water contents of some phlogopite (n = 4) exceeds the upper limit that can be structurally accommodated in the hydroxyl sites of F-free micas (approximately 4 to 5 wt %; Deer et al., 1992).

4.5.2 Halogen (Cl and F) contents

Amphibole Cl and F contents range from 70 to 340 µg g^{-1} (average is 185 µg g^{-1}) and from 465 to 1580 µg g^{-1} (average is 982 µg g^{-1}), respectively. Phlogopite Cl and F contents range from 168 to 934 µg g^{-1} (average is 427 µg g^{-1}) and from 435 to 2090 µg g^{-1} (average is 922 µg g^{-1}), respectively (Figure 53 and Table 12). Shiveluch vein amphibole and phlogopite are enriched in Cl relative to amphibole reported from mantle xenoliths from Avachinsky volcano (40 to 111 µg g^{-1}; Bénard et al., 2017) but are depleted in Cl relative to most olivine-hosted melt inclusions from Shiveluch volcanic rocks (Figure 53; Iveson et al., *in prep*) and from volcanic rocks along the Kamchatka arc (384 to 1237 µg g^{-1}; Churikova et al., 2007; Portnyagin et al., 2007). Phlogopite grains from *SHIV-16-12-06* are enriched in Cl and depleted in F compared to phlogopite from the other Shiveluch xenoliths and are identical in Cl

and F contents to some Shiveluch and Kamchatka arc high-Mg# olivine-hosted melt inclusions (Figure 53; Iveson et al., *in prep*).

Table 12. *Water, Li and halogen (Cl and F) data of Shiveluch hydrous vein minerals*

Sample	Mineral	H_2O* (wt %)	Li* (µg g^{-1})	F* (µg g^{-1})	Cl* (µg g^{-1})
SH98X-16	Am	2.58	1.40	469.01	71.88
		2.61	1.23	501.11	67.15
		2.61	1.80	626.91	120.98
		2.34	2.66	466.15	248.99
		2.32	2.49	583.16	220.40
		2.87	1.65	761.00	122.69
	Phl	4.47	2.25	587.15	259.74
		4.48	2.39	604.41	167.82
		4.67	2.45	637.20	211.52
		4.53	2.45	639.14	179.89
		4.81	2.61	736.57	209.61
		4.89	2.71	759.26	216.90
SHIV-16-12-06	Phl	4.89	2.18	475.05	652.27
		4.80	1.97	477.59	706.07
		6.74	1.86	494.37	934.16
		4.74	1.18	436.26	685.58
		4.57	1.99	469.14	728.94
		4.92	2.07	479.62	801.34
SHX03-17	Phl	5.25	3.05	1378.62	399.88
		4.77	2.90	1196.33	428.11
		5.08	3.03	1172.88	416.63
		5.02	2.86	1270.92	470.22
	Am	2.65	2.00	873.17	95.95
		2.73	2.08	919.82	124.20
SHX03-18	Am	2.33	3.17	1508.38	211.34
		2.25	3.22	1503.98	193.76
	Phl	4.26	4.20	1742.44	332.66
		4.36	3.90	2082.18	271.49
SHX03-04	Am	2.23	2.50	1581.37	338.79
		2.55	2.41	1472.19	286.42
	Phl	4.81	3.04	1729.30	556.33

Abbreviations: Am = amphibole and Phl = phlogopite.
* Uncertainties of amphibole and phlogopite H_2O, Li, F and Cl concentrations are 8 and 11 % RSD, 29 and 27 % RSD, 48 and 56 % RSD and 50 and 52 % RSD, respectively.

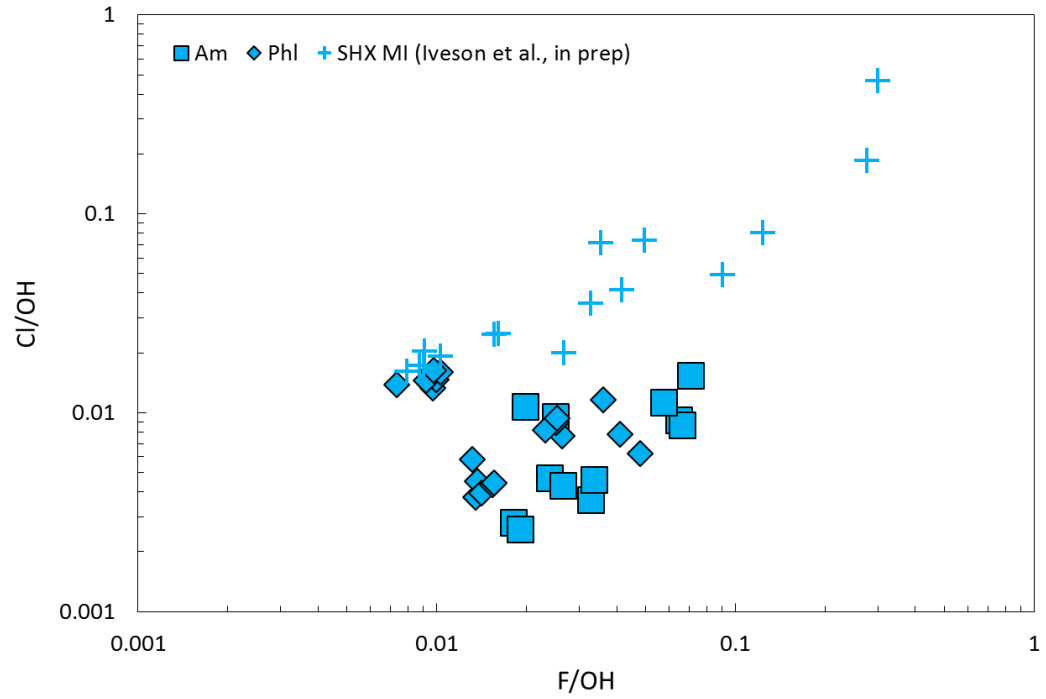

Figure 53. *Hydroxyl site composition of Shiveluch vein amphibole and phlogopite and halogen/OH of Shiveluch high-Mg# olivine-hosted melt inclusions (MI; Iveson et al., in prep).*

In amphibole there is an inverse covariation between Cl abundance and both SiO_2 and MgO (Figure 54A and C), whereas Al_2O_3 and FeO show positive covariation (Figure 54B and D). With the exception of FeO, these relationships are also observed in phlogopite, although fewer analyses were made. The fluid mobile elements Rb, Ba and Li covary positively with Cl in amphibole, while only Li shows a similar relationship with F in both amphibole and phlogopite (Figure 55).

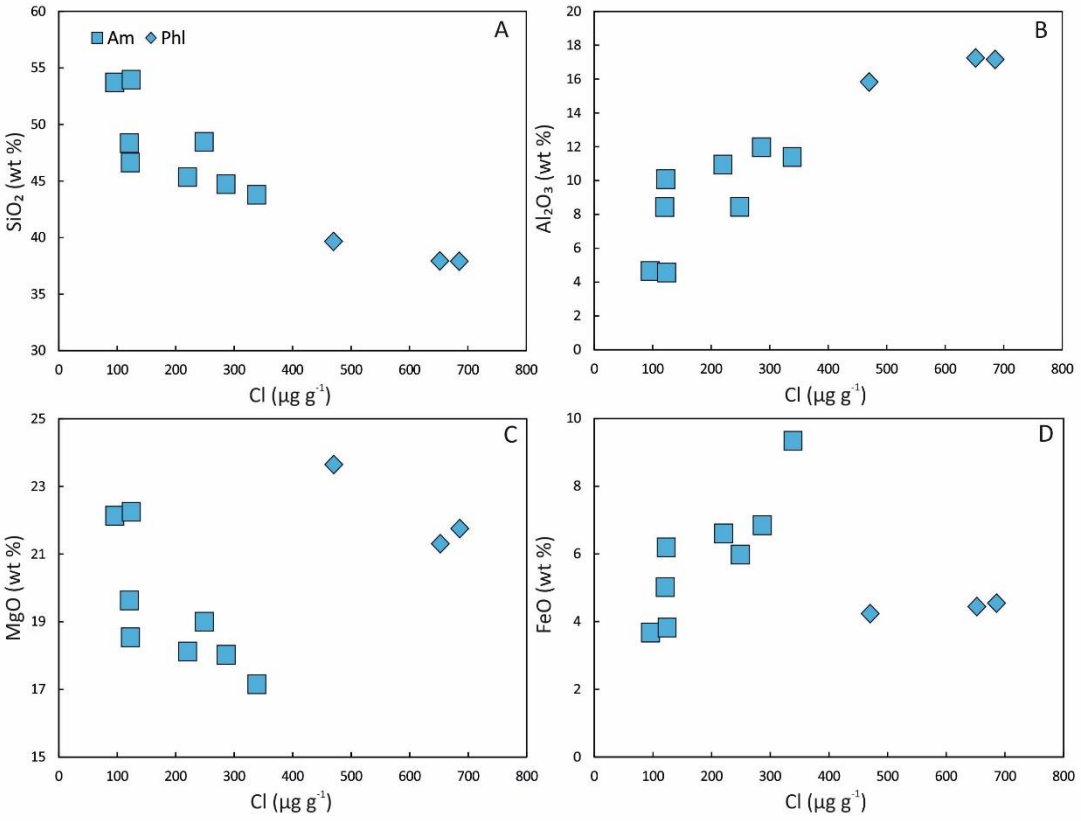

Figure 54. *A) to D) Major element abundances versus Cl concentration in Shiveluch vein amphibole and phlogopite.*

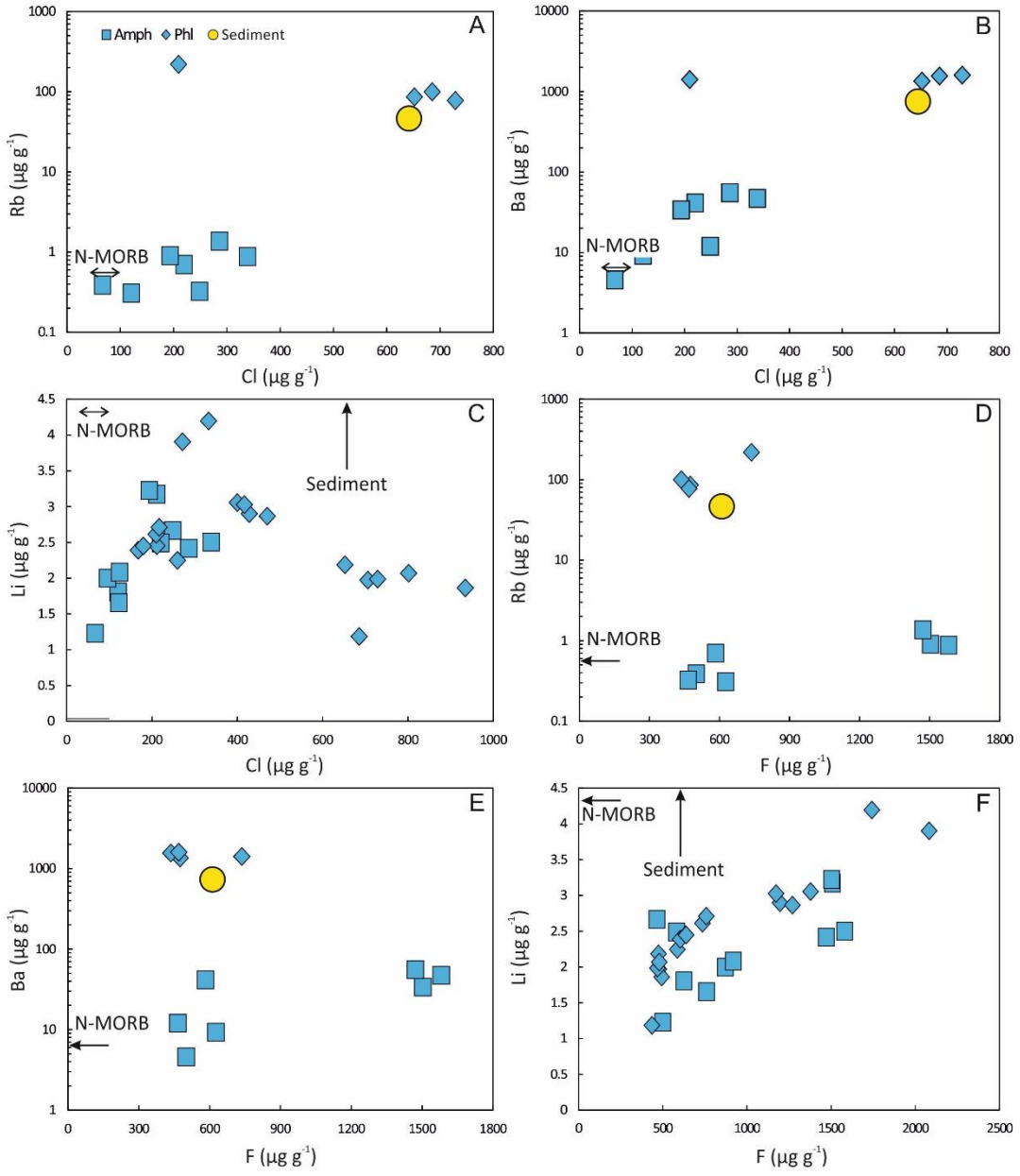

Figure 55. *A) to C) Fluid-mobile element abundances (Rb, Ba and Li) versus Cl and D) to F) F concentrations in Shiveluch vein amphibole and phlogopite. N-MORB is from Sun and McDonough (1989) and Urann et al. (2017), trace element Kamchatka sediment concentrations are from Plank (2014) and Cl and F concentrations of sediment derived from continental crust are from Barnes et al. (2018).*

4.6 Discussion

4.6.1 Depletion of Shiveluch peridotites

The majority of Shiveluch ultramafic xenoliths consist of harzburgites and dunites. It has been experimentally demonstrated that dunites are the products of extensive melt-rock reactions in the subarc mantle (Kelemen, 1990) and therefore cannot be used to estimate the degree of melt depletion. Percolation of basaltic melt through refractory mantle peridotite will produce olivine-saturated liquid. This liquid will retain high Mg# as it would equilibrate with the wall rock mantle peridotite and precipitate high Mg# olivine upon cooling, similar to the high Mg# olivine of the reactant refractory mantle peridotite (Kelemen, 1990).

Unlike dunite, harzburgite is a residual mantle lithology produced after extensive melt extraction from the subarc mantle. Veined Shiveluch harzburgites investigated in this chapter contain low modal percentages of primary orthopyroxene (< 16 %; Figure 40 and Table 8) and clinopyroxene (< 1 %; Figure 40 and Table 8) suggesting that these harzburgites were formed by previous melt extraction. The estimated degree of mantle melting is 18 % via Cr# of residual spinel (Hellebrand et al., 2001). Peridotite modal mineral abundances record larger degree of mantle melting of more than 20 % (Baker and Stolper, 1994), which is consistent with the absence of clinopyroxene in most of these samples. All clinopyroxene would have been consumed by 29 % wet melting of the subarc mantle (Bizimis et al., 2000).

The high degrees of melt extraction recorded in Shiveluch harzburgites might have been enhanced by elevated mantle temperature due to asthenospheric mantle flow around the edge of the subducting Pacific plate (Yogodzinski et al., 2001;

Münker et al., 2004). Shiveluch andesites possess geochemical signatures almost identical to those of adakites which are characterized by high Sr/Y (> 35) and low Y (< 18 μg g^{-1}; Defant and Drummond, 1990; Churikova et al., 2001; Yogodzinski et al., 2001). The 1964 host andesite also has adakite-like geochemical characteristics with Sr/Y = 38 and Y = 13.1 μg g^{-1}. The occurrence of adakite-like volcanic rocks at Shiveluch (Kepezhinskas et al., 1997; Yogodzinski et al., 2001; Münker et al., 2004) indicated that the mantle temperature was high enough to cause partial melting of the top of the subducting slab of otherwise old and cold Pacific plate subducting at a relatively shallow angle (35°; Gorbatov et al., 1997).

Similar to Avachinsky peridotites, the high Cr# of spinel and olivine forsterite component coupled with the high degrees of melt extraction preclude the origin of Shiveluch xenoliths as fragments of the SCLM (Figure 44B) or inclusions of older mantle veins. It has been demonstrated that the composition of the subarc mantle under the EVF and CKD approximates that of depleted N-MORB (Churikova et al., 2001; Churikova et al., 2007). Furthermore, the lack of evidence for subducted slabs older than 50 Ma under Kamchatka (Levin et al., 2002) indicates that the current metasomatized mantle xenoliths are representative of subarc metasomatism in the past 50 Ma.

4.6.2 Metasomatic processes in Shiveluch subarc mantle

Relatively little is known about metasomatic processes occurring in the subarc mantle beneath Shiveluch. It has been proposed that the hydrous veins cross-cutting Shiveluch mantle xenoliths are deuteric, i.e. they crystallized in equilibrium with water-rich magmatic fluids (Bryant et al., 2007). However, the low B and negative $\delta^{11}B$ of the vein amphibole and phlogopite suggested that they were produced in

equilibrium with fluids and melts derived from the AOC (Tomanikova et al., 2019). In the following section I elaborate on the proposed magmatic versus mantle origins of the hydrous vein minerals in Shiveluch mantle xenoliths and the extent and nature of metasomatic processes occurring in Shiveluch subarc mantle via the use of major and trace elements.

4.6.2.1 Evidence for multiple pulses of metasomatic activity from mineral major element compositions

Major element composition of melts in equilibrium with vein amphibole were calculated after Zhang et al. (2017). A broad range of amphibole equilibrium melt compositions, spanning from basalt to dacite, were calculated for xenolith *SHX03-04* whereas in the other Shiveluch veins, amphibole equilibrium melts cluster at either basaltic andesite or dacitic composition (Figure 56).

Two vein amphibole populations were recognized based on their major element compositions and equilibrium melt major element compositions. The first 'early-stage' vein amphibole population is located either at vein edges or in vein centres adjacent to orthopyroxene or phlogopite and is classified as pargasite, magnesiohastingsite and edenite (Figure 47B; Leake et al., 1997). It is slightly enriched in Na_2O and Al_2O_3 relative to the late-stage amphibole population and records equilibration with basalt and basaltic andesite similar in composition to high Mg# olivine-hosted melt inclusions from Shiveluch volcanic rocks (Figure 56; Iveson et al., *in prep*). Therefore, it is suggested that the early-stage vein amphibole equilibrated with basaltic melt in the lithospheric mantle (Figure 57 and Equation 23). Only a few grains (n = 7) of the early-stage amphibole were identified in *SHX03-04*.

The second 'late-stage' vein amphibole population is located at selvages and at vein centres adjacent to interstitial albite-rich plagioclase (i.e. Na-rich) and is classified as magnesiohornblende and tschermakite (Figure 47A; Leake et al., 1997). It records equilibration with dacite and rhyolite identical to evolved amphibole- and plagioclase-hosted melt inclusions from Shiveluch arc volcanic rocks (Humphreys et al., 2008). Selvage and vein amphibole located at vein edges that connect to the selvage record equilibration with the most evolved melts (dacites). In *SH98X-16* and *SHX03-04*, amphibole equilibrium melt composition shifts from dacitic to andesitic moving away from the selvage into the centre of the vein. The intruding dacitic melt re-equilibrated with the pre-existing vein minerals (i.e. amphibole, phlogopite and orthopyroxene) and vice versa as it percolated into the vein centre, thus shifting its composition from dacitic to andesitic in harzburgite *SH98X-16* (Figure 58 Inset B):

$$NaCa_2(Mg_4Al)(Si_6Al_2)O_{22}(OH)_2 + MgSiO_3 + KMg_3AlSi_3O_{10}(OH)_2 + melt\ (4SiO_2) \rightarrow Ca_2(Mg_4Al)(Si_7Al)O_{22}(OH)_2 + NaAlSi_3O_8 + MgSiO_3 + KMg_3AlSi_3O_{10}(OH)_2 \quad \textbf{Equation 25}$$

In harzburgite *SHX03-18*, amphibole equilibrium melt composition also shifts linearly from dacitic to andesitic moving closer to the harzburgite-selvage interface. Reactive percolation of dacitic melt into the mantle harzburgite immediately prior to the eruption produced a narrow reaction zone in which the intruding melt shifted its composition from dacitic to andesitic:

$2Mg_2SiO_4 + MgSiO_3 + KMg_3AlSi_3O_{10}(OH)_2 + melt\ (2\ CaO,\ ½\ Na_2O,\ 1½\ Al_2O_3,\ 8\ SiO_2\ and\ H_2O) \rightarrow Ca_2(Mg_4Al)(Si_7Al)O_{22}(OH)_2 + NaAlSi_3O_8 + MgSiO_3 + KMg_3AlSi_3O_{10}(OH)_2$ **Equation 26**

It has been proposed that andesitic melt compositions are products of mixing between basaltic and evolved melts in the upper crustal magma reservoirs (Reubi and Blundy, 2009). Their study demonstrated bimodal distribution of melt inclusion compositions in arc volcanic rocks with peaks centred at basaltic and silicic compositions and andesitic compositional gap which is inconsistent with the widespread eruption of andesite at arc volcanoes. Consistent with the study of Reubi and Blundy (2009), reaction of dacitic melt with the pre-existing mantle lithospheric veins and mantle harzburgite in Shiveluch xenoliths produces andesitic melt (Figure 56). Furthermore, Humphreys et al. (2006) demonstrated that Shiveluch upper-crustal magma chamber is formed by accumulation of small magma batches of both mafic and felsic compositions. They found quenched mafic andesite enclaves consisting of amphibole, plagioclase, orthopyroxene and oxides in the host andesite. The bulk composition of the enclave is more mafic than that of the host andesite indicating that it formed from a rapidly undercooled basaltic melt (Blundy and Sparks, 1992). The volume of the basaltic melt must have been very small relative to the host andesite in order to by-pass crystallization of the liquidus and near-liquidus assemblage of olivine, clinopyroxene and plagioclase (Blundy and Sparks, 1992). Apart from mafic magma, small batches of felsic magma were identified via complex plagioclase zoning (Humphreys et al., 2006). Cores of sieve plagioclase phenocrysts are albitic and record crystallization in dacitic magma whereas its rims have higher anorthite component (i.e Ca-plagioclase endmember) and record

crystallization in more mafic magma (Humphreys et al., 2006). Interstitial plagioclase in Shiveluch veins is albite-rich which therefore indicates that the late-stage amphibole re-equilibrated with evolved dacitic melt in the upper crustal magma chamber (Figure 58).

Alternatively, the early-stage vein amphibole might have re-equilibrated with the evolved melt in the lithospheric mantle at the crust-mantle boundary. Complex zoning of high-Mg# olivine phenocrysts from Shiveluch basaltic maar deposit and the high P-T- fO_2 conditions of olivine crystallization equivalent to 18 to 30 km depth indicated that olivine re-equilibrated with melts of both basaltic and more evolved compositions in the lithospheric mantle (Gordeychik et al., 2018). The final mafic melt-olivine overgrowth formed in only 1 to 10 days, which is consistent with the rapid onset of the eruption required to transport mantle xenoliths to the surface (Gordeychik et al., 2018).

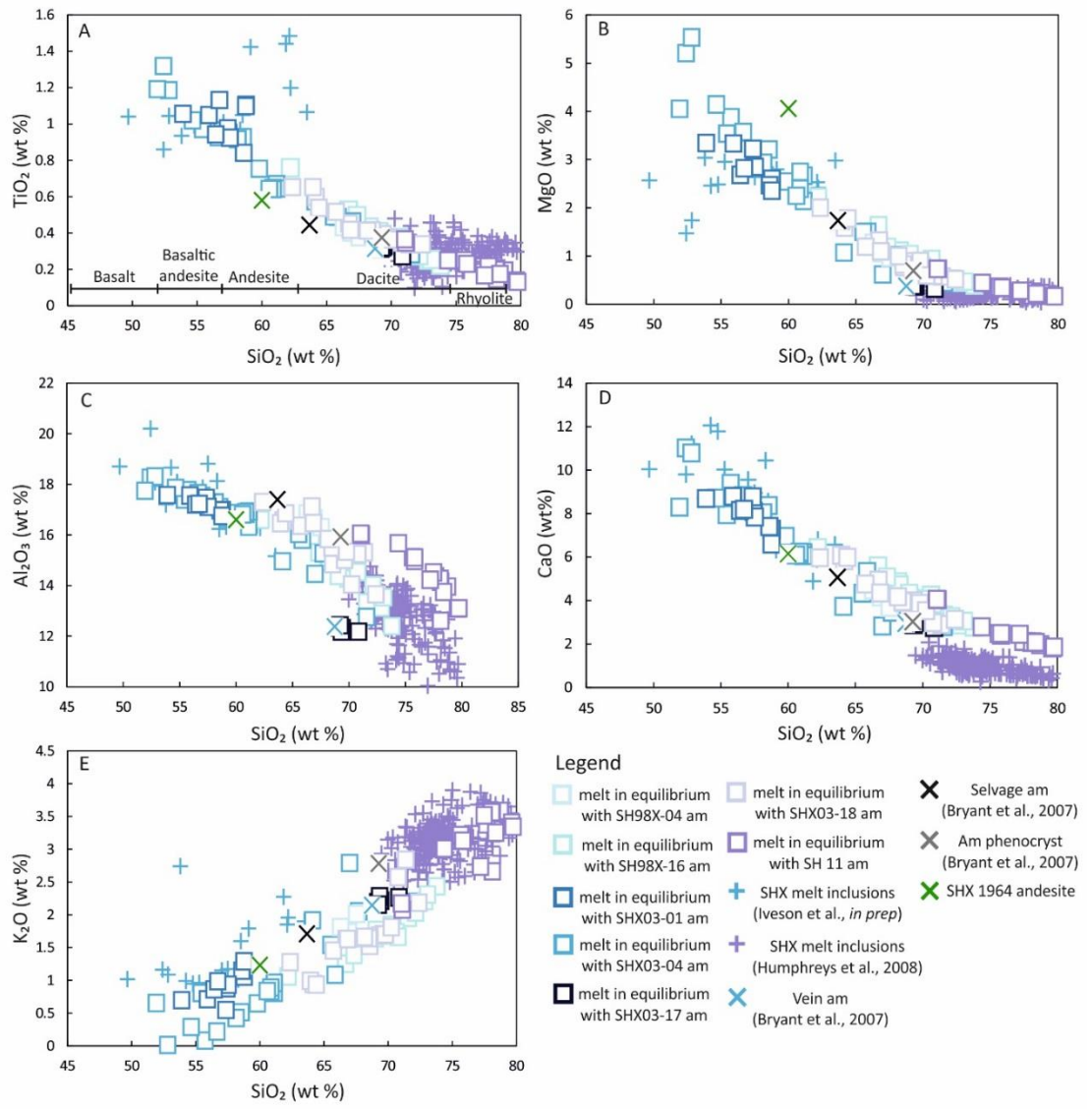

Figure 56. *A) to E) Major element composition and classification of melts in equilibrium with Shiveluch vein amphibole and amphibole from reaction zone in SH11 calculated after Zhang et al. (2017). Melt classification scheme is adopted from Le Bas et al. (1986). Shiveluch melt inclusions are from Iveson et al. (in prep) and Humphreys et al. (2008) and vein amphibole, selvage amphibole and amphibole phenocryst are from Bryant et al. (2007).*

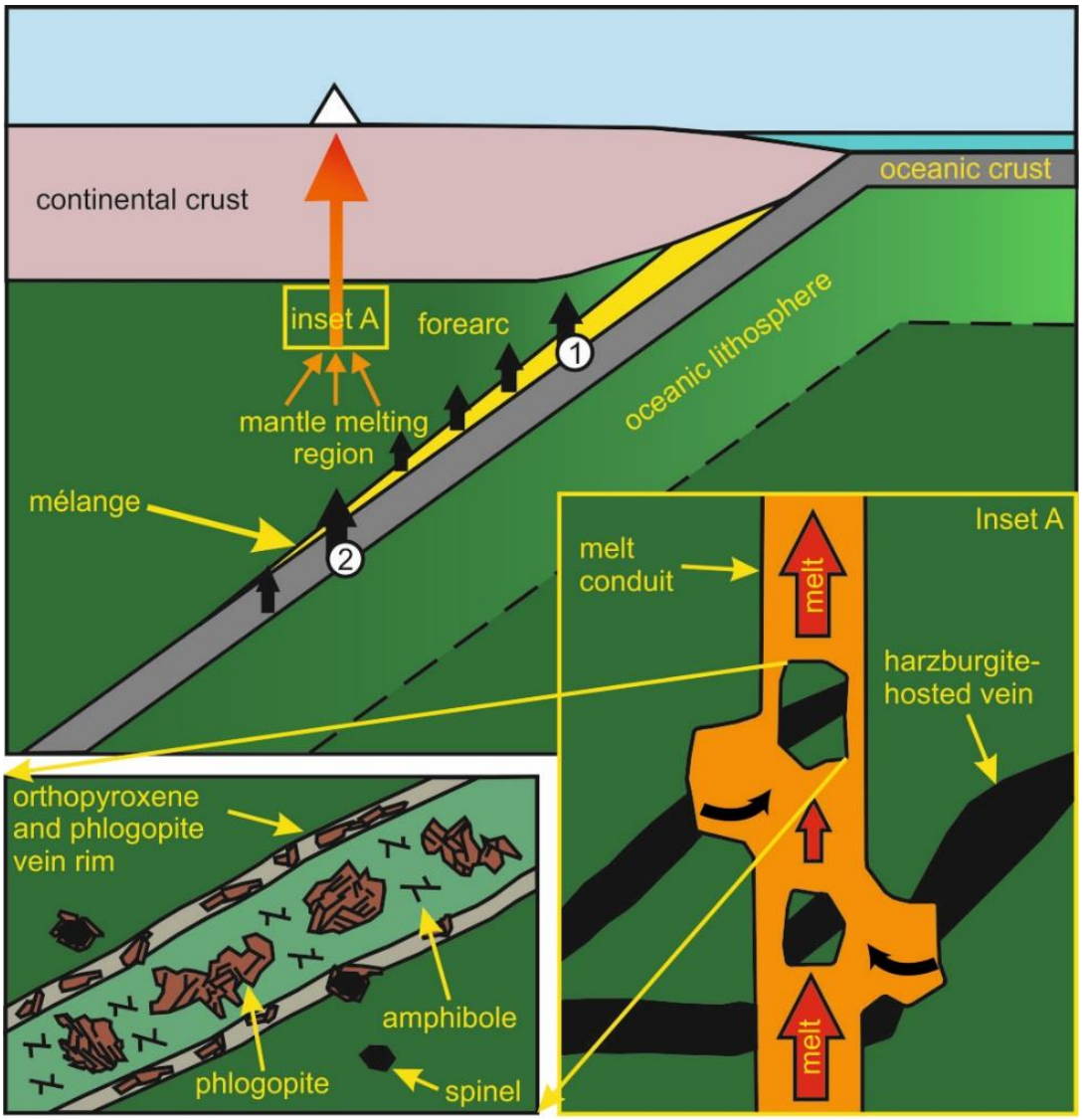

Figure 57. *Generation of veined mantle lithosphere underneath the Shiveluch. Slab-derived melts and fluids (black arrows) percolate through an inter-connected vein network through the lithospheric mantle (zoom-in on inset A), fragments of which are entrained into magma (orange arrows) on its way up to the surface (inset A). The position of inset A corresponds to the depth from which the xenoliths were derived (30-50 km).*

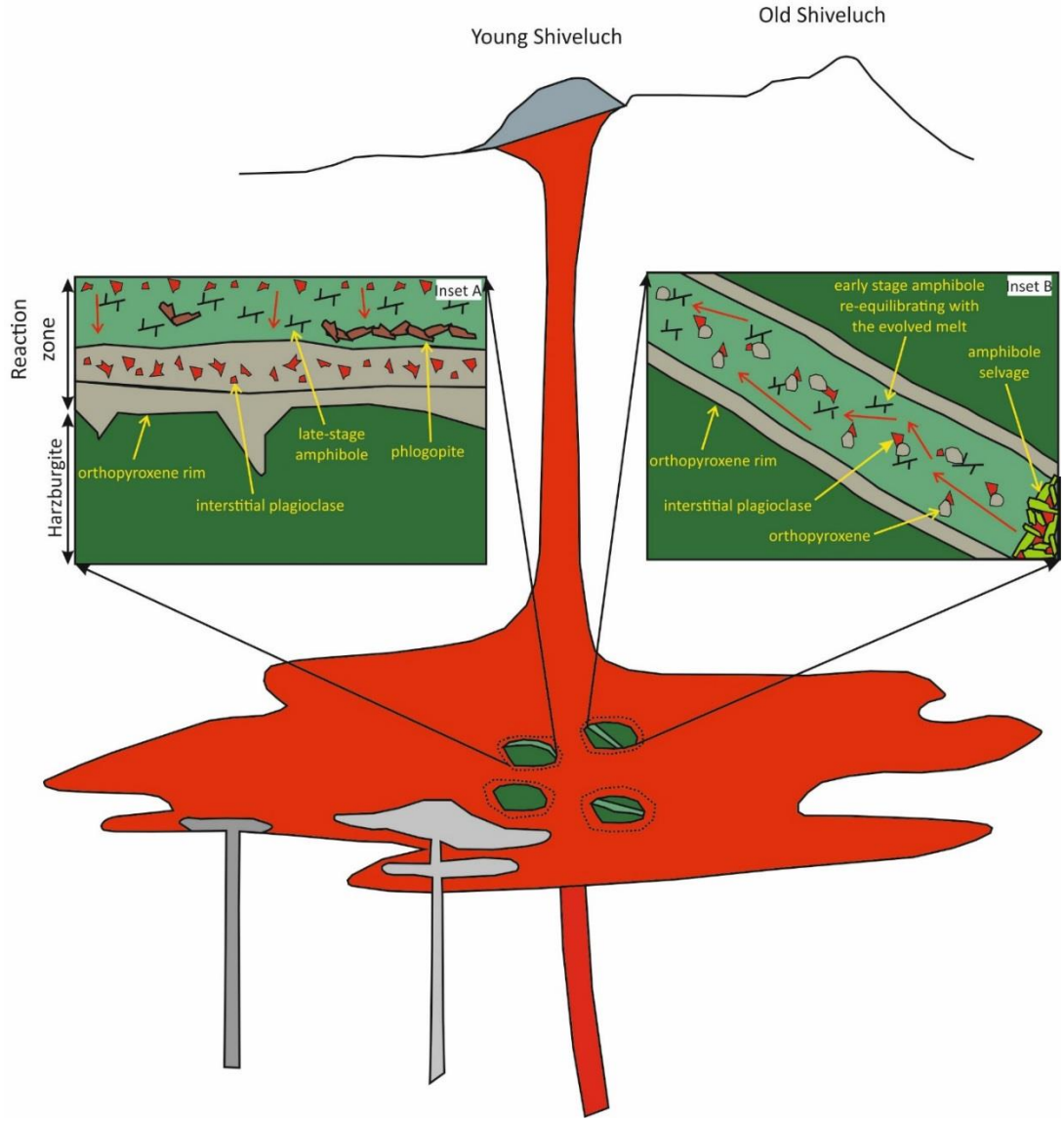

Figure 58. *Late-stage melt-rock reactions taking place in the upper crustal magma chamber. Inset A illustrates a reaction zone between harzburgite SHX03-18 and dacite (red arrows). Inset B illustrates percolation of dacitic melt (red arrows) through a pre-existing vein in SHX03-04. Both melt-rock reaction types occur immediately prior to the eruption. Figure is modified after Humphreys et al. (2006).*

4.6.2.2 Evidence for multiple pulses of metasomatic activity from mineral trace element compositions

Amphibole trace element compositions presented in this chapter belong to the late-stage vein amphibole that equilibrated with evolved melts. Shiveluch late-stage

vein amphibole is enriched in all incompatible trace elements relative to phlogopite, particularly in Th, U and REE, and is enriched in LREE relative to HREE (i.e. concave-up REE distribution patterns; Figure 50B). Trace element (Rb, Sr, Pb, Zr, Nb, La, Ce, Nd, Sm, Gd, Dy, Ho, Er, Yb, Lu, Y) composition of melts in equilibrium with vein amphibole were calculated after Humphreys et al. (2019) who applied multiple regression analysis to experimental calcic amphibole synthesized at a wide range of conditions (P = 0.2 to 2.5 GPa and T = 780 to 1100 °C). Their method allows for temperature- and pressure-independent calculation of trace element partition coefficients from amphibole major element composition, which exerts the main control on trace element partitioning into amphibole (Nandedkar et al., 2016; Humphreys et al., 2019). The REE composition of melts in equilibrium with Shiveluch early-stage vein amphibole could not have been constrained because of the lack of trace element composition data for this amphibole population.

The REE composition of melts in equilibrium with Shiveluch late-stage vein amphibole are identical to that of average evolved amphibole- and plagioclase-hosted melt inclusions from Shiveluch volcanic rocks (Humphreys et al., 2008) and average primitive (high-Mg#) continental andesite (Kelemen et al., 2003). Experimental study on the origin of high-Mg# andesites by Wood and Turner (2009) demonstrated that they formed in equilibrium with harzburgite at P > 0.7 GPa in the lithospheric mantle. Their high SiO_2 and MgO contents were attributed to equilibration with olivine and orthopyroxene in the residual harzburgite. Indeed, high-Mg# andesite can commonly form in Shiveluch subarc mantle because of its highly depleted (i.e. harzburgitic) composition (section 4.6.1) and could have percolated through the veins to produce the early-stage amphibole (Equation 23).

Alternatively, high Mg# andesite can be formed by mixing of ultramafic xenoliths and evolved melts as recorded by the REE composition of dacitic and andesitic melts in equilibrium with late-stage amphibole (Figure 50B). Furthermore, it is concluded that fractional crystallization of high-Mg# andesitic parental melt can produce REE signature of the evolved dacitic melt trapped in amphibole- and plagioclase-hosted melt inclusions via removal of REE from the fractionating melt by crystallization of amphibole and clinopyroxene.

Unlike amphibole, phlogopite is enriched in Rb, Ba, Pb and Cs (Figure 51A) and is depleted in REE (often below detection limit; Figure 51B) relative to the primitive mantle (McDonough and Sun, 1995). Phlogopite containing chlorite lamellae is REE enriched relative to phlogopite free of chlorite lamellae and its REE distribution trend is similar to that of the host andesite (Figure 52). Therefore, it is suggested that melt with which phlogopite last equilibrated is related to the host andesite.

The high Nb/U and Cs/U of phlogopite grains indicate percolation of a hydrous melt derived from melting of the AOC and dehydration of forearc serpentinite, respectively (Figure 59A; Foley et al., 2000 and Peters et al., 2017). The mixed signature might indicate physical mixing of the two liquids in the lithospheric subarc mantle or serpentinite-derived fluid flux-melting of the AOC.

Dehydration of forearc serpentinite characteristically releases LILE, ^{11}B, Li, LREE, U and Cl (John et al., 2011; Spandler et al., 2014) and produces elevated Cs/U and Rb/U relative to abyssal serpentinite (Peters et al., 2017). In oxidizing oceanic environment, serpentinization leads to U enrichment whereas in the forearc, reduced sediment-derived fluids mobilize Cs relative to U (Peters et al., 2017). Shiveluch phlogopite possesses higher Rb/U values than that observed in forearc

serpentinite (Figure 59B) because Rb and other LILE (e.g. Ba) are more compatible in phlogopite (LaTourrette et al., 1995). Trace element composition of melt in equilibrium with Shiveluch phlogopite could not have been constrained because of the lack of comprehensive trace element phlogopite-melt partitioning studies (LaTourrette et al., 1995). However, trace element composition of fluid in equilibrium with Shiveluch phlogopite was constrained using partition coefficients from Adam et al. (2014). These fluid compositions lie within forearc serpentinite field (Peters et al., 2017) indicating ubiquitous percolation of forearc serpentinite-derived fluids through Shiveluch subarc mantle. Some Shiveluch phlogopite grains possess $\delta^{11}B$ higher than that of the depleted mantle (> -7.1 ‰; Marschall et al., 2017) which has also been attributed to percolation of a small amount of forearc serpentinite-derived fluids (Tomanikova et al., 2019).

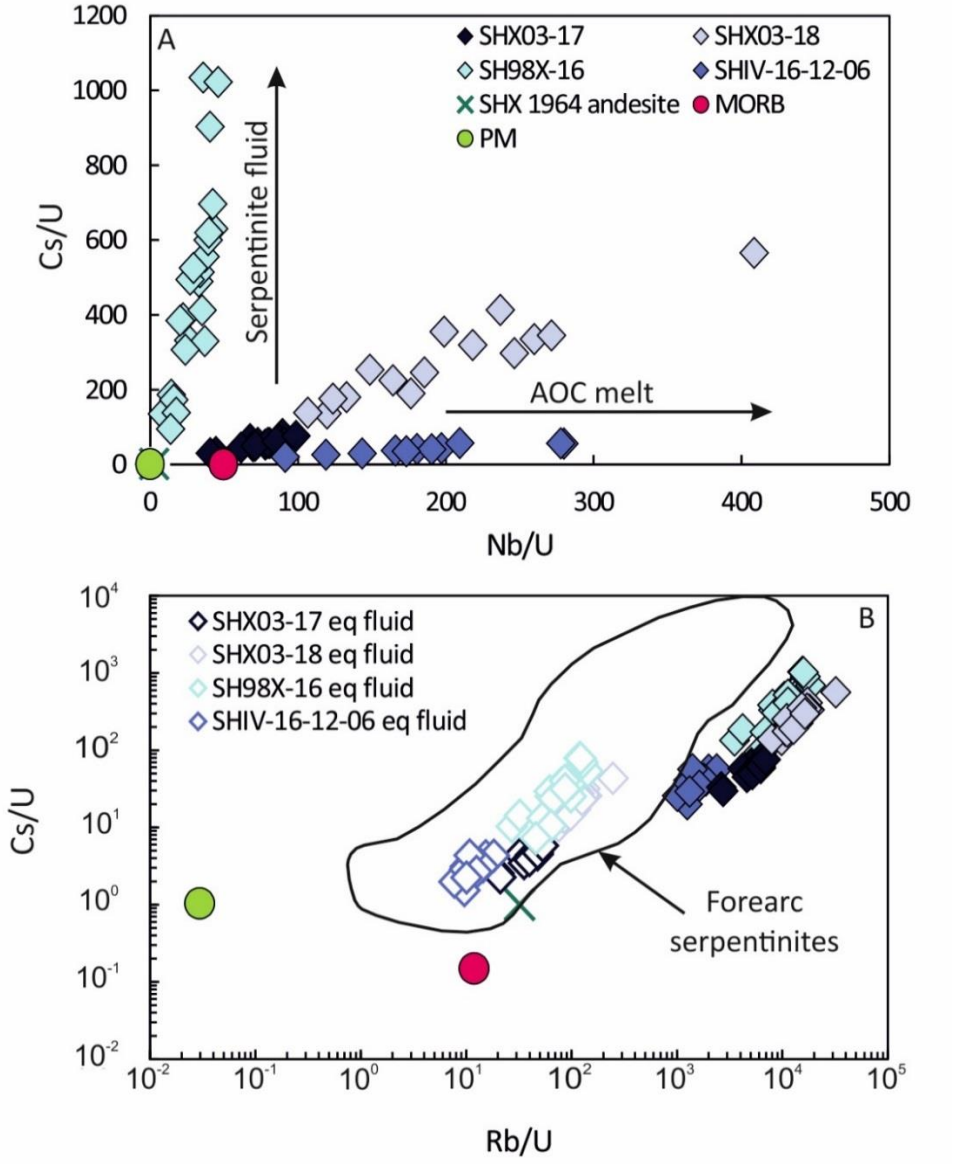

Figure 59. *Shiveluch phlogopite trace element ratios characteristic of A) forearc serpentinite dehydration (Cs/U) and altered oceanic crust (AOC) melting (Nb/U) and B) forearc serpentinite dehydration. All phlogopite grains possess high Cs/U and Rb/U typical for forearc serpentinites (Peters et al., 2017) and the majority of phlogopite grains possess high Nb/U characteristic of AOC melts in equilibrium with rutile (Foley et al., 2000). Compositions of melt in equilibrium with phlogopite were calculated from partitioning coefficients taken from Adam et al. (2014). Forearc serpentinite field is from Peters et al. (2017), primitive mantle (PM) is from McDonough and Sun (1995) and MORB is from Sun and McDonough (1989).*

4.6.3 Hydroxyl site occupancy of hydrous vein minerals

4.6.3.1 Excess H_2O in phlogopite

Water contents of vein amphibole and phlogopite range from 2.23 to 2.87 wt % and from 4.26 to 6.74 wt %, respectively (Table 12). Amphibole typically contains 2 to 3 wt % H_2O, equivalent to up to 2 atoms per formula unit in the hydroxyl site whereas mica typically contains 4 to 5 wt % H_2O, equivalent to up to 4 atoms per formula unit in the hydroxyl site (Deer et al., 1992). However, Shiveluch phlogopite contains H_2O in excess of the maximum estimated 5 wt% (Deer et al., 1992). The highly reproducible SIMS analyses and the ubiquitous presence of chlorite lamellae in phlogopite grains exploiting its cleavage planes (Figure 41 and Figure 42) indicate that an incomplete phlogopite-chlorite reaction must have elevated H_2O contents of phlogopite (chlorite can contain up to 13 wt % water; Deer et al., 1992). Chlorite lamellae occur in most phlogopite in all Shiveluch samples and at times might not have been avoided during analysis. Similar phlogopite-chlorite replacement reactions were observed in Franklin Marble Formation, Farber Quarry, Franklin, New Jersey, whereby phlogopite was replaced by chlorite along discrete lamellae on µm-scale through a low-temperature hydrothermal process (Yau et al., 1984):

$$KMg_3AlSi_3O_{10}(OH)_2 + melt\ (2\ MgO, ½\ Al_2O_3\ and\ 6\ H_2O) \rightarrow \quad \textbf{Equation 27}$$
$$Mg_5Al(AlSi_3O_{10})(OH)_8 + melt\ (½\ K_2O)$$

Phlogopite alteration to chlorite is attributed to percolation of evolved melts in Shiveluch magma chamber imminently prior to eruption, which also formed

selvage-related late-stage vein amphibole (Figure 56). Unlike the late-stage amphibole that was produced by dissolution-re-crystallization of the early-stage vein amphibole population, phlogopite was altered into chlorite along discrete planes (Figure 41 and Figure 42). The absence of interstitial plagioclase in between phlogopite grains indicates that the evolved melt reacted with phlogopite along cleavage planes to produce chlorite lamellae and propagated through phlogopite grains towards the vein centres.

4.6.3.2 Chlorine in amphibole and phlogopite

The unusually high concentration of H_2O in some Shiveluch phlogopite grains, and the generally high H_2O concentration in all of the hydrous phases in the veins suggests that their hydroxyl sites are predominantly occupied by H_2O (/OH) leaving a limited capacity for Cl and F (Figure 53). The strong incompatibility of Cl in mantle amphibole and phlogopite is a consequence of "the Mg-Cl crystallographic avoidance principle" (e.g. Munoz and Swenson, 1981; Oberti et al., 1993 and references therein). In Cl-rich amphibole, the larger ionic radius of Cl is accommodated by Fe^{2+} substitution for Mg^{2+} and by Al^{3+} substitution for Si^{4+}, both substitutions expanding and thus distorting octahedral and tetrahedral sites, respectively. This substitution principle is demonstrated in Figure 54 in which amphibole Cl content increases with decreasing MgO and increasing FeO. Chlorine anions tend to bond with Fe^{2+} in the octahedral site and with larger alkalis, such as K, in the A site in amphibole and in the interlayer site in mica (Volfinger et al., 1985; Oberti et al., 1993). In phlogopite, the interlayer site that contains K is, however, too small to accommodate the large Cl^- (Volfinger et al., 1985). Therefore, Mg-rich vein amphibole and phlogopite in Shiveluch xenoliths can accommodate

only trace amounts of Cl (up to 350 µg g^{-1} and up to 950 µg g^{-1}, respectively; Figure 53).

Amphibole major element composition and thus its capacity to incorporate Cl is mostly affected by fO_2 and melt chemistry, particularly its halogen content (Iveson et al., 2017). Experiments conducted at low fO_2 (< NNO +1.0) yielded amphibole with lower MgO and higher Fe^{2+} contents, while Fe^{3+} content did not differ from amphibole that crystallized from more oxidized melts. Thus, relatively higher Fe^{2+} contents (and hence lower Mg#) of amphibole crystallizing under reducing conditions increases the amount of Cl that can be accommodated in the structure. Under more oxidizing conditions, Cl generally strongly partitions into an exsolved fluid phase, rather than remaining in the melt or the growing amphibole due to lower Fe^{2+} contents of the amphibole. The presence of other halogens, particularly F, and their abundance in both the melt and amphibole also exerts a strong control on Cl partitioning into amphibole. Iveson et al. (2017) observed a decrease in Cl partitioning into amphibole with increased F content of amphibole and melt.

4.6.3.3 Fluorine in amphibole and phlogopite

Unlike Cl, F is compatible in both mantle amphibole (Bénard et al., 2017) and phlogopite (Edgar and Pizzolato, 1995), F contents range from 465 to 1580 µg g^{-1} and from 435 to 2090 µg g^{-1}, respectively in Shiveluch hydrous vein minerals (Figure 53). In biotite and phlogopite, F content is controlled by mineral structure and fluid and/or melt composition with which the mica last equilibrated (Munoz, 1984; Guidotti, 1984; Speer, 1984 and references therein). Magnesium-rich biotite contains more F than Fe-rich biotite, consistent with “the Fe-F avoidance principle” (Munoz, 1984; Guidotti, 1984; Speer, 1984 and references therein). Equally,

trioctahedral mica (e.g. phlogopite) whose octahedral site is fully occupied by divalent cations tend to incorporate more F relative to dioctahedral mica whose octahedral site is partially vacant (Robert et al., 1993). In dioctahedral micas, octahedral substitutions involving Ti^{4+} and Al^{3+} create vacancies ($2M^{2+} = Ti^{4+}$ + [vacancy] and $3M^{2+} = 2Al^{3+}$ + [vacancy], respectively; Finch, 1995) which favour incorporation of OH^- relative to F^- into the hydroxyl site (Robert et al., 1993). Polar OH^- preferentially sits next to octahedral vacancies in mica, where H^+ bonds with O^{2-} of the adjacent tetrahedra, such as is typical in dioctahedral mica (e.g. muscovite; Robert et al., 1993). In contrast, OH^- in trioctahedral mica acts as a single anion whose H^+ does not interact with tetrahedral O^{2-}. Thus, F^- can readily replace OH^- in phlogopite and, similarly in amphibole (Robert et al., 1993), if available in fluid and/or melt with which the hydrous mineral last equilibrated.

Partitioning of F in favour of amphibole and phlogopite is also affected by fluid and melt composition, specifically by speciation of F and melt H_2O content. Fluorine forms complexes with Si and Al in aluminosilicate melts (Dalou et al., 2015) and its solubility dramatically increases at higher melt H_2O contents (Dalou and Mysen, 2015; Bénard et al., 2017). In contrast, Cl complexes with alkalis and alkaline earth metals such as Na, K and Ca (Webster and De Vivo, 2002; Dalou et al., 2015; Webster et al., 2015) and its solubility decreases at higher melt H_2O contents (Dalou and Mysen, 2015). Therefore, it has been proposed that Cl/F is a sensitive indicator of dissolved water content of magmas (Dalou et al., 2014; Dalou and Mysen, 2015).

4.6.4 Melt halogen (Cl and F) composition

The halogen composition of melt that last equilibrated with Shiveluch hydrous vein minerals has been constrained by partition coefficients of Cl and F between amphibole, phlogopite and melt at upper-crustal and subarc mantle pressure-temperature conditions, respectively (Edgar and Pizzolato, 1995; Iveson et al., 2017). Fluorine content of melt in equilibrium with Shiveluch phlogopite ranges from 280 to 1600 µg g^{-1} (Edgar and Pizzolato, 1995) and that of melt in equilibrium with late-stage vein amphibole ranges from 28 to 480 µg g^{-1} (Table 13; Iveson et al., 2017). The high F content of melt in equilibrium with phlogopite is attributed to dehydration of F-rich minerals such as amphibole, phengite and lawsonite in the increasingly deeper parts of the AOC (Portnyagin et al., 2007; Churikova et al., 2007). Chlorine content of melt in equilibrium with phlogopite cannot be calculated at present. In previous studies it has been noted that synthetic phlogopite does not incorporate Cl, whose distribution coefficient between phlogopite and melt and/or fluid remains unknown (Munoz and Swenson, 1981; Volfinger et al., 1985). The concentration of Cl in melt in equilibrium with late-stage amphibole ranges from 190 to 900 µg g^{-1} at 5.9 % H_2O melt content, but rises to 2850 µg g^{-1} at the lower 4.3 % H_2O melt content (Table 13; Dalou et al., 2014). Lower Cl melt concentrations ranging from 194 to 518 µg g^{-1} at 2.52 % H_2O content (Table 13) were estimated from late-stage amphibole major element compositions following the method of Giesting and Filiberto (2014) and average evolved amphibole- and plagioclase-hosted melt inclusion water content from Humphreys et al. (2008):

$$K_{Cl} = \frac{\left(\frac{X_{Cl}}{X_{OH}}\right)_{amphibole}}{\left(\frac{[Cl]}{[OH]}\right)_{melt}} \qquad \textit{Equation 28}$$

where

$$ln\,K_{Cl} = \frac{6.59K}{(Na + {}^{A}\square)} - 0.679Mg + 0.487{}^{[6]}Fe \qquad \textbf{\textit{Equation 29}}$$

and X is the mole fraction of an anion in the O(3) site and K, Na, $^{A}\square$ (vacancy in amphibole A site), Mg and $^{[6]}$Fe are amounts of each component in amphibole in atoms per formula unit.

The model of Giesting and Filiberto (2014) was calibrated for water-saturated shallow crustal magmatic environments corresponding to a narrow temperature and pressure range of 800 to 850 °C and 1.85 to 3 kbar, respectively. Thus, the melt composition estimates calculated after Giesting and Filiberto (2014) might be more applicable to Shiveluch late-stage vein amphibole that equilibrated with evolved melts than those calculated after Dalou et al. (2014).

Melts that equilibrated with late-stage vein amphibole do not have the same halogen (Cl and F) compositions as those recorded in Shiveluch olivine-hosted melt inclusions which are enriched in both Cl and F (Figure 60; Iveson et al., *in prep*). Olivine-hosted melt inclusions record primary basaltic melts trapped during the formation of high-Mg# olivine in the lithospheric subarc mantle whereas the late-stage vein amphibole records equilibration with evolved dacitic melts in the upper-crustal magma chamber prior to the eruption. However, melts that equilibrated with the late-stage vein amphibole differ in Cl concentration from evolved Shiveluch amphibole- and plagioclase-hosted melt inclusions (average Cl = 1480 µg g^{-1}; Humphreys et al., 2008). Evolved melts stored in the magma chamber commonly lose exsolved volatiles such as H_2O and Cl via degassing, which would shift Cl composition of evolved melts in the magma chamber to lower values. Melt inclusions trapped in high-Mg# olivine, and potentially in amphibole and

plagioclase phenocrysts, cannot readily lose Cl and F via degassing and diffusive re-equilibration through the host olivine (Bucholz et al., 2013) and therefore record higher Cl contents than those of the calculated evolved melts in equilibrium with the late-stage amphibole. Consistent with the affinity of Cl for H_2O-rich fluid phase and its consequent degassing from evolved magmas, experimental studies of Cl solubility across a range of melt compositions (at P < 3 kbar) demonstrate that primitive basaltic melts have much higher Cl solubilities relative to more evolved dacitic and rhyolitic melts stored at the same conditions (Webster et al., 1999; Chevychelov and Suk, 2003; Webster et al., 2015).

Table 13. *Calculated Cl, F and Cl/OH of amphibole equilibrium melt*

Sample	Mineral	Cl*	Cl†	F min[#]	F max[#]	Cl/OH[§]	Cl[§]
SH98X-16	Am 1	604.00	190.15	28.20	142.12	nd	nd
	Am 2	564.30	177.65	30.13	151.85	nd	nd
	Am 3	1016.63	320.05	37.70	189.97	0.011	269.08
	Am 4	2092.32	658.69	28.03	141.26	0.021	517.74
	Am 5	1852.14	583.08	35.07	176.72	0.015	388.13
	Am 6	1031.00	324.57	45.76	230.60	0.008	193.56
SHX03-17	Am 1	806.30	253.83	52.51	264.60	0.017	430.55
	Am 2	1043.71	328.57	55.31	278.73	0.021	517.06
SHX03-18	Am 1	1775.99	559.11	90.70	457.08	nd	nd
	Am 2	1628.28	512.61	90.44	455.75	nd	nd
SHX03-04	Am 1	2847.00	896.28	95.09	479.20	0.018	451.73
	Am 2	2406.85	757.71	88.53	446.12	0.020	496.84

Abbreviations: Am = amphibole, nd = not determined

*D_{Cl} from run CD2H4 at 4.3 % H_2O melt content (Dalou et al., 2014)

†D_{Cl} from run CD2H6 at 5.9 % H_2O melt content (Dalou et al., 2014)

D_F from runs 1-14-02 and 1-16-14A with corresponding analytical errors of 1.05 and 0.11, respectively (Iveson et al., 2017)

[§]Calculated after Giesting and Filiberto (2014) with statistically significant r value ranging from 0.86 to 0.95 and r^2 value ranging from 0.7 to 0.84 and average H_2O melt content of 2.52 ± 1.47 wt% from Humphreys et al. (2008)

Halogen (Cl and F) composition of melt generated by flux-induced partial melting of the depleted MORB mantle (DMM) lherzolite has been calculated via the

following non-modal batch melting equation originally adopted from Johnson et al. (1990) and later modified by Eiler et al. (2000):

$$C_i^{arc\ magmas} = \frac{C_i^{DMM} + \alpha x\left(C_{H_2O}^{slab\ flux}\right)^{-1}\left(C_i^{slab\ flux} - C_i^{DMM}\right)}{\bar{D}_i^{lherzolite/arc\ magma} + x(1 - \bar{P}_i^{lherzolite/arc\ magma})} \qquad \textbf{Equation 30}$$

The above equation is often adopted (e.g. Dalou et al., 2014; Van den Bleeken and Koga, 2015; Bénard et al., 2017) to model melt content of an element *i* generated by various degrees of melting (denoted by *x*) of the DMM fluxed by AOC-derived fluids and melts. Chlorine and F composition of the DMM is 0.24 and 6.75 µg g^{-1}, respectively (average values taken from Urann et al., 2017), AOC-derived fluid is 9390 and 990 µg g^{-1}, respectively (Straub and Layne, 2003), AOC-derived melt is 14800 and 13700 µg g^{-1}, respectively (LeVoyer et al., 2010) and granitic melt is 3500 and 39000 µg g^{-1}, respectively (Webster et al., 2004). Water content of the AOC-derived fluid is 25 wt % (Straub and Layne, 2003) and that of the AOC-derived melt is 44.5 wt % (LeVoyer et al., 2010). The rate of flux melting (α) is defined as the amount of H_2O added to the lherzolite divided by the degree of mantle melting (i.e. addition of 1 wt % H_2O causes 10 wt % partial melting; Eiler et al., 2000). Experimentally determined melt water contents of 2.6, 4.9 and 5.9 wt % (Dalou et al., 2014) were selected to calculate α values reflecting increasing levels of mantle metasomatism.

Bulk distribution coefficients of Cl and F between spinel lherzolite and melt ($D_i^{lherzolite/melt}$) and bulk melt partition coefficients ($P_i^{lherzolite/melt}$) were constrained from distribution coefficients between olivine, orthopyroxene, clinopyroxene (mineral proportions were taken from Workman and Hart, 2005) and melt (stoichiometric coefficients of minerals participating in hydrous melting at 1.2 GPa

were taken from Gaetani and Grove (1998) and distribution coefficients were taken from Dalou et al. (2014).

Shiveluch high-Mg# olivine-hosted melt inclusions lie along the DMM-AOC melt mixing line (Figure 60A) rather than the DMM-AOC fluid mixing line (Figure 60B). Relatively low to intermediate degrees of mantle melting (< 5 %) triggered by influx of hydrous AOC-derived melt (< 4.9 % H_2O, but mostly < 2.6 % H_2O) are required to produce melt identical to that trapped in Shiveluch high-Mg# olivine-hosted melt inclusions (Figure 60A). Some Shiveluch olivine-hosted melt inclusions possess higher F contents than could have been successfully modelled based on the halogen estimate of the AOC-derived melt (Figure 60A; Le Voyer et al., 2010). It has been demonstrated that melts derived from increasingly deeper parts of the AOC (up to 180 km depth-to-slab) have higher F abundances than melts derived from shallower parts of the AOC (100 km depth-to-slab; Portnyagin et al., 2007). The breakdown of amphibole and phengite in the AOC mobilizes F which becomes readily soluble in the increasingly SiO_2-rich AOC-derived melts (Portnyagin et al., 2007; Dalou et al., 2015; Debret et al., 2016).

In contrast to Shiveluch high-Mg# olivine-hosted melt inclusions, the estimated Cl and F composition of melts (both Cl and F < 500 µg g^{-1}) that equilibrated with Shiveluch late-stage amphibole can not be interpreted via the mantle melting model because these evolved melts originated in the upper crutal magma chamber rather than in the subarc mantle. Their halogen (Cl and F) compositions lie at the lower range of evolved melt inclusions from arc volcanic rocks (Aiuppa et al., 2009 and references therein), and are lower than those from Shiveluch (Cl = 900 to 2400 µg g^{-1}; Humphreys et al., 2008). In these evolved hydrous melts, Cl and F were likely lost

via degassing (Pyle and Mather, 2009). Additionally, F might have been taken up by a F-rich mineral such as fluorite, topaz or zinnwaldite (e.g. Webster et al., 2004).

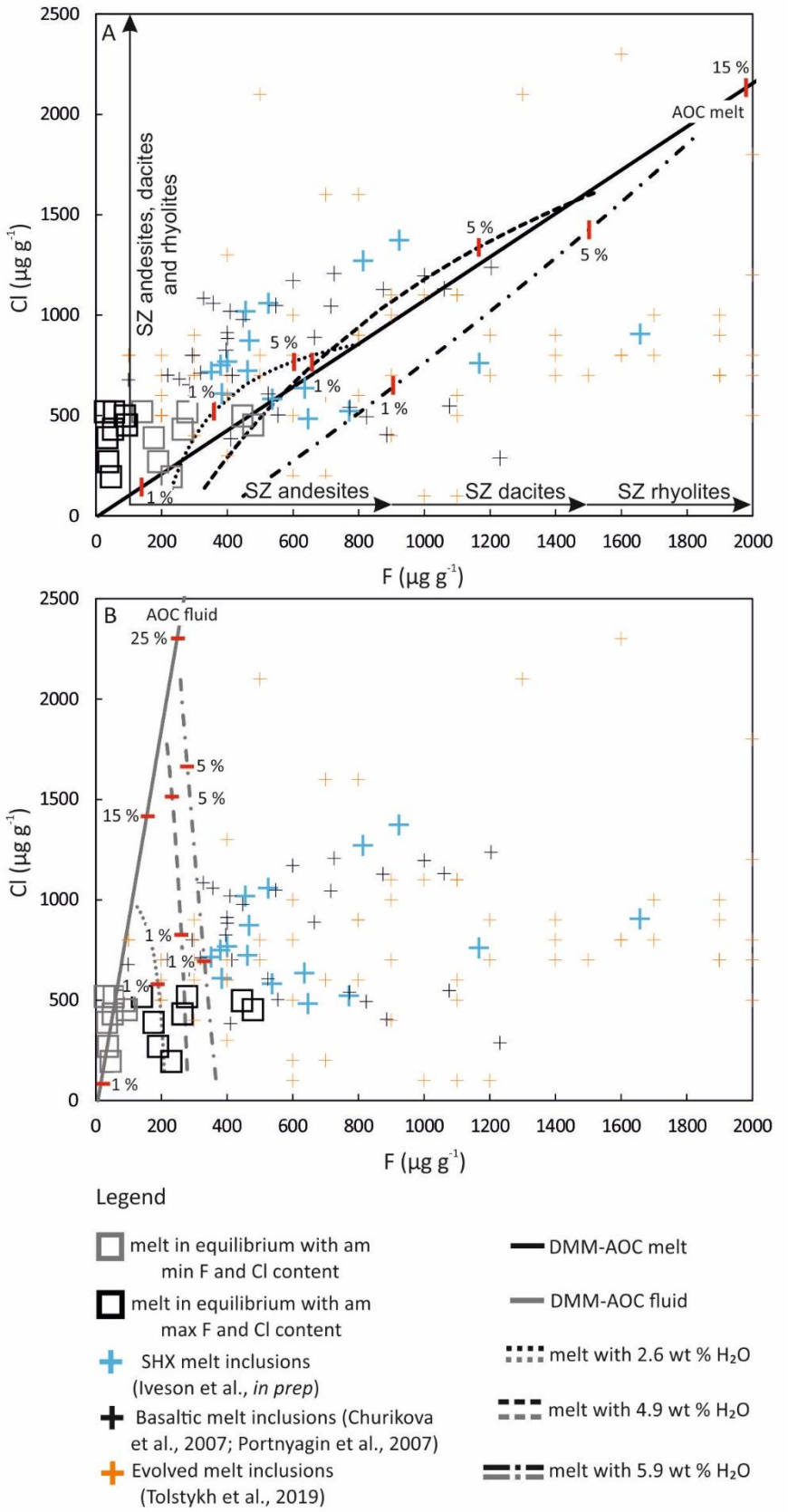

Figure 60. *Halogen (Cl and F) composition of melts in equilibrium with Shiveluch vein amphibole calculated after Giesting and Filiberto (2014) and from* $D_F^{am/mel}$ *(Iveson et al.,*

2017), high-Mg# olivine-hosted melt inclusions from Shiveluch volcanic rocks (Iveson et al., in prep), olivine-hosted basaltic melt inclusions from volcanic rocks from across the Kamchatka arc (Churikova et al., 2007; Portnyagin et al., 2007), evolved melt inclusions from Ichinsky volcano, Kamchatka (Tolstykh et al., 2019) and mixing relationship between the depleted MORB mantle (DMM; Urann et al., 2017) and AOC-derived melt in A) and mixing relationship between the DMM (Urann et al., 2017) and AOC-derived fluid (Straub and Layne, 2003) in B). Dashed and dotted lines correspond to modelled compositions of melt generated via flux melting of the DMM (Urann et al., 2017) caused by AOC-derived melt (LeVoyer et al., 2010) and AOC-derived fluid (Straub and Layne, 2003) in A) and B), respectively. Water contents of the modelled melts range from 2.6 % to 4.9 % and 5.9 % (Dalou et al., 2014). Tick marks correspond to the degree of mantle melting (in %). Black arrows correspond to the range of Cl and F compositions of melt inclusions in arc andesites, dacites and rhyolites, whose Cl abundances range from 100 to 8500 µg g^{-1}, 100 to 3000 µg g^{-1} and 100 to 7500 µg g^{-1}, respectively and those of F range from 100 to 900 µg g^{-1}, 100 to 1500 µg g^{-1} and 100 to 5000 µg g^{-1}, respectively (Aiuppa et al., 2009 and references therein).

4.7 Conclusions

- Shiveluch ultramafic xenoliths represent fragments of depleted subarc lithospheric mantle with estimated degree of melting exceeding 20 %.
- Subsequent to extensive melt extraction, Shiveluch xenoliths were metasomatized by hydrous melts percolating through a network of veins consisting of amphibole, phlogopite, two pyroxenes and plagioclase (Figure 41).
- Veins and the hydrous minerals within them record variable chemical signatures attributed to multiple pulses of metasomatic activity.
- Early-stage vein amphibole formed in equilibrium with basaltic melt (Figure 56) similar to that of high-Mg# olivine-hosted melt inclusions (Iveson et al., *in prep*) in the lithospheric subarc mantle. Late-stage vein amphibole formed in equilibrium with dacitic melt (Figure 56) identical to that of amphibole- and plagioclase-hosted melt inclusions (Humphreys et al., 2008) in the upper-crustal magma reservoir. The evolved dacitic melt shifted its

composition to andesitic as it percolated through and reacted with the mantle harzburgite and the pre-existing veins.

- REE distribution trends and abundances of melts in equilibrium with late-stage vein amphibole (Figure 50B) are identical to those of amphibole- and plagioclase-hosted melt inclusions (Humphreys et al., 2008) and high-Mg# continental andesite (Kelemen et al., 2003). It is suggested that the evolved melt compositions recorded in the amphibole- and plagioclase-hosted melt inclusions were produced by fractional crystallization of high-Mg# andesite.
- Phlogopite formed in equilibrium with melts of mixed AOC melt (high Nb/U) and forearc serpentinite fluid signature (high Cs/U and Rb/U; Figure 59). The mixed signature can be attained by physical mixing of the two liquids in the lithospheric mantle or by serpentinite-derived fluid flux-melting of the AOC.
- Fluorine composition of melt that equilibrated with Shiveluch phlogopite ranges from 280 to 1600 µg g^{-1}, which can be attributed to sampling of increasingly deeper parts of the AOC (Portnyagin et al., 2007; Churikova et al., 2007). Chlorine composition of this melt remains unknown because of the lack of Cl partitioning studies between phlogopite and melt.
- Chlorine and F composition of melt in equilibrium with late-stage vein amphibole ranges from 270 to 518 µg g^{-1} and from 28 to 480 µg g^{-1}, respectively. The low Cl and F composition of the evolved melt that equilibrated with late-stage vein amphibole indicates xenolith interaction with already degassed melt in the upper crustal magma chamber (Figure 60).

- Secondary chlorite replacing phlogopite formed in equilibrium with the host andesite during the eruption (Figure 52).

Chapter 5
A limited role for metasomatized sub-arc mantle in the generation of boron isotope signatures of arc volcanic rocks

5.1 Introduction

Direct observation of the processes of element transfer and isotope fractionations associated with slab dehydration in subduction zones is not possible. However, the classic study of Tatsumi (1989) suggested that a hydrous component released from dehydrating slabs in subduction zones is responsible for the depression of the wet solidus in depleted mantle wedge harzburgite, thus generating fluid-mobile element (FME)-enriched arc volcanic rocks. Contrary to what is seen at mid-ocean ridges, elevated water contents of the subarc mantle control the extensive melting in subduction zones (Kelley et al., 2006). Subsequently, it has been suggested that a slab-derived hydrous fluid or melt percolates through the subarc mantle via an interconnected vein network (Pirard and Hermann, 2015; Plümper et al., 2016), comprising metasomatic mineral phases such as hornblende, phlogopite and two pyroxenes (Figure 16 and Figure 41). Previous studies (e.g. Kepezhinskas et al., 1995; Kepezhinskas and Defant, 1996) speculated that metasomatic veins could be mantle reservoirs of slab-derived elements which, upon melting, will generate the characteristic FME-rich signature of arc volcanic rocks. In this model, the role of the subducting hydrated oceanic plate is central to the generation of FME-enriched arc volcanic rocks, since both primitive mantle and MORB-source mantle contain only traces of FME (McDonough and Sun, 1995; Marschall et al., 2017).

Rocks from the subarc mantle are rarely exposed at the Earth's surface. This, in turn, imposes constraints on our knowledge of the metasomatic processes taking place below the volcanic arcs. The Kamchatka arc is exceptional as rare veined mantle xenoliths have been recovered from several volcanoes along the arc, allowing insights of the subarc mantle to be gained (Kepezhinskas et al., 1995; Kepezhinskas and Defant, 1996; Arai et al., 2003; Bryant et al., 2007; Ishimaru et al., 2007; Arai et al., 2007; Halama et al., 2009; Ionov, 2010; Ionov et al., 2011; Bénard and Ionov, 2012; Ionov et al., 2013; Bénard and Ionov, 2013; Bénard et al., 2017; Siegrist et al., 2019). Previous Kamchatka studies have demonstrated that depleted, harzburgitic, subarc mantle has been extensively metasomatized by hydrous slab-derived fluids and melts, forming amphibole- and phlogopite-bearing veins. The major and trace element characteristics of these veins suggest a transition from fluid-induced mantle metasomatism at the volcanic front and in the southern part of the Central Kamchatka depression (Kepezhinskas and Defant, 1996; Arai et al., 2003; Ishimaru et al., 2007; Arai et al., 2007; Halama et al., 2009; Ionov, 2010; Ionov et al., 2011; Ionov et al., 2013; Bénard et al., 2017) to mostly melt-induced mantle metasomatism at its northern part (Kepezhinskas et al., 1995; Bryant et al., 2007; Ionov et al., 2013).

Boron and $\delta^{11}B$ (the per mil difference between the $^{11}B/^{10}B$ of a sample and NIST 951 boric acid) have been widely used in studies of slab-derived fluids in subduction zones (e.g. de Hoog and Savov, 2018 and references therein). Boron and its isotopic composition (as $\delta^{11}B$) are particularly sensitive tracers of slab-derived metasomatic agents because of the highly fluid-mobile nature of B (Hervig et al., 2002). Boron is enriched in subducting oceanic lithosphere relative to B-poor mantle (e.g., Marschall

et al., 2017) and a wide range of values of $\delta^{11}B$ (ca. 70 ‰) is preserved in natural materials (e.g. de Hoog and Savov, 2018 and references therein). However, this versatile tracer has not been employed previously in the investigation of FME budgets in metasomatized (veined) subarc mantle xenoliths.

This chapter reports measurements of B contents and $\delta^{11}B$ of vein minerals from selected Avachinsky (*AVX-16-03-10, AVX-16-03-20* and *AVX-16-03-24*) and Shiveluch *(SH98X-16, SHX03-04, SHX03-17, SHX03-18* and *SHIV-16-22-06)* mantle xenoliths which demonstrate that metasomatic veins formed by the percolation of hydrous melts and fluids through the subarc mantle cannot play a significant role in the generation of arc magmas.

5.2 Results

Boron contents and $\delta^{11}B$ ratios of the hydrous vein minerals (amphibole and phlogopite), nominally anhydrous mantle minerals (olivine and pyroxene), and plagioclase were measured by secondary ion mass spectrometry (SIMS) using a Cameca 1270 ion microprobe at the University of Edinburgh (see section 2.3.1).

Avachinsky hydrous vein minerals are low in B (0.2 to 0.9 µg g^{-1}) and possess light $\delta^{11}B$ (- 16.6 to - 3.6 ‰), whereas B contents of Shiveluch hydrous vein minerals extend to values as high as 3.1 µg g^{-1} and higher $\delta^{11}B$ (- 13.8 to + 0.9 ‰; Figure 61A and Table 14). Nominally anhydrous mantle minerals olivine and orthopyroxene have low B contents (0.3 to 1.4 µg g^{-1} and 0.3 to 2.1 µg g^{-1}, respectively) and low $\delta^{11}B$ (- 13.8 to - 3.2 ‰ and - 13.7 to - 4.9 ‰, respectively; Figure 61B and Table 14). Vein minerals in Kamchatka mantle xenoliths are only slightly enriched in B relative to depleted mantle (Marschall et al., 2017), and their

$\delta^{11}B$ do not extend to the higher end of the range of $\delta^{11}B$ observed in Kamchatka arc volcanic rocks (B = 11.2 to 36.3 µg g^{-1}; $\delta^{11}B$= -3.7 to +5.6 ‰; Ishikawa et al., 2001). The low B contents and $\delta^{11}B$ of the nominally anhydrous mantle minerals are comparable to previous studies of mantle composition (Harvey et al., 2014 and references therein; Marschall et al., 2017) and will not be discussed further.

Two amphibole populations were identified in Shiveluch and Avachinsky mantle xenoliths based on their major element compositions and the compositions of melts that they equilibrated with (see sections 3.5.4.1 and 4.6.2.1). The early-stage vein amphibole population equilibrated with basaltic andesitic melt in the lithospheric mantle whereas the late-stage vein amphibole population equilibrated with more evolved dacitic to rhyolitic melt in the upper-crustal magma chamber. In Avachinsky veins, amphibole B content and $\delta^{11}B$ is averaged due to the very low amphibole B content which creates large $\delta^{11}B$ uncertainties. Average amphibole B content and $\delta^{11}B$ reported for *AVX-16-03-24* and *AVX-16-03-20* correspond to the late-stage amphibole population and those reported for *AVX-16-03-10* correspond to both the early-stage and late-stage amphibole populations. In Shiveluch veins, amphibole B content and $\delta^{11}B$ were analyzed in both amphibole populations except for *SHX03-18* and *SH98X-16* which contains only the late-stage amphibole. The early-stage amphibole in *SHX03-04* possesses negative $\delta^{11}B$ (- 10.33 to - 6.43 ‰) whereas that of the late-stage amphibole is somewhat less negative (- 2.54 ‰).

No difference in B content and $\delta^{11}B$ was observed in chlorite-bearing phlogopite relative to chlorite-free phlogopite. Phlogopite SIMS spots in *SHX03-18* are free of chlorite lamellae and only two and three phlogopite SIMS spots potentially

containing chlorite lamellae were identified in *SHX03-04* and *SHX03-17*, respectively.

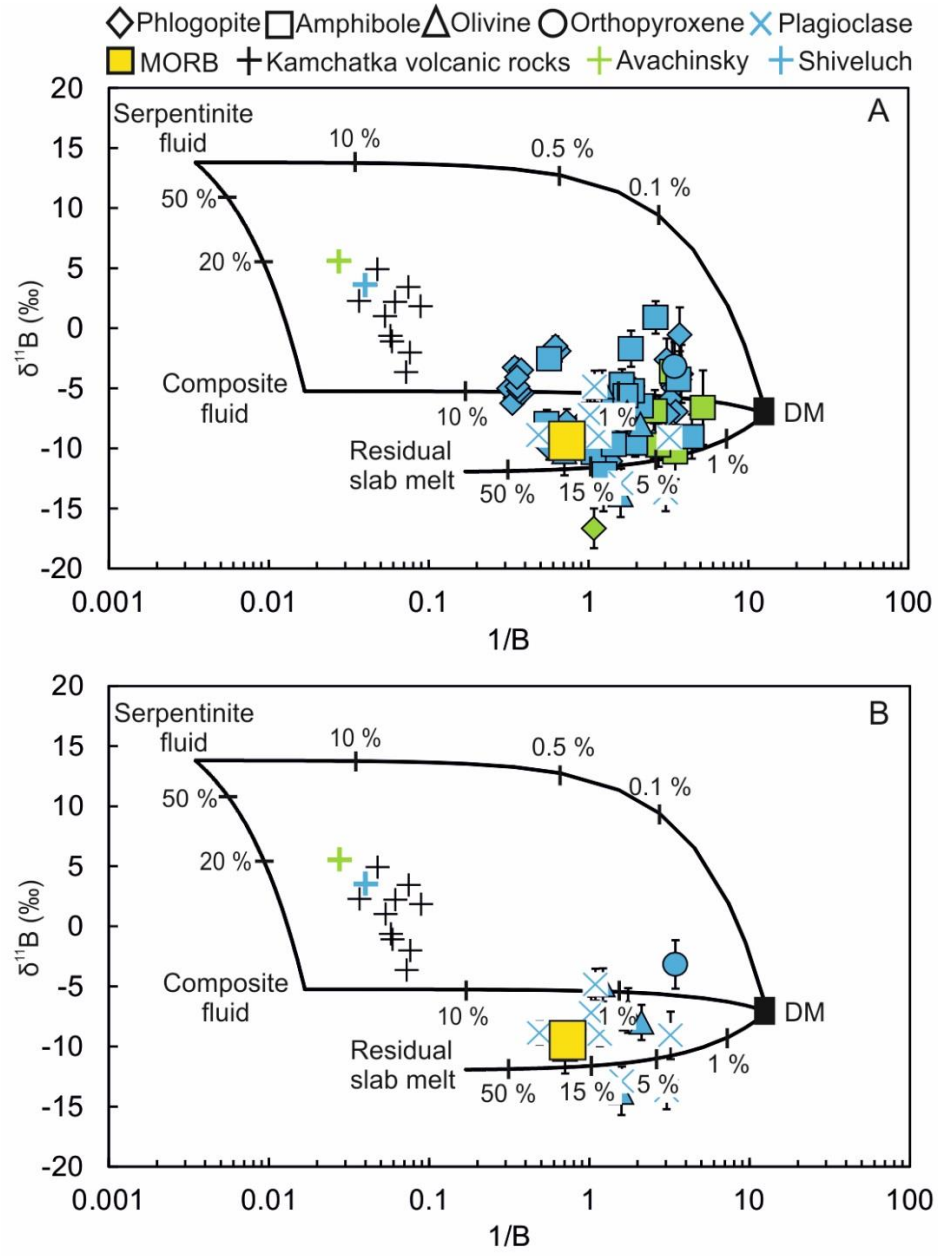

Figure 61. *A) and B) $\delta^{11}B$ vs 1/B in vein minerals in Avachinsky (green) and Shiveluch (blue) mantle xenoliths, Kamchatka volcanic rocks (Ishikawa et al., 2001) and MORB (Marschall et al., 2017) and the mixing relationship between depleted mantle (DM; Marschall et al., 2017), serpentinite fluid (Tonarini et al., 2011), composite slab fluid released at 120 km depth and residual slab melt (calculated after Tonarini et al., 2011 with an additional dehydration stage at 25 km corresponding to 80 % B loss in the fore arc; Savov et al., 2007). Composite fluid comprises 99 % fluid released from altered oceanic crust and 1 % fluid released from sediment. All symbols are larger than the error bars unless shown.*

Table 14. *Boron contents and $\delta^{11}B$ of vein minerals in Avachinsky and Shiveluch mantle xenoliths*

Sample	Mineral	B ($\mu g\ g^{-1}$)	$\delta^{11}B$ (‰)	$\delta^{11}B$ 1σ (‰)
AVX-16-03-10	Am	0.29	-10.28	2.28
		0.37	-9.72	1.79
		0.38	-6.89	1.76
AVX-16-03-20	Am	0.3 (5)*	-3.60	3.20
AVX-16-03-24	Am	0.19 (8)	-6.60	3.10
	Phl	0.81	-13.58	1.65
		0.93	-16.65	1.65
SHIV-16-12-06	Phl	2.85	-5.78	0.67
		3.13	-5.01	0.61
		2.99	-6.24	0.59
		2.89	-3.26	0.75
		2.60	-5.37	0.67
		2.64	-3.47	0.68
		2.70	-5.23	0.62
		2.78	-4.85	0.60
		2.80	-4.08	0.63
		1.61	-1.49	0.80
	Ol	0.57	-7.01	1.86
		1.42	-10.26	1.98
		0.82	-4.89	1.38
		0.47	-8.00	1.46
		0.63	-13.84	1.86
SHX03-04	Am	0.47	-6.46	1.74
		0.93	-10.33	1.15

		1.82	-7.94	0.93
		1.76	-2.54	0.89
	Phl	1.37	-7.79	1.06
		1.05	-9.26	1.09
		1.76	-9.96	0.98
	Pl	0.92	-4.85	1.32
		0.31	-9.08	1.97
		0.97	-7.22	1.36
SHX03-17	Am	0.92	-7.21	1.67
	Phl	0.76	-10.19	1.68
		1.02	-7.34	1.53
		1.02	-9.89	1.27

Abbreviations: Am = amphibole, Phl = phlogopite, Ol = olivine, Opx = orthopyroxene, Pl = plagioclase. *Number of mineral analyses per sample.

5.3 Discussion

Sources of the hydrous veins were investigated through a B elemental-isotopic mixing model incorporating four mantle B end-members known to date, the depleted mantle (DM; Marschall et al., 2017), serpentinite fluid liberated at 120 depth-to-slab (Tonarini et al., 2011), composite slab fluid comprising AOC- and sediment-derived fluid and residual slab melt (Table 15).

Table 15. *Mixing model input parameters*

End-member	B (µg g^{-1})	$\delta^{11}B$ (‰)
DM (Marschall et al., 2017)	0.077	- 7.1
Serpentinite fluid released at 120 km depth (Tonarini et al., 2011)	289	+ 13.8
Composite fluid (calculated after Tonarini et al., 2011)	59.6	- 5.2
Residual slab melt (calculated after Tonarini et al., 2011)	5.9	- 11.9

Composite fluid comprises 99% AOC-derived fluid and 1% sediment-derived fluid reflecting the maximum estimated sediment proportion of the subducting Pacific plate underneath Kamchatka (Kersting and Arculus, 1995; Kepezhinskas et al., 1997; Turner et al., 1998; Churikova et al., 2001). Nankai sediment B contents (80 µg g^{-1}) and $\delta^{11}B$ (- 4 ‰; You et al., 1995) were used in the calculation of the composite fluid composition and B contents (26 µg g^{-1}) and $\delta^{11}B$ (+ 5.5 ‰) of the AOC were taken from Leeman et al. (2004). Water contents of Nankai sediments was estimated to be 6.25 wt % (Plank, 2014) and that of the AOC to be 3.7 wt % (Rüpke et al., 2004). Elemental and isotopic B composition of the composite fluid released at 120 depth-to-slab was calculated via a set of mass balance equations after Marschall et al. (2006) under the assumption that B is linked to water release from the subducting lithologies in the slab. The subducting slab was dehydrated at 200 °C, corresponding to the 80 % loss of B in the fore arc (Savov et al., 2007) followed by further slab dehydration at 250, 600 and 650 °C (water loss in sediments with increasing depth of a cold subducting slab; Rüpke et al., 2004) and finally at 720 °C, corresponding to the AOC water loss under the Kamchatka volcanic arc front (Rüpke et al., 2004; Syracuse et al., 2010). The $\delta^{11}B$ of melts does not fractionate during fractional crystallization (e.g. Kuritani et al., 2005) and thus the model

applies to both vein types irrespective of their origin (i.e. lithospheric mantle vs. upper-crustal magma chamber).

Contrary to earlier predictions of metasomatized mantle wedge playing a fundamental role in generating the characteristic FME enriched arc volcanic rocks (e.g. Kepezhinskas et al., 1995; Kepezhinskas and Defant, 1996), the low B abundances and $\delta^{11}B$ of the metasomatized subarc mantle are unexpected. The majority of vein compositions can be reproduced by mixing of variable amounts of three components: (i) isotopically light composite slab fluid, (ii) residual slab melt and (iii) the depleted mantle (Figure 61 and Table 15). Slab-derived fluids can be generated either by dehydration of mélange diapirs in the subarc mantle under the arc front (Savov et al., 2007; Nielsen and Marschall, 2017 and references therein) and/or by serpentine breakdown in the fore arc, followed by dehydration of altered oceanic crust (AOC) by chlorite and amphibole breakdown under the arc front, as previously proposed in Kamchatka subduction zone model (Konrad-Schmolke and Halama, 2014). Other hydrous minerals typically constituting the AOC, such as lawsonite and phengite, are absent in the top 10 km of the subducting slab in Kamchatka and are therefore not likely to contribute B to the subarc mantle (Konrad-Schmolke and Halama, 2014).

Dehydration of sediments and AOC, in response to rising pressure and temperature with ongoing subduction, leads to B isotopic fractionation between fluids and silicates, specifically ^{11}B depletion in silicates. Trigonally-coordinated ^{11}B preferentially partitions into fluids and tetrahedrally-coordinated ^{10}B into silicate minerals and melts in low pH environments (Kakihana et al., 1977; Peacock and Hervig, 1999; Hervig et al., 2002; Wunder et al., 2005; Pabst et al., 2012; Konrad-

Schmolke and Halama, 2014). Therefore, vein amphibole and phlogopite preserving low $\delta^{11}B$ (i.e., < -7 ‰) may have equilibrated with slab fluid released by chlorite dehydration in the AOC (Rüpke et al., 2004; Konrad-Schmolke and Halama, 2014) or residual slab melt generated at > 120 km depth-to-slab, assuming vertical transport of the released fluid or melt. In cold subduction zones, fully hydrated AOC and sediments dehydrate in several steps before they are subducted to 120 km (Rüpke et al., 2004), where they release isotopically light B upon their dehydration (Figure 61). Isotopically light fluid, however, could have also been released by dehydration of serpentinite which interacted with sediment (Cannaò et al., 2015).

The higher $\delta^{11}B$ (> -5 ‰) of some of the vein minerals requires at least some forearc serpentinite fluid influx ($\delta^{11}B$ = ~ 14 ‰; Tonarini et al., 2011) into the subarc mantle. Vein amphibole with the highest $\delta^{11}B$ requires up to 15 % of its B content to be derived from serpentinite and 85 % from a composite lithology comprising 99 % AOC and 1 % sediment (Figure 61). Alternatively, the positive $\delta^{11}B$ fluid could have been derived by dehydration of the lower-AOC (McCaig et al., 2018). The most serpentinized lower crustal gabbro drilled at Hess Deep by the IODP Expedition 345 possesses positive $\delta^{11}B$ (25.6 ‰; McCaig et al., 2018). Indeed, Shiveluch lies above a subducting transform fault, which could have exposed the lower oceanic crust and the upper lithospheric mantle to seawater percolation prior to subduction (Manea et al., 2014).

My data demonstrate a negligible contribution to the otherwise large outfluxes of boron at volcanic arcs. The veins represent a volumetrically minor mantle B end-member with insufficient B concentrations to significantly skew the composition of the erupted arc volcanic rocks. Instead, a slab-derived component, enriched in ^{11}B

must transit relatively rapidly through the mantle wedge (Figure 62). In Kamchatka, the limited sedimentary pile (435 m of ashy-siliceous clay; Plank, 2014) and the AOC are not likely to carry B deeper than the fore arc as more than 80 % of their original boron contents is released during shallow slab dehydration (Savov et al., 2007) and its further dehydration under the arc front releases isotopically light fluids ($\delta^{11}B$ = -5.2 ‰; Figure 61).

Several prior studies have established that serpentinite can host up to 80 µg g^{-1} B and retain high $\delta^{11}B$ signature of up to +25 ‰ in shallow subduction settings (Benton et al., 2001; Scambelluri and Tonarini, 2012; Harvey et al., 2014; De Hoog and Savov, 2018 and references therein). The results of my model suggest that fluids from dehydration of subducted forearc serpentinite and AOC, rather than metasomatized veins in the subarc mantle, are responsible for the boron elemental and isotopic signature of Kamchatka arc volcanic rocks (Figure 61; Ishikawa et al., 2001; Churikova et al., 2007).

It has been shown that the initially high $\delta^{11}B$ of slab fluid rapidly decreases as it moves away from the dehydration site (Prigent et al., 2018), unless the fluid flow is focused in an interconnected vein network (Figure 62; Pirard and Hermann, 2015; Plümper et al., 2016). The fluid flow through this vein network must be rapid for only limited chemical exchange to occur between the vein minerals and the percolating slab-derived fluid (e.g. John et al., 2012). Large variations of $\delta^{11}B$ in amphibole and phlogopite in samples *SHX03-18, SHX03-04* and *SH98X-16* (Figure 61 and Table 14) suggest that the veins investigated in this study sampled multiple pulses of slab-derived fluids and melts originating from different depths. Alternatively, the slab-derived fluids and melts could have been sourced by mélange

diapirs in the mantle wedge (Nielsen and Marschall, 2017 and references therein) which are composed of a mixture of slab and hydrated forearc mantle lithologies with variable $\delta^{11}B$ compositions.

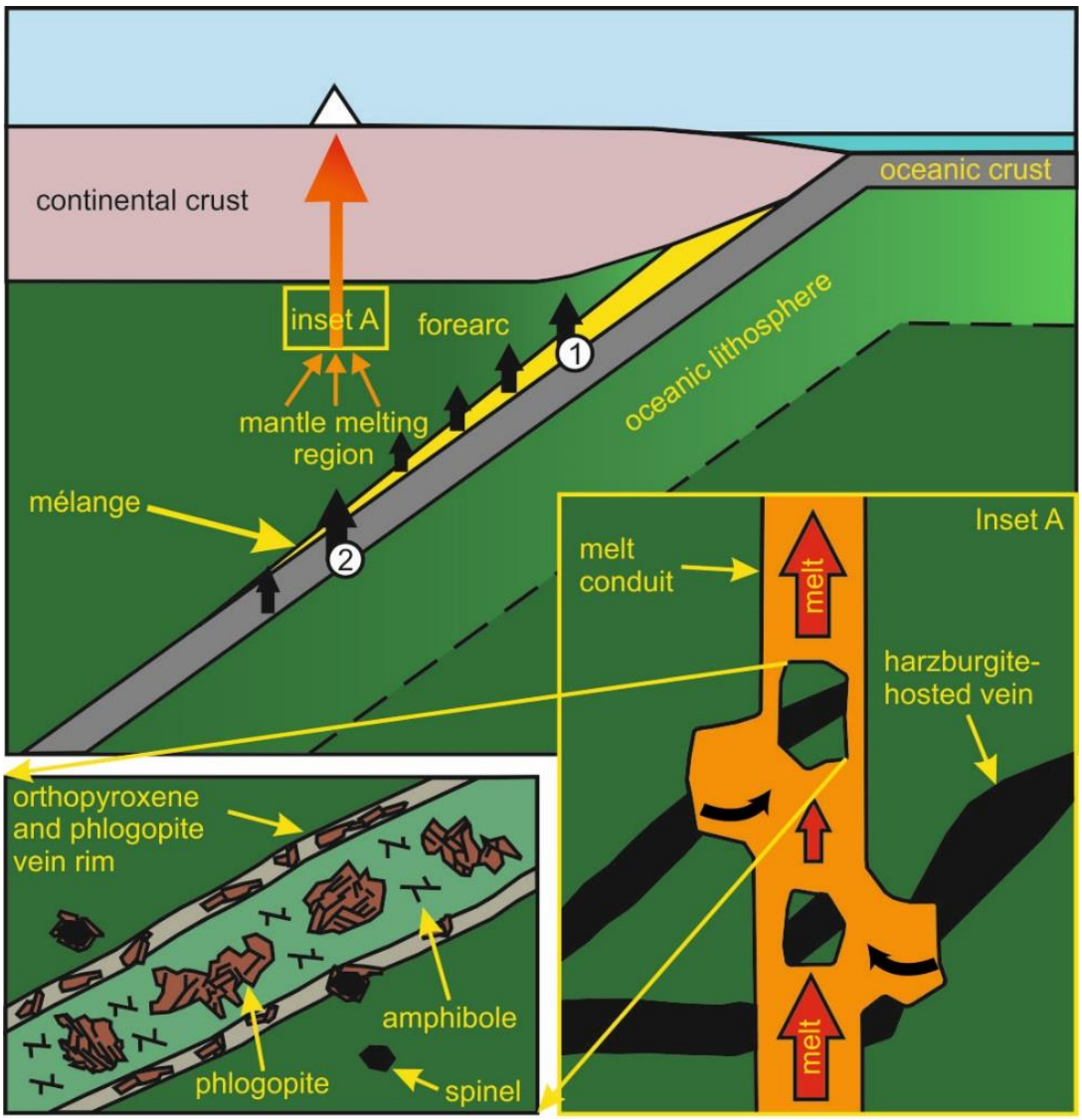

Figure 62. *In Kamchatka, slab-derived fluids (black arrows) can be generated either by mélange diapir dehydration in the mantle wedge (Nielsen and Marschall, 2017) or by (1) serpentine breakdown in the fore arc and (2) chlorite and amphibole breakdown in the AOC at 90-120 km depth-to-slab. B-rich, isotopically heavy slab-derived fluid is transferred through the sub-arc mantle by an interconnected network of veins cross-cutting the mantle harzburgite, fragments of which are entrained into magma (orange arrows) on its way up to the surface (inset A). Inset A position corresponds to the depth from which the xenoliths were derived (30-50 km).*

5.4 Conclusions

- Vein amphibole in Avachinsky mantle xenoliths is low in B (0.2 to 0.9 µg g^{-1}) and possesses negative $\delta^{11}B$ (- 16.6 to - 3.6 ‰), whereas vein hydrous minerals (amphibole and phlogopite) in Shiveluch mantle xenoliths extend to B values as high as 3.1 µg g^{-1} and higher $\delta^{11}B$ (- 13.8 to + 0.9 ‰).
- The veins record multiple pulses of fluids and melts percolating through the subarc mantle, ranging from isotopically light AOC-derived fluids and residual melts to isotopically heavy forearc serpentinite-derived fluids (Figure 61).
- The B contents and $\delta^{11}B$ of vein minerals in Kamchatka arc xenoliths from Shiveluch and Avachinsky volcanoes are inconsistent with their providing a significant contribution to the boron budget of Kamchatka arc volcanic products.
- The fluid flow appears to be focused in veins connecting either the slab dehydration sites or mélange diapirs with the magma generation region to facilitate the rapid transport of heavy B to arc magmas and limited interaction with the vein minerals (Figure 62).

Chapter 6
Discussion and conclusions

A transect from the volcanic front to the rear-arc Kamchatka mantle wedge integrating petrological and geochemical data presented in Chapters 3,4 and 5 is described here. The results are then compared to mantle xenoliths recovered from other volcanic arcs. Finally, recommendations for future research are outlined at the end of this chapter.

6.1 Transect through the Kamchatka subarc mantle

Mantle xenoliths recovered from Shiveluch, Avachinsky and Bakening volcanoes offer insights into progressively deeper portions of the subarc mantle underlying Kamchatka. Avachinsky and Shiveluch volcanoes are located in the volcanic front at ~ 120 and 90 km depth-to-slab, respectively (Figure 2; Gorbatov et al., 1997), whereas Bakening volcano is located in the rear-arc at ~ 200 km depth-to-slab (Figure 2; Gorbatov et al., 1997). Ultramafic xenoliths found at Shiveluch and Avachinsky volcanoes are compositionally different from those found at Bakening. Peridotites, specifically harzburgites, are the most common mantle rock type erupted at Shiveluch and Avachinsky (Figure 14 and Figure 40), whereas pyroxenites dominate the mantle rocks erupted at Bakening (Figure 14). Equilibration pressure estimates indicate that Shiveluch and Avachinsky peridotites were derived from depths of 30 to 43.5 km (Figure 49) and 33 to 36 km (Figure 26), respectively. This depth range corresponds to the lithospheric subarc mantle close to the crust-mantle boundary which is located at 35 km in Kamchatka (Levin et al., 2002). In contrast,

Bakening peridotites and pyroxenites were derived from greater depths of 45 to 55.5 km (Figure 26), also corresponding to the lithospheric subarc mantle.

The increasing depth-to-slab from the volcanic front to the rear-arc affects the degree of melting. At the volcanic front, the estimated degree of melt extraction exceeds 20 %. It is likely that the estimated degree of melt extraction exceeds 29 % as primary clinopyroxene is absent in both Shiveluch and Avachinsky peridotites (Bizimis et al., 2000). Consistently high degrees of melt extraction ranging from 28 to 35 % at Avachinsky were previously constrained by Ionov (2010). At the rear-arc, the estimated degree of melt extraction is lower than that at the volcanic front and ranges from 8 to 11 %. In cold subduction zones, the subducting plate dehydrates in several stages before it reaches rear-arc depth (Rüpke et al., 2004). The forearc is fluxed with sediment-derived and serpentinite breakdown fluids (e.g. DeHoog and Savov, 2018 and references therein), the subarc is fluxed with amphibole, chlorite and antigorite breakdown fluids (Rüpke et al., 2004; Konrad-Schmolke and Halama, 2014) and the rear-arc is fluxed with phengite breakdown fluids (e.g. Churikova et al., 2007; Portnyagin et al., 2007; Bénard et al., 2017). Thus, the rear-arc mantle under Bakening is fluxed with lower volume of slab-derived fluids than the subarc mantle under Shiveluch and Avachinsky, which, in turn, triggers lower degrees of partial melting of the rear-arc mantle.

Mantle xenoliths recovered from the volcanic front differ in metasomatic style from those recovered from the rear-arc. Shiveluch and Avachinsky peridotites are cross-cut by both, anhydrous orthopyroxene-rich (Figure 16F and Figure 17B) and hydrous amphibole- and phlogopite-rich veins (Figure 16E, Figure 17, Figure 41 and Figure 42). These veins record multiple episodes of metasomatism. Bakening

peridotites are not cross-cut by any veins. Instead, they contain secondary clinopyroxene overgrowing primary olivine and orthopyroxene (Figure 18).

At Shiveluch, the earliest metasomatic episode recorded in mantle xenoliths is the formation of dunite veins. A silica-undersaturated melt percolating through the depleted harzburgite dissolved orthopyroxene to form dunite (Equation 20). Melt produced by the dunite-forming melt-rock reaction became silica-saturated because of the dissolution of orthopyroxene, and produced anhydrous orthopyroxene-rich veins (Equation 21). Subsequently, Shiveluch dunites were cross-cut by hydrous amphibole- and phlogopite-rich veins (Equation 19 and Equation 23). Based on the occurrence of amphibole inclusions in phlogopite in *SHX03-17* (Figure 42A), it has been established that the early-stage vein amphibole crystallized before phlogopite in Shiveluch hydrous veins. The early-stage vein amphibole equilibrated with basaltic to basaltic andesitic melt similar in composition to the high-Mg# olivine-hosted melt inclusions from Shiveluch volcanic rocks (Figure 56; Iveson et al., *in prep*), but its trace element composition remains unknown. Phlogopite equilibrated with melts possessing trace element characteristics of both, AOC-derived melt (i.e. high Nb/U in Figure 59A) and forearc serpentinite-derived fluid (i.e. high Cs/U and Rb/U in Figure 59B; Peters et al., 2017). Furthermore, the low B contents (0.2 to 3.1 µg g^{-1}; Table 14) and isotopically variable $\delta^{11}B$ (-13.8 to +0.9 ‰; Table 14) of Shiveluch vein phlogopite and amphibole also demonstrated a mixed signature of isotopically light AOC-derived fluids and residual melts with small amounts (up to 15 %; Figure 61) of isotopically heavy forearc serpentinite-derived fluids. The mixed signature of AOC-derived melt and forearc serpentinite-derived fluid could have been attained either by serpentinite-derived fluid flux-melting of the AOC (Figure 1A) or by mélange diapir melting in the mantle melting region (Figure 1B;

e.g. Nielsen and Marschall, 2017 and references therein). The former scenario necessitates transport of the residual AOC-derived hydrous melt through veins connecting the AOC melting site with the mantle melting region (John et al., 2012; Pirard and Hermann, 2015; Plümper et al., 2016). Consistent with the model of melt transport through veins rather than mélange diapirs, the high F content (from 280 to 1600 μg g^{-1}) of melt that equilibrated with Shiveluch phlogopite is attributed to sampling increasingly deeper parts of the AOC via the breakdown of F-rich minerals such as amphibole, phengite and lawsonite (Portnyagin et al., 2007; Churikova et al., 2007; Bénard et al., 2017).

At Avachinsky, the earliest metasomatic episode recorded in mantle xenoliths is the percolation of K-rich melt forming phlogopite intergrown with olivine (Figure 16E and Equation 19) and percolation of silica-undersaturated basaltic melt forming dunite veins (Figure 16C and Equation 20). Avachinsky xenoliths were subsequently metasomatized by silica-saturated melts forming anhydrous orthopyroxene-rich veins (Figure 16D and Equation 21) which were later re-fertilized by CaO- and SiO_2-rich melt that produced secondary clinopyroxene (Figure 16D and Equation 22). Finally, the re-fertilized anhydrous veins were overgrown by clinopyroxene and amphibole that equilibrated with hydrous mafic melt (Figure 16F and Equation 23). Trace element composition of the calculated melt in equilibrium with vein clinopyroxene (Figure 27) and amphibole in *AVX-16-03-24 (*Figure 34*)* is identical to that of boninite (Hickey and Frey, 1982; Pearce et al., 1992; Kelemen et al., 2003). Boninites are primitive arc melts with high MgO (> 8 wt %) and SiO_2 (> 53 wt %) contents that are derived from an ultra-depleted mantle source (up to 20 % melt depletion) subsequently metasomatized by AOC-derived fluids and melts formed during the early stages of subduction (Hickey and Frey, 1982; Pearce et al.,

1992). Similar anhydrous orthopyroxene-rich veins cross-cutting Avachinsky peridotites have been reported by Halama et al. (2009), Bénard and Ionov (2012) and Bénard and Ionov (2013), who also demonstrated that the veins formed in equilibrium with boninitic melt. Consistent with the above, the low B contents (0.2 to 0.9 µg g^{-1}; Table 14) and negative $\delta^{11}B$ (-16.6 to -3.6 ‰; Table 14) of Avachinsky vein amphibole indicates percolation of residual AOC-derived melts and fluids, occasionally mixed with a small amount of serpentinite-derived fluid (up to 2 %; Figure 61). Equally, Bénard et al. (2017) demonstrated that mantle melts that equilibrated with minerals in websterite and orthopyroxenite veins cross-cutting Avachinsky harzburgites are strongly enriched in Cl and F, respectively, which was attributed to different melt sources. The high Cl content of SiO_2-rich picrite and high-Ca boninite percolating through the websterite veins was attributed to high degrees of mantle melting triggered by pervasive percolation of Cl-rich fluids liberated from serpentinite and the AOC dehydration under the arc (Bénard et al., 2017), whereas the high F content of low-Ca boninite percolating through the orthopyroxenite veins was attributed to low degrees of mantle melting triggered by F-rich liquids released via amphibole and/or mica breakdown in the residual AOC (Bénard et al., 2017).

At Bakening, only two metasomatic episodes were recorded in mantle xenoliths, the formation of dunite veins (Figure 18 and Equation 20) and re-fertilization (Figure 18 and Equation 22) of both, peridotites and pyroxenites. The low forsterite component in olivine (maximum Fo_{87}), olivine NiO content (from 0.04 to 0.35 wt %) and spinel Cr# (maximum spinel Cr# = 30) are much lower than those of Shiveluch and Avachinsky mantle xenoliths (Figure 19,Figure 20 and Figure 36). Combined with the elevated clinopyroxene HREE abundances (Figure 29, Figure 30

and Figure 31), the low olivine Fo and NiO contents indicated that Bakening peridotites equilibrated with melt derived from partial melting of pyroxenite. The pyroxenite melt was mixed with < 1 % carbonatite melt which elevated LREE of Bakening clinopyroxene (Figure 38).

6.2 Magmatic overprint in the upper-crustal magma chamber

Shiveluch and Avachinsky xenoliths have been affected by magmatic processes occurring in the upper crustal magma chamber immediately prior to their transport to the surface (Figure 58). The second population of late-stage vein amphibole (classified as magnesiohornblende and tschermakite) formed in most of the pre-existing hydrous amphibole- and phlogopite-rich veins that equilibrated in the mantle. The late-stage vein amphibole is located at selvages and at vein centres adjacent to interstitial albite-rich plagioclase (i.e. Na-rich) and records equilibration with evolved dacitic to rhyolitic melts (Figure 37 and Figure 56). Progressive reaction of the evolved melt with the pre-existing vein minerals shifted the composition of the reactant melt from dacitic/rhyolitic to andesite (Equation 25). Occasionally, a new set of hydrous amphibole-rich veins and reaction zone was produced during the interaction of the evolved melt with harzburgites *AVX-16-03-20* and *SHX03-18*, respectively (Equation 26). Incompatible trace element abundances of vein amphibole in *AVX-16-03-20* (Figure 33B) are identical to that of selvage-related vein amphibole from a similar Avachinsky peridotite that formed in late-stage melt-rock interaction prior to the eruption (Bénard and Ionov, 2013).

The estimated Cl contents and trace element compositions of melts in equilibrium with the late-stage vein amphibole in Shiveluch xenoliths are identical to those of

upper-crustal melts trapped in evolved amphibole-and plagioclase-hosted melt inclusions from Shiveluch volcanic rocks (Humphreys et al., 2008) and average primitive (high-Mg#) andesite (Figure 50B; Kelemen et al., 2003). Similar to boninites, primitive andesitic melts originate as wet mantle melts in equilibrium with olivine and orthopyroxene in the refractory harzburgite (Wood and Turner, 2009). Therefore, it is suggested that the early-stage Shiveluch vein amphibole equilibrated with primitive andesitic melt and that fractional crystallization of such melt in the upper crustal magma chamber produced the evolved dacitic and rhyolitic melt trapped in amphibole- and plagioclase-hosted Shiveluch melt inclusions.

The low Cl (270 to 518 µg g^{-1}) and F (28 to 480 µg g^{-1}; Figure 60) contents of the melt in equilibrium with the late-stage Shiveluch vein amphibole indicates that the xenoliths interacted with a degassed evolved melt in the upper crustal magma chamber (Figure 60) similar to that trapped in amphibole- and plagioclase-hosted melt inclusions (Humphreys et al., 2008).

All Kamchatka mantle xenoliths described here have interacted with the host magma that brought them to the surface. Shiveluch and Avachinsky mantle xenoliths were entrained into andesitic melt which reacted with phlogopite to form chlorite. Phlogopite is commonly replaced by chlorite along its cleavage planes in both, Shiveluch and Avachinsky mantle xenoliths (Figure 42A and Figure 16E, respectively). The REE distribution trend of phlogopite containing chlorite lamellae is similar to that of the host andesite (Figure 52) indicating that the secondary chlorite lamellae formed in equilibrium with the host andesite shortly prior to the eruption. Bakening mantle xenoliths were entrained into basaltic magma which infiltrated both peridotites and pyroxenites along grain boundaries and formed

symplectite made up of olivine and glass that rapidly quenched upon the eruption (Figure 18F).

6.3 Implications for the classic metasomatized mantle wedge melting model

The classic model of partial melting of metasomatized subarc mantle generating volatile and FME-rich arc volcanic rocks (e.g. Kepezhinskas et al., 1995; Kepezhinskas and Defant, 1996) is challenged with the studied B contents and $\delta^{11}B$ of vein minerals in Shiveluch and Avachinsky mantle xenoliths. In contrast to the vein minerals depleted in B (0.2 to 3.1 µg g^{-1}) and negative in $\delta^{11}B$ (- 16.6 to + 0.9 ‰), Kamchatka arc volcanic rocks possess higher B contents (up to 36.3 µg g^{-1}; Ishikawa et al., 2001) and more positive $\delta^{11}B$ (up to + 5.58 ‰; Ishikawa et al., 2001). The high B contents and positive $\delta^{11}B$ of Kamchatka arc volcanic rocks was attributed to the influx of serpentinite-derived fluid (~ 20 % of fluid derived from serpentinite dehydration) whereas the low B contents and negative $\delta^{11}B$ of vein minerals in mantle xenoliths was attributed to the influx of AOC-derived fluids and melts and a small amount of serpentinite-derived fluids (Figure 61). Thus, the inconsistency in B contents and $\delta^{11}B$ between the vein minerals and Kamchatka arc volcanic rocks indicates that partial melting of metasomatized mantle alone cannot provide a significant contribution to the boron budget of Kamchatka arc. Instead, fluid flow through the subarc mantle appears to be focused in veins that connect slab dehydration sites with the magma generation region to facilitate the rapid transport of heavy B to arc magmas with limited interaction with the vein minerals (Figure 62; John et al., 2012).

6.4 Implications for the serpentinized slab mantle dehydration model

It has been proposed that subducting fracture zones are capable of releasing higher than normal amounts of water and FME such as B into the subarc mantle (Manea et al., 2014). Large portions of a fractured oceanic plate are hydrated by seawater that can percolate as deep as the lithospheric mantle. Contrary to slab bending faults, fracture zones are the only known tectonic features that allow fluxing of the oceanic lithospheric mantle by B-rich fluids (McCaig et al., 2018).

Shiveluch volcano is located above such subducting fracture zone (the Aleutian transform fault, Figure 2), which is expected to release large quantities of water during serpentinite breakdown and thus, trigger extensive partial melting of the subarc mantle. However, I demonstrated that vein minerals in mantle xenoliths equilibrated with fluids and melts generated by dehydration and melting of the AOC (Figure 61). Only a small amount of serpentinite-derived fluids (< 15 %) was required to elevate $\delta^{11}B$ of some vein minerals. The lack of serpentinite-derived fluid signature in Shiveluch mantle xenoliths have been caused by rapid pulsed fluid flow through the subarc mantle as indicated by the discrepancy in B contents and $\delta^{11}B$ between vein minerals in mantle xenoliths and the erupted arc volcanic rocks. Indeed, dehydration of serpentinized slab lithospheric mantle was proposed to trigger partial melting of the CKD subarc mantle and elevate B contents of volcanic rocks erupted at CKD volcanoes (Figure 9; Konrad-Schmolke and Halama, 2014; Konrad-Schmolke et al., 2016).

6.5 Comparison with other volcanic arcs

Spinel peridotites are not exclusive to Kamchatka arc, similar rocks have been recovered from volcanic arcs all over the world such as at the Mexican Volcanic Belt (Luhr et al., 1989; Luhr and Aranda-Gómez, 1997; Blatter and Carmichael, 1998; Mukasa et al., 2007), the Luzon arc in the Philippines (Maury et al., 1992), the Tabar-Lihir-Tanga-Feni arc in Papua New Guinea (McInnes et al., 2001; Gregoire et al., 2001) and the West Bismarck arc in Papua New Guinea (Tollan et al., 2017), among others.

The common feature of arc mantle xenoliths is their initially extremely depleted composition (the maximum estimated degree of melt depletion is 30 %) that is subsequently overprinted by highly oxidized fluids and melts (most often referred to as slab-derived aqueous fluids with dissolved silicate component) originating from the subducting AOC. These metasomatic fluids and melts precipitate a range of secondary minerals including orthopyroxene, clinopyroxene, amphibole and phlogopite, either in veins or in interstitial melt pockets.

The ultramafic xenoliths entrained in andesites from El Peñon, Mexico, contain interstitial amphibole that is compositionally distinct from that found at the selvage and in the groundmass of the host andesite (Mukasa et al., 2007). It has been demonstrated that the interstitial amphibole is a product of slab-derived fluid interaction with the depleted subarc mantle (Blatter and Carmichael, 1998) and that the amphibole-rich peridotite is residual to an earlier melt extraction event taking place prior to its entrainment into the host andesite (Mukasa et al., 2007). Similar to amphibole in El Peñon xenoliths, the formation of the early-stage vein amphibole that equilibrated with basaltic and basaltic andesitic melt in Shiveluch and

Avachinsky xenoliths was attributed to a melt-rock reaction (Equation 23) occurring in the subarc mantle prior to the entrainment of mantle xenoliths into the host magma.

Phlogopite lherzolites have also been recovered from the Mexican arc volcanoes at the Ventura-Espíritu Santo volcanic field (Luhr and Aranda-Gómez, 1997). Its formation was attributed to hydrous Fe-rich melt that produced Fe-enriched peridotite containing phlogopite veinlets. Unlike in Shiveluch and Avachinsky xenoliths, the edges of phlogopite grains in this Fe-rich lherzolite are resorbed and consist of Ti-rich rim that was produced during interaction with the host magma (Luhr and Aranda-Gómez, 1997).

Contrastingly, phlogopite in Shiveluch and Avachinsky xenoliths is replaced by chlorite along its cleavage planes (Figure 16E and Figure 42A), which is the product of mantle xenolith interaction with the host magma.

6.6 Future work

Suggested directions of future research are outlined below.

- *Trace element and halogen analyses of the early-stage vein amphibole in Shiveluch xenoliths.* The early-stage vein amphibole is far less abundant than the late-stage vein amphibole and occurs only in two Shiveluch (*SHX03-01* and *SHX03-04*) and one Avachinsky (*AVX-16-03-10*) peridotites. Complementary to the B elemental-isotopic mixing model (Figure 61), the trace element composition of the early-stage vein amphibole could be used to better constrain the composition of melt in equilibrium with this mantle-derived amphibole.

- *Trace elemental partitioning experiments (including B) between phlogopite and melt.* An incomplete set of partition coefficients exists for equilibrium trace elemental exchange between phlogopite and melt at subarc conditions (LaTourrette et al., 1995). This precludes the use of phlogopite commonly occurring in metasomatized arc peridotites as a proxy for mantle-derived melt compositions and in melting models of metasomatized mantle.
- *Chlorite dehydration experiments*. Unlike the composition of serpentinite-derived fluids, the composition of fluids derived from dehydration of chlorite has not been reported yet. It has been demonstrated that dehydration of forearc serpentinite in, or adjacent to, the AOC produces chlorite harzburgite that is then subducted to the subarc depth where it dehydrates (Padrón-Navarta et al., 2011). Therefore, it is important to constrain the composition of chlorite-derived fluid, including its B abundances and $\delta^{11}B$.

- Investigation of micro-meter scale mineral textures such as the alteration of phlogopite to chlorite (observed in all Shiveluch and Avachinsky phlogopite-bearing xenoliths) and spinel exsolution mechanism in clinopyroxene (observed in all Bakening xenoliths except for websterites *BAK-16-22-32* and *BAK-16-22-42*).

References

Adam, J., Locmelis, M., Afonso, J.C., Rushmer, T. and Fiorentini, M.L. 2014. The capacity of hydrous fluids to transport and fractionate incompatible elements and metals within the Earth's mantle. *Geochemistry, Geophysics, Geosystems*. **15**(6), pp.2241–2253.

Aiuppa, A., Baker, D.R. and Webster, J.D. 2009. Halogens in volcanic systems. *Chemical Geology*. **263**(1–4), pp.1–18.

Arai, S. 1994. Characterization of spinel peridotites by olivine-spinel compositional relationships: Review and interpretation. *Chemical Geology*. **113**(3–4), pp.191–204.

Arai, S. 1992. Chemistry of chromian spinel in volcanic rocks as a potential guide to magma chemistry. *Mineralogical Magazine*. **56**, pp.173–184.

Arai, S., Abe, N. and Ishimaru, S. 2007. Mantle peridotites from the Western Pacific. *Gondwana Research*. **11**(1–2), pp.180–199.

Arai, S., Ishimaru, S. and Okrugin, V.M. 2003. Metasomatized hazburgite xenoliths from Avacha volcano as fragments of mantle wedge of the Kamchatka arc: Implication for the metasomatic agent. *Island Arc*. **12**(2), pp.233–246.

Avdeiko, G.P., Savelyev, D.P., Palueva, A.A. and Popruzhenko, S. V. 2007. Evolution of the Kurile-Kamchatkan volcanic arcs and dynamics of the Kamchatka-Aleutian junction *In*: J. C. Eichelberger, E. Gordeev, P. Izbekov, M. Kasahara and J. Lees, eds. *Volcanism and subduction: The Kamchatka region*. Washington, DC: American Geophysical Union, pp.37–55.

Baker, M.B. and Stolper, E.M. 1994. Determining the composition of high-pressure mantle melts using diamond aggregates. *Geochimica et Cosmochimica Acta*. **58**(13), pp.2811–2827.

Barnes, J.D., Manning, C.E., Scambelluri, M. and Selverstone, J. 2018. The behavior of halogens during subduction-zone processes *In*: D. E. Harlov and L. Aranovich, eds. *The role of halogens in terrestrial and extraterrestrial geochemical processes*. Cham: Springer International Publishing, pp.545–590.

Beattie, P., Ford, C. and Russell, D. 1991. Partition coefficients for olivine-melt and orthopyroxene-melt systems. *Contributions to Mineralogy and Petrology*. **109**(2), pp.212–224.

Bénard, A. and Ionov, D.A. 2012. A new petrogenetic model for low-Ca boninites: Evidence from veined sub-arc xenoliths on melt-mantle interaction and melt fractionation. *Geochemistry, Geophysics, Geosystems*. **13**(1), pp.1–14.

Bénard, A. and Ionov, D.A. 2013. Melt- and fluid-rock interaction in supra-subduction lithospheric mantle: Evidence from andesite-hosted veined peridotite xenoliths. *Journal of Petrology*. **54**(11), pp.2339–2378.

Bénard, A., Klimm, K., Woodland, A.B., Arculus, R.J., Wilke, M., Botcharnikov, R.E., Shimizu, N., Nebel, O., Rivard, C. and Ionov, D.A. 2018. Oxidising agents in sub-arc mantle melts link slab devolatilisation and arc magmas.

Nature Communications. **9**(1), pp.1–10.

Bénard, A., Koga, K.T., Shimizu, N., Kendrick, M.A., Ionov, D.A., Nebel, O. and Arculus, R.J. 2017. Chlorine and fluorine partition coefficients and abundances in sub-arc mantle xenoliths (Kamchatka, Russia): Implications for melt generation and volatile recycling processes in subduction zones. *Geochimica et Cosmochimica Acta*. **199**, pp.324–350.

Benton, L.D., Ryan, G. and Tera, F. 2001. Boron isotope systematics of slab fluids as inferred from a serpentine seamount, Mariana forearc. *Earth and Planetary Science Letters*. **187**, pp.273–282.

Bizimis, M., Salters, V.J.M. and Bonatti, E. 2000. Trace and REE content of clinopyroxenes from supra-subduction zone peridotites. Implications for melting and enrichment processes in island arcs. *Chemical Geology*. **165**(1–2), pp.67–85.

Blatter, D.L. and Carmichael, I.S.E. 1998. Hornblende peridotite xenoliths from central Mexico reveal the highly oxidized nature of subarc upper mantle. *Geology*. (11), pp.1035–1038.

Blundy, J.D. and Sparks, R.S.J. 1992. Petrogenesis of mafic inclusions in granitoids of the Admello Massif, Italy. *Journal of Petrology*. **33**(5), pp.1039–1104.

Boyd, F.R. and Mertzman, S.A. 1987. Composition and structure of the Kaapvaal lithosphere, southern Africa *In*: B. O. Mysen, ed. *Magmatic Processes: Physicochemical Principles*. The Geological Society Special Publications, pp.13–24.

Boyd, F.R., Pokhilenko, N.P., Pearson, D.G., Mertzman, S.A., Sobolev, N. V. and Finger, L.W. 1997. Composition of the Siberian cratonic mantle: evidence from Udachnaya peridotite xenoliths. *Contributions to Mineralogy and Petrology*. **128**(2–3), pp.228–246.

Braitseva, O.A., Bazanova, L.I., Melekestsev, I. V. and Sulerzhitsky, L.D. 1998. Large Holocene eruptions of Avacha volcano, Kamchatka (7250-3700 14C years B.P.). *Volcanology and Seismology*. **20**, pp.1–27.

Braitseva, O.A., Melekestsev, I. V., Ponomareva, V. V. and Sulerzhitsky, L.D. 1995. Ages of calderas, large explosive craters and active volcanoes in the Kuril-Kamchatka region, Russia. *Bulletin of Volcanology*. **57**(6), pp.383–402.

Brey, G.P. and Kohler, T. 1990. Geothermobarometry in four-phase lherzolites II. New thermobarometers, and practical assessment of existing thermobarometers. *Journal of Petrology*. **31**(6), pp.1353–1378.

Bryant, J.A., Yogodzinski, G.M. and Churikova, T.G. 2007. Melt-mantle interactions beneath the Kamchatka arc: Evidence from ultramafic xenoliths from Shiveluch volcano. *Geochemistry, Geophysics, Geosystems*. **8**(4).

Bucholz, C.E., Gaetani, G.A., Behn, M.D. and Shimizu, N. 2013. Post-entrapment modification of volatiles and oxygen fugacity in olivine-hosted melt inclusions. *Earth and Planetary Science Letters*. **374**, pp.145–155.

Cannaò, E., Agostini, S., Scambelluri, M., Tonarini, S. and Godard, M. 2015. B, Sr and Pb isotope geochemistry of high-pressure Alpine metaperidotites monitors fluid-mediated element recycling during serpentinite dehydration in subduction

mélange (Cima di Gagnone, Swiss Central Alps). *Geochimica et Cosmochimica Acta*. **163**, pp.80–100.

Castellana, B. 1998. *Geology, chemostratigraphy, and petrogenesis of the Avachinsky volcano, Kamchatka, Russia*.

Chevychelov, V.Y. and Suk, N.I. 2003. Influence of the composition of magmatic melt on the solubility of metal chlorides at pressures of 0.1-3.0 kbar. *Petrology*. **11**(1), pp.68–81.

Churikova, T., Dorendorf, F. and Wörner, G. 2001. Sources and fluids in the mantle wedge below Kamchatka, evidence from across-arc geochemical variation. *Journal of Petrology*. **42**(8), pp.1567–1593.

Churikova, T., Wörner, G., Mironov, N. and Kronz, A. 2007. Volatile (S, Cl and F) and fluid mobile trace element compositions in melt inclusions: Implications for variable fluid sources across the Kamchatka arc. *Contributions to Mineralogy and Petrology*. **154**(2), pp.217–239.

Dalou, C., Koga, K.T., Le Voyer, M. and Shimizu, N. 2014. Contrasting partition behavior of F and Cl during hydrous mantle melting: implications for Cl/F signature in arc magmas. *Progress in Earth and Planetary Science*. **1**(1), pp.1–17.

Dalou, C., Le Losq, C., Mysen, B.O. and Cody, G.D. 2015. Solubility and solution mechanisms of chlorine and fluorine in aluminosilicate melts at high pressure and high temperature. *American Mineralogist*. **100**(10), pp.2272–2283.

Dalou, C. and Mysen, B.O. 2015. The effect of H2O on F and Cl solubility and solution mechanisms of in aluminosilicate melts at high pressure and high temperature. *American Mineralogist*. **100**(2–3), pp.633–643.

Debret, B., Koga, K.T., Cattani, F., Nicollet, C., Van den Bleeken, G. and Schwartz, S. 2016. Volatile (Li, B, F and Cl) mobility during amphibole breakdown in subduction zones. *Lithos*. **244**, pp.165–181.

Deer, W.A., Howie, R.A. and Zussman, J. 1992. *An introduction to the rock-forming minerals* 2nd ed. Harlow, England: Pearson Education Limited.

Defant, M.J. and Drummond, M.S. 1990. Derivation of some modern arc magmas by melting of young subducted lithosphere. *Nature*. **347**, pp.662–665.

DeHoog, J.C.M., Monteleone, B.D., Savov, I.P., Marschall, H.R. and Zack, T. 2017. Matrix effects in B isotope analysis of silicate minerals by SIMS. *Goldschmidt abstracts*., p.872.

DeHoog, J.C.M. and Savov, I.P. 2018. Boron isotopes as a tracer of subduction zone processes *In*: H. R. Marschall and G. Foster, eds. *Boron isotopes: The fifth element*. Cham: Springer International Publishing, pp.217–247.

Dorendorf, F., Churikova, T., Koloskov, A. and Worner, G. 2000. Late Pleistocene to Holocene activity at Bakening volcano and surrounding monogenetic centers (Kamchatka): Volcanic geology and geochemical evolution. *Journal of Volcanology and Geothermal Research*. **104**(1–4), pp.131–151.

Droop, G.T.R. 1987. A general equation for estimating Fe3+ concentrations in ferromagnesian silicates and oxides from microprobe analyses, using

stoichiometric criteria. *Mineralogical Magazine*. **51**(361), pp.431–435.

Duggen, S., Portnyagin, M., Baker, J., Ulfbeck, D., Hoernle, K., Garbe-Schönberg, D. and Grassineau, N. 2007. Drastic shift in lava geochemistry in the volcanic-front to rear-arc region of the Southern Kamchatkan subduction zone: Evidence for the transition from slab surface dehydration to sediment melting. *Geochimica et Cosmochimica Acta*. **71**(2), pp.452–480.

Edgar, A.D. and Pizzolato, L.A. 1995. An experimental study of partitioning of fluorine between K-richterite, apatite, phlogopite, and melt at 20 kbar. *Contributions to Mineralogy and Petrology*. **121**(3), pp.247–257.

Eiler, J.M., Crawford, A., Elliott, T., Farley, K.A., Valley, J.W. and Stolper, E.M. 2000. Oxygen isotope geochemistry of oceanic arc lavas. *Journal of Petrology*. **41**(2), pp.229–256.

Elliott, T. 2004. Tracers of the slab *In*: J. M. Eiler, ed. *Geophysical Monograph Series*. Washington, DC: American Geophysical Union, pp.23–45.

Ferlito, C. 2011. Bimodal geochemical evolution at Sheveluch stratovolcano, Kamchatka, Russia: Consequence of a complex subduction at the junction of the Kuril Kamchatka and Aleutian island arcs. *Earth-Science Reviews*. **105**(1–2), pp.49–69.

Finch, A. 1995. Metasomatic overprinting by juvenile igneous fluids, Igdlerfigsalik, South Greenland. *Contributions to Mineralogy and Petrology*. **122**(1–2), pp.11–24.

Foley, S.F., Barth, M.G. and Jenner, G.A. 2000. Rutile/melt partition coefficients for trace elements and an assessment of the influence of rutile on the trace element characteristics of subduction zone magmas. *Geochimica et Cosmochimica Acta*. **64**(5), pp.933–938.

Frey, F.A., John Suen, C. and Stockman, H.W. 1985. The Ronda high temperature peridotite: Geochemistry and petrogenesis. *Geochimica et Cosmochimica Acta*. **49**(11), pp.2469–2491.

Gaetani, G.A. and Grove, T.L. 1998. The influence of water on melting of mantle peridotite. *Contributions to Mineralogy and Petrology*. **131**(4), pp.323–346.

Giesting, P.A. and Filiberto, J. 2014. Quantitative models linking igneous amphibole composition with magma Cl and OH content. *American Mineralogist*. **99**(4), pp.852–865.

Gorbach, N., Portnyagin, M. and Tembrel, I. 2013. Volcanic structure and composition of Old Shiveluch volcano, Kamchatka. *Journal of Volcanology and Geothermal Research*. **263**, pp.193–208.

Gorbatov, A., Kostoglodov, V., Suarez, G. and Gordeev, E. 1997. Seismicity and structure of the Kamchatka subduction zone. *Journal of Geophysical Research*. **102**, pp.17883–17898.

Gordeychik, B., Churikova, T., Kronz, A., Sundermeyer, C., Simakin, A. and Wörner, G. 2018. Growth of, and diffusion in, olivine in ultra-fast ascending basalt magmas from Shiveluch volcano. *Scientific Reports*. **8**(1).

Green, T.H., Blundy, J.D., Adam, J. and Yaxley, G.M. 2000. SIMS determination of

trace element partition coefficients between garnet, clinopyroxene and hydrous basaltic liquids at 2-7.5 GPa and 1080-1200°C. *Lithos*. **53**(3–4), pp.165–187.

Gregoire, M., McInnes, B.I.A. and Reilly, S.Y.O. 2001. Hydrous metasomatism of oceanic sub-arc mantle, Lihir, Papua New Guinea Part 2 . Trace element characteristics of slab-derived fluids. *Lithos*. **59**, pp.91–108.

Grove, T.L., Chatterjee, N., Parman, S.W. and Médard, E. 2006. The influence of H2O on mantle wedge melting. *Earth and Planetary Science Letters*. **249**(1–2), pp.74–89.

Guidotti, C. V. 1984. Micas in metamorphic rocks *In*: S. W. Bailey, ed. *Micas*. Chelsea: Mineralogical Society of America, pp.357–456.

Halama, R., Savov, I.P., Rudnick, R.L. and McDonough, W.F. 2009. Insights into Li and Li isotope cycling and sub-arc metasomatism from veined mantle xenoliths, Kamchatka. *Contributions to Mineralogy and Petrology*. **158**(2), pp.197–222.

Hall, R. 2002. Cenozoic geological and plate tectonic evolution of SE Asia and the SW Pacific. *Journal of Asian Earth Sciences*. **20**, pp.353–431.

Harvey, J., Garrido, C.J., Savov, I., Agostini, S., Padrón-Navarta, J.A., Marchesi, C., López Sánchez-Vizcaíno, V. and Gómez-Pugnaire, M.T. 2014. 11B-rich fluids in subduction zones: The role of antigorite dehydration in subducting slabs and boron isotope heterogeneity in the mantle. *Chemical Geology*. **376**, pp.20–30.

Harvey, J., Yoshikawa, M., Hammond, S.J. and Burton, K.W. 2012. Deciphering the trace element characteristics in Kilbourne hole peridotite xenoliths: Melt-rock interaction and metasomatism beneath the Rio Grande Rift, SW USA. *Journal of Petrology*. **53**(8), pp.1709–1742.

Hawkesworth, C.J., Turner, S.P., McDermott, F., Peate, D.W. and van Calsteren, P. 1997. U-Th isotopes in arc magmas: Implications for element transfer from the subducted crust. *Science*. **276**, pp.551–555.

Hellebrand, E., Snow, J.E., Dick, H.J. and Hofmann, A.W. 2001. Coupled major and trace elements as indicators of the extent of melting in mid-ocean-ridge peridotites. *Nature*. **410**, pp.677–681.

Hervig, R.L., Moore, G.M., Williams, L.B., Peacock, S.M., Holloway, J.R. and Roggensack, K. 2002. Isotopic and elemental partitioning of boron between hydrous fluid and silicate melt. *American Mineralogist*. **87**(5–6), pp.769–774.

Hickey, R.L. and Frey, F.A. 1982. Geochemical characteristics of boninite series volcanics: Implications for their source. *Geochimica et Cosmochimica Acta*. **46**(11), pp.2099–2115.

Hirschmann, M.M. 2000. Mantle solidus: Experimental constraints and the effects of peridotite composition. *Geochemistry, Geophysics, Geosystems*. **1**.

Hochstaedter, A.G., Kepezhinskas, P. and Defant, M. 1996. Insights into the volcanic arc mantle wedge from magnesian lavas from the Kamchatka arc. *Journal of Geophysical Research*. **101**(B1), pp.697–712.

Humphreys, M.C.S. 2006. *Andesite petrogenesis and magmatic processes at Shiveluch Volcano, Kamchatka*. University of Bristol.

Humphreys, M.C.S., Blundy, J.D. and Sparks, R.S.J. 2006. Magma evolution and open-system processes at Shiveluch Volcano: Insights from phenocryst zoning. *Journal of Petrology*. **47**(12), pp.2303–2334.

Humphreys, M.C.S., Blundy, J.D. and Sparks, R.S.J. 2008. Shallow-level decompression crystallisation and deep magma supply at Shiveluch Volcano. *Contributions to Mineralogy and Petrology*. **155**, pp.45–61.

Humphreys, M.C.S., Cooper, G.F., Zhang, J., Loewen, M., Kent, A.J.R., Macpherson, C.G. and Davidson, J.P. 2019. Unravelling the complexity of magma plumbing at Mount St. Helens: A new trace element partitioning scheme for amphibole. *Contributions to Mineralogy and Petrology*. **174**(9).

Ionov, D.A. 2010. Petrology of mantle wedge lithosphere: New data on supra-subduction zone peridotite xenoliths from the andesitic Avacha volcano, Kamchatka. *Journal of Petrology*. **51**(1–2), pp.327–361.

Ionov, D.A., Bénard, A. and Plechov, P.Y. 2011. Melt evolution in subarc mantle: Evidence from heating experiments on spinel-hosted melt inclusions in peridotite xenoliths from the andesitic Avacha volcano (Kamchatka, Russia). *Contributions to Mineralogy and Petrology*. **162**(6), pp.1159–1174.

Ionov, D.A., Bénard, A., Plechov, P.Y. and Shcherbakov, V.D. 2013. Along-arc variations in lithospheric mantle compositions in Kamchatka, Russia: First trace element data on mantle xenoliths from the Klyuchevskoy Group volcanoes. *Journal of Volcanology and Geothermal Research*. **263**, pp.122–131.

Ionov, D.A., Bodinier, J.L., Mukasa, S.B. and Zanetti, A. 2002. Mechanisms and sources of mantle metasomatism: Major and trace element compositions of peridotite xenoliths from Spitsbergen in the context of numerical modelling. *Journal of Petrology*. **43**(12), pp.2219–2259.

Ionov, D.A. and Seitz, H.M. 2008. Lithium abundances and isotopic compositions in mantle xenoliths from subduction and intra-plate settings: Mantle sources vs. eruption histories. *Earth and Planetary Science Letters*. **266**(3–4), pp.316–331.

Ishikawa, T., Tera, F. and Nakazawa, T. 2001. Boron isotope and trace element systematics of the three volcanic zones in the Kamchatka arc. *Geochimica et Cosmochimica Acta*. **65**(24), pp.4523–4537.

Ishimaru, S. and Arai, S. 2008. Calcic amphiboles in peridotite xenoliths from Avacha volcano, Kamchatka, and their implications for metasomatic conditions in the mantle wedge *In*: M. Coltorti and M. Gregoire, eds. *Metasomatism in oceanic and continental lithospheric mantle*. London: The Geological Society Special Publications, pp.35–55.

Ishimaru, S. and Arai, S. 2011. Peculiar Mg-Ca-Si metasomatism along a shear zone within the mantle wedge: Inference from fine-grained xenoliths from Avacha volcano, Kamchatka. *Contributions to Mineralogy and Petrology*. **161**(5), pp.703–720.

Ishimaru, S., Arai, S., Ishida, Y., Shirasaka, M. and Okrugin, V.M. 2007. Melting and multi-stage metasomatism in the mantle wedge beneath a frontal arc inferred from highly depleted peridotite xenoliths from the Avacha volcano,

southern Kamchatka. *Journal of Petrology*. **48**(2), pp.395–433.

Iveson, A.A., Webster, J.D., Rowe, M.C. and Neill, O.K. 2017. Major element and halogen (F, Cl) mineral-melt-fluid partitioning in hydrous rhyodacitic melts at shallow crustal conditions. *Journal of Petrology*. **58**(12), pp.2465–2492.

John, T., Gussone, N., Podladchikov, Y.Y., Bebout, G.E., Dohmen, R., Halama, R., Klemd, R., Magna, T. and Seitz, H.M. 2012. Volcanic arcs fed by rapid pulsed fluid flow through subducting slabs. *Nature Geoscience*. **5**(7), pp.489–492.

John, T., Scambelluri, M., Frische, M., Barnes, J.D. and Bach, W. 2011. Dehydration of subducting serpentinite: Implications for halogen mobility in subduction zones and the deep halogen cycle. *Earth and Planetary Science Letters*. **308**(1–2), pp.65–76.

Johnson, K.T.M., Dick, H.J.B. and Shimizu, N. 1990. Melting in the oceanic upper mantle: An ion microprobe study of diopsides in abyssal peridotites. *Journal of Geophysical Research*. **95**(B3), p.2661.

Kakihana, H., Kotaka, M., Satoh, S., Nomura, M. and Okamoto, M. 1977. Fundamental studies on the ion-exchange separation of boron isotopes. *Bulletin of the chemical society of Japan*. **50**(1), pp.158–163.

Kelemen, P.B. 1990. Reaction between ultramafic rock and fractionating basaltic magma I. phase relations, the origin of calc-alkaline magma series, and the formation of discordant dunite. *Journal of Petrology*. **31**(1), pp.51–98.

Kelemen, P.B., Hanghoj and Greene 2003. One view of the geochemistry of subduction-related magmatic arcs, with an emphasis on primitive andesite and lower crut *In*: R. L. Rudnick, H. D. Holland and K. K. Turekian, eds. *Treatise on Geochemistry*. Oxford: Elsevier, pp.593–659.

Kelley, K.A., Plank, T., Grove, T.L., Stolper, E.M., Newman, S. and Hauri, E. 2006. Mantle melting as a function of water content beneath back-arc basins. *Journal of Geophysical Research*. **111**(B09208).

Kepezhinskas, P. and Defant, M.J. 1996. Constraining styles of mantle metasomatism above subduction zones: Constraints from ultramafic xenoliths in Kamchatka *In*: G. E. Bebout, D. W. Scholl, S. H. Kirby and J. P. Platt, eds. *Subduction: Top to Bottom*. Washington, DC: American Geophysical Union, pp.307–314.

Kepezhinskas, P., McDermott, F., Defant, M.J., Hochstaedter, A., Drummond, M.S., Hawkesworth, C.J., Koloskov, A., Maury, R.C. and Bellon, H. 1997. Trace element and Sr-Nd-Pb isotopic constraints on a three-component model of Kamchatka arc petrogenesis. *Geochimica et Cosmochimica Acta*. **61**(3), pp.577–600.

Kepezhinskas, P.K., Defant, M.J. and Drummond, M.S. 1995. Na metasomatism in the island-arc mantle by slab melt-peridotite interaction: Evidence from mantle xenoliths in the north Kamchatka arc. *Journal of Petrology*. **36**(6), pp.1505–1527.

Kersting, A.B. and Arculus, R.J. 1995. Pb systematics of Klyuchevskoy Volcano, Kamchatka, and North Pacific sediments: Implications for magma genesis and sediment recycling in the Kamchatkan Arc. *Earth and Planetary Science*

Letters. **136**, pp.133–148.

Koloskov, A. V., Martynov, Y.A. and Ananiev, V. V. 2017. New isotope–geochemical and mineralogical data on the ultramafic xenoliths in the volcanic rocks of the Kamchatka–Koryak region: Two types of mantle protolith in the modern island-arc system. *Russian Journal of Pacific Geology*. **11**(2), pp.95–109.

Konrad-Schmolke, M. and Halama, R. 2014. Combined thermodynamic-geochemical modeling in metamorphic geology: Boron as tracer of fluid-rock interaction. *Lithos*. **208**–**209**, pp.393–414.

Konrad-Schmolke, M., Halama, R. and Manea, V.C. 2016. Slab mantle dehydrates beneath Kamchatka—Yet recycles water into the deep mantle. *Geochemistry, Geophysics, Geosystems*. **17**(8), pp.2987–3007.

Kuritani, T., Kitagawa, H. and Nakamura, E. 2005. Assimilation and fractional crystallization controlled by transport process of crustal melt: Implications from an alkali basalt-dacite suite from Rishiri Volcano, Japan. *Journal of Petrology*. **46**(7), pp.1421–1442.

Lander, A. V. and Shapiro, M.N. 2007. The origin of the modern Kamchatka subduction zone *In*: J. C. Eichelberger, E. Gordeev, P. Izbekov, M. Kasahara and J. Lees, eds. *Volcanism and Subduction: The Kamchatka Region*. Washington, DC: American Geophysical Union, pp.57–64.

LaTourrette, T., Hervig, R.L. and Holloway, J.R. 1995. Trace element partitioning between amphibole, phlogopite, and basanite melt. *Earth and Planetary Science Letters*. **135**, pp.13–30.

Leake, B.E., Woolley, A.R., Arps, C.E.S., Birch, W.D., Gilbert, M.C., Grice, J.D., Hawthorne, F.C., Kato, A., Kisch, H.J., Krivovichev, V.G., Linthout, K., Laird, J., Mandarino, J.A., Maresch, W.V., Nickel, E.H., Rock, N.M.S., Schumacher, J.C., Smith, D.C., Stephenson, N.C.N., Ungaretti, L., Whittaker, E.J.W. and Youzhi, G. 1997. Nomenclature of amphiboles: Report of the subcommittee on amphiboles of the international mineralogical association, commission on new minerals and mineral names. *The Canadian Mineralogist*. **35**, pp.219–246.

LeBas, M.J., Le Maitre, R.N., Streckeisen, A. and Zanettin, B. 1986. A chemical classification of volcanic rocks based on the total alkali-silica diagram. *Journal of Petrology*. **27**(3), pp.745–750.

Leeman, W.P., Tonarini, S., Chan, L.H. and Borg, L.E. 2004. Boron and lithium isotopic variations in a hot subduction zone - The southern Washington Cascades. *Chemical Geology*. **212**(1–2), pp.101–124.

LeRoux, V., Bodinier, J.L., Tommasi, A., Alard, O., Dautria, J.M., Vauchez, A. and Riches, A.J.V. 2007. The Lherz spinel lherzolite: Refertilized rather than pristine mantle. *Earth and Planetary Science Letters*. **259**(3–4), pp.599–612.

Levin, V., Park, J., Brandon, M., Lees, J., Peyton, V., Gordeev, E. and Ozerov, A. 2002. Crust and upper mantle of Kamchatka from teleseismic receiver functions. *Tectonophysics*. **358**(1–4), pp.233–265.

Levin, V., Shapiro, N.M., Park, J. and Ritzwoller, M.H. 2002. Seismic evidence for catastrophic slab loss beneath Kamchatka. *Nature*. **418**, pp.763–767.

Levin, V., Shapiro, N.M., Park, J. and Ritzwoller, M.H. 2005. Slab portal beneath the western Aleutians. *Geology*. **33**(4), pp.253–256.

LeVoyer, M., Rose-Koga, E.F., Shimizu, N., Grove, T.L. and Schiano, P. 2010. Two contrasting H2O-rich components in primary melt inclusions from Mount Shasta. *Journal of Petrology*. **51**(7), pp.1571–1595.

Luhr, J.F., Allan, J.F., Carmichael, I.S.E., Nelson, S.A. and Hasenaka, T. 1989. Primitive calc-alkaline and alkaline rock types from the western Mexican Volcanic Belt. *Journal of Geophysical Research*. **94**(B4), pp.4515–4530.

Luhr, J.F. and Aranda-Gómez, J.J. 1997. Mexican peridotite xenoliths and tectonic terranes: Correlations among vent location, texture, temperature, pressure, and oxygen fugacity. *Journal of Petrology*. **38**(8), pp.1075–1112.

Manea, V.C., Leeman, W.P., Gerya, T., Manea, M. and Zhu, G. 2014. Subduction of fracture zones controls mantle melting and geochemical signature above slabs. *Nature Communications*. **5**, p.5095.

Marschall, H.R., Ludwig, T., Altherr, R., Kalt, A. and Tonarini, S. 2006. Syros metasomatic tourmaline: Evidence for very high-δ11 B fluids in subduction zones. *Journal of Petrology*. **47**(10), pp.1915–1942.

Marschall, H.R., Wanless, V.D., Shimizu, N., Pogge von Strandmann, P.A.E., Elliott, T. and Monteleone, B.D. 2017. The boron and lithium isotopic composition of mid-ocean ridge basalts and the mantle. *Geochimica et Cosmochimica Acta*. **207**, pp.102–138.

Mattioli, G.S. and Wood, B.J. 1988. Magnetite activities across the MgAl2O4-Fe3O4 spinel join, with application to thermobarometric estimates of upper mantle oxygen fugacity. *Contributions to Mineralogy and Petrology*. **98**(2), pp.148–162.

Maury, R., Defant, M.J. and Joron, J.-L. 1992. Metasomatism of the sub-arc mantle inferred from trace elements in Philippine xenoliths. *Nature*. **360**, pp.661–663.

McCaig, A.M., Titarenko, S.S., Savov, I.P., Cliff, R.A., Banks, D., Boyce, A. and Agostini, S. 2018. No significant boron in the hydrated mantle of most subducting slabs. *Nature Communications*. **9**(1).

McDonough, W.F. and Sun 1995. The composition of the Earth. *Chemical Geology*. **2541**(94), pp.223–253.

McInnes, B.I.A., Gregoire, M., Binns, R.A., Herzig, P.M. and Hannington, M.D. 2001. Hydrous metasomatism of oceanic sub-arc mantle, Lihir, Papua New Guinea: Petrology and geochemistry of fluid-metasomatised mantle wedge xenoliths. *Earth and Planetary Science Letters*. **188**(1–2), pp.169–183.

Mercier, J.C.C. and Nicolas, A. 1975. Textures and fabrics of upper-mantle peridotites as illustrated by xenoliths from basalts. *Journal of Petrology*. **16**(2), pp.454–487.

Moore, M., Chakhmouradian, A.R., Mariano, A.N. and Sidhu, R. 2015. Evolution of rare-earth mineralization in the Bear Lodge carbonatite, Wyoming: Mineralogical and isotopic evidence. *Ore Geology Reviews*. **64**, pp.499–521.

Morimoto, N. 1988. Nomenclature of pyroxenes. *Mineralogy and Petrology*. **39**(1),

pp.55–76.

Morris, J.D., Leeman, W.P. and Tera, F. 1990. The subducted component in island arc lavas: Constraints from Be isotopes and B-Be systematics. *Nature*. **344**, pp.31–36.

Mukasa, S.B., Blatter, D.L. and Andronikov, A. V. 2007. Mantle peridotite xenoliths in andesite lava at El Peñon, central Mexican Volcanic Belt: Isotopic and trace element evidence for melting and metasomatism in the mantle wedge beneath an active arc. *Earth and Planetary Science Letters*. **260**(1–2), pp.37–55.

Münker, C., Wörner, G., Yogodzinski, G. and Churikova, T. 2004. Behaviour of high field strength elements in subduction zones: Constraints from Kamchatka-Aleutian arc lavas. *Earth and Planetary Science Letters*. **224**(3–4), pp.275–293.

Munoz, J.L. 1984. F-OH and Cl-OH exchange in micas with applications to hydrothermal ore deposits *In*: S. W. Bailey, ed. *Micas*. Chelsea: Mineralogical Society of America, pp.469–491.

Munoz, J.L. and Swenson, A. 1981. Chloride-hydroxyl exchange in biotite and estimation of relative HCl/HF activities in hydrothermal fluids. *Economic Geology*. **76**(8), pp.2212–2221.

Nandedkar, R.H., Hürlimann, N., Ulmer, P. and Müntener, O. 2016. Amphibole–melt trace element partitioning of fractionating calc-alkaline magmas in the lower crust: an experimental study. *Contributions to Mineralogy and Petrology*. **171**(8–9).

Nekrylov, N., Portnyagin, M. V., Kamenetsky, V.S., Mironov, N.L., Churikova, T.G., Plechov, P.Y., Abersteiner, A., Gorbach, N. V., Gordeychik, B.N., Krasheninnikov, S.P., Tobelko, D.P., Shur, M.Y., Tetroeva, S.A., Volynets, A.O., Hoernle, K. and Wörner, G. 2018. Chromium spinel in Late Quaternary volcanic rocks from Kamchatka: Implications for spatial compositional variability of subarc mantle and its oxidation state. *Lithos*. **322**, pp.212–224.

Nielsen, S.G. and Marschall, H.R. 2017. Geochemical evidence for mélange melting in global arcs. *Science Advances*. **3**.

O'Neill, H.S.C. 1981. The transition between spinel lherzolite and garnet lherzolite, and its use as a geobarometer. *Contributions to Mineralogy and Petrology*. **77**(2), pp.185–194.

O'Neill, H.S.C. and Wall, V.J. 1987. The olivine-orthopyroxene-spinel oxygen geobarometer, the nickel precipitation curve, and the oxygen fugacity of the Earth' s upper mantle. *Journal of Petrology*. **28**, pp.1169–1191.

Oberti, R., Ungaretti, L., Cannillo, E. and Hawthorne, F.C. 1993. The mechanism of Cl incorporation into amphibole. *American Mineralogist*. **78**, pp.746–752.

Pabst, S., Zack, T., Savov, I.P., Ludwig, T., Rost, D., Tonarini, S. and Vicenzi, E.P. 2012. The fate of subducted oceanic slabs in the shallow mantle: Insights from boron isotopes and light element composition of metasomatized blueschists from the Mariana forearc. *Lithos*. **132**–**133**, pp.162–179.

Padrón-Navarta, J.A., Sánchez-Vizcaí, V.L., Garrido, C.J. and Gómez-Pugnaire, M.T. 2011. Metamorphic record of high-pressure dehydration of antigorite serpentinite to chlorite harzburgite in a subduction setting (Cerro del Almirez,

Nevado-Filábride complex, Southern Spain). *Journal of Petrology*. **52**(10), pp.2047–2078.

Parkinson, I.J. and Pearce, J.A. 1998. Peridotites from the Izu-Bonin-Mariana forearc (ODP Leg 125): Evidence for mantle melting and melt-mantle interaction in a supra-subduction zone setting. *Journal of Petrology*. **39**(9), pp.1577–1618.

Peacock, S.M. and Hervig, R.L. 1999. Boron isotopic composition of subduction-zone metamorphic rocks. *Chemical Geology*. **160**(4), pp.281–290.

Pearce, J.A., van der Laan, S.R., Arculus, R.J., Murton, B.J., Ishii, T., Peate, D.W. and Parkinson, I.J. 1992. Boninite and harzburgite from Leg 125 (Bonin-Mariana Forearc): A case study of magma genesis during the initial stages of subduction. *Proceedings of the Ocean Drilling Program, Scientific Results*. **125**, pp.623–662.

Peters, D., Bretscher, A., John, T., Scambelluri, M. and Pettke, T. 2017. Fluid-mobile elements in serpentinites: Constraints on serpentinisation environments and element cycling in subduction zones. *Chemical Geology*. **466**, pp.654–666.

Peyton, V., Levin, V., Park, J., Brandon, M., Lees, J., Gordeev, E. and Ozerov, A. 2001. Mantle flow at a slab edge: Seismic anisotropy in the Kamchatka region. *Geophysical Research Letters*. **28**(2), pp.379–382.

Pirard, C. and Hermann, J. 2015. Focused fluid transfer through the mantle above subduction zones. *Geology*. **43**(10), pp.915–918.

Plank, T. 2014. The chemical composition of subducting sediments *In*: H. D. Holland and K. K. Turekian, eds. *Treatise on Geochemistry: Second Edition*. Amsterdam; Boston: Elsevier Ltd., pp.607–629.

Plümper, O., John, T., Podladchikov, Y.Y., Vrijmoed, J.C. and Scambelluri, M. 2016. Fluid escape from subduction zones controlled by channel-forming reactive porosity. *Nature Geoscience*. **10**, pp.150–156.

Ponomareva, V., Kyle, P., Pevzner, M., Sulerzhitsky, L. and Hartman, M. 2007. Holocene eruptive history of Shiveluch volcano, Kamchatka peninsula, Russia *In*: J. C. Eichelberger, E. Gordeev, P. Izbekov, M. Kasahara and J. Lees, eds. *Volcanism and subduction: The Kamchatka region*. Washington, DC: American Geophysical Union, pp.263–282.

Portnyagin, M., Hoernle, K., Plechov, P., Mironov, N. and Khubunaya, S. 2007. Constraints on mantle melting and composition and nature of slab components in volcanic arcs from volatiles (H2O, S, Cl, F) and trace elements in melt inclusions from the Kamchatka arc. *Earth and Planetary Science Letters*. **255**(1–2), pp.53–69.

Portnyagin, M. and Manea, V.C. 2008. Mantle temperature control on composition of arc magmas along the Central Kamchatka Depression. *Geology*. **36**(7), pp.519–522.

Prigent, C., Guillot, S., Agard, P., Lemarchand, D., Soret, M. and Ulrich, M. 2018. Transfer of subduction fluids into the deforming mantle wedge during nascent subduction: Evidence from trace elements and boron isotopes (Semail ophiolite, Oman). *Earth and Planetary Science Letters*. **484**, pp.213–228.

Putirka, K.D. 2008. Thermometers and barometers for volcanic systems. *Reviews in Mineralogy and Geochemistry*. **69**(1), pp.61–120.

Pyle, D.M. and Mather, T.A. 2009. Halogens in igneous processes and their fluxes to the atmosphere and oceans from volcanic activity: A review. *Chemical Geology*. **263**, pp.110–121.

Reubi, O. and Blundy, J. 2009. A dearth of intermediate melts at subduction zone volcanoes and the petrogenesis of arc andesites. *Nature*. **461**, pp.1269–1273.

Robert, J.-L., Beny, J.-M., Ventura, G. Della and Hardy, M. 1993. Fluorine in micas: crystal-chemical control of the OH-F distribution between trioctahedral and dioctahedral sites. *European Journal of Mineralogy*. **5**(1), pp.7–18.

Rudnick, R.L., McDonough, W.F. and Chappell, B.W. 1993. Carbonatite metasomatism in the northern Tanzanian mantle: Petrographic and geochemical characteristics. *Earth and Planetary Science Letters*. **114**(4), pp.463–475.

Rüpke, L.H., Morgan, J.P., Hort, M. and Connolly, J.A.D. 2004. Serpentine and the subduction zone water cycle. *Earth and Planetary Science Letters*. **223**(1–2), pp.17–34.

Ryan, W.B.F., Carbotte, S.M., Coplan, J.O., O'Hara, S., Melkonian, A., Arko, R., Weissel, R.A., Ferrini, V., Goodwillie, A., Nitsche, F., Bonczkowski, J. and Zemsky, R. 2009. Global multi-resolution topography synthesis. *Geochemistry, Geophysics, Geosystems*. **10**(3).

Savelieva, G.N., Batanova, V.G. and Sobolev, A. V. 2016. Pyroxene–Cr-spinel exsolution in mantle lherzolites of the Syum-Keu ophiolite massif (Arctic Urals). *Russian Geology and Geophysics*. **57**(10), pp.1419–1436.

Savov, I.P., Ryan, J.G., D'Antonio, M. and Fryer, P. 2007. Shallow slab fluid release across and along the Mariana arc-basin system: Insights from geochemistry of serpentinized peridotites from the Mariana fore arc. *Journal of Geophysical Research: Solid Earth*. **112**(9).

Scambelluri, M. and Tonarini, S. 2012. Boron isotope evidence for shallow fluid transfer across subduction zones by serpentinized mantle. *Geology*. **40**(10), pp.907–910.

Siegrist, M., Yogodzinski, G., Bizimis, M., Fournelle, J., Churikova, T., Dektor, C. and Mobley, R. 2019. Fragments of metasomatized forearc: Origin and implications of mafic and ultramafic xenoliths from Kharchinsky volcano, Kamchatka. *Geochemistry, Geophysics, Geosystems*. **20**.

Sobolev, A. V., Hofmann, A.W., Kuzmin, D. V., Yaxley, G.M., Arndt, N.T., Chung, S.L., Danyushevsky, L. V., Elliott, T., Frey, F.A., Garcia, M.O., Gurenko, A.A., Kamenetsky, V.S., Kerr, A.C., Krivolutskaya, N.A., Matvienkov, V. V., Nikogosian, I.K., Rocholl, A., Sigurdsson, I.A., Sushchevskaya, N.M. and Teklay, M. 2007. The amount of recycled crust in sources of mantle-derived melts. *Science*. **316**(5823), pp.412–417.

Sobolev, A. V., Hofmann, A.W., Sobolev, S. V. and Nikogosian, I.K. 2005. An olivine-free mantle source of Hawaiian shield basalts. *Nature*. **42**(4), pp.417–421.

Soustelle, V., Tommasi, A., Demouchy, S. and Ionov, D.A. 2010. Deformation and

fluid-rock interaction in the supra-subduction mantle: Microstructures and water contents in peridotite xenoliths from the Avacha volcano, Kamchatka. *Journal of Petrology*. **51**(1–2), pp.363–394.

Spandler, C., Pettke, T. and Hermann, J. 2014. Experimental study of trace element release during ultrahigh-pressure serpentinite dehydration. *Earth and Planetary Science Letters*. **391**, pp.296–306.

Speer, J.A. 1984. Micas in igneous rocks *In*: S. W. Bailey, ed. *Micas*. Chelsea: Mineralogical Society of America, pp.299–349.

Straub, S.M., LaGatta, A.B., Martin-Del Pozzo, A.L. and Langmuir, C.H. 2008. Evidence from high-Ni olivines for a hybridized peridotite/pyroxenite source for orogenic andesites from the central Mexican Volcanic Belt. *Geochemistry, Geophysics, Geosystems*. **9**(3).

Straub, S.M. and Layne, G.D. 2003. The systematics of chlorine, fluorine, and water in Izu arc front volcanic rocks: Implications for volatile recycling in subduction zones. *Geochimica et Cosmochimica Acta*. **67**(21), pp.4179–4203.

Streckeisen A. 1979. Classification and nomenclature of volcanic rocks, lamprophyres, carbonatites, and melilitic rocks: Recommendations and suggestions of the IUGS Subcommission on the Systematics of Igneous Rocks. *Geology*. **7**, pp.331–335.

Sun, S. and McDonough, W.F. 1989. Chemical and isotopic systematics of oceanic basalts : implications for mantle composition and processes *In*: A. D. Saunders and M. J. Norry, eds. *Magmatism in the ocean basins*. Oxford, London, Edinburgh, Boston, Melbourne: Geological Society Special Publication, pp.313–345.

Syracuse, E.M., van Keken, P.E., Abers, G.A., Suetsugu, D., Bina, C., Inoue, T., Wiens, D. and Jellinek, M. 2010. The global range of subduction zone thermal models. *Physics of the Earth and Planetary Interiors*. **183**(1–2), pp.73–90.

Tatsumi, Y. 1989. Migration of fluid phases and genesis of basalt magmas in subduction zones. *Journal of Geophysical Research*. **94**(B4), pp.4697–4707.

Tollan, P.M.E., Dale, C.W., Hermann, J., Davidson, J.P. and Arculus, R.J. 2017. Generation and modification of the mantle wedge and lithosphere beneath the West Bismarck Island Arc: Melting, metasomatism and thermal history of peridotite xenoliths from Ritter Island. *Journal of Petrology*. **58**(8), pp.1475–1510.

Tolstykh, M.L., Pevzner, M.M., Naumov, V.B. and Babansky, A.D. 2019. Characteristics of acid melts that produced the tephra of Pleistocene–Holocene eruptions of Ichinsky volcano, Kamchatka: Evidence from melt inclusions. *Geochemistry International*. **57**(3), pp.243–265.

Tomanikova, L., Savov, I.P., Harvey, J., de Hoog, J.C.M., Churikova, T.G., Gordeychik, B. and Yogodzinski, G.M. 2019. A limited role for metasomatized subarc mantle in the generation of boron isotope signatures of arc volcanic rocks. *Geology*. **47**(6), pp.517–521.

Tonarini, S., Leeman, W.P. and Leat, P.T. 2011. Subduction erosion of forearc mantle wedge implicated in the genesis of the South Sandwich Island (SSI) arc:

Evidence from boron isotope systematics. *Earth and Planetary Science Letters*. **301**(1–2), pp.275–284.

Turner, S., McDermott, F., Hawkesworth, C. and Kepezhinskas, P. 1998. A U-series study of lavas from Kamchatka and the Aleutians: Constraints on source composition and melting processes. *Contributions to Mineralogy and Petrology*. **133**(3), pp.217–234.

Ulmer, P. and Trommsdorff, V. 1999. Phase relations of hydrous mantle subducting to 300 km *In*: Y. Fei, C. M. Bertka and B. O. Mysen, eds. *Mantle petrology: Field observations and high pressure experimentation*. Houston: The Geochemical Society, pp.259–281.

Urann, B.M., Le Roux, V., Hammond, K., Marschall, H.R., Lee, C.T.A. and Monteleone, B.D. 2017. Fluorine and chlorine in mantle minerals and the halogen budget of the Earth's mantle. *Contributions to Mineralogy and Petrology*. **172**(51).

VandenBleeken, G. and Koga, K.T. 2015. Experimentally determined distribution of fluorine and chlorine upon hydrous slab melting, and implications for F-Cl cycling through subduction zones. *Geochimica et Cosmochimica Acta*. **171**, pp.353–373.

Volfinger, M., Robert, J.L., Vielzeuf, D. and Neiva, A.M.R. 1985. Structural control of the chlorine content of OH-bearing silicates (micas and amphiboles). *Geochimica et Cosmochimica Acta*. **49**(1), pp.37–48.

Volynets, A.O., Churikova, T.G., Wörner, G., Gordeychik, B.N. and Layer, P. 2010. Mafic Late Miocene-Quaternary volcanic rocks in the Kamchatka back arc region: Implications for subduction geometry and slab history at the Pacific-Aleutian junction. *Contributions to Mineralogy and Petrology*. **159**(5), pp.659–687.

Webster, J., Thomas, R., Förster, H.J., Seltmann, R. and Tappen, C. 2004. Geochemical evolution of halogen-enriched granite magmas and mineralizing fluids of the Zinnwald tin-tungsten mining district, Erzgebirge, Germany. *Mineralium Deposita*. **39**(4), pp.452–472.

Webster, J.D., Kinzler, R.J. and Mathez, E.A. 1999. Chloride and water solubility in basalt and andesite melts and implications for magmatic degassing. *Geochimica et Cosmochimica Acta*. **63**(5), pp.729–738.

Webster, J.D., Vetere, F., Botcharnikov, R.E., Goldoff, B., McBirney, A. and Doherty, A.L. 2015. Experimental and modeled chlorine solubilities in aluminosilicate melts at 1 to 7000 bars and 700 to 1250 °C: Applications to magmas of Augustine Volcano, Alaska. *American Mineralogist*. **100**(2–3), pp.522–535.

Webster, J.D. and De Vivo, B. 2002. Experimental and modeled solubilities of chlorine in aluminosilicate melts, consequences of magma evolution, and implications for exsolution of hydrous chloride melt at Mt. Somma-Vesuvius. *American Mineralogist*. **87**(8–9), pp.1046–1061.

Wood, B.J., Bryndzia, L.T. and Johnson, K.E. 1990. Mantle oxidation state and its relationship to tectonic environment and fluid speciation. *Science*. **248**(4953),

pp.337–345.

Wood, B.J. and Turner, S.P. 2009. Origin of primitive high-Mg andesite: Constraints from natural examples and experiments. *Earth and Planetary Science Letters*. **283**(1–4), pp.59–66.

Workman, R.K. and Hart, S.R. 2005. Major and trace element composition of the depleted MORB mantle (DMM). *Earth and Planetary Science Letters*. **231**(1–2), pp.53–72.

Wunder, B., Meixner, A., Romer, R.L., Wirth, R. and Heinrich, W. 2005. The geochemical cycle of boron: Constraints from boron isotope partitioning experiments between mica and fluid. *Lithos*. **84**(3–4), pp.206–216.

Yau, Y.C., Anovitz, L.M., Essene, E.J. and Peacor, D.R. 1984. Phlogopite-chlorite reaction mechanisms and physical conditions during retrograde reactions in the Marble Formation, Franklin, New Jersey. *Contributions to Mineralogy and Petrology*. **88**(3), pp.299–306.

Yogodzinski, G.M., Lees, J.M., Churikova, T.G., Dorendorf, F., Wöerner, G. and Volynets, O.N. 2001. Geochemical evidence for the melting of subducting oceanic lithosphere at plate edges. *Nature*. **409**, pp.500–504.

You, C.F., Chan, L.H., Spivack, A.J. and Gieskes, J.M. 1995. Lithium, boron, and their isotopes in sediments and pore waters of Ocean Drilling Program site 808, Nankai Trough: Implications for fluid expulsion in accretionary prisms. *Geology*. **23**(1), pp.37–40.

Zhang, J., Humphreys, M.C.S., Cooper, G.F., Davidson, J.P. and Macpherson, C.G. 2017. Magma mush chemistry at subduction zones, revealed by new melt major element inversion from calcic amphiboles. *American Mineralogist*. **102**(6), pp.1353–1367.

Zhu, Y., Chen, J., Xue, Y., Feng, W. and Jiang, J. 2018. Spinel and orthopyroxene exsolved from clinopyroxene in the Haladala pluton in the middle Tianshan (Xinjiang, China). *Mineralogy and Petrology*. **112**(4), pp.465–479.

Appendix A
Mineral major and minor element compositions

***Table A16**. Major and minor element compositions of olivine in Shiveluch, Avachinsky and Bakening mantle xenoliths*

Sample	Mineral ID	SiO_2	TiO_2	Al_2O_3	Cr_2O_3	FeO	NiO	MnO	MgO	CaO	Na_2O	K_2O	Total	Mg#	Comment
SHX03-04	Ol_01	39.76	bdl	bdl	bdl	14.91	nd	0.36	45.33	0.02	bdl	bdl	100.39	84.42	host rock contact
	Ol_01	39.71	bdl	bdl	0.01	14.49	nd	0.36	45.54	0.01	bdl	bdl	100.14	84.85	host rock contact
	Ol_02	40.20	bdl	bdl	0.01	11.57	nd	0.27	47.87	0.01	bdl	bdl	99.92	88.05	host rock contact
	Ol_03	39.34	bdl	bdl	0.01	15.58	nd	0.37	44.72	0.01	bdl	bdl	100.04	83.65	host rock contact
	Ol_03	39.58	bdl	bdl	bdl	14.63	nd	0.36	45.18	0.01	bdl	bdl	99.76	84.63	host rock contact
	Ol_05	40.51	bdl	bdl	0.01	11.17	nd	0.23	48.48	bdl	bdl	bdl	100.40	88.55	hydrous vein contact
	Ol_05	40.71	bdl	bdl	bdl	10.54	nd	0.23	49.07	bdl	bdl	0.01	100.55	89.24	hydrous vein contact
	Ol_06	40.43	bdl	bdl	bdl	11.72	nd	0.27	48.07	0.01	bdl	bdl	100.50	87.97	hydrous vein contact
	Ol_07	40.50	bdl	bdl	bdl	10.65	nd	0.22	48.96	bdl	bdl	bdl	100.34	89.12	hydrous vein contact
	Ol_08	40.63	bdl	bdl	bdl	9.08	nd	0.18	49.78	bdl	bdl	0.01	99.68	90.72	
	Ol_08	40.67	bdl	bdl	0.01	9.04	nd	0.18	49.91	bdl	bdl	0.01	99.82	90.77	
	Ol_09	40.57	bdl	bdl	0.01	10.64	nd	0.23	48.84	bdl	bdl	bdl	100.28	89.11	hydrous vein contact
	Ol_09	40.56	bdl	bdl	0.02	11.02	nd	0.24	48.87	0.01	bdl	bdl	100.72	88.77	hydrous vein contact
	Ol_10	40.69	bdl	bdl	0.01	10.89	nd	0.22	48.69	0.01	bdl	bdl	100.51	88.85	hydrous vein contact
	Ol_10	40.43	0.01	bdl	bdl	11.11	nd	0.25	48.32	0.01	bdl	bdl	100.13	88.57	hydrous vein contact
	Ol_10	40.30	bdl	bdl	0.01	11.51	nd	0.26	48.12	0.01	bdl	0.01	100.21	88.17	hydrous vein contact
	Ol_01_R	40.39	bdl	bdl	0.17	9.15	0.23	0.18	51.42	0.01	nd	nd	101.54	90.92	spinel contact
	Ol_01_C	40.51	bdl	bdl	0.03	9.32	0.23	0.19	50.46	bdl	nd	nd	100.74	90.61	
	Ol_02_R	40.51	bdl	0.01	0.53	9.23	0.23	0.18	50.73	bdl	nd	nd	101.42	90.74	spinel contact
	Ol_02_C	40.50	bdl	bdl	0.03	9.11	0.25	0.19	50.43	0.01	nd	nd	100.52	90.79	
	Ol_03_R	40.66	0.01	bdl	0.55	9.26	0.21	0.18	50.49	0.01	nd	nd	101.36	90.67	spinel contact
	Ol_03_C	40.15	bdl	bdl	0.07	9.28	0.24	0.18	49.87	0.02	nd	nd	99.80	90.55	
	Ol_04_R	40.65	bdl	bdl	0.62	9.33	0.26	0.17	50.60	0.01	nd	nd	101.64	90.63	spinel contact
	Ol_04_C	40.55	0.01	bdl	0.43	9.28	0.24	0.17	50.67	bdl	nd	nd	101.35	90.68	
	Ol_05_R	40.51	0.01	bdl	0.21	9.25	0.24	0.17	50.25	0.01	nd	nd	100.65	90.64	spinel contact
	Ol_05_C	40.56	bdl	bdl	0.02	9.44	0.26	0.18	50.18	0.01	nd	nd	100.64	90.45	
	Ol_06_R	40.31	bdl	0.01	0.39	9.32	0.26	0.17	49.94	0.01	nd	nd	100.40	90.52	spinel contact
	Ol_06_C	40.36	bdl	bdl	0.08	9.31	0.24	0.18	50.56	0.01	nd	nd	100.74	90.63	

Abbreviations: Ol = olivine, R = rim, C = centre, bdl = below detection limit, nd = not determined. *Note:* all oxides are in wt %.

***Table A16**. Continued*

Sample	Mineral ID	SiO_2	TiO_2	Al_2O_3	Cr_2O_3	FeO	NiO	MnO	MgO	CaO	Na_2O	K_2O	Total	Mg#	Comment
SHX03-01	Ol_02	40.98	bdl	bdl	0.01	9.17	0.41	0.10	50.54	0.02	bdl	bdl	101.21	90.76	
	Ol_02	41.06	0.01	bdl	bdl	9.17	0.42	0.10	50.33	0.02	bdl	bdl	101.09	90.73	
	Ol_03	40.96	bdl	bdl	bdl	9.29	0.41	0.10	50.40	0.02	bdl	bdl	101.20	90.63	
	Ol_08	40.88	bdl	bdl	bdl	9.24	0.38	0.12	50.50	0.02	bdl	bdl	101.14	90.69	
	Ol_09	41.04	bdl	bdl	bdl	9.23	0.39	0.11	50.24	0.02	bdl	0.01	101.03	90.66	
	Ol_10	41.24	bdl	bdl	bdl	9.22	0.42	0.11	50.33	0.02	bdl	bdl	101.33	90.68	
SHX03-18	Ol_12	41.35	0.01	bdl	bdl	8.64	0.36	0.17	51.04	0.02	bdl	bdl	101.57	91.33	hydrous vein contact
	Ol_12	41.42	bdl	bdl	0.01	8.25	0.33	0.16	51.53	0.01	bdl	bdl	101.71	91.76	hydrous vein contact
	Ol_12	41.28	bdl	bdl	bdl	7.91	0.30	0.15	51.90	0.01	bdl	0.01	101.57	92.12	hydrous vein contact
	Ol_13	41.67	0.01	bdl	bdl	7.60	0.37	0.14	52.17	0.01	bdl	bdl	101.96	92.44	hydrous vein contact
	Ol_13	41.64	bdl	bdl	bdl	7.41	0.29	0.13	52.40	0.01	bdl	bdl	101.89	92.65	hydrous vein contact
	Ol_13	41.52	bdl	bdl	bdl	7.15	0.29	0.14	52.81	0.01	bdl	bdl	101.91	92.94	hydrous vein contact
	Ol_14	41.64	bdl	bdl	0.01	7.54	0.28	0.15	52.04	0.01	bdl	bdl	101.68	92.48	hydrous vein contact
	Ol_15	41.55	bdl	bdl	bdl	7.19	0.31	0.13	52.20	bdl	bdl	bdl	101.39	92.82	
	Ol_16	41.15	bdl	bdl	bdl	9.12	0.61	0.18	50.38	0.02	bdl	bdl	101.46	90.78	hydrous vein contact
	Ol_16	41.23	bdl	bdl	bdl	8.69	0.44	0.16	50.77	0.01	bdl	bdl	101.29	91.24	hydrous vein contact
	Ol_16	41.20	bdl	bdl	bdl	8.55	0.41	0.16	51.09	0.01	bdl	bdl	101.40	91.42	hydrous vein contact
	Ol_17	41.47	bdl	bdl	bdl	6.78	0.23	0.13	52.84	bdl	bdl	bdl	101.46	93.28	hydrous vein contact
	Ol_17	41.48	bdl	bdl	bdl	6.93	0.29	0.13	52.64	0.01	bdl	bdl	101.47	93.12	hydrous vein contact
	Ol_17	41.59	bdl	bdl	0.01	6.81	0.29	0.14	52.57	0.01	bdl	bdl	101.42	93.22	hydrous vein contact
	Ol_18	41.66	bdl	bdl	bdl	6.85	0.23	0.13	52.95	0.02	bdl	bdl	101.85	93.23	hydrous vein contact
	Ol_18	41.65	bdl	bdl	bdl	6.78	0.25	0.13	52.61	0.01	bdl	0.01	101.43	93.25	hydrous vein contact
	Ol_18	41.77	bdl	bdl	0.01	6.86	0.23	0.15	53.11	0.01	bdl	bdl	102.15	93.24	hydrous vein contact
	Ol_19	41.59	bdl	bdl	0.02	6.60	0.23	0.14	52.72	0.01	bdl	bdl	101.30	93.43	hydrous vein contact
	Ol_19	41.55	bdl	bdl	bdl	6.60	0.27	0.13	52.78	0.01	bdl	bdl	101.34	93.44	hydrous vein contact
	Ol_19	41.49	0.01	bdl	bdl	7.60	0.25	0.15	51.85	0.01	bdl	bdl	101.35	92.40	hydrous vein contact
	Ol_20	41.78	bdl	bdl	bdl	6.64	0.22	0.13	52.85	0.01	bdl	bdl	101.63	93.42	hydrous vein contact

Abbreviations: Ol = olivine, R = rim, C = centre, bdl = below detection limit. *Note:* all oxides are in wt %.

Table A16. *Continued*

Sample	Mineral ID	SiO_2	TiO_2	Al_2O_3	Cr_2O_3	FeO	NiO	MnO	MgO	CaO	Na_2O	K_2O	Total	Mg#	Comment
SHX03-18	Ol_20	41.71	bdl	bdl	bdl	6.64	0.25	0.14	52.98	0.01	bdl	bdl	101.73	93.43	hydrous vein contact
	Ol_20	41.74	0.01	bdl	bdl	6.62	0.25	0.13	52.73	0.01	bdl	bdl	101.50	93.42	hydrous vein contact
	Ol_01_R	41.01	0.01	bdl	0.27	6.37	0.27	0.14	52.83	0.01	nd	nd	100.90	93.66	
	Ol_01_C	41.01	0.01	bdl	0.05	6.56	0.27	0.12	52.74	0.01	nd	nd	100.77	93.47	
	Ol_02	41.23	bdl	bdl	0.01	6.90	0.25	0.13	52.48	0.02	nd	nd	101.01	93.13	
SHX-No-No	Ol_21	40.93	bdl	bdl	bdl	7.01	0.32	0.15	52.25	0.01	bdl	bdl	100.66	92.99	
	Ol_22	41.02	bdl	bdl	bdl	6.95	0.34	0.14	52.25	0.01	bdl	bdl	100.72	93.06	
	Ol_22	40.95	bdl	bdl	0.01	6.95	0.36	0.14	52.09	0.01	bdl	bdl	100.51	93.03	
	Ol_22	41.00	bdl	bdl	bdl	7.01	0.35	0.15	52.10	0.01	bdl	0.01	100.62	92.98	
	Ol_23	41.09	bdl	bdl	bdl	8.06	0.32	0.18	50.97	0.02	bdl	bdl	100.64	91.85	
	Ol_23	41.04	bdl	bdl	0.01	8.27	0.32	0.20	50.87	0.02	bdl	bdl	100.73	91.64	host rock contact
	Ol_23	41.15	0.01	bdl	0.01	7.92	0.29	0.19	51.19	0.01	bdl	bdl	100.78	92.01	
	Ol_24	41.02	bdl	bdl	bdl	8.45	0.33	0.20	50.72	0.01	bdl	bdl	100.73	91.45	host rock contact
	Ol_25	41.36	bdl	bdl	bdl	6.98	0.37	0.14	52.05	0.01	bdl	bdl	100.91	93.00	
	Ol_25	41.38	0.01	bdl	bdl	7.00	0.37	0.14	52.27	0.01	bdl	0.01	101.19	93.01	
	Ol_25	41.43	bdl	bdl	bdl	6.97	0.37	0.13	51.95	0.01	bdl	bdl	100.87	93.00	
	Ol_26	41.37	bdl	bdl	bdl	6.94	0.32	0.15	52.23	0.01	bdl	bdl	101.03	93.06	
	Ol_27	41.45	bdl	bdl	bdl	6.91	0.30	0.15	52.27	0.01	bdl	bdl	101.09	93.10	
	Ol_28	41.46	bdl	bdl	bdl	6.96	0.31	0.14	52.27	0.01	bdl	bdl	101.17	93.04	
	Ol_29	41.38	bdl	bdl	bdl	6.97	0.33	0.14	52.09	bdl	bdl	bdl	100.91	93.02	
	Ol_30	41.58	bdl	bdl	0.01	7.00	0.33	0.16	52.39	0.01	bdl	bdl	101.47	93.03	
	Ol_30	41.43	bdl	bdl	0.01	7.01	0.34	0.16	52.31	0.01	bdl	bdl	101.28	93.00	
	Ol_30	41.47	0.01	bdl	0.02	7.03	0.31	0.15	52.51	0.01	bdl	bdl	101.50	93.02	
	Px_11	40.94	bdl	bdl	bdl	6.90	0.37	0.15	50.94	0.02	bdl	bdl	99.33	92.93	
	Px_15	41.11	bdl	bdl	bdl	7.00	0.35	0.13	51.29	0.01	bdl	bdl	99.90	92.89	
SHX03-17	Ol_01	41.41	bdl	bdl	0.29	8.18	0.24	0.19	51.09	0.01	nd	nd	101.41	91.75	spinel contact
	Ol_02	45.55	0.01	0.14	0.22	7.51	0.21	0.18	47.91	0.02	nd	nd	101.74	91.92	spinel contact

Abbreviations: Ol and Px = olivine, R = rim, C = centre, bdl = below detection limit, nd = not determined. *Note:* all oxides are in wt %.

Table A16. *Continued*

Sample	Mineral ID	SiO_2	TiO_2	Al_2O_3	Cr_2O_3	FeO	NiO	MnO	MgO	CaO	Na_2O	K_2O	Total	Mg#	Comment
SHX03-17	Ol_03	41.17	bdl	bdl	0.41	8.60	0.23	0.18	51.19	0.01	nd	nd	101.80	91.38	spinel contact
	Ol_06	41.22	0.01	bdl	0.43	8.27	0.23	0.18	51.62	0.01	nd	nd	101.96	91.75	spinel contact
	Ol_07	40.93	bdl	bdl	0.46	8.30	0.27	0.18	51.05	0.01	nd	nd	101.20	91.64	spinel contact
	Ol_12	41.13	bdl	bdl	0.01	8.26	0.23	0.18	51.62	0.01	nd	nd	101.44	91.76	
	Ol_13	41.04	bdl	bdl	0.01	8.45	0.25	0.17	51.25	0.02	nd	nd	101.18	91.53	
	Ol_14	40.99	bdl	bdl	bdl	8.40	0.25	0.18	51.38	0.01	nd	nd	101.21	91.60	
	Ol_15	41.48	bdl	bdl	bdl	8.18	0.23	0.17	51.66	0.01	nd	nd	101.72	91.84	
	Ol_16	41.14	bdl	bdl	0.01	8.15	0.24	0.17	51.36	0.01	nd	nd	101.07	91.83	
	Ol_17	41.12	bdl	bdl	bdl	8.28	0.26	0.18	51.30	0.01	nd	nd	101.14	91.69	
	Ol_18	41.07	bdl	bdl	bdl	8.34	0.26	0.19	51.21	0.01	nd	nd	101.07	91.63	
	Ol_19	41.13	bdl	bdl	bdl	8.39	0.24	0.18	51.31	0.01	nd	nd	101.27	91.59	
	Ol_20	41.14	0.01	bdl	0.01	8.36	0.21	0.17	51.29	0.06	nd	nd	101.23	91.62	
SHIV-16-12-06	Ol_02	40.30	nd	nd	bdl	10.05	0.18	0.1	49.52	bdl	nd	nd	100.21	89.77	
	Ol_03	40.15	nd	nd	0.17	10.17	0.19	0.13	49.69	0.05	nd	nd	100.55	89.70	
	Ol_04	40.36	nd	nd	bdl	10.63	0.21	0.13	49.06	0.47	nd	nd	100.87	89.16	
	Ol_05	40.29	nd	nd	bdl	10.56	0.22	0.14	47.35	1.04	nd	nd	99.59	88.88	
	Ol_06	40.20	nd	nd	bdl	10.78	0.21	0.13	48.73	0.06	nd	nd	100.10	88.96	
	Ol_07	40.16	nd	nd	bdl	10.77	0.21	0.13	48.79	0.31	nd	nd	100.37	88.98	
	Ol_08	40.50	nd	nd	bdl	11.01	0.22	0.15	48.38	0.02	nd	nd	100.27	88.68	
	Ol_09	40.21	nd	nd	0.01	10.92	0.23	0.14	48.96	0.08	nd	nd	100.53	88.88	
	Ol_10	40.28	nd	nd	bdl	11.02	0.23	0.13	48.89	0.03	nd	nd	100.58	88.77	
	Ol_13	40.18	nd	nd	0.02	10.35	0.21	0.15	49.30	0.02	nd	nd	100.23	89.46	
	Ol_14	39.15	nd	nd	bdl	14.95	0.19	0.13	45.28	0.17	nd	nd	99.87	84.37	host rock contact
	Ol_15	39.01	nd	nd	bdl	16.25	0.22	0.14	44.03	0.02	nd	nd	99.66	82.84	host rock contact
	Ol_16	40.07	nd	nd	bdl	10.37	0.18	0.13	49.70	0.02	nd	nd	100.46	89.52	
AVX-16-03-24	Ol_01	40.86	0.01	bdl	bdl	9.27	0.36	0.15	49.71	0.07	nd	nd	100.43	90.53	
	Ol_02	40.63	bdl	bdl	0.01	9.75	0.38	0.14	49.30	0.07	nd	nd	100.27	90.01	

Abbreviations: Ol = olivine, bdl = below detection limit, nd = not determined. *Note:* all oxides are in wt %.

Table A16. *Continued*

Sample	Mineral ID	SiO_2	TiO_2	Al_2O_3	Cr_2O_3	FeO	NiO	MnO	MgO	CaO	Na_2O	K_2O	Total	Mg#	Comment
AVX-16-03-24	Ol_03	40.68	bdl	bdl	bdl	9.95	0.40	0.14	49.15	0.07	nd	nd	100.40	89.79	
	Ol_04	40.07	bdl	bdl	bdl	10.15	0.37	0.14	48.85	0.08	nd	nd	99.65	89.56	
	Ol_06	40.40	bdl	bdl	0.01	10.03	0.40	0.15	49.37	0.07	nd	nd	100.43	89.77	
	Ol_07	40.46	bdl	bdl	0.02	9.63	0.38	0.14	49.46	0.07	nd	nd	100.15	90.15	
	Ol_08	40.62	bdl	bdl	0.01	9.74	0.38	0.16	49.21	0.07	nd	nd	100.19	90.00	
	Ol_09	40.60	bdl	bdl	bdl	10.02	0.39	0.15	49.25	0.06	nd	nd	100.48	89.75	
	Ol_10	40.64	bdl	bdl	0.01	10.15	0.37	0.14	48.98	0.08	nd	nd	100.36	89.58	
	Ol_11	40.65	bdl	bdl	0.01	9.88	0.41	0.13	49.12	0.06	nd	nd	100.26	89.86	
	Ol_12	40.78	bdl	bdl	bdl	10.13	0.41	0.16	49.08	0.06	nd	nd	100.63	89.62	
	Ol_13	40.60	bdl	bdl	0.01	9.91	0.39	0.15	49.24	0.06	nd	nd	100.36	89.85	
	Ol_14	40.54	bdl	bdl	bdl	10.16	0.40	0.15	48.97	0.07	nd	nd	100.30	89.57	
	Ol_15	40.52	bdl	bdl	bdl	10.18	0.40	0.16	49.06	0.07	nd	nd	100.39	89.57	
AVX-16-03-23	Ol_16	40.78	bdl	bdl	bdl	10.08	0.38	0.14	49.08	0.07	nd	nd	100.53	89.67	
	Ol_18	40.77	bdl	bdl	bdl	10.02	0.39	0.15	49.22	0.07	nd	nd	100.61	89.75	
	Ol_19	41.19	bdl	bdl	bdl	9.56	0.37	0.14	49.79	0.07	nd	nd	101.12	90.27	
	Ol_20	40.96	bdl	bdl	bdl	9.55	0.37	0.15	49.57	0.07	nd	nd	100.67	90.25	
	Ol_21	41.01	bdl	bdl	bdl	9.57	0.38	0.14	49.58	0.08	nd	nd	100.76	90.23	
	Ol_22	40.81	bdl	bdl	bdl	9.84	0.39	0.15	49.50	0.08	nd	nd	100.77	89.96	
	Ol_23	40.95	bdl	bdl	0.01	9.68	0.37	0.15	49.45	0.07	nd	nd	100.68	90.11	
	Ol_24	40.93	bdl	bdl	bdl	9.66	0.36	0.14	49.39	0.07	nd	nd	100.54	90.11	
	Ol_26	40.77	bdl	bdl	0.01	10.09	0.40	0.16	49.12	0.07	nd	nd	100.62	89.66	
	Ol_27	40.70	bdl	bdl	bdl	9.97	0.41	0.15	49.29	0.07	nd	nd	100.59	89.81	
	Ol_28	40.90	bdl	bdl	bdl	9.97	0.42	0.15	48.99	0.06	nd	nd	100.49	89.75	
	Ol_29	40.76	bdl	bdl	bdl	9.74	0.39	0.14	49.35	0.06	nd	nd	100.45	90.03	
	Ol_30	40.82	bdl	bdl	bdl	9.70	0.39	0.13	49.33	0.06	nd	nd	100.43	90.06	

Abbreviations: Ol = olivine, bdl = below detection limit, nd = not determined. *Note:* all oxides are in wt %.

Table A16. *Continued*

Sample	Mineral ID	SiO_2	TiO_2	Al_2O_3	Cr_2O_3	FeO	NiO	MnO	MgO	CaO	Na_2O	K_2O	Total	Mg#	Comment
AVX-16-03-20	Ol_31	41.03	bdl	bdl	0.01	8.65	0.35	0.15	50.43	0.08	nd	nd	100.69	91.22	
	Ol_32	40.88	0.01	bdl	0.03	8.54	0.37	0.13	50.38	0.09	nd	nd	100.43	91.31	
	Ol_33	41.00	bdl	bdl	0.01	8.19	0.38	0.13	50.83	0.08	nd	nd	100.63	91.71	
	Ol_34	40.83	bdl	bdl	0.01	8.36	0.38	0.13	50.68	0.09	nd	nd	100.48	91.53	
	Ol_35	40.93	bdl	bdl	0.02	8.41	0.36	0.13	50.72	0.09	nd	nd	100.67	91.49	
	Ol_36	40.62	bdl	bdl	0.01	8.26	0.37	0.14	50.71	0.08	nd	nd	100.18	91.62	
	Ol_37	40.68	bdl	bdl	bdl	8.29	0.36	0.13	50.67	0.08	nd	nd	100.22	91.59	
	Ol_38	40.88	bdl	bdl	bdl	8.34	0.36	0.14	50.75	0.08	nd	nd	100.55	91.56	
	Ol_39	40.71	bdl	bdl	bdl	8.17	0.38	0.13	50.74	0.10	nd	nd	100.23	91.71	
	Ol_40	39.66	bdl	bdl	bdl	14.80	0.41	0.41	44.79	0.10	nd	nd	100.17	84.35	hydrous vein contact
	Ol_41	39.17	bdl	bdl	0.01	16.50	0.42	0.49	43.32	0.10	nd	nd	100.02	82.39	hydrous vein contact
	Ol_42	39.22	bdl	bdl	bdl	15.86	0.44	0.48	43.83	0.11	nd	nd	99.94	83.12	hydrous vein contact
	Ol_43	39.55	bdl	bdl	bdl	14.81	0.41	0.44	44.77	0.10	nd	nd	100.07	84.35	hydrous vein contact
	Ol_44	39.44	bdl	bdl	bdl	15.32	0.40	0.44	44.50	0.10	nd	nd	100.21	83.81	hydrous vein contact
	Ol_45	39.53	bdl	bdl	bdl	15.56	0.41	0.47	44.37	0.11	nd	nd	100.43	83.56	hydrous vein contact
AVX-16-03-10	Ol_01	40.14	nd	nd	bdl	11.97	0.37	0.15	47.31	0.04	nd	nd	99.98	87.57	hydrous vein contact
	Ol_02	40.34	nd	nd	bdl	11.48	0.39	0.14	47.54	0.03	nd	nd	99.91	88.07	hydrous vein contact
	Ol_03	39.98	nd	nd	bdl	11.19	0.42	0.13	47.76	0.03	nd	nd	99.52	88.38	hydrous vein contact
	Ol_04	40.65	nd	nd	bdl	9.70	0.39	0.15	49.16	0.04	nd	nd	100.09	90.03	
	Ol_05	40.58	nd	nd	0.01	8.70	0.39	0.13	50.26	0.03	nd	nd	100.09	91.15	
	Ol_06	40.19	nd	nd	0.02	10.93	0.38	0.14	48.37	0.09	nd	nd	100.12	88.74	
	Ol_07	40.23	nd	nd	0.01	8.90	0.39	0.13	50.30	0.04	nd	nd	100.00	90.97	
	Ol_09	40.50	nd	nd	bdl	8.80	0.39	0.14	50.07	0.64	nd	nd	100.55	91.02	
	Ol_10	40.48	nd	nd	bdl	9.74	0.41	0.15	49.14	0.02	nd	nd	99.94	89.99	
	Ol_11	40.35	nd	nd	bdl	10.46	0.40	0.14	48.77	0.03	nd	nd	100.16	89.25	
	Ol_13	40.59	nd	nd	bdl	9.43	0.40	0.14	49.31	0.02	nd	nd	99.89	90.31	
	Ol_14	40.73	nd	nd	0.01	8.61	0.39	0.14	50.20	0.03	nd	nd	100.10	91.22	

Abbreviations: Ol = olivine, bdl = below detection limit, nd = not determined. *Note:* all oxides are in wt %.

Table A16. *Continued*

Sample	Mineral ID	SiO_2	TiO_2	Al_2O_3	Cr_2O_3	FeO	NiO	MnO	MgO	CaO	Na_2O	K_2O	Total	Mg#	Comment
AVX-16-03-10	Ol_15	40.74	nd	nd	0.01	8.57	0.39	0.15	50.22	0.02	nd	nd	100.10	91.26	
	Ol_17	40.94	nd	nd	0.18	8.52	0.37	0.14	49.90	0.04	nd	nd	100.10	91.25	
	Opx_13	40.17	nd	nd	bdl	9.75	0.42	0.16	49.82	0.56	nd	nd	100.89	90.11	
AVX-16-03-02	Ol_25	40.75	0.01	bdl	0.02	8.90	0.41	0.14	50.17	0.04	bdl	nd	100.43	90.95	
	Ol_26	40.72	bdl	bdl	bdl	8.92	0.40	0.14	50.34	0.03	bdl	nd	100.54	90.96	
	Ol_27	40.67	bdl	bdl	bdl	9.00	0.40	0.15	50.38	0.02	bdl	nd	100.62	90.89	
	Ol_28	40.74	bdl	bdl	bdl	8.99	0.40	0.14	50.26	0.03	0.01	nd	100.57	90.88	
	Ol_29	40.86	bdl	bdl	0.02	8.92	0.41	0.12	50.39	0.04	bdl	nd	100.76	90.97	
	Ol_31	40.60	0.01	bdl	0.20	8.80	0.40	0.13	50.32	0.07	bdl	nd	100.54	91.07	
	Ol_31	40.75	bdl	bdl	0.01	8.71	0.40	0.13	50.09	0.06	bdl	nd	100.15	91.11	
	Ol_32	40.65	bdl	bdl	bdl	8.72	0.41	0.13	50.40	0.06	bdl	nd	100.39	91.15	
	Ol_33	40.63	bdl	bdl	0.22	8.74	0.40	0.12	49.97	0.06	bdl	nd	100.14	91.06	
	Ol_33	40.67	bdl	bdl	0.01	8.72	0.41	0.13	49.75	0.06	bdl	nd	99.76	91.04	
	Ol_34	40.64	bdl	bdl	0.02	9.03	0.41	0.14	49.67	0.04	bdl	nd	99.95	90.74	
	Ol_35	40.45	bdl	bdl	bdl	8.93	0.40	0.13	49.94	0.03	bdl	nd	99.89	90.88	
	Ol_36	40.62	bdl	bdl	bdl	9.16	0.41	0.14	49.75	0.02	0.01	nd	100.09	90.64	
	Ol_37	40.59	bdl	bdl	0.01	8.87	0.41	0.13	49.80	0.04	bdl	nd	99.83	90.92	
	Ol_38	40.69	0.02	bdl	0.02	8.87	0.40	0.13	49.92	0.03	0.01	nd	100.08	90.93	
	Ol_39	40.79	bdl	bdl	0.02	8.89	0.40	0.14	49.79	0.02	bdl	nd	100.04	90.90	
	Ol_40	40.70	0.01	bdl	0.01	8.94	0.39	0.14	49.74	0.04	0.01	nd	99.98	90.84	
AVX-16-03-07	Ol_41	40.40	bdl	bdl	0.17	9.31	0.38	0.15	49.62	0.06	0.01	nd	100.08	90.47	
	Ol_41	40.44	bdl	bdl	0.01	9.39	0.39	0.13	49.82	0.02	bdl	nd	100.19	90.44	
	Ol_42	40.40	bdl	bdl	bdl	9.46	0.40	0.14	50.04	0.02	bdl	nd	100.47	90.41	
	Ol_43	40.40	0.01	bdl	0.02	9.43	0.39	0.15	49.82	0.02	0.01	nd	100.27	90.40	
	Ol_45	40.84	bdl	bdl	0.01	9.16	0.38	0.14	49.81	0.02	bdl	nd	100.35	90.64	
	Ol_46	40.56	0.01	bdl	0.01	9.17	0.39	0.14	49.60	0.03	bdl	nd	99.93	90.60	
	Ol_47	40.33	0.01	bdl	0.01	9.59	0.39	0.14	49.30	0.02	bdl	nd	99.78	90.16	

Abbreviations: Ol and Opx = olivine, bdl = below detection limit, nd = not determined. *Note:* all oxides are in wt %.

Table A16. *Continued*

Sample	Mineral ID	SiO_2	TiO_2	Al_2O_3	Cr_2O_3	FeO	NiO	MnO	MgO	CaO	Na_2O	K_2O	Total	Mg#	Comment
AVX-16-03-07	Ol_48	40.50	bdl	bdl	bdl	9.15	0.36	0.14	49.67	0.06	bdl	nd	99.87	90.63	
	Ol_49	40.47	0.01	bdl	0.01	9.32	0.39	0.12	49.71	0.02	bdl	nd	100.05	90.48	
	Ol_50	40.46	bdl	bdl	0.01	9.14	0.33	0.13	50.10	0.04	bdl	nd	100.19	90.72	
	Ol_51	40.50	bdl	bdl	0.01	9.37	0.38	0.15	49.80	0.03	bdl	nd	100.25	90.45	
	Ol_52	40.36	bdl	bdl	0.01	9.64	0.38	0.14	49.45	0.02	bdl	nd	99.99	90.14	
	Ol_53	40.59	bdl	bdl	bdl	9.14	0.40	0.14	49.88	0.02	bdl	nd	100.17	90.67	
	Ol_54	40.52	bdl	bdl	0.01	9.04	0.36	0.13	50.04	0.05	bdl	nd	100.13	90.80	
	Ol_55	40.57	0.01	bdl	0.01	9.44	0.38	0.14	49.92	0.02	0.01	nd	100.50	90.41	
	Ol_56	40.57	0.01	bdl	0.01	9.41	0.38	0.13	49.58	0.02	bdl	nd	100.11	90.37	
	Ol_57	40.55	bdl	bdl	bdl	9.45	0.38	0.14	49.59	0.02	bdl	nd	100.13	90.34	
	Ol_58	40.45	0.01	bdl	0.01	9.45	0.39	0.13	49.65	0.02	bdl	nd	100.12	90.35	
BAK-16-22-04	Ol_01	39.63	nd	nd	0.19	13.10	0.27	0.22	47.00	0.10	nd	nd	100.51	86.47	
	Ol_01	40.15	nd	nd	0.01	12.95	0.27	0.21	47.11	0.04	nd	nd	100.74	86.64	
	Ol_02	40.32	nd	nd	0.22	12.19	0.27	0.20	47.99	0.05	nd	nd	101.25	87.53	
	Ol_02	40.15	nd	nd	0.01	12.64	0.28	0.20	47.25	0.04	nd	nd	100.57	86.95	
	Ol_03	39.77	nd	nd	0.22	12.90	0.27	0.21	47.13	0.07	nd	nd	100.56	86.69	
	Ol_03	40.22	nd	nd	0.09	12.90	0.28	0.21	46.66	0.05	nd	nd	100.41	86.57	
	Ol_04	39.33	nd	nd	0.21	13.04	0.27	0.22	47.09	0.09	nd	nd	100.24	86.55	
	Ol_05	39.95	nd	nd	0.25	13.03	0.27	0.22	46.56	0.10	nd	nd	100.37	86.43	
	Ol_05	40.17	nd	nd	0.01	12.63	0.27	0.20	47.04	0.04	nd	nd	100.38	86.90	
	Ol_06	40.21	nd	nd	0.02	12.88	0.27	0.22	46.75	0.14	nd	nd	100.48	86.61	
	Ol_06	40.30	nd	nd	0.01	12.76	0.27	0.21	46.90	0.05	nd	nd	100.50	86.75	
	Ol_07	39.84	nd	nd	0.01	12.52	0.27	0.20	47.55	0.16	nd	nd	100.54	87.13	
	Ol_01 R	40.79	bdl	bdl	0.04	12.75	0.27	nd	47.56	0.07	bdl	bdl	101.50	86.92	spinel contact
	Ol_02 R	40.53	bdl	bdl	0.03	12.81	0.26	nd	47.20	0.12	bdl	bdl	100.95	86.78	clinopyroxene contact
	Ol_03 R	39.64	bdl	bdl	0.19	12.92	0.26	nd	46.35	0.03	bdl	bdl	99.38	86.47	spinel contact
	Ol_06 R	40.08	0.03	bdl	0.05	12.40	0.26	nd	46.86	0.09	bdl	bdl	99.76	87.07	spinel contact

Abbreviations: Ol = olivine, R = rim, bdl = below detection limit, nd = not determined. *Note:* all oxides are in wt %.

Table A16. *Continued*

Sample	Mineral ID	SiO_2	TiO_2	Al_2O_3	Cr_2O_3	FeO	NiO	MnO	MgO	CaO	Na_2O	K_2O	Total	Mg#	Comment
BAK-16-22-04	Ol_08 C	40.07	0.03	bdl	bdl	12.62	0.27	nd	46.80	bdl	bdl	bdl	99.79	86.86	
	Ol_09 C	39.96	bdl	bdl	0.02	12.54	0.26	nd	46.86	bdl	0.02	bdl	99.66	86.94	
	Ol_10 C	38.57	bdl	bdl	0.01	19.49	0.12	nd	40.76	0.11	bdl	bdl	99.06	78.84	
	Ol_16 R	39.84	0.02	bdl	bdl	12.93	0.28	nd	46.10	0.06	bdl	bdl	99.22	86.41	
	Ol_17 R	39.69	0.01	bdl	bdl	12.74	0.23	nd	46.36	0.13	bdl	bdl	99.15	86.64	
BAK-16-22-01B	Ol_01	38.12	0.03	bdl	0.01	21.30	0.17	0.61	39.05	0.21	bdl	bdl	99.50	76.57	host rock contact
	Ol_02	38.31	0.01	bdl	bdl	20.56	0.19	0.54	39.69	0.19	bdl	bdl	99.50	77.48	host rock contact
	Ol_03	38.86	bdl	bdl	bdl	17.69	0.24	0.35	42.33	0.02	bdl	bdl	99.50	81.00	host rock contact
	Ol_04	39.42	0.01	0.01	bdl	14.26	0.26	0.21	45.23	bdl	bdl	bdl	99.39	84.97	
	Ol_06	39.61	bdl	bdl	0.02	13.70	0.27	0.19	45.82	bdl	bdl	bdl	99.61	85.63	
	Ol_07	39.75	bdl	bdl	0.02	13.59	0.27	0.21	45.77	0.07	bdl	bdl	99.68	85.72	
	Ol_08	39.72	0.01	bdl	bdl	13.71	0.27	0.22	45.71	bdl	bdl	bdl	99.63	85.59	
	Ol_09	39.57	0.01	bdl	0.02	13.70	0.28	0.21	45.60	0.01	bdl	bdl	99.39	85.57	
	Ol_10	39.66	0.01	bdl	0.02	13.73	0.27	0.21	45.48	0.07	bdl	bdl	99.43	85.52	
	Ol_11	39.57	0.01	bdl	0.01	13.70	0.28	0.21	45.64	bdl	bdl	bdl	99.44	85.58	
	Ol_12	39.21	bdl	0.37	0.30	13.28	0.29	0.20	46.20	0.03	bdl	bdl	99.88	86.11	
	Ol_13	39.65	0.01	bdl	bdl	13.80	0.30	0.20	45.71	0.04	bdl	bdl	99.71	85.51	
	Ol_14	39.77	0.01	bdl	bdl	14.00	0.27	0.21	45.91	0.01	bdl	bdl	100.17	85.39	
	Ol_15	40.06	0.01	bdl	0.01	13.80	0.29	0.22	46.09	0.03	bdl	bdl	100.50	85.62	
	Ol_16	39.80	bdl	bdl	0.18	13.89	0.28	0.21	46.45	bdl	bdl	bdl	100.80	85.63	
	Ol_17	40.24	0.01	bdl	0.16	13.67	0.27	0.20	45.52	bdl	bdl	bdl	100.07	85.58	
BAK-16-22-01A	Ol_18	38.55	0.01	bdl	0.01	20.14	0.21	0.38	40.66	0.11	bdl	bdl	100.06	78.25	
	Ol_19	38.61	0.01	bdl	bdl	20.04	0.23	0.34	40.85	0.02	bdl	bdl	100.10	78.41	
	Ol_20	38.38	bdl	bdl	0.01	19.37	0.22	0.33	41.29	0.07	bdl	bdl	99.68	79.16	
	Ol_21	38.42	0.01	bdl	bdl	19.48	0.24	0.31	41.27	0.02	bdl	bdl	99.75	79.06	
	Ol_22	38.46	0.01	bdl	bdl	20.95	0.19	0.44	39.95	0.04	bdl	bdl	100.04	77.27	
	Ol_23	38.62	0.01	bdl	0.01	18.98	0.22	0.32	41.29	0.04	bdl	bdl	99.48	79.50	

Abbreviations: Ol = olivine, C = centre, R = rim, bdl = below detection limit. *Note:* all oxides are in wt %.

Table A16. *Continued*

Sample	Mineral ID	SiO_2	TiO_2	Al_2O_3	Cr_2O_3	FeO	NiO	MnO	MgO	CaO	Na_2O	K_2O	Total	Mg#	Comment
BAK-16-22-09	Ol_24	39.26	0.01	bdl	bdl	12.39	0.33	0.17	47.07	0.01	bdl	bdl	99.23	87.13	
	Ol_24	39.33	0.01	bdl	bdl	12.41	0.31	0.19	46.93	bdl	bdl	bdl	99.17	87.08	
	Ol_25	39.17	bdl	bdl	0.02	12.58	0.30	0.18	46.63	0.01	bdl	bdl	98.89	86.85	
	Ol_27	39.03	bdl	bdl	0.15	12.62	0.32	0.21	46.61	0.10	bdl	bdl	99.04	86.81	
	Ol_28	39.28	0.01	bdl	0.01	12.25	0.34	0.19	47.13	bdl	bdl	bdl	99.20	87.27	
	Ol_30	39.34	bdl	bdl	0.01	12.32	0.31	0.18	47.10	0.01	bdl	bdl	99.27	87.20	
BAK-16-22-03	Ol_01	39.40	0.01	bdl	0.01	16.99	0.19	0.32	43.30	0.12	bdl	bdl	100.35	81.95	host rock contact
	Ol_01	39.96	0.01	bdl	0.01	13.92	0.26	0.21	46.13	bdl	0.01	bdl	100.51	85.52	
	Ol_02	38.40	0.03	bdl	0.01	21.30	0.10	0.58	39.44	0.18	bdl	bdl	100.04	76.74	host rock contact
	Ol_02	38.94	bdl	bdl	bdl	19.58	0.14	0.47	41.11	0.12	0.01	bdl	100.37	78.91	
	Ol_02	39.38	bdl	bdl	0.01	17.31	0.19	0.34	43.10	0.02	0.03	bdl	100.38	81.61	
	Ol_02	39.81	0.01	bdl	0.01	14.96	0.24	0.24	45.39	0.01	bdl	bdl	100.65	84.39	
	Ol_03	39.92	bdl	bdl	bdl	13.98	0.26	0.19	46.05	0.01	bdl	bdl	100.41	85.45	
	Ol_03	40.04	bdl	bdl	0.14	13.84	0.21	0.20	46.28	0.01	bdl	bdl	100.72	85.63	
	Ol_04	39.80	0.01	bdl	0.01	14.64	0.20	0.23	45.49	0.03	bdl	bdl	100.43	84.70	
	Ol_05	40.16	0.01	bdl	0.13	13.89	0.28	0.20	46.27	bdl	bdl	bdl	100.94	85.58	
	Ol_05	39.96	bdl	bdl	0.01	13.93	0.25	0.20	45.89	0.01	bdl	bdl	100.26	85.44	
	Ol_06	39.90	0.01	bdl	0.17	13.75	0.22	0.21	46.31	0.10	bdl	bdl	100.66	85.72	
	Ol_06	40.02	bdl	bdl	0.02	13.95	0.21	0.20	46.08	0.01	bdl	bdl	100.49	85.48	
	Ol_07	40.19	bdl	0.01	0.15	13.98	0.25	0.22	46.20	bdl	bdl	bdl	101.00	85.48	
	Ol_07	40.01	0.01	bdl	0.08	13.87	0.25	0.21	46.26	0.01	bdl	bdl	100.68	85.60	
	Ol_07	39.95	0.01	bdl	0.10	14.07	0.24	0.21	46.22	0.02	bdl	bdl	100.82	85.41	
	Ol_07	40.05	0.01	bdl	0.01	14.02	0.25	0.22	46.08	0.04	bdl	bdl	100.67	85.42	
	Ol_08	38.77	0.06	bdl	0.02	21.01	0.10	0.57	39.76	0.16	0.01	bdl	100.46	77.13	host rock contact
	Ol_08	39.16	0.01	bdl	bdl	19.11	0.14	0.45	41.60	0.10	bdl	bdl	100.58	79.50	host rock contact
	Ol_08	39.64	bdl	bdl	0.01	15.78	0.15	0.27	44.73	bdl	bdl	bdl	100.59	83.47	host rock contact
	Ol_08	39.86	0.01	bdl	0.01	14.26	0.18	0.22	45.79	0.01	bdl	bdl	100.32	85.12	host rock contact

Abbreviations: Ol = olivine, bdl = below detection limit. *Note:* all oxides are in wt %.

Table A16. *Continued*

Sample	Mineral ID	SiO_2	TiO_2	Al_2O_3	Cr_2O_3	FeO	NiO	MnO	MgO	CaO	Na_2O	K_2O	Total	Mg#	Comment
BAK-16-22-03	Ol_09	40.15	0.01	bdl	0.01	13.96	0.31	0.21	46.28	bdl	bdl	bdl	100.92	85.52	
	Ol_10	39.69	0.01	bdl	bdl	15.60	0.23	0.25	44.67	bdl	bdl	bdl	100.46	83.61	
	Ol_11	40.04	bdl	bdl	bdl	14.02	0.23	0.20	46.10	bdl	bdl	bdl	100.60	85.42	
	Ol_12	40.11	0.01	bdl	0.01	14.14	0.22	0.21	46.03	0.01	bdl	bdl	100.74	85.29	
	Ol_13	39.80	bdl	bdl	0.01	13.93	0.17	0.22	45.85	bdl	bdl	bdl	99.97	85.43	
	Ol_14	40.21	0.01	bdl	0.01	13.91	0.21	0.21	46.04	0.01	bdl	bdl	100.60	85.51	
	Ol_15	39.93	bdl	bdl	0.01	13.86	0.19	0.21	46.23	0.01	bdl	bdl	100.43	85.60	
	Ol_16	40.00	bdl	bdl	0.01	13.83	0.24	0.21	45.83	bdl	bdl	bdl	100.12	85.52	
	Ol_17	40.23	bdl	bdl	bdl	13.94	0.23	0.23	46.19	bdl	bdl	bdl	100.82	85.52	
	Ol_17	39.99	0.01	bdl	bdl	13.87	0.17	0.21	46.14	bdl	bdl	bdl	100.38	85.57	
BAK-16-22-32	Ol_18	38.78	0.02	bdl	0.03	20.27	0.11	0.32	40.67	0.06	bdl	bdl	100.27	78.14	
	Ol_19	38.99	0.02	bdl	0.03	20.30	0.15	0.31	40.74	0.10	bdl	bdl	100.64	78.15	
	Ol_20	38.97	0.02	bdl	0.02	20.27	0.04	0.30	40.85	0.07	bdl	bdl	100.54	78.22	
	Ol_21	38.95	0.02	0.04	0.02	20.31	0.15	0.31	40.92	0.08	bdl	bdl	100.80	78.22	
	Ol_22	39.06	0.02	bdl	0.01	20.12	0.10	0.33	41.01	0.09	bdl	bdl	100.75	78.41	
	Ol_23	39.04	0.03	bdl	0.02	19.86	0.08	0.30	41.13	0.09	bdl	0.01	100.56	78.68	
	Ol_24	38.96	0.02	bdl	0.01	20.20	0.14	0.31	40.81	0.09	bdl	bdl	100.53	78.26	

Abbreviations: Ol = olivine, bdl = below detection limit. *Note:* all oxides are in wt %.

Table A17*. Major and minor element compositions of spinel in Shiveluch, Avachinsky and Bakening mantle xenolith*

Sample	Mineral ID	SiO_2	TiO_2	Al_2O_3	Cr_2O_3	FeO	NiO	MnO	MgO	CaO	Total	Mg#	Cr#	Comment
SHX03-17	Spl_01	bdl	0.37	8.44	45.78	32.95	0.18	0.46	8.68	bdl	96.87	43.80	78.45	
	Spl_02	bdl	0.27	9.80	45.10	31.31	0.11	0.41	10.04	bdl	97.05	49.80	75.54	
	Spl_02	bdl	0.25	7.65	47.06	31.78	0.11	0.41	9.58	bdl	96.83	48.18	80.50	
	Spl_03C	bdl	0.28	7.57	48.41	30.95	0.12	0.42	9.41	bdl	97.16	47.40	81.09	
	Spl_03	bdl	0.31	8.69	43.88	32.58	0.13	0.42	9.45	bdl	95.46	47.75	77.20	pyroxene contact
	Spl_04	bdl	0.32	9.59	43.21	33.23	0.16	0.38	9.73	bdl	96.63	48.24	75.14	pyroxene contact
	Spl_04C	bdl	0.26	7.36	47.51	32.04	0.11	0.41	9.38	bdl	97.08	47.20	81.24	
	Spl_05	bdl	0.28	9.17	46.99	30.32	0.10	0.42	9.97	bdl	97.25	49.67	77.47	olivine contact
	Spl_05C	bdl	0.28	7.56	47.40	31.80	0.08	0.44	9.60	bdl	97.16	48.15	80.80	
	Spl_06	bdl	0.29	9.26	46.39	30.88	0.11	0.42	10.24	bdl	97.59	50.60	77.07	olivine contact
	Spl_06C	bdl	0.28	7.48	48.36	31.17	0.08	0.43	9.75	bdl	97.56	48.77	81.27	
	Spl_07	bdl	0.25	9.51	47.95	28.70	0.10	0.41	10.06	bdl	96.98	50.35	77.19	olivine contact
	Spl_07C	bdl	0.28	7.71	49.08	30.12	0.10	0.44	9.71	bdl	97.44	48.75	81.02	
	Spl_08	bdl	0.42	8.25	43.10	35.12	0.14	0.43	9.39	bdl	96.84	46.54	77.80	olivine contact
	Spl_08C	bdl	0.31	7.15	46.66	33.03	0.11	0.44	9.24	bdl	96.93	46.48	81.40	
	Spl_09	bdl	0.34	9.66	42.76	33.38	0.17	0.40	9.94	bdl	96.65	49.09	74.81	olivine contact
	Spl_09C	bdl	0.28	7.24	47.34	32.50	0.12	0.42	9.54	bdl	97.44	47.73	81.44	
	Spl_10	bdl	0.30	10.54	42.47	31.75	0.14	0.41	10.08	bdl	95.68	50.24	73.00	olivine contact
	Spl_10C	bdl	0.29	8.49	46.93	31.21	0.11	0.42	9.76	bdl	97.21	48.72	78.76	
SHX03-18	Spl_01	bdl	0.44	16.12	47.29	20.00	0.09	0.32	13.52	bdl	97.78	64.04	66.31	
	Spl_02	bdl	0.37	15.30	46.31	21.90	0.12	0.31	13.45	bdl	97.76	63.85	67.00	olivine contact
	Spl_02C	bdl	0.44	15.31	48.55	20.01	0.10	0.32	13.50	bdl	98.22	63.93	68.02	
	Spl_03	bdl	0.22	13.86	47.89	22.60	0.09	0.34	12.27	bdl	97.27	59.63	69.86	
	Spl_04	bdl	0.39	14.45	48.58	20.80	0.09	0.33	12.83	bdl	97.47	61.71	69.28	
	Spl_05	bdl	0.19	15.24	44.96	23.36	0.11	0.30	12.96	bdl	97.14	62.17	66.43	

Abbreviations: Spl = spinel, C = centre, bdl = below detection limit. *Note:* all oxides are in wt %.

Table A17. *Continued*

Sample	Mineral ID	SiO_2	TiO_2	Al_2O_3	Cr_2O_3	FeO	NiO	MnO	MgO	CaO	Total	Mg#	Cr#	Comment
SHX03-04	Spl_01	bdl	0.42	12.94	30.41	44.71	0.28	0.56	6.11	0.03	95.45	30.31	61.19	inside vein
	Spl_02	bdl	0.41	12.77	32.13	41.26	0.25	0.43	8.59	bdl	95.84	41.60	62.79	inside vein
	Spl_03	bdl	0.33	13.82	30.66	43.49	0.26	0.54	6.67	0.01	95.77	32.89	59.82	inside vein
	Spl_05	bdl	0.41	12.69	33.58	39.99	0.25	0.42	8.82	bdl	96.15	42.74	63.97	hydrous vein contact
	Spl_06	bdl	0.25	15.74	31.81	39.61	0.35	0.49	7.57	0.06	95.87	37.28	57.56	inside vein
	Spl_07	bdl	0.27	15.35	32.59	39.77	0.31	0.50	7.66	0.03	96.49	37.49	58.76	inside vein
	Spl_09	bdl	0.34	15.91	34.12	35.46	0.22	0.40	10.03	bdl	96.48	48.10	58.99	hydrous vein contact
	Spl_10	bdl	0.22	20.44	32.55	30.96	0.41	0.36	11.21	bdl	96.15	53.24	51.65	
	Spl_11	0.30	0.35	16.53	37.08	29.72	0.14	0.33	10.97	bdl	95.42	52.69	60.08	olivine contact
	Spl_11C	bdl	0.40	17.98	35.80	30.83	0.17	0.33	11.29	bdl	96.79	53.49	57.18	
	Spl_12	bdl	0.65	14.10	36.69	34.03	0.18	0.35	10.30	bdl	96.29	49.48	63.57	olivine contact
	Spl_12C	bdl	0.70	14.63	35.34	34.78	0.19	0.35	10.45	bdl	96.44	49.80	61.84	
	Spl_13	bdl	0.54	16.00	35.33	32.95	0.17	0.34	10.79	bdl	96.13	51.57	59.70	olivine contact
	Spl_13C	bdl	0.54	16.09	34.96	33.24	0.17	0.33	10.79	bdl	96.11	51.48	59.31	
	Spl_14	bdl	0.41	18.90	35.76	29.03	0.14	0.32	11.52	bdl	96.08	54.78	55.93	olivine contact
	Spl_14C	bdl	0.43	18.38	36.40	29.35	0.14	0.33	11.47	bdl	96.49	54.46	57.06	
	Spl_15	bdl	0.44	13.97	36.68	33.48	0.16	0.36	10.45	bdl	95.53	50.73	63.79	olivine contact
	Spl_15C	bdl	0.54	15.08	33.76	35.76	0.20	0.35	10.54	bdl	96.23	50.14	60.03	
	Spl_16	bdl	0.43	18.20	35.16	30.70	0.15	0.32	11.41	bdl	96.38	54.07	56.45	
SHIV-16-12-06	Spl_01	bdl	0.52	12.42	40.54	33.29	0.09	0.39	9.47	0.12	96.84	46.44	68.65	
	Spl_01	bdl	0.54	11.38	40.51	33.85	0.10	0.38	9.35	0.12	96.23	46.20	70.48	
	Spl_02	bdl	0.95	10.55	42.52	33.31	0.10	0.38	9.23	0.11	97.16	45.18	73.00	
	Spl_03	bdl	0.46	13.21	41.43	30.90	0.08	0.35	9.88	0.12	96.43	48.63	67.79	
	Spl_03	bdl	0.52	11.15	44.80	31.01	0.07	0.38	9.33	0.11	97.38	46.18	72.95	
	Spl_04	bdl	0.47	6.63	43.32	37.43	0.09	0.40	8.01	0.11	96.48	40.43	81.43	
	Spl_05	bdl	1.00	7.94	42.07	36.75	0.13	0.40	8.48	0.11	96.89	41.87	78.04	
	Spl_06	bdl	0.84	8.57	43.25	35.36	0.10	0.41	8.39	0.11	97.03	41.68	77.20	

Abbreviations: Spl = spinel, C = centre, bdl = below detection limit. *Note:* all oxides are in wt %.

Table A17. *Continued*

Sample	Mineral ID	SiO_2	TiO_2	Al_2O_3	Cr_2O_3	FeO	NiO	MnO	MgO	CaO	Total	Mg#	Cr#	Comment
SHIV-16-12-06	Spl_07	bdl	0.90	8.75	43.81	34.65	0.11	0.38	8.44	0.11	97.15	41.83	77.05	
	Spl_08	bdl	0.79	12.58	43.05	31.08	0.11	0.37	9.42	0.12	97.51	45.97	69.66	
	Spl_09	bdl	1.01	10.22	41.50	35.03	0.11	0.38	8.73	0.11	97.10	42.76	73.15	
	Spl_10	bdl	0.46	12.84	45.96	28.32	0.07	0.37	9.43	0.13	97.58	46.64	70.60	
AVX-16-03-24	Spl_01	bdl	0.07	13.90	52.75	19.14	0.07	0.29	11.29	bdl	97.51	55.64	71.80	
	Spl_02	bdl	0.05	13.29	53.93	18.71	0.05	0.31	11.34	bdl	97.68	56.01	73.13	
	Spl_04	bdl	0.06	13.39	53.30	19.72	0.05	0.31	10.97	bdl	97.81	54.23	72.75	
	Spl_05	bdl	0.06	13.07	53.65	19.27	0.06	0.30	11.13	bdl	97.54	55.15	73.36	
	Spl_06	bdl	0.05	13.04	53.66	19.83	0.04	0.35	10.57	bdl	97.54	52.67	73.41	
	Spl_07	bdl	0.05	12.89	54.20	19.69	0.04	0.33	10.64	bdl	97.83	52.86	73.82	
	Spl_08	bdl	0.05	12.85	50.65	22.18	0.07	0.33	10.93	0.01	97.06	54.35	72.55	
	Spl_09	bdl	0.05	13.29	52.60	19.93	0.09	0.30	11.29	bdl	97.55	55.79	72.64	
	Spl_10	bdl	0.04	12.70	55.18	18.22	0.05	0.30	11.19	bdl	97.69	55.49	74.46	
	Spl_11	bdl	0.09	16.89	48.98	19.26	0.07	0.30	12.09	bdl	97.68	58.36	66.05	
	Spl_12	bdl	0.07	18.08	48.09	18.89	0.10	0.28	12.21	bdl	97.72	58.60	64.09	
	Spl_13	bdl	0.09	14.84	51.38	19.60	0.07	0.28	11.43	bdl	97.69	55.92	69.91	
AVX-16-03-23	Spl_14	bdl	0.08	14.33	51.98	19.93	0.08	0.31	11.02	bdl	97.74	54.24	70.87	
	Spl_15	bdl	0.05	13.29	53.34	19.32	0.08	0.29	11.49	0.01	97.87	56.56	72.92	
	Spl_16	bdl	0.07	14.19	51.94	19.86	0.07	0.29	11.36	bdl	97.77	55.72	71.05	
	Spl_17	bdl	0.05	13.90	52.27	19.66	0.08	0.29	11.47	bdl	97.73	56.35	71.61	
	Spl_19	bdl	0.07	13.86	53.26	19.40	0.07	0.28	11.48	bdl	98.42	56.05	72.05	
	Spl_20	bdl	0.09	12.41	55.28	18.60	0.07	0.30	11.58	bdl	98.33	56.91	74.93	

Abbreviations: Spl = spinel, bdl = below detection limit. *Note:* all oxides are in wt %.

Table A17. *Continued*

Sample	Mineral ID	SiO_2	TiO_2	Al_2O_3	Cr_2O_3	FeO	NiO	MnO	MgO	CaO	Total	Mg#	Cr#	Comment
AVX-16-03-20	Spl_21	bdl	0.02	17.59	45.94	20.88	0.13	0.26	12.93	bdl	97.74	61.66	63.67	
	Spl_22	bdl	0.02	17.79	45.55	20.92	0.12	0.25	13.06	bdl	97.72	62.16	63.20	
	Spl_23	bdl	0.03	17.11	45.37	22.02	0.14	0.30	12.45	bdl	97.42	59.84	64.01	
	Spl_24	bdl	0.08	16.59	43.48	24.98	0.15	0.49	11.30	bdl	97.07	55.10	63.74	
	Spl_25	bdl	0.02	19.88	46.68	17.20	0.09	0.24	13.59	bdl	97.71	64.15	61.17	
	Spl_26	bdl	0.02	18.79	45.65	19.88	0.11	0.28	13.07	bdl	97.81	62.03	61.97	
	Spl_27	bdl	0.06	18.06	44.38	21.74	0.13	0.27	12.82	bdl	97.46	61.09	62.25	
	Spl_28	bdl	0.02	17.88	45.49	20.80	0.13	0.26	12.89	bdl	97.46	61.56	63.06	
	Spl_29	bdl	0.03	16.62	45.32	23.54	0.12	0.39	11.52	bdl	97.55	55.88	64.65	
AVX-16-03-10	Spl_03	bdl	0.08	24.93	38.45	19.14	0.17	0.19	14.93	0.13	98.03	68.09	50.85	
	Spl_04	bdl	0.07	25.58	37.42	18.80	0.17	0.19	15.45	0.13	97.81	70.13	49.53	
	Spl_05	bdl	0.08	26.95	36.44	18.60	0.19	0.18	15.22	0.12	97.77	68.87	47.56	
	Spl_06	bdl	0.08	26.19	36.87	18.88	0.18	0.19	15.06	0.12	97.56	68.52	48.57	
	Spl_07	bdl	0.08	25.33	38.58	19.03	0.17	0.20	14.85	0.11	98.36	67.51	50.54	
	Spl_08	bdl	0.07	24.85	38.80	19.16	0.16	0.20	14.82	0.12	98.19	67.61	51.16	
	Spl_09	bdl	0.08	25.94	36.88	19.60	0.19	0.20	14.83	0.12	97.84	67.48	48.82	
	Spl_10	bdl	0.10	24.29	39.34	19.07	0.17	0.22	14.64	0.11	97.94	67.16	52.08	
	Spl_10	bdl	0.09	23.35	40.43	19.22	0.15	0.23	14.40	0.11	97.98	66.39	53.74	
AVX-16-03-02	Spl_11	0.03	0.09	18.62	43.89	19.99	0.14	0.24	13.01	0.02	96.01	62.71	61.26	
	Spl_11	bdl	0.07	24.31	37.05	19.71	0.17	0.21	14.14	0.01	95.66	66.21	50.56	
	Spl_12	bdl	0.05	21.82	40.14	20.03	0.18	0.23	13.69	bdl	96.14	64.76	55.24	
	Spl_12	bdl	0.02	17.28	45.26	20.15	0.15	0.25	12.87	bdl	95.99	62.60	63.73	
	Spl_13	0.01	0.07	18.54	43.68	19.99	0.13	0.25	13.05	0.02	95.75	63.13	61.24	
	Spl_13	bdl	0.05	18.16	44.19	20.01	0.16	0.23	13.12	0.01	95.93	63.43	62.01	
	Spl_14	bdl	0.03	18.11	44.48	19.70	0.15	0.25	13.02	0.03	95.78	63.26	62.23	
	Spl_15	bdl	0.04	17.96	44.57	19.87	0.15	0.25	12.99	0.01	95.83	63.10	62.48	
	Spl_16	bdl	0.06	18.74	43.39	19.92	0.14	0.25	13.25	bdl	95.75	63.91	60.83	

Abbreviations: Spl = spinel, bdl = below detection limit. *Note:* all oxides are in wt %.

Table A17. *Continued*

Sample	Mineral ID	SiO_2	TiO_2	Al_2O_3	Cr_2O_3	FeO	NiO	MnO	MgO	CaO	Total	Mg#	Cr#	Comment
AVX-16-03-02	Spl_16	bdl	0.05	17.89	44.57	20.24	0.13	0.24	13.11	bdl	96.24	63.28	62.56	
	Spl_17	bdl	0.04	18.16	46.21	18.80	0.13	0.26	13.22	bdl	96.81	63.64	63.06	
	Spl_18	bdl	0.07	18.48	43.81	20.36	0.16	0.25	13.08	bdl	96.23	63.14	61.39	
	Spl_19	bdl	0.06	19.11	43.78	20.08	0.13	0.25	13.19	0.02	96.63	63.16	60.58	
	Spl_20	bdl	0.04	17.98	46.18	18.96	0.11	0.23	13.11	bdl	96.62	63.17	63.28	
	Spl_21	bdl	0.03	17.57	45.57	19.93	0.14	0.25	13.04	bdl	96.55	63.02	63.50	
	Spl_22	bdl	0.03	17.82	45.39	19.68	0.14	0.25	13.09	bdl	96.40	63.20	63.08	
	Spl_23	bdl	0.04	17.79	45.63	19.71	0.13	0.27	12.96	bdl	96.54	62.70	63.24	
	Spl_24	bdl	0.06	17.61	45.36	20.11	0.15	0.24	12.81	bdl	96.34	62.03	63.34	
	Spl_25	bdl	0.04	17.70	45.70	20.15	0.15	0.26	13.10	bdl	97.12	62.92	63.39	
AVX-16-03-07	Spl_26	bdl	0.06	19.61	41.55	20.47	0.15	0.25	13.26	0.01	95.36	63.94	58.70	
	Spl_26	bdl	0.05	18.98	43.13	20.46	0.15	0.24	13.11	0.01	96.13	63.05	60.39	
	Spl_27	bdl	0.04	19.26	44.51	19.16	0.12	0.24	13.18	bdl	96.52	63.18	60.78	
	Spl_28	bdl	0.07	17.84	46.30	19.32	0.12	0.26	12.83	bdl	96.74	62.00	63.52	
	Spl_29	bdl	0.05	19.66	43.82	19.25	0.12	0.25	13.00	bdl	96.15	62.52	59.92	
	Spl_30	bdl	0.05	19.75	44.43	18.68	0.12	0.24	13.23	bdl	96.52	63.31	60.15	
	Spl_31	bdl	0.05	20.05	43.22	19.27	0.12	0.23	13.17	bdl	96.12	63.12	59.11	
	Spl_32	bdl	0.05	19.66	45.29	18.05	0.10	0.25	13.26	bdl	96.65	63.43	60.71	
	Spl_33	bdl	0.05	20.13	43.80	18.50	0.11	0.24	13.30	bdl	96.13	63.75	59.35	
	Spl_34	bdl	0.05	19.75	45.16	17.85	0.10	0.25	13.32	bdl	96.47	63.77	60.53	
	Spl_35	bdl	0.04	19.73	44.13	18.72	0.12	0.24	13.21	bdl	96.20	63.43	60.00	
	Spl_36	bdl	0.03	20.05	44.76	17.84	0.11	0.25	13.23	bdl	96.30	63.63	59.96	
	Spl_37	bdl	0.05	19.49	44.00	19.55	0.12	0.24	13.15	bdl	96.59	62.91	60.24	
	Spl_38	bdl	0.06	20.43	43.49	18.60	0.13	0.24	13.41	bdl	96.37	63.97	58.82	
	Spl_39	bdl	0.07	20.08	43.41	18.99	0.12	0.23	13.14	bdl	96.05	62.99	59.19	
	Spl_40	bdl	0.07	20.40	42.08	20.05	0.14	0.23	13.23	bdl	96.21	63.15	58.05	
	Spl_41	bdl	0.05	21.25	41.95	19.35	0.15	0.22	13.39	bdl	96.37	63.70	56.97	

Abbreviations: Spl = spinel, bdl = below detection limit. *Note:* all oxides are in wt %.

Table A17. *Continued*

Sample	Mineral ID	SiO_2	TiO_2	Al_2O_3	Cr_2O_3	FeO	NiO	MnO	MgO	CaO	Total	Mg#	Cr#	Comment
AVX-16-03-07	Spl_42	0.10	0.06	19.10	42.44	19.24	0.13	0.24	12.89	0.01	94.21	63.04	59.85	
	Spl_43	bdl	0.06	19.53	45.95	17.62	0.11	0.23	13.29	bdl	96.80	63.52	61.22	
BAK-16-22-04	Spl_01	bdl	0.52	38.40	20.30	22.22	0.23	0.17	14.82	0.12	96.78	64.09	26.18	
	Spl_02	bdl	0.50	37.11	20.16	24.43	0.25	0.19	14.85	0.11	97.61	63.92	26.71	
	Spl_02	bdl	0.48	36.19	20.39	23.99	0.24	0.19	14.81	0.12	96.41	64.61	27.43	
	Spl_03	bdl	0.49	37.30	20.40	23.73	0.25	0.17	14.72	0.11	97.18	63.64	26.84	
	Spl_04	bdl	0.49	37.10	20.41	23.64	0.22	0.17	15.08	0.11	97.23	65.01	26.96	
	Spl_04	bdl	0.48	37.63	20.75	22.87	0.23	0.19	14.73	0.11	97.00	63.82	27.01	
	Spl_05	bdl	0.65	37.65	21.01	21.05	0.24	0.19	16.32	0.19	97.30	69.70	27.24	
	Spl_05	bdl	0.49	37.49	20.81	22.93	0.23	0.17	13.82	0.11	96.05	60.73	27.13	
	Spl_07	bdl	0.43	36.82	19.37	23.45	0.26	0.17	15.06	0.11	95.67	65.85	26.08	
	Spl_07	bdl	0.43	37.88	19.85	23.02	0.24	0.16	15.03	0.12	96.72	65.05	26.01	
	Spl_08	bdl	0.61	35.36	21.25	23.96	0.23	0.17	14.68	0.26	96.52	64.28	28.74	
	Spl_09	bdl	0.60	34.31	21.39	22.96	0.23	0.18	15.15	0.22	95.05	67.13	29.49	
	Spl_10	0.09	0.41	35.77	19.64	22.65	0.22	0.20	15.51	0.55	95.04	68.87	26.91	exsolution in cpx
	Spl_11	0.04	0.49	35.60	20.91	23.09	0.21	0.20	14.89	0.55	95.98	66.02	28.27	exsolution in cpx
	Spl_12	0.57	0.49	35.51	18.50	23.37	0.23	0.17	15.18	0.83	94.85	67.09	25.90	exsolution in cpx
	Spl_13	bdl	0.47	36.25	21.98	21.56	0.24	0.21	15.34	0.11	96.17	67.05	28.92	
	Spl_13	bdl	0.46	36.78	21.13	23.57	0.24	0.19	13.83	0.11	96.31	60.85	27.82	
	Spl_14	bdl	0.45	36.17	21.25	23.72	0.23	0.19	14.28	0.12	96.40	62.64	28.27	
	Spl_15	bdl	0.52	35.79	20.30	24.73	0.23	0.18	14.92	0.11	96.79	64.76	27.57	
	Spl_15	bdl	0.50	36.29	20.43	24.65	0.24	0.19	14.18	0.12	96.60	62.00	27.41	
BAK-16-22-01B	Spl_01	bdl	0.29	38.41	13.92	29.61	0.18	0.30	13.18	bdl	95.88	57.62	19.56	
	Spl_02	bdl	0.26	42.18	14.77	22.62	0.19	0.17	15.57	bdl	95.76	66.57	19.02	
	Spl_03	bdl	0.27	41.76	14.80	22.48	0.20	0.18	15.59	bdl	95.28	66.99	19.21	
	Spl_04	bdl	0.28	41.21	15.57	23.31	0.19	0.17	15.14	0.01	95.88	65.04	20.22	
	Spl_05	bdl	0.30	39.14	16.87	24.29	0.21	0.18	14.80	0.01	95.80	64.18	22.43	

Abbreviations: Spl = spinel, cpx = clinopyroxene, bdl = below detection limit. *Note:* all oxides are in wt %.

Table A17. *Continued*

Sample	Mineral ID	SiO_2	TiO_2	Al_2O_3	Cr_2O_3	FeO	NiO	MnO	MgO	CaO	Total	Mg#	Cr#	Comment
BAK-16-22-01B	Spl_07	bdl	0.25	37.47	18.38	24.84	0.20	0.22	14.33	bdl	95.70	62.93	24.76	
	Spl_08	0.03	0.25	43.64	12.59	22.21	0.22	0.16	15.82	bdl	94.93	67.58	16.21	
	Spl_08	bdl	0.24	44.05	12.89	21.79	0.22	0.16	15.92	bdl	95.28	67.77	16.41	
	Spl_09	bdl	0.30	37.83	18.66	23.49	0.17	0.17	14.92	0.01	95.54	65.09	24.86	
	Spl_10	bdl	0.25	41.72	15.03	22.75	0.19	0.17	15.53	0.01	95.65	66.58	19.46	
	Spl_11	bdl	0.34	40.12	15.72	22.82	0.19	0.17	15.40	0.02	94.78	66.80	20.81	
	Spl_12	0.10	0.23	41.48	13.12	23.79	0.20	0.16	14.96	bdl	94.07	64.92	17.51	
	Spl_12	bdl	0.26	42.73	13.63	23.24	0.22	0.16	15.31	bdl	95.55	65.51	17.62	
	Spl_13	bdl	0.29	39.78	16.66	23.30	0.18	0.18	14.95	0.01	95.35	64.90	21.94	
	Spl_14	bdl	0.40	33.33	22.35	25.82	0.15	0.23	13.39	0.01	95.68	59.80	31.03	
	Spl_15	0.01	0.28	42.27	13.58	23.40	0.22	0.17	15.12	bdl	95.05	65.08	17.73	
BAK-16-22-09	Spl_16	0.02	0.36	42.33	18.94	20.36	0.25	0.17	15.27	bdl	97.71	64.55	23.08	
	Spl_19	0.01	0.87	37.84	18.25	27.89	0.13	0.33	11.73	0.20	97.25	51.42	24.44	
	Spl_20	0.03	0.61	41.40	17.29	23.15	0.16	0.25	14.36	0.20	97.47	61.31	21.89	
	Spl_23	0.01	0.47	45.61	19.12	15.13	0.19	0.16	17.39	0.02	98.11	71.56	21.96	
	Spl_24	bdl	0.51	42.92	19.96	19.25	0.16	0.20	14.72	0.09	97.81	62.42	23.78	
	Spl_25	bdl	0.50	45.00	19.84	16.90	0.17	0.19	16.10	bdl	98.70	66.63	22.82	
	Spl_26	bdl	0.46	40.76	19.81	20.56	0.25	0.16	15.50	bdl	97.51	65.79	24.59	
BAK-16-22-03	Spl_02	bdl	0.30	39.78	17.51	23.96	0.20	0.17	15.53	0.13	97.61	66.19	22.80	
	Spl_03	bdl	0.32	39.59	17.44	23.77	0.23	0.20	15.49	0.12	97.18	66.28	22.81	
	Spl_04	0.34	0.25	39.44	14.92	23.56	0.18	0.19	16.41	0.65	95.94	70.62	20.24	exsolution in cpx
	Spl_05	0.01	0.27	41.62	13.70	25.26	0.25	0.17	15.35	0.11	96.74	65.32	18.09	
	Spl_05	bdl	0.25	41.87	13.92	24.77	0.21	0.15	15.78	0.12	97.07	66.72	18.24	
	Spl_06	bdl	0.89	37.06	16.19	27.39	0.19	0.19	14.61	0.12	96.65	62.61	22.67	
	Spl_07	bdl	0.41	40.08	16.59	25.05	0.21	0.21	14.85	0.11	97.51	63.37	21.73	
	Spl_08	bdl	1.12	34.14	17.45	30.64	0.29	0.31	13.10	0.13	97.17	56.79	25.53	
	Spl_09	1.70	0.22	43.44	12.28	22.34	0.23	0.16	17.95	0.14	98.48	70.55	15.95	

Abbreviations: Spl = spinel, cpx = clinopyroxene, bdl = below detection limit. *Note:* all oxides are in wt %.

Table A17*. Continued*

Sample	Mineral ID	SiO_2	TiO_2	Al_2O_3	Cr_2O_3	FeO	NiO	MnO	MgO	CaO	Total	Mg#	Cr#	Comment
BAK-16-22-03	Spl_09	bdl	0.20	45.14	13.19	22.22	0.23	0.15	16.59	0.11	97.83	68.90	16.39	
	Spl_10	bdl	0.22	44.18	13.10	23.14	0.17	0.16	16.04	0.12	97.13	67.34	16.59	
	Spl_11	bdl	0.27	39.56	15.55	26.04	0.28	0.17	14.74	0.12	96.74	63.48	20.87	
	Spl_12	bdl	0.25	41.30	14.88	24.93	0.28	0.16	15.06	0.11	96.99	64.40	19.47	
	Spl_13	bdl	0.23	42.38	14.04	24.07	0.25	0.17	15.45	0.12	96.71	65.72	18.18	
	Spl_14	bdl	0.25	39.78	15.07	26.01	0.24	0.18	14.85	0.12	96.49	63.93	20.26	
	Spl_15	bdl	0.28	40.58	14.94	25.51	0.22	0.18	14.86	0.12	96.70	63.72	19.81	
	Spl_16	bdl	0.28	37.72	16.35	27.76	0.22	0.20	14.22	0.12	96.87	61.67	22.53	
	Spl_17	0.01	1.37	39.92	15.12	24.60	0.26	0.18	15.47	0.17	97.11	64.75	20.26	
	Spl_18	bdl	0.71	40.08	17.28	23.33	0.22	0.19	15.42	0.15	97.38	65.36	22.43	
	Spl_19	bdl	0.28	43.43	14.17	22.44	0.25	0.16	16.54	0.13	97.39	69.26	17.96	
	Spl_20	bdl	0.97	43.93	13.04	22.33	0.24	0.14	16.42	0.19	97.29	68.06	16.61	
BAK-16-22-32	Spl_21	0.02	0.42	56.46	1.29	22.37	0.29	0.13	16.07	0.11	97.17	64.56	1.51	
	Spl_22	bdl	0.55	55.35	2.80	21.81	0.21	0.13	15.96	0.16	96.98	64.43	3.28	
	Spl_23	0.02	0.33	52.10	2.94	24.59	0.26	0.13	16.16	0.12	96.66	65.95	3.65	
	Spl_24	0.01	0.43	54.36	2.67	23.87	0.26	0.13	15.71	0.12	97.57	63.44	3.19	
	Spl_25	bdl	0.31	52.61	2.43	24.45	0.19	0.13	16.30	0.27	96.69	66.58	3.00	
	Spl_26	bdl	0.32	55.20	1.37	23.82	0.23	0.12	16.09	0.11	97.26	64.80	1.64	
	Spl_27	bdl	0.31	54.80	1.41	23.56	0.21	0.14	16.06	0.11	96.61	65.20	1.70	
	Spl_28	bdl	0.33	53.47	1.92	24.35	0.20	0.12	16.46	0.12	96.96	66.50	2.35	
	Spl_29	bdl	0.28	55.82	1.41	22.88	0.23	0.14	16.44	0.12	97.31	66.02	1.67	
	Spl_30	bdl	0.39	57.19	2.29	19.43	0.26	0.15	17.25	0.11	97.08	68.81	2.62	
	Spl_31	bdl	0.40	57.23	1.48	22.17	0.29	0.13	16.16	0.11	97.98	64.36	1.71	
	Spl_32	bdl	0.37	57.29	1.53	21.91	0.23	0.12	16.26	0.11	97.81	64.80	1.75	
	Spl_33	bdl	0.32	55.38	1.34	24.39	0.25	0.12	16.11	0.11	98.02	64.43	1.59	
	Spl_34	bdl	0.27	55.10	1.39	23.82	0.27	0.13	16.49	0.11	97.57	66.15	1.66	
	Spl_35	bdl	0.34	51.04	4.06	25.54	0.25	0.13	16.08	0.12	97.56	65.35	5.07	

Abbreviations: Spl = spinel, bdl = below detection limit. *Note:* all oxides are in wt %.

Table A17. *Continued*

Sample	Mineral ID	SiO_2	TiO_2	Al_2O_3	Cr_2O_3	FeO	NiO	MnO	MgO	CaO	Total	Mg#	Cr#	Comment
BAK-16-22-32	Spl_36	0.04	0.32	51.09	4.04	25.63	0.24	0.14	15.93	0.11	97.55	64.80	5.04	
	Spl_37	0.01	0.35	50.40	3.85	25.57	0.16	0.15	16.44	0.12	97.03	66.92	4.87	
	Spl_38	bdl	0.30	54.36	1.57	24.40	0.27	0.13	16.45	0.11	97.59	66.07	1.91	
	Spl_39	bdl	0.46	54.90	2.83	22.36	0.27	0.15	16.42	0.12	97.51	65.96	3.35	
	Spl_40	0.01	0.34	54.16	1.74	24.25	0.26	0.16	16.27	0.11	97.30	65.63	2.11	
	Spl_41	bdl	0.39	54.32	3.09	23.07	0.15	0.20	16.09	0.12	97.44	64.99	3.67	
	Spl_42	bdl	0.29	51.87	3.40	24.70	0.20	0.14	16.36	0.12	97.09	66.58	4.21	
	Spl_43	0.02	0.29	51.18	4.07	24.28	0.19	0.13	16.06	0.12	96.34	65.95	5.07	

Abbreviations: Spl = spinel, bdl = below detection limit. *Note:* all oxides are in wt %.

***Table A18**. Major and minor element compositions of orthopyroxene in Shiveluch, Avachinsky and Bakening mantle xenoliths*

Sample	Mineral ID	SiO_2	TiO_2	Al_2O_3	Cr_2O_3	FeO	NiO	MnO	MgO	CaO	Na_2O	K_2O	Total	Mg#	Comment
SHX03-04	Ol_04	54.81	0.12	1.36	0.02	11.79	nd	0.43	30.67	0.37	bdl	bdl	99.57	82.25	
	Opx_03	55.59	0.01	0.38	0.01	12.03	nd	0.53	29.67	0.62	bdl	bdl	98.86	81.46	hydrous vein orthopyroxene
	Opx_05	56.06	0.02	0.37	0.02	11.51	nd	0.53	30.06	0.61	bdl	0.01	99.17	82.32	hydrous vein orthopyroxene
	Opx_06R	56.24	0.01	1.21	0.02	8.70	nd	0.32	32.53	0.26	bdl	bdl	99.30	86.95	hydrous vein orthopyroxene
	Opx_06R	55.72	0.02	0.88	0.01	10.46	nd	0.48	30.80	0.56	bdl	bdl	98.92	83.99	hydrous vein orthopyroxene
	Opx_06C	56.02	0.02	1.28	0.02	9.23	nd	0.37	31.89	0.31	bdl	bdl	99.12	86.02	hydrous vein orthopyroxene
	Opx_07	55.95	0.02	1.41	0.01	9.21	nd	0.35	32.04	0.33	bdl	bdl	99.33	86.11	hydrous vein orthopyroxene
	Opx_08	56.62	0.02	0.66	bdl	9.03	nd	0.39	32.40	0.35	bdl	bdl	99.47	86.48	hydrous vein orthopyroxene
	Opx_13	56.75	bdl	0.63	bdl	8.52	nd	0.34	32.74	0.26	bdl	bdl	99.24	87.26	hydrous vein orthopyroxene
	Opx_18	56.67	0.13	1.19	0.01	9.01	nd	0.48	32.48	0.38	bdl	bdl	100.36	86.53	
	Opx_20	54.95	0.12	1.61	bdl	12.93	nd	0.44	29.25	0.40	0.02	0.01	99.74	80.12	
	Opx_21	54.79	0.13	1.48	0.01	11.92	nd	0.45	29.97	0.42	bdl	bdl	99.16	81.76	
	Opx_01	55.46	0.06	0.27	bdl	11.95	0.12	0.50	30.19	0.93	nd	nd	99.48	81.82	hydrous vein orthopyroxene
	Opx_02	55.13	0.01	0.56	bdl	11.93	0.09	0.48	30.56	0.50	nd	nd	99.27	82.03	hydrous vein orthopyroxene
	Opx_03	55.20	0.02	0.47	bdl	11.89	0.13	0.47	30.54	0.63	nd	nd	99.37	82.07	hydrous vein orthopyroxene
	Opx_04	55.40	0.02	0.54	0.01	10.60	0.11	0.40	31.61	0.61	nd	nd	99.30	84.16	hydrous vein orthopyroxene
	Opx_05	54.56	0.01	1.61	0.01	10.61	0.10	0.41	31.08	0.61	nd	nd	99.00	83.92	hydrous vein orthopyroxene
SHX03-01	Opx_01	54.40	0.29	1.33	0.02	12.39	nd	0.38	29.88	0.39	0.02	bdl	99.10	81.12	
	Opx_02	54.84	0.21	1.58	bdl	11.83	nd	0.52	30.32	0.35	bdl	bdl	99.64	82.04	
	Opx_03	54.26	0.08	0.77	0.02	12.17	nd	0.45	29.43	1.09	bdl	bdl	98.27	81.17	
	Opx_04	54.00	0.05	1.01	0.10	12.97	nd	0.28	29.04	0.68	bdl	bdl	98.13	79.97	
	Opx_05	55.45	0.08	1.06	0.04	11.81	nd	0.57	30.62	0.22	bdl	bdl	99.86	82.20	
	Opx_06	55.92	0.05	1.07	0.10	8.56	nd	0.45	32.84	0.28	bdl	bdl	99.26	87.24	
	Opx_07	54.33	0.03	1.62	0.10	13.30	nd	0.15	29.26	0.38	bdl	bdl	99.18	79.68	
	Opx_08	54.72	0.15	1.02	0.07	11.25	nd	0.13	30.68	0.20	bdl	bdl	98.22	82.94	
	Opx_09	56.14	0.04	1.25	0.11	6.37	nd	0.12	34.06	0.74	bdl	bdl	98.84	90.49	
	Opx_10	56.78	0.04	1.90	0.15	6.46	nd	0.12	34.17	0.55	bdl	bdl	100.17	90.40	

Abbreviations: Ol and Opx = orthopyroxene, R = rim, C = centre, bdl = below detection limit, nd = not determined. *Note:* all oxides are in wt %.

Table A18. *Continued*

Sample	Mineral ID	SiO_2	TiO_2	Al_2O_3	Cr_2O_3	FeO	NiO	MnO	MgO	CaO	Na_2O	K_2O	Total	Mg#	Comment
SHX03-01	Opx_11	56.45	0.09	1.40	0.43	6.46	nd	0.13	33.72	0.66	bdl	0.01	99.34	90.29	
	Opx_12	56.38	0.05	0.92	0.06	6.68	nd	0.12	33.77	0.43	bdl	0.01	98.40	90.01	
	Opx_13	56.49	0.14	0.99	0.18	6.48	nd	0.12	33.82	0.81	bdl	bdl	99.03	90.29	
	Opx_4	57.68	0.08	0.64	0.12	6.25	0.10	0.14	34.86	1.04	bdl	0.01	100.93	90.86	
	Opx_5	57.14	0.05	1.22	0.10	6.66	0.09	0.13	35.02	0.28	bdl	bdl	100.70	90.36	
	Opx_6	57.25	0.13	0.83	0.10	6.62	0.09	0.13	35.02	0.47	bdl	bdl	100.65	90.42	
	Opx_7	57.06	0.05	1.17	0.14	6.39	0.09	0.12	36.00	0.34	bdl	0.02	101.39	90.94	
	Opx_11	57.11	0.03	0.35	bdl	9.63	0.22	0.32	32.79	0.59	bdl	bdl	101.05	85.85	
SHX03-18	Opx_01	56.93	0.04	0.62	bdl	6.41	nd	0.37	34.21	0.45	0.01	bdl	99.04	90.49	hydrous vein orthopyroxene
	Opx_02	56.87	0.13	0.33	bdl	6.46	nd	0.35	34.24	0.48	bdl	bdl	98.87	90.43	hydrous vein orthopyroxene
	Opx_03	56.35	0.07	0.27	bdl	10.10	nd	0.36	31.43	0.42	0.02	bdl	99.02	84.72	hydrous vein orthopyroxene
	Opx_04	56.78	0.05	0.30	bdl	9.86	nd	0.34	31.61	0.50	bdl	bdl	99.45	85.11	hydrous vein orthopyroxene
	Opx_05C	56.82	0.09	0.41	bdl	9.77	nd	0.37	31.57	0.71	bdl	0.02	99.77	85.20	hydrous vein orthopyroxene
	Opx_05R	56.80	0.06	0.21	bdl	9.79	nd	0.34	31.64	0.57	bdl	bdl	99.41	85.21	hydrous vein orthopyroxene
	Opx_06	56.65	0.07	0.49	bdl	9.71	nd	0.41	31.19	0.58	bdl	0.04	99.14	85.13	hydrous vein orthopyroxene
	Opx_07	56.70	0.07	0.37	0.01	9.83	nd	0.37	31.66	0.54	0.01	bdl	99.56	85.17	hydrous vein orthopyroxene
	Opx_08	56.32	0.13	0.41	bdl	10.02	nd	0.36	31.11	0.86	bdl	bdl	99.21	84.70	hydrous vein orthopyroxene
	Opx_09	56.51	0.07	0.50	bdl	10.07	nd	0.20	31.42	0.63	bdl	bdl	99.40	84.75	hydrous vein orthopyroxene
	Opx_10	56.44	0.07	0.28	bdl	9.99	nd	0.31	31.52	0.55	bdl	bdl	99.19	84.90	hydrous vein orthopyroxene
	Opx_10	57.56	0.08	0.25	bdl	5.89	nd	0.31	35.15	0.20	bdl	0.01	99.45	91.41	hydrous vein orthopyroxene
	Opx_10	56.53	0.09	0.29	0.01	9.11	nd	0.33	31.89	0.74	bdl	bdl	98.99	86.18	hydrous vein orthopyroxene
	Opx_11	56.64	0.04	0.13	bdl	9.21	nd	0.31	32.17	0.60	bdl	bdl	99.10	86.16	hydrous vein orthopyroxene
	Opx_12	56.73	0.05	0.19	bdl	9.18	nd	0.33	31.92	0.75	bdl	bdl	99.16	86.11	hydrous vein orthopyroxene
	Opx_13	56.58	0.02	0.18	bdl	8.93	nd	0.20	31.67	0.97	bdl	bdl	98.55	86.34	hydrous vein orthopyroxene
	Opx_14	56.50	0.06	0.26	bdl	9.11	nd	0.27	31.51	1.03	bdl	bdl	98.75	86.05	hydrous vein orthopyroxene
	Opx_15	57.50	0.10	0.52	0.02	6.71	nd	0.28	34.29	0.13	bdl	bdl	99.56	90.10	hydrous vein orthopyroxene
	Opx_16	57.14	0.10	0.61	bdl	8.48	nd	0.30	32.79	0.42	0.01	bdl	99.85	87.33	hydrous vein orthopyroxene

Abbreviations: Opx = orthopyroxene, R = rim, C = centre, bdl = below detection limit, nd = not determined. *Note:* all oxides are in wt %.

Table A18. *Continued*

Sample	Mineral ID	SiO_2	TiO_2	Al_2O_3	Cr_2O_3	FeO	NiO	MnO	MgO	CaO	Na_2O	K_2O	Total	Mg#	Comment
SHX03-18	Opx_17	56.53	0.04	0.65	bdl	9.16	nd	0.29	32.11	0.53	bdl	bdl	99.31	86.21	hydrous vein orthopyroxene
	Opx_18	56.46	0.03	0.47	bdl	9.11	nd	0.25	31.84	0.52	bdl	bdl	98.68	86.17	hydrous vein orthopyroxene
	Opx_19	56.53	0.01	1.24	0.03	8.79	nd	0.16	32.38	0.39	bdl	bdl	99.54	86.78	hydrous vein orthopyroxene
	Opx_20	56.85	0.06	0.35	bdl	7.89	nd	0.30	33.19	0.32	0.01	0.01	98.96	88.23	hydrous vein orthopyroxene
SHX03-17	Opx_01	55.85	bdl	0.89	bdl	9.69	0.07	0.46	32.93	0.23	nd	nd	100.13	85.82	hydrous vein orthopyroxene
	Opx_02	56.68	bdl	0.72	bdl	8.25	0.06	0.35	34.03	0.20	nd	nd	100.29	88.02	hydrous vein orthopyroxene
	Opx_03	56.53	bdl	1.87	bdl	6.75	0.08	0.22	34.66	0.18	nd	nd	100.30	90.15	hydrous vein orthopyroxene
	Opx_04	56.81	0.01	0.63	0.02	7.86	0.09	0.39	34.19	0.21	nd	nd	100.20	88.57	hydrous vein orthopyroxene
	Opx_05	56.59	bdl	0.85	bdl	8.13	0.06	0.37	33.79	0.20	nd	nd	99.98	88.11	hydrous vein orthopyroxene
	Opx_06	56.46	bdl	0.77	bdl	7.86	0.05	0.34	34.02	0.22	nd	nd	99.71	88.53	hydrous vein orthopyroxene
	Opx_07	56.96	0.01	0.90	0.02	6.67	0.08	0.22	35.10	0.20	nd	nd	100.17	90.36	hydrous vein orthopyroxene
	Opx_08	56.62	0.01	0.68	0.01	7.61	0.08	0.32	34.30	0.19	nd	nd	99.80	88.93	hydrous vein orthopyroxene
	Opx_09	56.77	bdl	0.75	0.01	8.14	0.06	0.35	33.90	0.20	nd	nd	100.19	88.12	hydrous vein orthopyroxene
	Opx_10	56.86	bdl	0.87	bdl	8.06	0.06	0.34	33.88	0.19	nd	nd	100.26	88.22	hydrous vein orthopyroxene
	Opx_11	56.52	bdl	1.01	bdl	8.30	0.07	0.36	33.62	0.19	nd	nd	100.07	87.83	hydrous vein orthopyroxene
	Opx_12	56.88	bdl	0.72	bdl	8.00	0.06	0.37	33.85	0.19	nd	nd	100.07	88.29	hydrous vein orthopyroxene
	Opx_15	57.03	bdl	0.54	0.01	7.32	0.07	0.27	34.51	0.24	nd	nd	99.99	89.37	hydrous vein orthopyroxene
	Opx_05	57.86	0.02	0.56	0.37	5.78	0.05	0.21	36.56	0.05	nd	nd	101.45	91.86	spinel contact
	Opx_08	57.87	0.03	0.48	0.35	5.98	0.04	0.21	36.15	0.14	nd	nd	101.26	91.50	spinel contact
	Opx_09	57.17	0.03	0.55	0.43	5.78	0.05	0.20	36.37	0.07	nd	nd	100.66	91.81	spinel contact
	Opx_10	57.67	0.01	0.36	0.18	6.34	0.09	0.23	36.05	0.13	nd	nd	101.05	91.02	spinel contact
	Opx_11	58.09	0.02	0.33	bdl	5.66	0.07	0.18	36.89	0.02	nd	nd	101.26	92.07	

Abbreviations: Opx = orthopyroxene, bdl = below detection limit, nd = not determined. *Note:* all oxides are in wt %.

Table A18. *Continued*

Sample	Mineral ID	SiO_2	TiO_2	Al_2O_3	Cr_2O_3	FeO	NiO	MnO	MgO	CaO	Na_2O	K_2O	Total	Mg#	Comment
SHIV-16-12-06	Opx_01	54.15	0.12	0.99	0.01	12.71	0.05	0.55	29.49	0.92	nd	nd	98.98	80.52	host rock contact
	Opx_02	54.40	0.14	1.13	0.02	11.89	0.04	0.51	30.04	1.05	nd	nd	99.20	81.83	host rock contact
	Opx_03	55.77	0.03	1.26	0.02	7.39	0.04	0.22	33.87	0.63	nd	nd	99.22	89.09	
	Opx_04	54.13	0.02	3.15	0.02	7.81	0.06	0.19	33.00	0.45	nd	nd	98.84	88.27	
	Opx_05	53.79	0.02	3.76	0.01	7.87	0.04	0.19	32.77	0.46	nd	nd	98.91	88.13	
	Opx_06	54.31	0.02	3.09	0.01	7.83	0.06	0.18	33.08	0.41	nd	nd	99.00	88.27	
	Opx_07	54.25	0.02	3.02	0.01	7.78	0.05	0.21	33.17	0.47	nd	nd	98.98	88.37	
	Opx_08	54.91	0.07	2.15	0.07	7.55	0.05	0.21	33.55	0.61	nd	nd	99.16	88.78	
	Opx_09	54.99	0.10	2.01	0.08	7.42	0.06	0.19	33.48	0.74	nd	nd	99.08	88.94	
	Opx_10	54.22	0.04	2.85	0.01	7.67	0.05	0.21	33.10	0.59	nd	nd	98.74	88.49	
SHX-No-No	Opx_01	56.50	0.02	1.55	0.04	5.08	0.13	0.17	35.57	0.13	bdl	0.01	99.18	92.58	
	Opx_01	56.95	0.02	1.22	0.05	4.96	0.08	0.16	35.75	0.10	bdl	bdl	99.30	92.78	
	Opx_01	56.51	0.02	1.54	0.02	5.08	0.12	0.17	35.55	0.13	bdl	bdl	99.13	92.58	
	Opx_02	56.94	0.01	1.12	0.01	4.97	0.13	0.14	35.77	0.15	bdl	bdl	99.24	92.76	
	Opx_03	56.93	0.01	1.37	0.02	4.98	0.12	0.14	35.54	0.13	bdl	bdl	99.24	92.71	
	Opx_03	57.36	bdl	0.79	0.01	4.99	0.12	0.16	35.86	0.17	bdl	bdl	99.47	92.76	
	Opx_04	56.58	0.01	1.42	0.02	5.05	0.13	0.16	35.62	0.13	bdl	bdl	99.11	92.63	
	Opx_05	56.88	0.02	1.33	0.03	5.07	0.08	0.16	35.62	0.09	bdl	bdl	99.29	92.60	
	Opx_06	56.36	0.02	1.38	0.19	7.46	0.08	0.25	33.76	0.14	bdl	bdl	99.63	88.97	
	Opx_07	54.81	0.03	0.38	bdl	15.30	0.06	0.59	27.45	0.55	0.02	bdl	99.19	76.18	
	Opx_08	54.10	0.07	0.79	bdl	16.12	0.03	0.63	26.86	0.61	bdl	bdl	99.23	74.80	
	Opx_09	54.77	0.03	0.86	bdl	14.15	0.08	0.54	28.52	0.48	bdl	bdl	99.44	78.22	
	Opx_10	55.28	0.03	1.16	0.01	11.28	0.09	0.42	30.73	0.41	bdl	0.01	99.41	82.92	
	Opx_11	56.94	bdl	1.74	bdl	5.13	0.12	0.17	35.11	0.41	bdl	bdl	99.62	92.42	
	Opx_12	57.04	0.02	1.50	0.14	5.25	0.08	0.17	35.44	0.14	bdl	bdl	99.77	92.33	
	Opx_12	57.51	0.01	1.14	0.01	5.07	0.11	0.15	35.79	0.12	bdl	bdl	99.92	92.64	
	Opx_12	57.39	0.01	1.00	0.01	5.05	0.10	0.16	35.76	0.16	bdl	bdl	99.64	92.66	

Abbreviations: Opx = orthopyroxene, bdl = below detection limit, nd = not determined. *Note:* all oxides are in wt %.

Table A18. *Continued*

Sample	Mineral ID	SiO_2	TiO_2	Al_2O_3	Cr_2O_3	FeO	NiO	MnO	MgO	CaO	Na_2O	K_2O	Total	Mg#	Comment
SHX-No-No	Opx_12	57.75	0.02	1.12	0.01	5.11	0.09	0.17	35.74	0.12	0.01	bdl	100.14	92.57	
	Opx_13	57.87	0.02	0.51	0.04	4.90	0.06	0.16	36.21	0.11	bdl	bdl	99.87	92.94	
	Opx_13	57.67	0.01	0.79	0.02	5.05	0.06	0.24	35.87	0.12	bdl	bdl	99.84	92.68	
	Opx_13	58.35	bdl	0.10	0.01	4.75	0.09	0.16	36.35	0.12	bdl	bdl	99.93	93.16	
	Opx_13	57.09	0.03	1.76	0.02	5.17	0.09	0.17	35.62	0.08	bdl	bdl	100.04	92.46	
	Opx_14	57.59	0.01	0.99	0.02	5.10	0.11	0.16	35.92	0.14	bdl	bdl	100.03	92.63	
	Opx_14	57.58	0.05	0.97	0.01	5.27	0.09	0.17	35.74	0.30	bdl	bdl	100.19	92.35	
	Opx_14	57.47	0.01	1.25	0.02	5.13	0.10	0.16	35.90	0.10	0.01	bdl	100.16	92.58	
	Opx_15	57.73	0.02	0.82	0.03	4.89	0.08	0.15	36.14	0.15	bdl	bdl	100.00	92.94	
	Opx_15	57.35	0.02	1.05	0.13	4.93	0.08	0.17	35.79	0.14	bdl	bdl	99.65	92.83	
	Opx_16	58.06	bdl	0.37	bdl	4.82	0.11	0.11	36.30	0.11	bdl	bdl	99.88	93.07	
	Opx_17	58.03	bdl	0.46	0.01	4.84	0.08	0.15	36.14	0.17	bdl	bdl	99.89	93.01	
	Opx_19	57.47	0.02	1.09	0.03	5.04	0.07	0.18	35.81	0.09	bdl	0.01	99.81	92.67	
	Opx_20	57.88	0.01	0.57	0.01	4.88	0.09	0.16	36.20	0.17	bdl	bdl	99.95	92.97	

Abbreviations: Opx = orthopyroxene, bdl = below detection limit, nd = not determined. *Note:* all oxides are in wt %.

***Table A18**. Continued*

Sample	Mineral ID	SiO_2	TiO_2	Al_2O_3	Cr_2O_3	FeO	NiO	MnO	MgO	CaO	Na_2O	K_2O	Total	Mg#	Comment
AVX-16-03-24	Opx_16	57.42	0.01	0.67	0.08	5.02	0.12	0.13	35.21	0.93	nd	nd	99.58	92.60	hydrous vein orthopyroxene
	Opx_17	56.83	0.02	1.16	0.13	5.44	0.10	0.11	34.99	0.65	nd	nd	99.43	91.98	hydrous vein orthopyroxene
	Opx_19	56.47	0.01	0.87	0.44	6.81	0.07	0.16	33.97	0.65	nd	nd	99.47	89.89	hydrous vein orthopyroxene
	Opx_20	57.08	0.01	0.74	0.04	5.76	0.09	0.14	34.80	0.73	nd	nd	99.38	91.50	hydrous vein orthopyroxene
	Opx_22	56.31	0.04	1.02	0.10	7.22	0.09	0.16	33.57	0.68	nd	nd	99.19	89.23	hydrous vein orthopyroxene
	Opx_23	56.57	0.02	0.96	0.40	6.87	0.09	0.17	34.01	0.56	nd	nd	99.63	89.82	hydrous vein orthopyroxene
	Opx_25	57.13	0.01	0.94	0.09	5.96	0.08	0.14	34.57	0.65	nd	nd	99.57	91.18	hydrous vein orthopyroxene
	Opx_26	56.68	bdl	0.81	0.46	6.41	0.08	0.14	34.12	0.64	nd	nd	99.34	90.46	
	Opx_27	56.64	0.01	0.74	0.42	6.50	0.06	0.16	34.22	0.56	nd	nd	99.32	90.37	
	Opx_27	56.82	0.01	0.94	0.37	5.75	0.10	0.11	34.68	0.71	nd	nd	99.50	91.49	
	Opx_29	56.58	bdl	0.81	0.47	6.01	0.06	0.15	35.04	0.16	nd	nd	99.27	91.22	
	Opx_30	56.66	0.01	0.78	0.34	6.82	0.06	0.16	33.86	0.62	nd	nd	99.33	89.84	

Abbreviations: Opx = orthopyroxene, bdl = below detection limit, nd = not determined. *Note:* all oxides are in wt %.

Table A18. *Continued*

Sample	Mineral ID	SiO_2	TiO_2	Al_2O_3	Cr_2O_3	FeO	NiO	MnO	MgO	CaO	Na_2O	K_2O	Total	Mg#	Comment
AVX-16-03-23	Opx_46	57.21	0.05	0.55	0.12	4.91	0.12	0.09	35.55	0.80	nd	nd	99.39	92.81	anhydrous vein orthopyroxene
	Opx_46	57.22	0.05	0.56	0.11	4.90	0.13	0.08	35.46	0.79	nd	nd	99.29	92.80	anhydrous vein orthopyroxene
	Opx_47	56.88	0.02	0.50	0.09	5.74	0.08	0.15	35.12	0.59	nd	nd	99.18	91.60	anhydrous vein orthopyroxene
	Opx_48	57.10	0.03	1.36	0.05	5.76	0.09	0.14	33.81	0.84	nd	nd	99.17	91.27	anhydrous vein orthopyroxene
	Opx_50	57.15	0.04	0.53	0.10	4.65	0.12	0.09	35.62	0.73	nd	nd	99.05	93.18	anhydrous vein orthopyroxene
	Opx_51	57.40	0.03	0.50	0.07	5.22	0.09	0.12	35.27	0.92	nd	nd	99.61	92.34	anhydrous vein orthopyroxene
	Opx_52	56.72	0.03	0.18	0.03	7.59	0.04	0.20	34.06	0.15	nd	nd	99.01	88.89	anhydrous vein orthopyroxene
	Opx_53	57.16	0.02	0.57	0.06	5.85	0.10	0.13	34.96	0.43	nd	nd	99.27	91.41	anhydrous vein orthopyroxene
	Opx_54	56.15	0.02	0.87	0.24	7.02	0.07	0.17	33.73	0.70	nd	nd	98.98	89.55	anhydrous vein orthopyroxene
	Opx_56	56.81	0.04	0.58	0.06	5.94	0.10	0.13	34.64	0.75	nd	nd	99.05	91.23	anhydrous vein orthopyroxene
	Opx_57	57.45	0.02	0.09	0.05	5.85	0.07	0.18	35.40	0.18	nd	nd	99.28	91.51	anhydrous vein orthopyroxene
	Opx_58	55.79	0.02	2.39	bdl	5.50	0.24	0.10	34.59	0.44	nd	nd	99.08	91.81	anhydrous vein orthopyroxene
	Opx_59	56.48	0.02	1.29	0.20	5.88	0.07	0.12	34.95	0.41	nd	nd	99.43	91.38	anhydrous vein orthopyroxene
	Opx_60	57.22	0.02	0.44	0.04	5.88	0.12	0.14	34.86	0.61	nd	nd	99.34	91.35	anhydrous vein orthopyroxene

Abbreviations: Opx = orthopyroxene, bdl = below detection limit, nd = not determined. *Note:* all oxides are in wt %.

***Table A18**. Continued*

Sample	Mineral	SiO_2	TiO_2	Al_2O_3	Cr_2O_3	FeO	NiO	MnO	MgO	CaO	Na_2O	K_2O	Total	Mg#	Comment
AVX-16-03-23	Opx_62	57.30	0.01	0.30	0.19	5.92	0.11	0.15	34.99	0.69	nd	nd	99.66	91.33	
	Opx_63	56.66	0.01	0.78	0.39	6.66	0.08	0.16	34.16	0.54	nd	nd	99.43	90.14	
	Opx_64	56.47	0.01	0.76	0.34	6.77	0.09	0.17	33.73	0.79	nd	nd	99.13	89.88	
	Opx_65	56.25	0.04	1.16	0.07	7.37	0.11	0.18	33.31	0.79	nd	nd	99.28	88.95	
	Opx_66	55.84	0.01	1.76	0.18	6.81	0.06	0.15	34.02	0.17	nd	nd	99.01	89.91	
	Opx_67	56.58	0.02	1.04	0.27	6.68	0.06	0.16	34.33	0.36	nd	nd	99.49	90.16	
	Opx_68	55.96	0.01	1.64	0.32	6.85	0.07	0.15	34.16	0.23	nd	nd	99.39	89.89	
	Opx_69	56.88	0.02	0.99	0.13	6.57	0.07	0.15	34.65	0.21	nd	nd	99.67	90.38	
AVX-16-03-20	Opx_82	55.32	0.09	1.00	0.03	10.50	0.11	0.53	31.10	0.39	nd	nd	99.07	84.07	hydrous vein orthopyroxene
	Opx_83	55.59	0.06	1.15	0.20	9.86	0.12	0.47	31.47	0.55	nd	nd	99.48	85.04	hydrous vein orthopyroxene
	Opx_84	55.10	0.08	1.15	0.13	10.65	0.10	0.51	30.93	0.43	nd	nd	99.08	83.81	hydrous vein orthopyroxene
	Opx_85	55.36	0.08	0.87	0.01	10.79	0.10	0.55	31.02	0.38	nd	nd	99.15	83.67	hydrous vein orthopyroxene
	Opx_86	55.03	0.07	0.96	0.01	10.81	0.10	0.55	30.72	0.56	nd	nd	98.81	83.51	hydrous vein orthopyroxene
	Opx_87	55.03	0.04	1.45	0.28	9.74	0.10	0.41	31.65	0.47	nd	nd	99.17	85.28	hydrous vein orthopyroxene
	Opx_88	55.16	0.08	0.80	0.01	10.82	0.10	0.53	30.96	0.40	nd	nd	98.85	83.61	hydrous vein orthopyroxene
	Opx_89	54.43	0.08	1.74	0.05	10.35	0.08	0.49	30.49	1.02	nd	nd	98.74	84.00	hydrous vein orthopyroxene
	Opx_90	54.52	0.10	1.47	0.01	10.66	0.07	0.50	30.31	0.99	nd	nd	98.63	83.51	hydrous vein orthopyroxene
	Opx_92	56.45	bdl	1.12	0.29	5.49	0.08	0.14	34.75	0.68	nd	nd	99.00	91.86	
	Opx_93	55.96	0.01	1.05	0.23	5.18	0.08	0.14	34.74	0.67	nd	nd	98.03	92.28	
	Opx_94	56.09	0.01	1.66	0.39	5.63	0.09	0.15	34.62	0.60	nd	nd	99.25	91.63	
AVX-16-03-02	Opx_01	57.35	0.03	1.38	0.43	6.06	0.11	0.14	34.23	1.09	0.01	nd	100.82	90.96	
	Opx_02	56.94	0.01	1.55	0.49	5.97	0.11	0.14	33.99	1.07	bdl	nd	100.27	91.02	
	Opx_02	57.66	bdl	1.05	0.04	5.95	0.12	0.13	34.87	0.69	0.01	nd	100.53	91.26	
	Opx_03	57.32	0.02	1.27	0.37	5.86	0.10	0.15	34.20	1.22	0.01	nd	100.51	91.23	
	Opx_03	57.27	0.02	1.28	0.45	5.79	0.08	0.16	34.61	1.10	0.01	nd	100.78	91.41	
	Opx_04	57.13	0.01	1.33	0.45	6.11	0.09	0.14	33.89	1.37	bdl	nd	100.53	90.82	
	Opx_05	57.05	0.01	1.32	0.51	6.10	0.08	0.16	34.02	1.11	0.01	nd	100.38	90.85	

Abbreviations: Opx = orthopyroxene, bdl = below detection limit, nd = not determined. *Note:* all oxides are in wt %.

Table A18. *Continued*

Sample	Mineral ID	SiO_2	TiO_2	Al_2O_3	Cr_2O_3	FeO	NiO	MnO	MgO	CaO	Na_2O	K_2O	Total	Mg#	Comment
AVX-16-03-02	Opx_06	56.97	0.01	1.35	0.52	6.00	0.07	0.15	33.61	1.51	bdl	nd	100.20	90.89	
	Opx_07	56.88	bdl	1.37	0.53	5.99	0.09	0.14	34.01	1.11	0.01	nd	100.13	91.00	
	Opx_08	57.31	0.01	1.00	0.27	5.88	0.11	0.15	34.52	1.19	0.01	nd	100.45	91.27	anhydrous vein orthopyroxene
	Opx_09	57.13	0.02	1.37	0.31	6.26	0.10	0.15	34.17	0.78	bdl	nd	100.27	90.68	anhydrous vein orthopyroxene
	Opx_10	57.33	0.03	1.12	0.36	6.00	0.09	0.14	34.42	0.72	0.01	nd	100.23	91.09	anhydrous vein orthopyroxene
	Opx_10	56.73	0.01	0.30	0.27	4.02	0.08	0.07	34.90	1.11	0.03	nd	97.51	93.94	anhydrous vein orthopyroxene
	Opx_11	57.84	0.01	0.37	0.16	5.72	0.10	0.14	34.79	0.96	0.01	nd	100.09	91.55	anhydrous vein orthopyroxene
	Opx_11	57.19	0.02	1.07	0.27	6.02	0.10	0.15	33.96	1.13	0.01	nd	99.92	90.95	anhydrous vein orthopyroxene
	Opx_12	57.29	0.04	0.97	0.23	6.20	0.10	0.16	33.85	1.08	0.01	nd	99.93	90.67	anhydrous vein orthopyroxene
	Opx_13	57.23	0.03	1.19	0.33	6.08	0.09	0.15	34.20	0.95	0.01	nd	100.26	90.93	anhydrous vein orthopyroxene
	Opx_14	57.43	0.03	1.19	0.40	6.04	0.08	0.16	34.24	0.89	0.01	nd	100.47	90.99	anhydrous vein orthopyroxene
	Opx_15	57.35	0.02	1.04	0.24	6.26	0.10	0.15	34.01	1.17	bdl	nd	100.35	90.63	anhydrous vein orthopyroxene
	Opx_16	57.09	0.03	1.16	0.27	6.26	0.11	0.15	33.77	1.14	0.01	nd	99.99	90.57	anhydrous vein orthopyroxene
	Opx_17	57.36	0.03	1.16	0.32	6.09	0.09	0.16	33.94	1.31	bdl	nd	100.46	90.85	anhydrous vein orthopyroxene

Abbreviations: Opx = orthopyroxene, bdl = below detection limit, nd = not determined. *Note:* all oxides are in wt %.

***Table A18**. Continued*

Sample	Mineral ID	SiO_2	TiO_2	Al_2O_3	Cr_2O_3	FeO	NiO	MnO	MgO	CaO	Na_2O	K_2O	Total	Mg#	Comment
AVX-16-03-02	Opx_18	57.12	0.02	1.15	0.29	6.27	0.10	0.17	33.95	1.09	0.01	nd	100.17	90.61	anhydrous vein orthopyroxene
	Opx_19	57.62	0.02	0.83	0.16	6.24	0.09	0.16	34.71	0.64	0.02	nd	100.48	90.83	anhydrous vein orthopyroxene
	Opx_20	57.70	0.02	0.97	0.30	6.01	0.10	0.16	34.39	1.01	0.01	nd	100.67	91.07	anhydrous vein orthopyroxene
AVX-16-03-07	Opx_21	57.30	0.01	1.20	0.32	6.15	0.08	0.14	34.09	0.96	0.01	nd	100.27	90.81	
	Opx_21	56.55	0.02	1.42	0.45	6.38	0.08	0.17	33.89	0.83	0.01	nd	99.78	90.44	
	Opx_22	56.69	0.01	1.52	0.55	6.24	0.07	0.15	33.85	0.90	0.01	nd	100.00	90.62	
	Opx_23	56.48	bdl	1.89	0.67	6.35	0.09	0.16	33.85	0.82	bdl	nd	100.31	90.48	
	Opx_23	56.73	0.02	1.56	0.37	6.22	0.08	0.14	33.80	1.07	0.02	nd	100.00	90.65	
	Opx_24	57.21	0.01	1.14	0.30	6.08	0.10	0.14	34.59	0.86	0.01	nd	100.43	91.02	
	Opx_24	56.83	0.02	1.29	0.41	6.37	0.08	0.15	34.02	0.77	bdl	nd	99.93	90.50	
	Opx_25	56.49	0.01	1.60	0.59	6.18	0.08	0.16	33.41	1.50	0.01	nd	100.03	90.60	
	Opx_26	56.97	0.02	1.29	0.37	6.37	0.08	0.16	34.16	0.79	bdl	nd	100.21	90.52	
	Opx_27	56.51	0.01	1.65	0.61	6.30	0.09	0.16	33.97	0.86	0.01	nd	100.17	90.57	
	Opx_28	56.71	0.02	1.56	0.56	6.24	0.09	0.15	33.79	1.02	bdl	nd	100.15	90.61	

Abbreviations: Opx = orthopyroxene, bdl = below detection limit, nd = not determined. *Note:* all oxides are in wt %.

***Table A18**. Continued*

Sample	Mineral ID	SiO_2	TiO_2	Al_2O_3	Cr_2O_3	FeO	NiO	MnO	MgO	CaO	Na_2O	K_2O	Total	Mg#	Comment
AVX-16-03-07	Opx_29	57.08	0.02	1.07	0.25	6.44	0.08	0.16	33.78	1.15	bdl	nd	100.03	90.34	anhydrous vein orthopyroxene
	Opx_30	57.02	0.02	1.21	0.33	6.40	0.09	0.16	33.91	0.93	0.02	nd	100.09	90.42	anhydrous vein orthopyroxene
	Opx_31	56.73	0.03	1.65	0.31	6.36	0.09	0.15	34.01	0.71	0.01	nd	100.06	90.50	anhydrous vein orthopyroxene
	Opx_31	57.14	0.03	1.13	0.26	6.43	0.09	0.16	33.87	0.98	bdl	nd	100.10	90.37	anhydrous vein orthopyroxene
	Opx_32	56.84	0.01	1.30	0.39	6.44	0.08	0.15	34.15	0.80	bdl	nd	100.15	90.44	anhydrous vein orthopyroxene
	Opx_33	57.01	0.03	1.42	0.27	6.01	0.09	0.14	34.32	0.90	0.01	nd	100.19	91.05	anhydrous vein orthopyroxene
	Opx_33	56.92	0.02	1.44	0.43	6.32	0.09	0.14	34.02	0.74	bdl	nd	100.13	90.55	anhydrous vein orthopyroxene
	Opx_34	56.16	0.02	1.96	0.75	6.32	0.10	0.15	33.22	1.34	0.01	nd	100.03	90.35	anhydrous vein orthopyroxene
	Opx_35	56.68	0.02	1.60	0.59	6.36	0.09	0.15	34.12	0.79	bdl	nd	100.39	90.52	anhydrous vein orthopyroxene
	Opx_36	56.20	0.01	2.08	0.79	6.49	0.10	0.15	33.45	0.71	bdl	nd	99.97	90.18	anhydrous vein orthopyroxene
	Opx_37	57.18	0.02	1.31	0.36	6.37	0.07	0.15	33.73	1.12	0.01	nd	100.33	90.42	anhydrous vein orthopyroxene
	Opx_38	57.14	0.02	1.27	0.35	6.44	0.08	0.15	34.22	0.84	0.02	nd	100.53	90.45	anhydrous vein orthopyroxene
	Opx_39	57.41	0.02	1.29	0.33	6.38	0.08	0.15	34.26	0.66	0.02	nd	100.60	90.54	anhydrous vein orthopyroxene
	Opx_40	57.92	0.01	0.70	0.17	6.03	0.09	0.15	34.84	0.69	0.02	nd	100.61	91.15	anhydrous vein orthopyroxene
	Opx_40	57.08	0.03	1.24	0.29	6.44	0.09	0.17	34.32	0.77	bdl	nd	100.42	90.47	anhydrous vein orthopyroxene

Abbreviations: Opx = orthopyroxene, bdl = below detection limit, nd = not determined. *Note:* all oxides are in wt %.

Table A18. *Continued*

Sample	Mineral ID	SiO_2	TiO_2	Al_2O_3	Cr_2O_3	FeO	NiO	MnO	MgO	CaO	Na_2O	K_2O	Total	Mg#	Comment
AVX-16-03-07	Opx_41	57.10	0.02	1.34	0.42	6.41	0.09	0.17	33.94	0.88	0.01	nd	100.37	90.42	anhydrous vein orthopyroxene
	Opx_42	56.97	0.02	1.38	0.43	6.35	0.07	0.16	33.99	0.74	0.01	nd	100.12	90.51	anhydrous vein orthopyroxene
	Opx_43	56.77	0.02	1.51	0.49	6.43	0.09	0.16	33.83	0.81	bdl	nd	100.11	90.36	anhydrous vein orthopyroxene
AVX-16-03-10	Opx_01	55.71	0.01	1.96	0.62	5.98	0.08	0.15	34.87	0.74	nd	nd	100.11	91.23	
	Opx_02	53.31	0.04	4.56	bdl	7.99	0.11	0.21	32.65	0.61	nd	nd	99.48	87.92	hydrous vein 2 orthopyroxene
	Opx_03	55.56	0.02	2.01	0.62	5.85	0.08	0.13	34.96	0.72	nd	nd	99.95	91.41	
	Opx_05	55.74	0.02	1.92	0.52	6.26	0.08	0.14	34.49	0.89	nd	nd	100.05	90.76	hydrous vein 2 orthopyroxene
	Opx_06	53.97	0.04	3.94	0.01	7.60	0.11	0.20	33.39	0.53	nd	nd	99.79	88.68	
	Opx_07	56.68	0.01	0.92	0.06	6.58	0.08	0.17	35.35	0.55	nd	nd	100.41	90.54	hydrous vein 2 orthopyroxene
	Opx_08	56.67	0.01	0.89	0.30	5.61	0.09	0.13	35.81	0.65	nd	nd	100.15	91.93	
	Opx_09	56.72	0.01	0.96	0.21	5.69	0.10	0.12	35.66	0.64	nd	nd	100.11	91.78	anhydrous vein orthopyroxene
	Opx_10	56.86	0.01	0.97	0.12	5.61	0.10	0.11	35.89	0.59	nd	nd	100.27	91.93	
	Opx_11	57.07	0.01	0.63	0.02	5.75	0.08	0.13	36.27	0.28	nd	nd	100.25	91.84	anhydrous vein orthopyroxene
	Opx_12	55.78	0.09	1.57	0.03	7.20	0.12	0.23	34.21	0.78	nd	nd	100.02	89.43	hydrous vein 2 orthopyroxene
	Opx_14	54.33	0.04	2.69	0.03	7.36	0.09	0.19	34.80	0.64	nd	nd	100.18	89.39	hydrous vein 2 orthopyroxene

Abbreviations: Opx = orthopyroxene, bdl = below detection limit, nd = not determined. *Note:* all oxides are in wt %.

***Table A18**. Continued*

Sample	Mineral ID	SiO_2	TiO_2	Al_2O_3	Cr_2O_3	FeO	NiO	MnO	MgO	CaO	Na_2O	K_2O	Total	Mg#	Comment
AVX-16-03-10	Opx_15	56.73	0.01	1.06	0.23	5.69	0.08	0.15	35.44	0.68	nd	nd	100.07	91.73	
	Opx_16	56.71	0.01	1.08	0.40	5.73	0.08	0.15	35.49	0.45	nd	nd	100.11	91.69	
	Opx_17	55.52	0.01	1.98	0.60	5.73	0.09	0.13	35.08	0.63	nd	nd	99.77	91.60	
	Opx_18	55.36	0.01	2.03	0.64	5.79	0.09	0.14	34.16	1.72	nd	nd	99.95	91.31	
	Opx_19	55.28	0.01	2.10	0.73	5.87	0.07	0.13	34.78	0.97	nd	nd	99.95	91.35	
	Opx_20	55.51	0.01	2.11	0.71	5.83	0.09	0.14	34.83	0.76	nd	nd	99.99	91.41	
BAK-16-22-04	Opx_01	54.23	0.11	2.74	0.28	8.43	0.07	0.20	31.94	0.73	nd	nd	98.73	87.10	
	Opx_02	54.42	0.11	2.58	0.28	8.30	0.05	0.21	31.91	0.81	nd	nd	98.67	87.27	
	Opx_03	54.17	0.10	2.75	0.29	8.29	0.07	0.20	32.09	0.77	nd	nd	98.73	87.34	
	Opx_04	54.27	0.10	2.76	0.30	8.37	0.05	0.21	32.08	0.73	nd	nd	98.87	87.23	
	Opx_05	54.48	0.11	2.67	0.32	8.52	0.06	0.19	32.09	0.83	nd	nd	99.26	87.04	exsolution in cpx
	Opx_06	54.60	0.11	2.80	0.35	8.48	0.07	0.22	32.09	0.73	nd	nd	99.44	87.08	
BAK-16-22-01A	Opx_01	52.22	0.12	4.72	0.25	11.41	0.02	0.25	28.95	0.85	0.04	bdl	98.80	81.89	
	Opx_01	52.27	0.11	4.66	0.25	11.96	0.01	0.25	28.44	0.71	0.05	bdl	98.69	80.90	
	Opx_02	52.03	0.09	4.69	0.26	12.45	0.02	0.29	28.03	0.74	0.03	bdl	98.63	80.04	
	Opx_03	52.74	0.10	4.99	0.30	9.78	0.04	0.22	30.10	0.75	0.02	bdl	99.02	84.57	
	Opx_04	52.52	0.10	4.87	0.21	10.58	0.04	0.23	29.21	0.73	0.04	bdl	98.55	83.10	
	Opx_05	52.38	0.10	4.80	0.25	11.37	0.03	0.25	28.92	0.68	0.04	bdl	98.83	81.92	
	Opx_06	52.41	0.10	4.93	0.26	9.97	0.02	0.23	29.98	0.67	0.02	bdl	98.59	84.28	
	Opx_07	51.91	0.12	4.80	0.25	12.70	0.01	0.25	27.72	0.75	0.06	bdl	98.56	79.54	
BAK-16-22-01B	Opx_08	54.15	0.08	2.98	0.41	8.65	0.01	0.21	31.46	0.72	0.01	bdl	98.68	86.64	
	Opx_09	54.44	0.08	2.99	0.37	8.70	0.04	0.21	31.33	0.81	0.02	bdl	98.98	86.52	
	Opx_10	54.31	0.07	3.00	0.41	8.72	0.03	0.21	31.53	0.69	bdl	bdl	98.97	86.57	
	Opx_11	54.24	0.08	3.19	0.34	8.78	0.04	0.22	31.48	0.71	0.02	bdl	99.09	86.47	
	Opx_11	53.99	0.08	3.47	0.48	8.93	0.04	0.20	31.23	0.53	0.01	bdl	98.96	86.18	
	Opx_12	54.23	0.09	3.58	0.39	8.71	0.04	0.20	31.48	0.68	0.02	bdl	99.42	86.56	
	Opx_12	53.71	0.09	4.07	0.41	8.98	0.04	0.20	31.12	0.56	0.01	bdl	99.18	86.07	
	Opx_13	54.29	0.09	3.31	0.32	8.84	0.04	0.21	31.71	0.66	0.02	bdl	99.51	86.47	
	Opx_13	54.27	0.09	3.45	0.36	8.91	0.03	0.20	31.52	0.57	0.01	bdl	99.41	86.31	

Abbreviations: Opx = orthopyroxene, bdl = below detection limit, nd = not determined. *Note:* all oxides are in wt %.

Table A18. *Continued*

Sample	Mineral ID	SiO_2	TiO_2	Al_2O_3	Cr_2O_3	FeO	NiO	MnO	MgO	CaO	Na_2O	K_2O	Total	Mg#	Comment
BAK-16-22-05	Opx_14	52.74	0.10	4.73	0.23	9.91	0.02	0.23	29.95	0.74	0.03	bdl	98.68	84.34	
	Opx_14	52.65	0.10	4.90	0.26	10.00	0.04	0.23	30.00	0.69	0.02	bdl	98.89	84.25	
	Opx_15	52.77	0.11	4.90	0.24	9.87	0.02	0.22	29.99	0.70	0.02	bdl	98.83	84.42	
	Opx_16	52.54	0.10	4.88	0.27	9.86	0.02	0.22	30.01	0.75	0.03	bdl	98.67	84.43	
	Opx_17	52.84	0.10	4.80	0.26	9.85	0.03	0.22	29.97	0.86	0.02	bdl	98.94	84.42	
	Opx_18	52.80	0.11	4.71	0.27	9.92	0.04	0.22	30.03	0.69	0.03	bdl	98.80	84.37	
	Opx_19	53.96	0.17	3.81	0.26	9.62	0.02	0.22	29.82	1.61	0.04	bdl	99.53	84.67	
	Opx_19	52.89	0.10	4.92	0.24	10.03	0.02	0.23	30.33	0.69	0.03	bdl	99.47	84.35	
	Opx_20	53.21	0.10	4.92	0.24	9.79	0.02	0.22	30.35	0.82	0.03	bdl	99.72	84.68	
	Opx_21	53.02	0.10	5.11	0.27	9.99	0.03	0.22	30.18	0.69	0.01	bdl	99.63	84.33	
	Opx_22	52.84	0.11	5.01	0.21	11.20	0.03	0.26	28.83	0.68	0.07	bdl	99.25	82.10	
	Opx_22	52.95	0.12	5.02	0.25	10.40	0.01	0.22	29.70	0.69	0.05	bdl	99.41	83.58	
	Opx_22	53.23	0.11	4.88	0.23	9.89	0.03	0.20	30.09	0.70	0.02	bdl	99.37	84.43	
BAK-16-22-09	Opx_23	53.69	0.11	3.37	0.42	7.69	0.04	0.18	31.81	1.61	0.02	bdl	98.93	88.06	exsolution in cpx
	Opx_26	53.87	0.09	3.32	0.42	7.90	0.03	0.18	32.21	0.71	0.01	bdl	98.73	87.91	
	Opx_26	54.01	0.09	3.35	0.40	8.04	0.04	0.20	32.22	0.67	0.03	bdl	99.05	87.72	
	Opx_27	53.84	0.11	3.32	0.46	8.03	0.04	0.18	32.16	0.74	0.01	bdl	98.89	87.71	
	Opx_27	53.90	0.09	3.25	0.42	7.91	0.04	0.19	32.28	0.78	0.03	bdl	98.89	87.91	
	Opx_27	53.87	0.10	3.28	0.42	8.13	0.05	0.19	32.14	0.68	0.01	bdl	98.86	87.57	
	Opx_28	54.02	0.10	3.23	0.38	8.11	0.06	0.20	32.43	0.68	0.02	bdl	99.23	87.69	
BAK-16-22-03	Opx_01	54.39	0.09	3.22	0.31	9.12	0.05	0.21	31.46	0.69	0.03	bdl	99.57	86.01	
	Opx_02	53.94	0.08	3.50	0.44	9.07	0.02	0.21	31.38	0.60	0.01	bdl	99.25	86.04	
BAK-16-22-32	Opx_03	52.51	0.17	4.91	0.08	11.67	0.05	0.24	29.06	0.73	0.02	bdl	99.44	81.61	
	Opx_04	52.08	0.16	5.37	0.07	11.73	0.10	0.25	28.87	0.74	0.02	bdl	99.40	81.43	
	Opx_05	52.73	0.15	4.64	0.09	11.69	0.06	0.23	29.12	0.77	0.02	bdl	99.51	81.62	
	Opx_05	52.71	0.15	4.60	0.10	11.59	0.05	0.24	29.06	0.77	0.03	bdl	99.29	81.71	
	Opx_06	52.66	0.14	4.64	0.10	11.64	0.01	0.23	29.03	0.76	0.01	bdl	99.23	81.63	
	Opx_06	52.35	0.16	4.76	0.09	11.63	0.07	0.24	28.97	0.79	0.02	bdl	99.07	81.61	
	Opx_07	52.54	0.15	4.83	0.07	11.82	0.04	0.24	29.16	0.76	0.03	bdl	99.65	81.47	

Abbreviations: Opx = orthopyroxene, bdl = below detection limit, nd = not determined. *Note:* all oxides are in wt %.

***Table A18**. Continued*

Sample	Mineral ID	SiO_2	TiO_2	Al_2O_3	Cr_2O_3	FeO	NiO	MnO	MgO	CaO	Na_2O	K_2O	Total	Mg#	Comment
BAK-16-22-32	Opx_07	52.53	0.15	4.86	0.09	11.67	0.02	0.24	29.07	0.77	0.02	bdl	99.43	81.61	
	Opx_08	52.12	0.16	5.23	0.07	11.83	0.04	0.25	28.92	0.73	bdl	bdl	99.36	81.33	
	Opx_09	52.36	0.17	4.98	0.07	11.88	0.07	0.25	28.89	0.76	0.02	bdl	99.46	81.25	
	Opx_10	52.24	0.16	5.14	0.08	11.80	bdl	0.24	28.79	0.74	0.02	bdl	99.21	81.31	
	Opx_11	52.08	0.16	5.29	0.10	11.88	0.04	0.25	28.66	0.72	0.02	bdl	99.20	81.13	
	Opx_12	52.58	0.14	4.67	0.12	11.65	bdl	0.24	28.99	0.80	0.02	bdl	99.21	81.60	
	Opx_13	51.89	0.15	5.36	0.12	11.77	0.02	0.25	28.61	0.78	0.02	bdl	98.96	81.25	
	Opx_14	52.29	0.15	4.99	0.10	11.74	0.01	0.25	29.07	0.74	0.03	bdl	99.37	81.52	
	Opx_15	51.79	0.16	5.72	0.09	11.91	0.01	0.24	28.58	0.74	0.03	bdl	99.29	81.05	
	Opx_16	52.04	0.17	5.46	0.07	11.80	0.03	0.24	28.80	0.74	0.03	bdl	99.37	81.31	
	Opx_17	52.30	0.16	5.14	0.09	11.78	0.05	0.26	28.90	0.75	0.02	bdl	99.45	81.38	
	Opx_18	51.82	0.15	5.69	0.07	11.84	0.08	0.24	28.68	0.75	0.01	bdl	99.33	81.19	
	Opx_19	52.43	0.18	4.98	0.09	11.83	0.06	0.23	28.98	0.75	0.02	bdl	99.54	81.37	
	Opx_20	52.17	0.16	5.22	0.09	11.77	0.04	0.23	28.73	0.74	0.01	bdl	99.16	81.31	
	Opx_21	52.48	0.16	4.75	0.08	11.77	0.05	0.25	29.05	0.72	0.03	bdl	99.33	81.47	
	Opx_22	52.01	0.16	5.40	0.08	11.89	0.06	0.26	28.71	0.74	0.02	bdl	99.33	81.14	
BAK-16-22-42	Opx_23	53.46	0.09	4.11	0.41	9.96	0.09	0.23	30.66	0.72	0.02	bdl	99.74	84.58	
	Opx_24	53.58	0.09	4.02	0.37	10.07	0.05	0.24	30.53	0.74	0.02	bdl	99.70	84.39	
	Opx_25	53.34	0.10	4.22	0.32	10.04	0.04	0.22	30.58	0.65	0.02	bdl	99.53	84.44	
	Opx_26	53.61	0.10	4.25	0.33	10.20	0.04	0.25	30.61	0.67	0.04	bdl	100.08	84.25	
	Opx_27	53.50	0.10	4.12	0.29	9.86	0.07	0.22	30.83	0.72	0.04	bdl	99.75	84.78	
	Opx_27	53.60	0.09	4.14	0.29	9.97	0.04	0.24	30.62	0.66	0.02	bdl	99.68	84.55	
	Opx_28	53.57	0.10	4.16	0.33	9.75	0.05	0.23	30.60	0.80	0.04	bdl	99.63	84.83	
	Opx_28	53.45	0.10	4.23	0.33	9.99	0.03	0.22	30.56	0.67	0.02	bdl	99.61	84.49	
	Opx_29	53.72	0.10	4.04	0.30	9.90	0.06	0.22	30.64	0.77	0.03	bdl	99.77	84.65	
	Opx_30	53.77	0.09	4.05	0.29	10.01	0.05	0.22	30.66	0.67	0.03	bdl	99.84	84.51	
	Opx_31	53.64	0.09	4.12	0.32	10.21	0.07	0.25	30.63	0.67	0.03	bdl	100.02	84.24	
	Opx_32	53.82	0.09	4.08	0.32	10.21	0.07	0.24	30.71	0.65	0.02	bdl	100.23	84.27	
	Opx_33	53.53	0.10	4.08	0.32	10.25	0.07	0.23	30.68	0.66	0.03	bdl	99.96	84.21	

Abbreviations: Opx = orthopyroxene, bdl = below detection limit, nd = not determined. *Note:* all oxides are in wt %.

Table A18. *Continued*

Sample	Mineral ID	SiO_2	TiO_2	Al_2O_3	Cr_2O_3	FeO	NiO	MnO	MgO	CaO	Na_2O	K_2O	Total	Mg#	Comment
BAK-16-22-42	Opx_34	53.74	0.10	4.12	0.31	10.11	0.01	0.25	30.68	0.64	0.02	bdl	99.98	84.40	
	Opx_35	53.67	0.11	4.04	0.31	10.12	0.04	0.23	30.63	0.69	0.03	bdl	99.86	84.37	
	Opx_36	53.67	0.11	4.14	0.31	10.09	0.13	0.23	30.76	0.65	0.04	bdl	100.13	84.45	

Abbreviations: Opx = orthopyroxene, bdl = below detection limit, nd = not determined. *Note:* all oxides are in wt %.

Table A19*. Major and minor element compositions of clinopyroxene in Shiveluch, Avachinsky and Bakening mantle xenoliths*

Sample	Mineral ID	SiO_2	TiO_2	Al_2O_3	Cr_2O_3	FeO	NiO	MnO	MgO	CaO	Na_2O	K_2O	Total	Mg#	Comment
SHX03-04	Cpx_01	53.17	0.15	0.89	bdl	5.61	0.07	0.24	18.05	21.27	nd	nd	99.47	85.15	
	Cpx_02	52.62	0.34	1.57	0.01	5.59	0.09	0.22	16.40	22.55	nd	nd	99.38	83.94	
	Cpx_03	53.28	0.13	0.87	bdl	5.10	0.07	0.23	16.96	22.90	nd	nd	99.55	85.56	
	Cpx_04	53.67	0.15	0.58	0.04	5.07	0.18	0.23	17.35	22.30	nd	nd	99.56	85.91	
	Cpx_05	52.75	0.32	1.64	0.04	5.02	0.10	0.20	16.72	22.78	nd	nd	99.57	85.59	
AVX-16-03-24	Cpx_01	54.15	0.04	1.06	0.08	3.52	0.05	0.11	17.21	23.55	nd	nd	99.75	89.71	
	Cpx_02	54.46	0.01	0.96	0.04	2.52	0.03	0.08	17.98	23.61	nd	nd	99.68	92.71	
	Cpx_03	54.40	0.02	0.96	0.22	2.15	0.04	0.07	18.03	23.93	nd	nd	99.82	93.72	
	Cpx_04	54.00	0.05	1.14	0.08	2.91	0.06	0.12	17.15	23.88	nd	nd	99.40	91.29	
	Cpx_05	53.80	0.04	0.75	0.12	3.22	0.04	0.11	17.23	24.13	nd	nd	99.45	90.51	
	Cpx_06R	54.31	0.02	1.17	0.08	2.65	0.05	0.09	17.96	23.34	nd	nd	99.68	92.35	
	Cpx_06C	54.20	0.02	1.18	0.07	2.62	0.05	0.09	17.89	23.33	nd	nd	99.46	92.40	
	Cpx_07	53.83	0.04	0.96	0.09	3.17	0.06	0.12	17.32	23.96	nd	nd	99.55	90.70	
	Cpx_08	54.08	0.04	0.93	0.08	2.85	0.06	0.10	17.36	23.95	nd	nd	99.46	91.56	
	Cpx_09	54.39	0.01	0.99	0.05	2.52	0.03	0.09	18.05	23.47	nd	nd	99.61	92.74	
	Cpx_10	54.19	0.06	1.08	0.07	2.87	0.06	0.11	17.60	23.90	nd	nd	99.95	91.61	
	Cpx_11	54.40	0.02	1.09	0.11	2.50	0.05	0.07	17.98	23.58	nd	nd	99.80	92.75	
	Cpx_13	53.45	0.07	1.25	0.11	3.55	0.06	0.11	16.98	23.74	nd	nd	99.31	89.48	
	Cpx_14	53.69	0.06	1.08	0.08	2.80	0.04	0.10	17.35	24.13	nd	nd	99.33	91.71	
	Cpx_15	54.36	0.02	0.93	0.07	2.24	0.04	0.08	18.18	23.57	nd	nd	99.50	93.54	
AVX-16-03-23	Cpx_31	54.29	0.03	0.61	0.07	2.29	0.04	0.08	18.10	24.15	nd	nd	99.66	93.37	

Abbreviations: Cpx = clinopyroxene, R = rim, C = centre, bdl = below detection limit, nd = not determined. *Note:* all oxides are in wt %.

Table A19. *Continued*

Sample	Mineral ID	SiO_2	TiO_2	Al_2O_3	Cr_2O_3	FeO	NiO	MnO	MgO	CaO	Na_2O	K_2O	Total	Mg#	Comment
AVX-16-03-23	Cpx_32	54.78	0.05	0.46	0.08	1.77	0.06	0.05	18.66	24.01	nd	nd	99.92	94.94	
	Cpx_33	54.22	0.02	0.64	0.07	2.11	0.05	0.08	18.30	24.23	nd	nd	99.72	93.93	
	Cpx_34	54.30	0.07	0.76	0.17	1.92	0.07	0.06	18.49	23.88	nd	nd	99.72	94.51	
	Cpx_35	54.37	0.02	0.81	0.07	2.28	0.04	0.07	18.15	24.03	nd	nd	99.86	93.41	
	Cpx_36	54.48	0.04	0.55	0.15	1.97	0.06	0.05	18.45	24.16	nd	nd	99.89	94.35	
	Cpx_37	54.08	0.06	0.75	0.12	2.08	0.06	0.06	18.02	23.76	nd	nd	98.99	93.91	
	Cpx_38	54.36	0.06	0.66	0.15	2.11	0.06	0.06	18.21	23.83	nd	nd	99.49	93.89	
	Cpx_39	54.74	0.02	0.55	0.26	2.26	0.05	0.07	18.28	24.49	nd	nd	100.72	93.51	
	Cpx_40	54.41	0.05	0.55	0.12	1.87	0.07	0.05	18.51	24.03	nd	nd	99.65	94.62	
	Cpx_41	54.85	0.06	0.50	0.05	1.96	0.04	0.06	18.76	23.70	nd	nd	99.97	94.45	
	Cpx_42	54.66	bdl	0.53	0.17	1.99	0.05	0.06	18.57	23.61	nd	nd	99.63	94.33	
	Cpx_43	54.57	0.05	0.52	0.14	1.93	0.07	0.05	18.67	23.61	nd	nd	99.61	94.53	
	Cpx_44	54.22	0.04	0.62	0.04	1.87	0.06	0.05	18.17	24.58	nd	nd	99.64	94.55	
	Cpx_45	54.59	0.04	0.43	0.06	1.81	0.07	0.04	18.52	24.06	nd	nd	99.62	94.80	
	Cpx_61	54.41	0.01	0.59	0.49	2.27	0.06	0.07	18.20	23.96	nd	nd	100.07	93.45	
AVX-16-03-20	Cpx_71	51.93	0.25	2.61	bdl	5.93	0.03	0.32	15.68	22.91	nd	nd	99.67	82.50	
	Cpx_77	51.74	0.26	2.75	0.01	6.16	0.02	0.32	15.78	22.54	nd	nd	99.57	82.03	
	Cpx_78	51.24	0.33	2.92	0.01	6.41	0.01	0.30	15.85	21.80	nd	nd	98.85	81.51	
	Cpx_79	50.77	0.35	3.26	bdl	6.49	0.01	0.29	15.13	22.71	nd	nd	99.01	80.59	
	Cpx_81	50.98	0.35	3.03	0.01	6.68	0.02	0.34	15.29	22.46	nd	nd	99.16	80.32	
	Cpx_91	53.35	0.01	1.57	0.57	2.45	0.05	0.08	17.80	23.77	nd	nd	99.65	92.83	
AVX-16-03-02	Cpx_01	55.29	0.02	0.88	0.31	2.38	0.07	0.06	18.54	23.73	0.16	nd	101.43	93.27	
	Cpx_01	54.38	0.01	1.63	0.67	2.40	0.08	0.06	17.89	23.88	0.20	nd	101.19	93.01	
	Cpx_02	54.61	0.01	1.41	0.58	2.63	0.07	0.07	18.24	23.44	0.27	nd	101.33	92.51	
	Cpx_03	54.47	0.04	1.80	0.77	2.79	0.05	0.09	17.80	23.33	0.31	nd	101.44	91.92	
	Cpx_03	54.42	0.03	1.72	0.74	2.86	0.04	0.09	17.86	23.16	0.31	nd	101.24	91.75	
	Cpx_04	54.36	0.02	1.68	0.82	2.44	0.06	0.05	17.69	23.94	0.21	nd	101.28	92.82	
	Cpx_05	54.38	0.04	1.81	0.66	2.63	0.06	0.08	17.79	23.63	0.23	nd	101.31	92.35	

Abbreviations: Cpx = clinopyroxene, bdl = below detection limit, nd = not determined. *Note:* all oxides are in wt %.

Table A19. *Continued*

Sample	Mineral ID	SiO_2	TiO_2	Al_2O_3	Cr_2O_3	FeO	NiO	MnO	MgO	CaO	Na_2O	K_2O	Total	Mg#	Comment
AVX-16-03-02	Cpx_06	54.59	0.02	1.39	0.70	2.76	0.06	0.09	17.95	23.28	0.30	nd	101.14	92.07	
	Cpx_07	54.23	0.02	1.70	0.73	2.69	0.05	0.08	17.94	23.42	0.23	nd	101.09	92.25	
	Cpx_08	55.06	0.02	0.75	0.89	1.93	0.06	0.06	18.57	23.60	0.24	nd	101.18	94.50	
	Cpx_08	54.62	0.04	1.26	0.48	2.13	0.05	0.08	17.99	24.37	0.13	nd	101.14	93.76	
	Cpx_09	54.45	0.03	1.16	0.59	3.23	0.05	0.10	18.02	23.26	0.09	nd	100.98	90.86	
	Cpx_10	54.66	0.03	1.24	0.46	2.25	0.04	0.08	18.01	24.32	0.15	nd	101.23	93.46	
	Cpx_11	55.60	0.01	0.62	0.61	1.93	0.06	0.05	19.05	23.29	0.24	nd	101.46	94.62	
	Cpx_11	55.79	0.03	0.48	0.39	1.85	0.05	0.06	19.22	23.62	0.16	nd	101.67	94.87	
	Cpx_12	54.52	0.03	1.01	0.30	2.36	0.06	0.08	17.89	24.70	0.13	nd	101.07	93.12	
	Cpx_13	54.35	0.03	1.42	0.49	2.45	0.05	0.08	17.61	24.60	0.12	nd	101.19	92.75	
	Cpx_14	54.69	0.02	1.02	0.24	2.31	0.05	0.08	17.75	25.01	0.09	nd	101.25	93.20	
	Cpx_15	54.72	0.04	1.15	0.38	2.64	0.07	0.08	18.12	23.33	0.31	nd	100.83	92.45	
	Cpx_16	55.15	0.04	0.68	0.63	2.08	0.05	0.06	18.69	23.62	0.21	nd	101.21	94.13	
	Cpx_16	55.38	0.03	0.54	0.46	1.85	0.06	0.06	18.87	23.88	0.15	nd	101.27	94.79	
	Cpx_17	55.29	0.02	0.55	0.10	2.36	0.06	0.08	18.17	24.72	0.08	nd	101.42	93.20	
	Cpx_18	54.60	0.04	1.32	0.44	2.17	0.05	0.07	17.92	24.73	0.11	nd	101.44	93.64	
	Cpx_19	54.70	0.02	1.36	0.41	2.17	0.05	0.09	17.74	24.72	0.10	nd	101.34	93.58	
	Cpx_20	55.37	0.02	0.96	0.54	2.16	0.06	0.05	18.52	23.81	0.16	nd	101.64	93.87	
	Cpx_21	54.43	0.03	1.45	0.49	2.73	0.05	0.08	17.98	23.27	0.27	nd	100.76	92.15	
	Cpx_22	55.29	0.02	0.71	0.19	1.90	0.03	0.07	17.96	25.22	0.05	nd	101.43	94.40	
AVX-16-03-07	Cpx_23	54.07	0.03	1.87	0.91	2.16	0.05	0.07	17.35	24.57	0.17	nd	101.24	93.48	
	Cpx_24	54.62	0.03	1.40	0.33	2.57	0.04	0.07	17.86	24.24	0.12	nd	101.28	92.53	
	Cpx_24	53.80	0.08	2.15	0.75	2.75	0.08	0.08	17.60	23.29	0.28	nd	100.86	91.94	
	Cpx_25	53.98	0.08	2.21	0.77	2.66	0.06	0.07	17.69	23.43	0.27	nd	101.21	92.22	
	Cpx_26	54.65	0.05	1.58	0.53	2.25	0.05	0.06	17.88	24.00	0.17	nd	101.21	93.40	
	Cpx_27	55.45	0.02	0.71	0.43	2.10	0.02	0.06	18.21	24.21	0.17	nd	101.40	93.93	
	Cpx_28	55.04	0.02	1.00	0.48	2.12	0.05	0.06	18.04	24.16	0.22	nd	101.18	93.81	
	Cpx_29	53.84	0.03	1.93	0.55	2.55	0.04	0.08	17.70	24.24	0.11	nd	101.05	92.53	
	Cpx_29	54.01	0.04	1.93	0.58	2.51	0.02	0.07	17.62	24.19	0.15	nd	101.11	92.61	

Abbreviations: Cpx = clinopyroxene, bdl = below detection limit, nd = not determined. *Note:* all oxides are in wt %.

Table A19. *Continued*

Sample	Mineral ID	SiO_2	TiO_2	Al_2O_3	Cr_2O_3	FeO	NiO	MnO	MgO	CaO	Na_2O	K_2O	Total	Mg#	Comment
AVX-16-03-07	Cpx_30	54.69	0.04	1.32	0.47	2.46	0.02	0.07	18.22	24.27	0.09	nd	101.66	92.96	
	Cpx_31	54.39	0.05	1.50	0.75	2.08	0.04	0.08	17.47	24.57	0.16	nd	101.09	93.73	
	Cpx_32	54.86	0.02	0.98	0.40	2.10	0.04	0.06	18.13	24.26	0.14	nd	101.00	93.89	
	Cpx_33	54.18	0.04	1.65	0.53	2.42	0.03	0.06	17.69	24.21	0.14	nd	100.94	92.88	
	Cpx_34	53.63	0.11	2.27	0.86	2.57	0.06	0.07	17.63	23.28	0.27	nd	100.75	92.45	
	Cpx_35	54.22	0.07	2.00	0.51	2.27	0.06	0.08	17.12	24.46	0.15	nd	100.94	93.07	
	Cpx_35	53.71	0.08	2.14	0.53	2.25	0.05	0.09	17.05	24.45	0.14	nd	100.49	93.10	
	Cpx_36	54.25	0.03	1.65	0.55	2.57	0.09	0.07	17.46	23.79	0.15	nd	100.62	92.37	
	Cpx_36	54.18	0.01	1.86	0.53	2.77	0.05	0.07	17.71	23.47	0.23	nd	100.89	91.92	
	Cpx_37	54.22	0.03	1.54	0.60	2.42	0.03	0.09	17.76	24.33	0.06	nd	101.08	92.90	
	Cpx_38	53.84	0.04	2.07	0.73	2.91	0.06	0.09	17.65	23.34	0.23	nd	100.97	91.53	
	Cpx_38	53.52	0.05	2.35	0.80	2.89	0.05	0.09	17.43	23.24	0.25	nd	100.67	91.49	
	Cpx_39	53.18	0.04	2.09	0.72	2.92	0.04	0.09	17.48	23.15	0.25	nd	99.95	91.42	
	Cpx_39	54.68	0.01	0.96	0.46	2.24	0.05	0.08	18.16	24.49	0.06	nd	101.19	93.52	
AVX-16-03-10	Cpx_01	53.41	0.01	1.06	0.47	2.22	0.04	0.06	18.48	24.45	nd	nd	100.21	93.69	
	Cpx_02	54.06	0.01	1.07	0.37	2.32	0.07	0.07	18.52	24.27	nd	nd	100.76	93.43	
	Cpx_03	53.36	0.01	1.38	0.38	2.31	0.04	0.08	18.40	24.36	nd	nd	100.31	93.42	
	Cpx_04	52.49	0.03	2.34	0.97	2.09	0.04	0.08	17.80	24.61	nd	nd	100.44	93.83	
	Cpx_05	51.40	0.05	3.49	0.82	2.89	0.05	0.08	17.45	23.70	nd	nd	99.93	91.50	
	Cpx_06	53.69	0.02	1.21	0.40	2.41	0.06	0.08	18.52	24.13	nd	nd	100.52	93.21	
BAK-16-22-04	Cpx_01	51.72	0.33	3.48	0.66	3.84	0.02	0.12	16.25	23.27	nd	nd	99.70	88.29	
	Cpx_01	51.53	0.38	3.48	0.71	3.86	0.04	0.11	16.09	23.04	nd	nd	99.25	88.12	
	Cpx_02	50.67	0.47	5.18	0.68	5.36	0.05	0.14	16.79	19.48	nd	nd	98.82	84.80	
	Cpx_02	48.85	0.72	5.25	1.03	4.96	0.03	0.13	15.84	21.99	nd	nd	98.80	85.05	
	Cpx_03	51.01	0.47	3.82	0.78	3.84	0.02	0.09	15.91	23.35	nd	nd	99.29	88.08	
	Cpx_04	51.91	0.32	3.23	0.44	3.92	0.04	0.11	16.35	23.02	nd	nd	99.33	88.15	
	Cpx_05	51.73	0.32	3.15	0.43	3.75	0.04	0.11	16.19	23.24	nd	nd	98.94	88.51	
	Cpx_06	51.60	0.32	3.17	0.45	3.69	0.03	0.12	16.44	23.28	nd	nd	99.10	88.80	
	Cpx_06	51.90	0.32	3.19	0.40	3.83	0.03	0.11	16.41	23.19	nd	nd	99.38	88.42	

Abbreviations: Cpx = clinopyroxene, bdl = below detection limit, nd = not determined. *Note:* all oxides are in wt %.

Table A19. *Continued*

Sample	Mineral ID	SiO_2	TiO_2	Al_2O_3	Cr_2O_3	FeO	NiO	MnO	MgO	CaO	Na_2O	K_2O	Total	Mg#	Comment
BAK-16-22-04	Cpx_07	51.57	0.36	3.51	0.73	3.89	0.03	0.12	16.18	22.96	nd	nd	99.36	88.10	
	Cpx_08	51.97	0.34	3.25	0.45	3.92	0.04	0.13	16.33	23.14	nd	nd	99.56	88.12	
	Cpx_09	51.84	0.33	3.16	0.47	3.95	0.04	0.13	16.45	23.15	nd	nd	99.50	88.13	
	Cpx_10	51.44	0.34	3.49	0.60	3.84	0.04	0.12	16.19	23.12	nd	nd	99.18	88.24	
	Cpx_11	47.36	0.95	6.55	1.11	4.38	0.04	0.08	15.47	21.97	nd	nd	97.92	86.28	
	Cpx_12	48.85	0.67	5.39	1.04	4.81	0.04	0.09	16.06	22.19	nd	nd	99.14	85.61	contains spl exsolutions
	Cpx_13	51.12	0.38	3.78	0.75	3.92	0.04	0.11	15.90	22.95	nd	nd	98.94	87.85	contains spl exsolutions
	Cpx_14	51.90	0.29	3.19	0.54	3.75	0.03	0.10	16.08	23.16	nd	nd	99.04	88.43	contains spl exsolutions
BAK-16-22-01B	Cpx_01	51.80	0.28	4.03	0.86	4.07	0.02	0.13	15.79	22.59	0.58	bdl	100.15	87.37	
	Cpx_02	51.94	0.27	3.64	0.54	4.18	0.01	0.12	16.48	22.44	0.54	bdl	100.16	87.54	
	Cpx_02	51.31	0.33	4.62	1.02	4.19	0.02	0.12	15.61	22.62	0.60	bdl	100.43	86.93	
	Cpx_02	51.93	0.20	3.83	0.85	4.22	0.01	0.11	16.00	22.48	0.62	bdl	100.26	87.12	
	Cpx_03	50.74	0.38	5.08	0.88	4.29	0.02	0.11	15.30	22.56	0.61	bdl	99.97	86.40	
	Cpx_04	51.25	0.30	4.42	0.99	4.20	0.02	0.13	15.77	22.59	0.59	bdl	100.25	87.01	
	Cpx_05	51.64	0.26	4.01	0.88	4.11	0.02	0.13	15.84	22.65	0.57	bdl	100.11	87.28	
	Cpx_06	51.81	0.21	3.79	1.14	3.99	0.03	0.13	15.83	22.52	0.63	bdl	100.07	87.62	
	Cpx_07	52.09	0.26	3.86	0.55	4.26	0.01	0.10	16.14	22.70	0.53	bdl	100.50	87.10	
	Cpx_07	51.11	0.33	4.61	1.06	4.19	0.01	0.13	15.53	22.57	0.56	bdl	100.11	86.84	
	Cpx_08	51.03	0.35	4.83	0.98	4.31	0.02	0.12	15.41	22.66	0.56	bdl	100.27	86.43	
	Cpx_09	52.08	0.32	4.27	0.55	4.40	0.01	0.13	16.12	22.43	0.52	bdl	100.83	86.73	
	Cpx_09	51.74	0.33	4.35	0.62	4.28	0.01	0.11	15.96	22.79	0.51	bdl	100.71	86.91	
	Cpx_10	52.05	0.28	3.88	0.46	4.35	bdl	0.13	16.29	22.72	0.50	bdl	100.66	86.98	
	Cpx_10	50.84	0.37	4.77	1.03	4.29	0.03	0.12	15.51	22.73	0.54	bdl	100.23	86.57	
BAK-16-22-01A	Cpx_11	50.38	0.43	6.11	0.36	5.90	0.04	0.18	14.09	21.22	1.11	bdl	99.83	80.96	
	Cpx_11	50.40	0.39	5.85	0.38	5.07	0.02	0.15	15.18	21.77	0.68	bdl	99.89	84.21	
	Cpx_12	50.12	0.42	6.05	0.39	5.91	0.02	0.14	14.70	21.17	0.91	bdl	99.83	81.59	
	Cpx_12	50.29	0.42	5.97	0.39	5.14	0.01	0.12	15.12	21.84	0.73	bdl	100.03	83.98	
	Cpx_13	50.42	0.40	5.88	0.40	5.02	0.03	0.12	15.06	21.86	0.69	bdl	99.86	84.25	
	Cpx_14	50.69	0.35	5.87	0.41	5.65	0.03	0.15	14.57	21.26	0.99	bdl	99.98	82.13	

Abbreviations: Cpx = clinopyroxene, bdl = below detection limit, nd = not determined. *Note:* all oxides are in wt %.

Table A19. *Continued*

Sample	Mineral ID	SiO_2	TiO_2	Al_2O_3	Cr_2O_3	FeO	NiO	MnO	MgO	CaO	Na_2O	K_2O	Total	Mg#	Comment
BAK-16-22-01A	Cpx_15	50.50	0.39	5.82	0.33	5.05	0.01	0.13	15.06	21.78	0.74	bdl	99.81	84.16	
	Cpx_16	50.28	0.40	5.88	0.38	4.96	0.01	0.14	15.16	21.85	0.68	bdl	99.76	84.47	
	Cpx_17	50.42	0.39	6.01	0.40	5.40	0.02	0.16	14.66	21.37	0.92	bdl	99.74	82.87	
	Cpx_18	50.33	0.38	5.89	0.39	5.05	0.01	0.15	15.26	21.78	0.66	bdl	99.90	84.33	
	Cpx_19	49.75	0.41	6.14	0.40	5.10	0.01	0.15	15.49	21.74	0.64	bdl	99.84	84.39	
	Cpx_20	50.36	0.39	5.80	0.36	6.86	0.02	0.24	13.37	21.05	1.24	bdl	99.69	77.66	
BAK-16-22-05	Cpx_21	50.05	0.42	5.93	0.34	5.09	0.01	0.15	15.12	21.96	0.62	bdl	99.69	84.10	
	Cpx_21	50.04	0.42	6.05	0.38	5.06	bdl	0.13	15.16	21.87	0.63	bdl	99.75	84.22	
	Cpx_22	50.08	0.39	5.90	0.39	5.23	bdl	0.15	15.08	21.88	0.60	bdl	99.69	83.71	
	Cpx_22	49.99	0.40	5.88	0.36	5.02	0.02	0.13	15.05	21.99	0.61	bdl	99.46	84.22	
	Cpx_23	50.31	0.40	5.82	0.38	5.17	0.01	0.14	15.26	22.00	0.59	bdl	100.08	84.02	
	Cpx_23	49.89	0.42	5.99	0.38	5.05	bdl	0.14	14.94	21.79	0.62	bdl	99.23	84.05	
	Cpx_24	49.80	0.42	6.09	0.34	5.06	0.02	0.14	15.07	21.73	0.65	bdl	99.35	84.14	
	Cpx_25	50.05	0.41	5.99	0.38	5.02	0.01	0.14	15.03	21.87	0.64	bdl	99.55	84.21	
	Cpx_26	50.62	0.38	5.61	0.38	4.95	0.01	0.14	15.12	22.05	0.70	bdl	99.97	84.48	
	Cpx_26	50.32	0.39	5.64	0.35	5.10	0.01	0.14	15.17	21.92	0.62	bdl	99.67	84.14	
	Cpx_27	50.32	0.41	5.87	0.38	5.07	0.02	0.13	15.19	22.02	0.63	bdl	100.04	84.23	
	Cpx_27	50.40	0.41	6.03	0.36	5.04	bdl	0.14	15.26	21.79	0.65	bdl	100.08	84.37	
	Cpx_28	50.20	0.40	5.98	0.38	5.03	bdl	0.13	15.16	21.85	0.65	bdl	99.78	84.31	
	Cpx_29	50.16	0.40	5.84	0.38	4.97	0.03	0.13	15.05	21.98	0.63	bdl	99.57	84.37	
	Cpx_30	50.75	0.36	6.07	0.37	5.53	0.02	0.15	14.39	20.88	1.12	0.01	99.66	82.27	
	Cpx_30	50.43	0.38	5.79	0.41	4.90	bdl	0.14	15.08	22.04	0.67	bdl	99.85	84.57	
	Cpx_31	50.37	0.38	5.77	0.37	5.11	0.01	0.14	15.26	21.84	0.65	0.01	99.92	84.18	
	Cpx_32	50.20	0.40	5.83	0.37	5.08	0.01	0.13	15.10	22.10	0.61	bdl	99.83	84.12	
	Cpx_33	50.34	0.37	5.61	0.36	4.98	0.01	0.14	15.28	21.92	0.65	bdl	99.65	84.54	

Abbreviations: Cpx = clinopyroxene, bdl = below detection limit, nd = not determined. *Note:* all oxides are in wt %.

Table A19. *Continued*

Sample	Mineral ID	SiO_2	TiO_2	Al_2O_3	Cr_2O_3	FeO	NiO	MnO	MgO	CaO	Na_2O	K_2O	Total	Mg#	Comment
BAK-16-22-09	Cpx_33	50.13	1.61	3.06	0.07	7.66	bdl	0.21	14.32	22.16	0.55	bdl	99.77	76.91	contains opx and spl exsolutions
	Cpx_33	51.02	0.31	4.54	0.89	4.01	0.02	0.12	16.04	22.45	0.62	bdl	100.03	87.69	contains opx and spl exsolutions
	Cpx_33	51.07	0.32	4.45	0.83	4.05	0.02	0.13	16.14	22.51	0.58	0.01	100.09	87.65	contains opx and spl exsolutions
	Cpx_34	51.16	0.31	4.66	0.94	4.02	0.01	0.11	16.04	22.37	0.65	bdl	100.28	87.68	
	Cpx_35	51.19	0.31	4.64	0.93	3.95	0.01	0.11	16.04	22.35	0.66	bdl	100.19	87.85	contains spl exsolutions
	Cpx_36	51.53	0.28	4.17	0.64	4.03	0.02	0.12	16.46	22.52	0.55	bdl	100.34	87.91	
	Cpx_36	51.49	0.28	4.20	0.80	3.94	0.04	0.11	16.22	22.49	0.62	bdl	100.19	88.02	
	Cpx_37	51.51	0.30	4.28	0.71	4.11	0.01	0.12	16.34	22.30	0.58	0.01	100.27	87.63	contains spl and opx exsolutions
	Cpx_37	51.39	0.30	4.21	0.69	4.07	0.02	0.11	16.41	22.44	0.57	bdl	100.21	87.79	

Abbreviations: Cpx = clinopyroxene, bdl = below detection limit, nd = not determined. *Note:* all oxides are in wt %.

Table A19. *Continued*

Sample	Mineral ID	SiO_2	TiO_2	Al_2O_3	Cr_2O_3	FeO	NiO	MnO	MgO	CaO	Na_2O	K_2O	Total	Mg#	Comment
BAK-16-22-09	Cpx_37	51.47	0.25	3.95	0.92	3.95	0.01	0.13	16.44	22.28	0.58	bdl	99.98	88.11	
	Cpx_38	50.81	0.33	4.70	0.91	4.12	0.01	0.11	16.02	22.39	0.60	bdl	100.01	87.38	
	Cpx_39	51.36	0.28	4.31	0.82	3.94	0.02	0.12	16.22	22.33	0.62	bdl	100.02	88.00	contains spl exsolutions
	Cpx_40	50.97	0.31	4.54	0.97	3.97	0.03	0.11	16.09	22.40	0.63	bdl	100.02	87.83	contains spl exsolutions
	Cpx_41	50.96	0.30	4.57	0.97	3.96	0.02	0.11	16.13	22.41	0.62	bdl	100.04	87.89	contains opx and spl exsolutions
	Cpx_42	51.01	0.31	4.66	0.95	4.01	0.02	0.12	16.06	22.48	0.66	bdl	100.27	87.70	contains spl exsolutions
	Cpx_44	50.97	0.30	4.58	0.83	3.96	0.04	0.11	16.07	22.34	0.62	bdl	99.83	87.84	contains spl exsolutions
	Cpx_45	51.19	0.30	4.52	0.85	4.06	0.02	0.12	16.19	22.24	0.65	bdl	100.15	87.66	host rock contact and contains spl exsolutions
	Cpx_45	51.20	0.31	4.44	0.87	4.01	0.01	0.13	16.20	22.35	0.65	bdl	100.18	87.81	
	Cpx_47	51.01	0.30	4.36	0.72	4.06	0.02	0.12	16.29	22.27	0.59	bdl	99.74	87.73	contains opx and spl exsolutions

Abbreviations: Cpx = clinopyroxene, bdl = below detection limit, nd = not determined. *Note:* all oxides are in wt %.

Table A19. *Continued*

Sample	Mineral ID	SiO_2	TiO_2	Al_2O_3	Cr_2O_3	FeO	NiO	MnO	MgO	CaO	Na_2O	K_2O	Total	Mg#	Comment
BAK-16-22-03	Cpx_01	51.33	0.30	4.32	0.93	4.26	0.02	0.12	15.74	22.98	0.58	bdl	100.58	86.81	
	Cpx_02	51.18	0.33	4.54	0.70	4.35	0.02	0.12	15.69	22.89	0.52	bdl	100.33	86.54	
	Cpx_03	51.50	0.31	4.34	0.86	4.31	bdl	0.13	15.63	22.72	0.58	0.01	100.39	86.61	
	Cpx_04	48.91	1.09	5.14	0.75	6.60	bdl	0.14	14.42	22.42	0.44	bdl	99.92	79.55	
	Cpx_04	51.57	0.26	4.12	0.96	4.26	0.01	0.10	15.73	22.86	0.55	bdl	100.41	86.82	
	Cpx_05	51.36	0.33	4.38	0.75	4.34	0.02	0.12	15.71	22.98	0.55	bdl	100.54	86.59	
	Cpx_06	51.07	0.36	4.75	0.65	4.29	0.03	0.11	15.51	22.98	0.51	bdl	100.27	86.57	
	Cpx_07	50.84	0.36	4.98	0.69	4.43	0.03	0.11	15.44	22.93	0.52	bdl	100.33	86.14	
	Cpx_08	51.29	0.33	4.62	0.66	4.41	bdl	0.12	15.58	22.85	0.52	bdl	100.37	86.30	
	Cpx_09	50.67	0.41	5.33	0.68	4.50	0.05	0.11	15.21	22.82	0.54	bdl	100.33	85.75	
	Cpx_10	51.68	0.23	3.85	0.80	4.10	0.04	0.12	16.00	22.82	0.54	bdl	100.18	87.43	
	Cpx_11	51.91	0.27	3.94	0.72	4.25	0.01	0.12	15.74	22.75	0.54	bdl	100.26	86.85	
	Cpx_12	51.47	0.29	4.44	0.75	4.39	0.02	0.11	15.57	22.83	0.51	bdl	100.40	86.33	
	Cpx_13	51.34	0.31	4.63	0.79	4.34	0.04	0.12	15.39	22.61	0.56	bdl	100.13	86.34	
	Cpx_14	51.48	0.29	4.28	0.80	4.30	0.01	0.12	15.62	22.68	0.54	bdl	100.11	86.61	
BAK-16-22-32	Cpx_15	49.76	0.60	5.91	0.16	6.12	0.01	0.14	14.58	21.79	0.69	bdl	99.77	80.94	
	Cpx_15	49.72	0.62	5.97	0.20	6.07	0.08	0.15	14.55	21.66	0.70	0.01	99.74	81.02	
	Cpx_16	49.74	0.63	6.14	0.15	6.19	0.04	0.15	14.48	21.70	0.70	bdl	99.90	80.65	
	Cpx_16	49.53	0.64	6.15	0.22	6.14	0.10	0.15	14.45	21.64	0.72	bdl	99.73	80.76	
	Cpx_17	49.77	0.63	6.15	0.13	6.11	bdl	0.16	14.46	21.69	0.71	bdl	99.81	80.84	
	Cpx_18	49.43	0.65	6.39	0.09	6.16	0.01	0.15	14.39	21.75	0.69	bdl	99.73	80.62	
	Cpx_18	49.45	0.65	6.45	0.09	6.20	0.04	0.14	14.41	21.58	0.71	bdl	99.72	80.55	
	Cpx_18	49.16	0.68	6.67	0.12	6.15	bdl	0.16	14.19	21.58	0.70	bdl	99.42	80.44	
	Cpx_18	49.61	0.63	6.52	0.10	6.28	0.02	0.16	14.46	21.46	0.71	bdl	99.96	80.40	
	Cpx_18	49.50	0.64	6.54	0.11	6.19	0.03	0.14	14.36	21.69	0.73	bdl	99.92	80.53	
	Cpx_18	49.36	0.65	6.77	0.10	6.18	0.04	0.15	14.15	21.51	0.73	bdl	99.64	80.31	
	Cpx_19	49.68	0.65	6.33	0.10	6.17	0.04	0.14	14.38	21.58	0.71	bdl	99.79	80.59	
	Cpx_20	49.51	0.64	6.20	0.08	6.17	0.05	0.14	14.52	21.68	0.70	bdl	99.70	80.75	
	Cpx_21	49.77	0.63	6.08	0.11	6.12	bdl	0.15	14.50	21.54	0.69	bdl	99.58	80.86	

Abbreviations: Cpx = clinopyroxene, bdl = below detection limit, nd = not determined. *Note:* all oxides are in wt %.

Table A19. *Continued*

Sample	Mineral ID	SiO_2	TiO_2	Al_2O_3	Cr_2O_3	FeO	NiO	MnO	MgO	CaO	Na_2O	K_2O	Total	Mg#	Comment
BAK-16-22-32	Cpx_22	50.22	0.59	5.32	0.20	5.95	0.02	0.13	14.86	21.84	0.63	bdl	99.76	81.64	
	Cpx_23	49.78	0.61	6.01	0.14	6.12	0.02	0.16	14.57	21.68	0.69	bdl	99.78	80.92	
	Cpx_24	49.93	0.63	6.16	0.15	5.96	0.01	0.16	14.37	21.53	0.69	bdl	99.59	81.12	
	Cpx_24	49.47	0.67	6.31	0.13	6.03	bdl	0.14	14.34	21.75	0.67	bdl	99.50	80.91	
	Cpx_24	49.65	0.62	6.12	0.39	6.08	0.02	0.14	14.37	21.54	0.73	bdl	99.66	80.82	
BAK-16-22-42	Cpx_25	51.55	0.40	4.99	0.48	4.89	0.05	0.14	15.38	22.00	0.67	bdl	100.54	84.86	
	Cpx_25	51.53	0.38	4.98	0.50	4.85	0.01	0.13	15.33	21.98	0.65	bdl	100.34	84.93	
	Cpx_25	51.55	0.35	4.88	0.59	4.75	0.06	0.14	15.43	22.09	0.67	bdl	100.51	85.26	
	Cpx_25	51.56	0.37	5.00	0.44	4.80	0.03	0.13	15.55	22.14	0.61	bdl	100.62	85.22	
	Cpx_26	51.35	0.34	4.73	0.56	4.77	0.03	0.13	15.41	21.89	0.65	bdl	99.85	85.20	
	Cpx_27	51.30	0.37	4.93	0.46	4.74	0.06	0.13	15.50	22.10	0.62	bdl	100.20	85.34	
	Cpx_28	51.13	0.38	4.96	0.51	4.80	0.01	0.13	15.45	22.07	0.63	bdl	100.08	85.15	
	Cpx_29	51.51	0.36	4.86	0.46	4.69	0.04	0.13	15.50	22.16	0.64	bdl	100.36	85.47	
	Cpx_30	51.28	0.35	4.85	0.45	4.83	bdl	0.14	15.63	21.95	0.62	bdl	100.10	85.21	
	Cpx_30	51.42	0.35	4.94	0.42	4.71	0.05	0.13	15.55	22.02	0.63	bdl	100.21	85.48	
	Cpx_31	51.54	0.38	4.89	0.50	4.78	0.01	0.13	15.49	21.96	0.61	bdl	100.29	85.25	
	Cpx_32	51.48	0.40	5.04	0.48	4.74	0.06	0.13	15.41	21.88	0.67	bdl	100.30	85.27	
	Cpx_33	51.43	0.38	4.89	0.48	4.83	0.04	0.12	15.51	21.92	0.65	bdl	100.25	85.13	
	Cpx_33	51.19	0.39	4.99	0.47	4.76	bdl	0.13	15.38	21.94	0.63	bdl	99.88	85.19	
	Cpx_34	51.29	0.40	4.95	0.49	4.80	bdl	0.14	15.43	22.00	0.69	bdl	100.19	85.15	
	Cpx_35	51.30	0.39	5.02	0.50	4.78	0.04	0.12	15.38	21.91	0.63	bdl	100.08	85.16	
	Cpx_36	51.27	0.37	4.96	0.50	4.80	bdl	0.14	15.45	21.84	0.70	bdl	100.02	85.16	
	Cpx_37	51.29	0.41	5.02	0.48	4.73	0.01	0.14	15.43	22.08	0.67	bdl	100.27	85.32	
	Cpx_38	51.25	0.39	5.08	0.49	4.80	bdl	0.13	15.39	21.97	0.64	bdl	100.15	85.10	
	Cpx_39	51.04	0.38	5.05	0.50	4.81	0.05	0.12	15.49	22.06	0.66	bdl	100.16	85.16	
	Cpx_40	51.13	0.38	4.97	0.48	4.73	bdl	0.13	15.34	22.13	0.62	bdl	99.92	85.26	
	Cpx_41	51.29	0.38	5.05	0.51	4.81	0.02	0.13	15.44	22.02	0.64	bdl	100.28	85.13	
	Cpx_42	51.12	0.38	5.04	0.47	4.67	bdl	0.13	15.51	22.21	0.64	bdl	100.18	85.56	
	Cpx_43	51.29	0.39	4.99	0.44	4.68	0.05	0.13	15.52	22.11	0.68	bdl	100.29	85.52	

Abbreviations: Cpx = clinopyroxene, bdl = below detection limit, nd = not determined. *Note:* all oxides are in wt %.

Table A19. *Continued*

Sample	Mineral ID	SiO_2	TiO_2	Al_2O_3	Cr_2O_3	FeO	NiO	MnO	MgO	CaO	Na_2O	K_2O	Total	Mg#	Comment
BAK-16-22-42	Cpx_44	51.15	0.38	5.02	0.46	4.72	0.02	0.12	15.43	22.05	0.66	bdl	100.00	85.35	
	Cpx_45	51.20	0.39	4.93	0.47	4.77	0.01	0.13	15.47	22.09	0.67	bdl	100.13	85.26	
	Cpx_45	51.04	0.41	5.23	0.47	4.75	0.03	0.13	15.38	22.01	0.66	bdl	100.10	85.23	
	Cpx_45	51.24	0.38	5.07	0.50	4.76	0.06	0.14	15.42	21.97	0.66	bdl	100.19	85.24	
	Cpx_45	51.26	0.39	5.04	0.48	4.75	0.04	0.12	15.43	21.81	0.64	bdl	99.95	85.27	
	Cpx_45	51.44	1.53	2.30	0.04	6.74	0.04	0.23	14.68	22.19	0.82	0.01	100.01	79.51	

Abbreviations: Cpx = clinopyroxene, bdl = below detection limit, nd = not determined. *Note:* all oxides are in wt %.

Table A20. *Major and minor element compositions of amphibole in Shiveluch and Avachinsky mantle xenoliths*

Sample	Mineral ID	SiO_2	TiO_2	Al_2O_3	Cr_2O_3	FeO	NiO	MnO	MgO	CaO	Na_2O	K_2O	Total	Mg#	Comment
AVX-16-03-24	Am_01	53.82	0.04	4.76	0.08	2.49	0.08	0.06	23.83	11.70	0.76	0.11	97.73	94.46	
	Am_02	53.62	0.03	5.05	0.12	2.61	0.07	0.06	22.36	11.77	0.93	0.11	96.74	93.84	
	Am_03	53.79	0.04	4.69	0.15	2.49	0.08	0.07	23.01	11.87	0.83	0.11	97.22	94.27	
	Am_04	51.00	0.04	7.41	0.09	2.79	0.15	0.06	21.18	12.14	1.07	0.40	96.33	93.11	
	Am_05	52.13	0.03	6.69	0.33	2.63	0.09	0.04	21.90	11.78	1.02	0.16	96.79	93.70	
	Am_06	50.38	0.03	8.50	0.05	2.99	0.09	0.07	21.25	12.21	1.12	0.39	97.10	92.67	
	Am_07	49.74	0.05	9.19	0.01	3.25	0.05	0.04	20.68	11.80	1.49	0.22	96.55	91.90	
	Am_08	47.16	0.07	12.18	0.03	3.38	0.09	0.07	20.13	11.41	1.94	0.21	96.69	91.40	
	Am_09	50.32	0.04	8.62	0.05	3.05	0.05	0.10	20.85	11.86	1.25	0.30	96.51	92.42	
	Am_11	50.01	0.04	9.04	0.04	3.21	0.08	0.08	20.74	11.98	1.23	0.42	96.97	92.01	
	Am_12	47.97	0.31	10.25	0.39	3.32	0.13	0.06	20.11	12.11	1.74	0.16	96.55	91.53	
	Am_13	47.74	0.04	11.04	0.02	3.82	0.07	0.07	19.74	11.75	1.70	0.31	96.30	90.20	
	Am_14	47.69	0.03	11.28	bdl	4.03	0.07	0.05	19.88	11.69	1.70	0.29	96.71	89.77	
	Am_15	49.55	0.11	8.67	0.15	3.84	0.08	0.07	19.80	11.83	1.22	0.08	95.41	90.17	
	Am_16	48.28	0.03	11.01	0.05	4.01	0.04	0.07	20.69	11.57	1.67	0.26	97.67	90.19	
	Am_18	50.55	0.05	8.18	0.10	3.81	0.05	0.07	21.25	11.79	1.54	0.21	97.64	90.85	

Abbreviations: Am = amphibole. *Note:* all oxides are in wt %.

Table A20. *Continued*

Sample	Mineral ID	SiO_2	TiO_2	Al_2O_3	Cr_2O_3	FeO	NiO	MnO	MgO	CaO	Na_2O	K_2O	Total	Mg#	Comment
AVX-16-03-24	Am_19	49.66	0.03	8.72	0.07	4.07	0.08	0.04	20.36	11.97	1.19	0.42	96.61	89.93	
	Am_21	48.38	0.05	10.04	bdl	4.31	bdl	0.07	19.66	11.63	1.48	0.33	95.95	89.05	
	Am_22	48.44	0.05	10.36	0.09	3.98	0.05	0.04	19.90	11.83	1.68	0.27	96.70	89.90	
	Am_23	47.90	0.04	10.83	0.09	4.09	0.06	0.05	20.57	11.80	1.83	0.26	97.51	89.96	
	Am_26	47.92	0.04	11.01	0.05	4.40	0.06	0.04	20.68	11.71	1.83	0.25	97.98	89.34	
	Am_27	45.95	0.02	12.96	bdl	4.79	0.04	0.08	19.15	11.51	1.91	0.34	96.77	87.69	
	Am_28	47.15	0.06	11.30	0.06	4.41	0.08	0.07	20.06	11.82	1.69	0.41	97.29	89.02	
	Am_30	54.05	0.06	4.68	0.02	2.91	0.08	0.04	22.73	11.69	0.64	0.18	97.09	93.29	
	Am_31	51.54	0.07	7.39	0.02	3.28	0.11	0.08	21.93	11.64	1.13	0.19	97.39	92.25	
	Am_35	50.53	0.08	8.27	0.04	3.41	0.10	0.05	20.19	11.94	1.35	0.09	96.14	91.34	
	Am_36	52.24	0.02	6.61	0.05	3.18	0.08	0.06	21.82	11.61	1.05	0.18	96.98	92.44	
	Am_37	53.69	0.05	5.59	0.07	3.00	0.11	0.07	22.84	11.72	0.93	0.16	98.24	93.14	
	Am_38	50.41	0.05	8.32	0.05	3.42	0.07	0.08	21.07	12.03	1.29	0.23	97.05	91.65	
	Am_39	48.14	0.05	10.63	0.06	3.99	0.05	0.06	20.19	11.72	1.71	0.25	96.86	90.01	
	Am_40	53.64	0.02	5.10	0.05	2.90	0.07	0.04	22.29	11.80	0.83	0.13	96.88	93.21	
	Am_41	55.12	0.02	4.51	0.11	2.86	0.07	0.06	23.21	11.71	0.78	0.10	98.63	93.53	
	Am_42	54.99	0.02	4.11	0.17	2.83	0.09	0.06	23.23	11.82	0.64	0.10	98.15	93.61	
AVX-16-03-20	Am_01	46.78	0.66	10.14	nd	9.02	0.10	0.29	16.54	11.39	1.88	0.10	96.90	76.57	
	Am_02	45.11	0.83	11.37	nd	9.59	0.05	0.23	15.74	11.60	1.98	0.10	96.66	74.51	
	Am_03	46.60	0.61	9.90	nd	8.58	0.11	0.29	16.90	11.21	1.77	0.07	96.06	77.83	
	Am_04	45.18	0.77	11.19	nd	10.27	0.07	0.26	15.70	11.44	2.06	0.10	97.09	73.14	
	Am_05	45.17	0.79	11.23	nd	10.07	0.07	0.23	15.40	11.46	1.97	0.12	96.52	73.15	
	Am_06	46.72	0.70	10.46	nd	9.26	0.09	0.25	16.40	11.60	1.87	0.11	97.50	75.94	
	Am_08	46.03	0.87	11.45	nd	9.08	0.05	0.23	15.97	11.62	1.98	0.10	97.40	75.80	
	Am_09	45.26	0.88	11.36	nd	9.85	0.06	0.30	15.75	11.42	2.23	0.13	97.27	74.03	
	Am_10	46.46	0.81	11.12	nd	9.94	0.06	0.29	15.59	11.40	1.94	0.10	97.76	73.66	
	Am_11	44.47	0.94	12.39	nd	9.01	0.07	0.21	15.83	11.59	2.13	0.12	96.77	75.79	

Abbreviations: Am = amphibole, bdl = below detection limit, nd = not determined. *Note:* all oxides are in wt %.

Table A20. *Continued*

Sample	Mineral ID	SiO_2	TiO_2	Al_2O_3	Cr_2O_3	FeO	NiO	MnO	MgO	CaO	Na_2O	K_2O	Total	Mg#	Comment
AVX-16-03-20	Am_13	44.37	0.84	11.57	nd	9.48	0.06	0.25	15.49	11.59	2.08	0.11	95.85	74.43	
	Am_14	45.48	0.86	10.91	nd	10.01	0.06	0.25	15.77	11.47	1.88	0.11	96.91	73.73	
	Am_17	44.53	0.81	11.62	nd	9.21	0.05	0.21	15.92	11.80	2.20	0.12	96.49	75.49	
	Am_18	44.08	0.94	11.84	nd	9.66	0.04	0.23	15.69	11.53	1.98	0.12	96.11	74.31	
	Am_19	44.33	0.89	11.33	nd	9.99	0.07	0.28	15.69	11.57	2.16	0.11	96.54	73.67	
	Am_20	44.26	0.93	11.88	nd	10.00	0.05	0.22	15.58	11.57	2.12	0.13	96.87	73.51	
	Am_21	43.41	0.93	12.05	nd	10.41	0.05	0.26	15.03	11.47	2.18	0.13	95.97	72.00	
	Am_25	44.73	0.99	12.02	nd	9.60	0.05	0.24	15.52	11.62	2.29	0.12	97.20	74.24	
	Am_26	46.05	0.94	11.42	nd	9.20	0.06	0.23	15.99	11.75	2.13	0.12	97.93	75.60	
	Am_27	44.29	1.01	12.42	nd	9.82	0.05	0.22	15.50	11.60	2.37	0.13	97.41	73.78	
	Am_28	43.96	0.94	11.83	nd	10.38	0.06	0.26	15.09	11.53	2.08	0.12	96.27	72.15	
	Am_29	44.30	0.97	12.14	nd	9.52	0.05	0.21	15.72	11.74	2.30	0.15	97.11	74.65	
	Am_30	47.37	0.78	10.17	nd	9.61	0.09	0.32	16.27	11.26	1.88	0.10	98.02	75.11	
	Am_31	44.88	1.19	11.60	nd	9.79	0.08	0.29	15.63	11.33	2.14	0.12	97.11	73.99	
	Am_32	46.69	0.67	8.96	nd	8.81	0.08	0.26	16.65	11.35	1.89	0.09	95.46	77.11	
	Am_36	45.11	0.98	11.74	nd	8.77	0.07	0.20	16.02	11.52	2.12	0.16	96.82	76.50	
	Am_37	44.64	1.00	12.28	nd	9.89	0.07	0.20	15.47	11.65	2.25	0.13	97.64	73.59	
	Am_38	43.88	0.99	11.67	nd	10.16	0.04	0.26	15.10	11.51	2.20	0.13	96.03	72.58	
	Am_39	43.80	1.05	11.96	nd	9.51	0.05	0.21	15.45	11.59	2.19	0.16	96.03	74.32	
	Am_40	43.85	0.97	12.08	nd	10.21	0.05	0.22	15.11	11.67	2.15	0.13	96.52	72.50	
	Am_42	45.04	0.99	10.83	nd	10.39	0.03	0.28	15.40	11.26	2.07	0.10	96.47	72.55	
	Am_43	43.21	1.19	12.39	nd	10.92	0.04	0.24	14.55	11.56	2.07	0.16	96.34	70.36	
	Am_44	44.53	bdl	11.80	nd	10.48	0.04	0.26	15.07	11.46	2.08	0.13	95.86	71.93	
	Am_45	43.63	1.09	12.30	nd	10.31	0.06	0.24	15.09	11.62	2.35	0.13	96.95	72.29	
	Am_46	43.23	1.04	12.42	nd	9.46	0.03	0.18	15.29	11.62	2.07	0.15	95.50	74.22	
	Am_47	43.34	1.09	12.36	nd	9.84	0.05	0.22	15.23	11.51	2.36	0.16	96.16	73.40	

Abbreviations: Am = amphibole, bdl = below detection limit, nd = not determined. *Note:* all oxides are in wt %.

Table A20. *Continued*

Sample	Mineral ID	SiO_2	TiO_2	Al_2O_3	Cr_2O_3	FeO	NiO	MnO	MgO	CaO	Na_2O	K_2O	Total	Mg#	Comment
AVX-16-03-20	Am_48	44.18	1.06	12.43	nd	9.75	0.06	0.19	15.49	11.58	2.18	0.14	97.15	73.90	
	Am_49	45.40	1.13	11.45	nd	10.37	0.07	0.35	15.16	11.02	2.07	0.15	97.29	72.26	
	Am_50	45.14	1.02	11.66	nd	10.22	0.06	0.28	15.05	11.32	2.06	0.12	97.00	72.41	
AVX-16-03-10	Am_51	44.62	0.78	13.54	nd	7.30	0.07	0.12	17.18	11.33	2.47	0.18	97.59	80.74	
	Am_52	43.80	0.89	13.13	nd	6.82	0.07	0.10	17.34	11.34	2.36	0.15	96.01	81.93	
	Am_53	43.55	0.85	12.56	nd	8.32	0.09	0.13	16.48	11.28	2.30	0.15	95.70	77.93	
	Am_54	43.18	1.05	13.65	nd	8.65	0.06	0.12	15.88	11.51	2.40	0.15	96.66	76.58	
	Am_57	44.55	0.81	12.89	nd	7.74	0.10	0.16	17.10	11.23	2.33	0.16	97.13	79.75	
	Am_60	44.91	0.67	12.90	nd	6.06	0.10	0.09	17.63	11.37	2.32	0.16	96.24	83.82	
	Am_62	43.95	0.05	15.39	nd	5.70	0.14	0.08	17.58	11.36	2.50	0.21	96.96	84.61	
	Am_63	45.48	0.70	13.26	nd	6.45	0.08	0.10	17.56	11.46	2.20	0.14	97.44	82.91	
	Am_64	44.33	0.90	13.13	nd	7.01	0.10	0.09	17.12	11.83	2.40	0.14	97.05	81.32	
	Am_65	42.75	1.22	14.39	nd	7.50	0.10	0.11	16.34	11.62	2.59	0.16	96.77	79.51	
	Am_67	45.36	0.78	12.95	nd	7.12	0.08	0.11	17.06	11.57	2.34	0.16	97.54	81.02	
	Am_68	42.12	1.34	14.82	nd	8.39	0.07	0.12	15.86	11.63	2.51	0.17	97.04	77.11	
	Am_69	43.92	1.04	13.41	nd	7.90	0.07	0.12	16.41	11.44	2.40	0.18	96.98	78.73	
	Am_70	44.51	0.89	13.17	nd	6.99	0.07	0.10	16.98	11.43	2.32	0.16	96.67	81.23	
	Am_71	43.08	1.09	13.68	nd	8.28	0.05	0.12	15.73	11.48	2.38	0.17	96.07	77.20	
	Am_72	43.48	0.99	13.53	nd	7.05	0.07	0.12	16.98	11.52	2.41	0.16	96.32	81.10	
	Am_73	42.50	1.21	13.89	nd	9.72	0.07	0.14	15.06	11.58	2.38	0.14	96.71	73.40	
	Am_74	44.38	0.72	12.80	nd	6.77	0.11	0.11	17.24	11.48	2.36	0.16	96.20	81.94	
	Am_75	44.33	0.71	13.38	nd	6.80	0.06	0.13	17.32	11.25	2.34	0.13	96.47	81.94	
	Am_76	44.66	0.76	12.93	nd	6.41	0.08	0.11	17.69	11.15	2.32	0.15	96.28	83.11	
	Am_80	44.09	0.80	13.07	nd	7.24	0.07	0.11	17.07	11.44	2.32	0.15	96.38	80.78	
	Am_84	43.04	1.21	13.48	nd	8.78	0.09	0.13	15.71	11.52	2.46	0.15	96.62	76.12	
	Am_86	44.09	0.80	13.07	nd	6.99	0.08	0.12	17.46	11.35	2.34	0.17	96.46	81.66	

Abbreviations: Am = amphibole, nd = not determined. *Note:* all oxides are in wt %.

Table A20. *Continued*

Sample	Mineral ID	SiO_2	TiO_2	Al_2O_3	Cr_2O_3	FeO	NiO	MnO	MgO	CaO	Na_2O	K_2O	Total	Mg#	Comment
AVX-16-03-10	Am_87	43.66	0.79	13.04	nd	6.65	0.08	0.10	17.29	11.31	2.32	0.16	95.43	82.24	
	Am_88	42.74	1.17	13.66	nd	8.53	0.09	0.11	15.53	11.80	2.37	0.16	96.18	76.45	
	Am_89	44.51	0.71	12.96	nd	7.78	0.09	0.12	16.71	11.23	2.33	0.14	96.59	79.29	
	Am_90	42.44	1.24	13.61	nd	9.57	0.06	0.14	15.15	11.45	2.42	0.15	96.24	73.84	
	Am_91	47.66	bdl	10.22	nd	3.69	0.13	0.04	19.21	12.08	1.92	0.10	95.12	90.28	
	Am_93	44.21	0.11	15.08	nd	5.63	0.13	0.11	17.75	10.88	2.43	0.26	96.60	84.90	
	Am_94	44.63	0.89	13.01	nd	7.54	0.11	0.18	17.01	11.26	2.46	0.15	97.26	80.09	
	Am_95	44.68	0.66	13.45	nd	6.74	0.14	0.14	17.42	11.23	2.44	0.13	97.11	82.16	
	Am_96	43.90	0.90	12.87	nd	8.11	0.08	0.19	16.46	11.26	2.42	0.15	96.38	78.35	
	Am_97	45.43	0.82	12.25	nd	6.90	0.12	0.16	17.50	11.18	2.25	0.15	96.77	81.88	
	Am_98	43.54	0.13	15.38	nd	5.66	0.14	0.11	17.64	11.08	2.58	0.19	96.56	84.75	
	Am_99	44.49	0.10	14.10	nd	6.06	0.16	0.13	17.86	10.50	2.34	0.21	95.95	84.00	
	Am_100	45.14	0.64	12.22	nd	6.91	0.14	0.15	17.59	11.13	2.41	0.13	96.50	81.94	
SHX-03-04	Am_01	47.28	1.75	7.10	0.03	9.97	0.01	0.20	17.62	10.71	1.68	0.34	96.79	75.90	selvage amphibole
	Am_02	47.18	1.36	8.13	0.03	9.14	0.02	0.23	18.63	10.68	1.90	0.36	97.88	78.41	selvage amphibole
	Am_03	45.04	1.45	8.83	0.01	11.26	0.03	0.22	16.50	10.81	1.82	0.34	96.54	72.31	selvage amphibole
	Am_05	46.49	0.36	10.42	0.03	7.27	0.10	0.15	19.10	11.20	2.04	0.32	97.82	82.39	
	Am_06	51.57	0.25	5.51	0.01	6.78	0.11	0.17	20.53	11.29	1.07	0.18	97.58	84.37	
	Am_07	45.68	0.47	11.32	0.06	7.34	0.14	0.16	18.52	11.19	2.15	0.32	97.46	81.81	
	Am_08	45.31	0.27	11.98	0.01	6.43	0.25	0.10	18.71	11.23	1.98	0.45	96.80	83.83	
	Am_09	45.05	0.12	12.69	0.00	6.56	0.30	0.11	18.68	11.15	2.29	0.34	97.53	83.54	
	Am_10	43.71	0.20	13.51	0.03	6.64	0.20	0.14	18.24	10.82	2.29	0.39	96.25	83.03	
	Am_11	44.59	0.22	12.30	0.01	6.60	0.20	0.10	18.38	11.11	2.28	0.37	96.35	83.23	
	Am_12	43.97	0.24	13.34	0.01	6.30	0.19	0.12	18.70	11.37	2.40	0.49	97.23	84.10	
	Am_13	44.71	0.44	11.96	0.02	6.84	0.13	0.16	18.02	10.89	2.15	0.33	95.68	82.44	
	Am_16	45.81	0.31	9.96	0.00	7.86	0.15	0.17	17.84	11.09	1.74	0.34	95.48	80.17	

Abbreviations: Am = amphibole, bdl = below detection limit, nd = not determined. *Note:* all oxides are in wt %.

***Table A20**. Continued*

Sample	Mineral ID	SiO_2	TiO_2	Al_2O_3	Cr_2O_3	FeO	NiO	MnO	MgO	CaO	Na_2O	K_2O	Total	Mg#	Comment
SHX-03-04	Am_17	44.03	0.53	11.87	0.57	6.79	0.13	0.16	18.17	11.14	2.22	0.40	96.31	82.67	
	Am_18	44.12	0.58	12.76	0.11	7.79	0.16	0.16	18.09	11.06	2.40	0.36	97.79	80.53	
	Am_19	43.76	1.11	11.39	0.01	9.34	0.11	0.18	17.15	11.27	2.21	0.41	97.07	76.59	
	Am_21	43.88	0.71	11.47	0.04	9.66	0.13	0.21	16.88	10.81	2.10	0.41	96.41	75.70	
	Am_22	44.21	1.49	10.26	0.05	10.81	0.12	0.20	16.21	10.91	2.09	0.42	96.93	72.77	
	Am_23	43.23	0.67	12.41	0.68	7.85	0.14	0.18	17.66	10.58	2.36	0.34	96.44	80.03	
	Am_24	43.04	0.82	11.75	0.01	10.35	0.15	0.15	16.52	10.91	2.03	0.48	96.38	73.99	
	Am_25	44.83	0.62	11.20	0.11	8.89	0.20	0.21	17.51	10.99	2.21	0.38	97.32	77.84	
SH98X-04	Am_02	44.26	1.32	11.12	0.08	11.94	nd	0.27	14.49	11.00	2.13	0.31	97.03	68.38	selvage amphibole?
	Am_03	44.02	1.52	10.36	0.05	12.24	nd	0.31	14.56	10.95	2.11	0.39	96.58	67.95	selvage amphibole?
	Am_04	43.59	1.41	11.32	0.08	11.51	nd	0.24	14.57	11.26	2.08	0.40	96.54	69.28	selvage amphibole?
SH98X-16	Am_02	51.19	0.38	5.75	0.01	5.86	nd	0.16	20.16	11.81	1.26	0.19	96.79	85.98	
	Am_03	46.62	0.82	10.08	bdl	6.19	nd	0.12	18.54	11.93	1.86	0.34	96.52	84.22	
	Am_04	48.93	0.22	8.80	0.01	5.21	nd	0.13	19.65	12.10	1.59	0.53	97.21	87.06	
	Am_05	49.52	0.39	7.71	0.07	5.19	nd	0.12	19.86	12.11	1.45	0.36	96.92	87.20	
	Am_06	51.61	0.07	6.02	bdl	4.58	nd	0.13	20.92	12.01	1.20	0.14	96.78	89.07	
	Am_07	48.44	0.70	8.44	bdl	5.98	nd	0.15	19.00	12.04	1.58	0.33	96.69	84.99	
	Am_08	45.34	1.08	10.95	0.02	6.60	nd	0.20	18.12	11.40	2.05	0.39	96.24	83.03	
	Am_09	48.34	0.40	8.44	0.16	5.02	nd	0.14	19.63	11.97	1.54	0.32	95.96	87.45	
	Am_10	50.06	0.28	7.39	0.01	4.70	nd	0.15	20.30	12.05	1.46	0.24	96.79	88.51	
	Am_11	49.71	0.53	7.59	0.01	4.88	nd	0.14	20.08	11.87	1.51	0.30	96.67	88.01	
	Am_12	52.83	0.10	4.67	0.02	3.89	nd	0.12	21.60	12.38	0.89	0.18	96.72	90.82	
	Am_13	48.50	0.62	9.00	0.02	4.92	nd	0.13	19.55	11.91	1.72	0.25	96.77	87.62	
	Am_14	47.62	0.80	8.45	0.01	6.11	nd	0.15	18.85	11.80	1.75	0.32	95.88	84.61	
	Am_15	50.48	0.30	6.72	0.18	6.46	nd	0.13	19.16	11.87	1.26	0.34	97.08	84.10	
	Am_16	49.87	0.43	7.20	0.03	6.81	nd	0.15	18.86	11.71	1.48	0.30	96.98	83.15	

Abbreviations: Am = amphibole, bdl = below detection limit, nd = not determined. *Note:* all oxides are in wt %.

Table A20. *Continued*

Sample	Mineral ID	SiO_2	TiO_2	Al_2O_3	Cr_2O_3	FeO	NiO	MnO	MgO	CaO	Na_2O	K_2O	Total	Mg#	Comment
SH98X-16	Am_17	48.96	0.34	8.41	0.02	7.51	nd	0.17	18.41	11.41	1.51	0.30	97.16	81.37	
SHX03-17	Am_01	54.08	0.01	4.62	0.02	3.94	nd	0.10	21.81	11.62	0.91	0.13	97.39	90.79	
	Am_02	53.60	0.03	4.83	0.02	3.77	nd	0.15	22.04	11.46	0.83	0.10	97.00	91.25	
	Am_03	53.70	0.01	4.65	0.03	3.67	nd	0.13	22.13	11.50	0.92	0.07	96.93	91.48	
	Am_05	53.94	0.04	4.56	0.01	3.82	nd	0.17	22.25	11.48	0.83	0.11	97.22	91.21	
	Am_06	53.17	0.02	4.85	bdl	3.96	nd	0.16	21.75	11.33	0.92	0.09	96.37	90.73	
SHX03-01	Am_01	45.79	0.14	11.79	0.63	4.78	nd	0.05	19.36	11.43	2.44	0.51	97.10	87.83	
	Am_02	45.81	1.55	11.36	0.32	4.73	nd	0.05	18.72	11.46	2.39	0.45	96.92	87.57	
	Am_03	45.95	0.48	11.68	0.55	4.71	nd	0.05	18.97	11.65	2.26	0.43	96.88	87.78	
	Am_04	46.23	0.46	11.25	0.69	4.69	nd	0.08	18.96	11.79	2.19	0.48	96.99	87.81	
	Am_05	45.81	0.38	11.99	0.15	4.84	nd	0.08	19.12	11.62	2.28	0.48	96.99	87.56	
	Am_06	46.21	0.49	11.31	0.50	4.59	nd	0.07	19.40	11.75	2.25	0.45	97.09	88.27	
	Am_07	45.76	0.43	12.18	0.46	4.91	nd	0.06	19.02	11.62	2.33	0.50	97.34	87.34	
	Am_08	45.88	1.85	10.83	0.55	4.52	nd	0.05	18.76	11.41	2.50	0.44	96.87	88.09	
	Am_09	46.43	0.10	11.66	0.74	4.66	nd	0.06	19.14	11.50	2.23	0.44	97.18	87.97	
	Am_10	46.37	0.79	12.06	0.66	4.70	nd	0.09	18.91	11.53	2.26	0.46	97.96	87.76	
SHX03-18	Am_01	46.05	1.91	9.13	0.04	11.83	nd	0.21	14.97	11.29	1.82	0.51	97.97	69.28	
	Am_02	44.37	1.35	12.50	0.04	12.20	nd	0.15	14.24	11.45	2.03	0.35	98.86	67.54	
	Am_03	46.23	1.74	9.05	0.01	11.48	nd	0.23	15.25	11.05	1.89	0.49	97.55	70.30	
	Am_05	50.18	1.06	7.04	0.03	6.57	nd	0.13	19.01	11.48	1.46	0.34	97.37	83.76	
	Am_06	46.32	0.82	11.28	0.02	7.99	nd	0.15	17.31	11.22	2.14	0.32	97.69	79.42	
	Am_07	45.52	1.11	11.24	0.03	10.51	nd	0.20	15.70	10.87	2.06	0.46	97.89	72.69	
	Am_07	46.85	0.87	9.39	0.02	9.18	nd	0.20	16.99	11.09	1.76	0.40	96.87	76.73	
	Am_09	48.18	0.48	8.73	bdl	8.39	nd	0.22	17.92	10.88	1.70	0.30	96.93	79.19	
	Am_10	44.86	1.11	10.99	0.01	11.35	nd	0.21	15.13	11.04	2.08	0.42	97.41	70.38	
	Am_11	47.43	0.81	9.04	0.01	9.42	nd	0.22	17.01	10.94	1.79	0.36	97.27	76.28	
	Am_13	47.31	0.99	10.17	0.03	10.50	nd	0.23	16.30	10.88	1.92	0.43	98.89	73.45	

Abbreviations: Am = amphibole, bdl = below detection limit, nd = not determined. *Note:* all oxides are in wt %.

Table A20. *Continued*

Sample	Mineral ID	SiO_2	TiO_2	Al_2O_3	Cr_2O_3	FeO	NiO	MnO	MgO	CaO	Na_2O	K_2O	Total	Mg#	Comment
SHX03-18	Am_14	45.96	1.03	10.31	0.01	10.47	nd	0.21	16.04	11.07	1.91	0.42	97.59	73.19	
	Am_15	46.27	0.94	9.75	bdl	10.54	nd	0.20	16.27	10.97	1.76	0.40	97.38	73.34	
	Am_16	43.91	1.36	12.31	0.02	9.92	nd	0.18	15.63	11.28	2.23	0.51	97.45	73.75	
	Am_17	45.89	0.77	11.31	bdl	7.84	nd	0.13	17.34	11.12	1.97	0.40	96.92	79.75	
	Am_18	44.87	0.65	11.83	bdl	9.22	nd	0.14	16.31	11.20	2.08	0.44	96.77	75.92	
	Am_19	49.82	0.55	7.60	bdl	6.92	nd	0.16	18.95	11.15	1.47	0.27	97.09	82.98	

Abbreviations: Am = amphibole, bdl = below detection limit, nd = not determined. *Note:* all oxides are in wt %.

Table A21. *Major and minor element compositions of phlogopite in Shiveluch and Avachinsky mantle xenoliths*

Sample	Mineral ID	SiO_2	TiO_2	Al_2O_3	Cr_2O_3	FeO	NiO	MnO	MgO	CaO	Na_2O	K_2O	Total	Mg#	Comment
SH98X-16	Phl_01	37.81	0.64	15.96	0.05	7.53	nd	0.05	21.42	0.04	1.18	8.09	93.09	83.51	
	Phl_02	38.20	0.67	16.35	bdl	6.64	nd	0.03	22.03	0.02	1.08	8.18	93.45	85.54	
	Phl_03	38.16	0.68	16.14	bdl	6.28	nd	0.04	22.20	0.01	1.00	8.27	92.81	86.30	
	Phl_04	38.28	0.58	16.22	bdl	6.02	nd	0.03	22.71	0.04	1.02	8.31	93.46	87.04	
	Phl_05	38.46	0.56	16.38	bdl	5.43	nd	0.02	22.86	bdl	1.04	8.31	93.22	88.23	
	Phl_06	38.87	0.73	15.47	1.06	5.32	nd	0.04	22.92	0.01	0.86	8.44	93.89	88.47	
	Phl_07	39.09	0.77	15.54	1.03	5.36	nd	0.02	22.76	0.06	0.90	8.40	94.06	88.33	
	Phl_08	38.76	0.49	15.90	0.01	4.93	nd	0.03	22.95	0.03	0.85	8.68	92.70	89.24	
	Phl_10	38.76	0.46	15.94	0.99	5.05	nd	0.02	23.06	0.06	0.78	8.98	94.26	89.06	
	Phl_11	39.22	0.55	15.88	0.01	4.78	nd	0.03	23.63	0.01	0.80	8.70	93.75	89.80	
	Phl_12	38.50	0.55	15.78	0.07	4.87	nd	0.05	23.22	0.05	0.88	8.72	92.81	89.46	
	Phl_13	38.85	0.56	16.19	0.04	5.02	nd	0.02	23.16	0.03	0.97	8.47	93.40	89.15	
	Phl_14	39.01	0.60	15.65	0.01	4.83	nd	0.02	23.18	0.02	0.91	8.66	92.95	89.52	
	Phl_15	38.42	0.57	16.29	0.01	5.92	nd	0.03	22.47	0.04	0.97	8.23	93.18	87.12	
	Phl_18	38.22	0.64	16.00	0.01	6.62	nd	0.04	22.07	0.02	1.00	8.22	93.05	85.59	
	Phl_19	38.21	0.55	16.21	bdl	6.62	nd	0.02	21.89	0.03	1.00	8.17	92.94	85.48	

Abbreviations: Phl = phlogopite, bdl = below detection limit, nd = not determined. *Note:* all oxides are in wt %.

Table A21. *Continued*

Sample	Mineral ID	SiO_2	TiO_2	Al_2O_3	Cr_2O_3	FeO	NiO	MnO	MgO	CaO	Na_2O	K_2O	Total	Mg#	Comment
SH98X-16	Phl_20	38.43	0.62	16.23	bdl	6.22	nd	0.04	22.19	0.02	0.98	8.25	93.20	86.40	
SHX03-17	Phl_02	39.61	0.17	15.60	0.01	4.66	nd	0.03	23.69	0.05	1.06	8.24	93.45	90.06	
	Phl_03	40.51	0.10	15.33	0.07	4.20	nd	0.04	23.86	0.05	0.96	7.93	93.39	91.02	
	Phl_04	40.11	0.09	15.20	0.02	4.11	nd	0.01	24.16	0.07	1.02	8.23	93.32	91.28	
	Phl_05	39.66	0.10	15.83	0.03	4.24	nd	0.02	23.65	0.06	0.97	8.06	92.96	90.87	
	Phl_06	39.98	0.10	15.49	bdl	4.14	nd	0.04	23.93	0.08	0.91	7.98	92.99	91.15	
	Phl_07	39.37	0.10	16.01	bdl	4.42	nd	0.01	23.69	0.02	0.98	8.25	93.11	90.52	
	Phl_08	39.48	0.11	15.40	0.12	4.16	nd	0.03	24.04	0.02	1.03	8.25	92.70	91.15	
	Phl_09	40.29	0.10	15.78	0.01	4.07	nd	0.04	24.01	0.06	1.04	8.11	93.72	91.31	
	Phl_10	40.65	0.10	14.91	0.02	3.99	nd	0.01	24.62	0.06	0.91	7.81	93.27	91.66	
	Phl_11	40.53	0.11	15.07	0.91	3.85	nd	0.03	23.76	0.03	0.93	8.18	93.75	91.65	
	Phl_12	40.08	0.10	15.04	0.10	4.07	nd	0.01	24.17	0.04	0.99	8.05	92.87	91.37	
	Phl_13	39.70	0.11	15.22	0.02	4.12	nd	0.03	23.97	0.04	0.99	8.14	92.70	91.20	
	Phl_14	39.85	0.13	15.24	0.01	4.16	nd	0.02	24.14	0.03	0.94	8.06	92.96	91.18	
	Phl_15	40.10	0.11	14.96	bdl	4.17	nd	bdl	24.26	0.06	0.95	8.16	92.97	91.21	
	Phl_16	39.09	0.10	16.01	0.02	4.22	nd	0.02	23.71	bdl	1.03	8.49	92.97	90.92	
	Phl_17	39.17	0.14	16.20	0.02	4.33	nd	0.04	23.69	bdl	0.98	8.30	93.13	90.70	
	Phl_18	39.45	0.11	15.61	bdl	4.31	nd	0.03	24.02	0.01	0.98	8.37	93.03	90.86	
	Phl_19	38.54	0.15	15.99	0.02	4.38	nd	0.02	23.71	0.04	1.03	8.25	92.30	90.61	
SH98X-04	Phl_02	38.39	0.53	15.42	0.72	5.33	nd	0.02	22.51	0.03	1.04	8.30	92.48	88.27	
	Phl_03	39.58	0.48	14.30	0.45	5.10	nd	0.02	23.18	0.05	1.00	8.23	92.45	89.00	
	Phl_04	39.80	0.63	14.36	0.77	5.25	nd	0.01	23.37	0.06	0.84	8.17	93.34	88.81	
	Phl_05	40.27	0.59	14.21	0.68	5.04	nd	0.04	23.04	0.05	0.85	8.37	93.29	89.07	
	Phl_06	40.44	0.49	14.14	0.77	5.12	nd	0.02	23.18	0.01	0.86	8.40	93.55	88.97	
	Phl_07	38.56	0.65	15.09	0.78	5.37	nd	0.02	22.86	0.05	0.91	8.42	92.91	88.36	
	Phl_08	39.93	0.60	14.39	0.66	5.06	nd	0.01	23.00	0.05	0.85	8.37	92.98	89.01	
SHX03-18	Phl_01	40.62	1.25	16.33	bdl	6.48	nd	0.03	20.75	0.08	1.58	6.90	94.48	85.09	
	Phl_02	39.32	1.36	16.17	0.01	6.68	nd	0.02	21.38	0.02	1.59	7.13	94.11	85.09	

Abbreviations: Phl = phlogopite, bdl = below detection limit, nd = not determined. *Note:* all oxides are in wt %.

Table A21. *Continued*

Sample	Mineral ID	SiO_2	TiO_2	Al_2O_3	Cr_2O_3	FeO	NiO	MnO	MgO	CaO	Na_2O	K_2O	Total	Mg#	Comment
SHX03-18	Phl_03	38.95	1.10	16.24	0.01	6.55	nd	0.05	21.73	bdl	1.63	7.28	93.78	85.53	
	Phl_04	39.76	0.58	15.84	bdl	3.51	nd	0.02	23.62	0.01	1.19	7.87	92.74	92.30	
	Phl_05	39.35	1.05	15.55	0.03	6.30	nd	0.04	21.92	0.01	1.49	7.03	93.05	86.11	
	Phl_06	39.02	1.09	15.91	0.01	6.45	nd	0.04	21.85	bdl	1.63	7.01	93.43	85.79	
	Phl_07	38.29	1.14	15.68	0.01	6.69	nd	0.05	21.31	0.02	1.54	7.09	92.13	85.02	
	Phl_08	39.10	1.17	15.92	bdl	6.40	nd	0.04	21.46	0.01	1.55	7.07	92.95	85.65	
	Phl_09	39.85	1.15	15.59	bdl	6.91	nd	0.04	21.53	0.01	1.61	6.65	93.60	84.74	
	Phl_10	38.58	1.57	16.15	bdl	5.99	nd	0.02	21.67	0.02	1.50	7.21	93.14	86.57	
	Phl_11	38.04	1.24	15.89	bdl	6.89	nd	0.05	21.51	bdl	1.69	7.02	92.45	84.76	
	Phl_12	38.86	1.55	15.73	0.01	6.97	nd	0.03	21.23	bdl	1.68	7.03	93.45	84.44	
	Phl_13	39.20	1.10	15.94	bdl	7.00	nd	0.03	21.76	0.01	1.61	6.90	93.93	84.71	
	Phl_14	38.49	1.01	16.17	bdl	7.91	nd	0.06	20.65	bdl	1.62	7.07	93.14	82.31	
	Phl_15	37.95	1.03	15.97	bdl	7.71	nd	0.02	20.99	0.01	1.55	6.80	92.30	82.91	
SHX03-01	Phl_01	39.68	0.93	16.76	0.10	4.07	nd	0.01	23.14	0.03	1.78	7.21	93.99	91.02	
	Phl_02	40.00	0.79	15.94	0.78	3.86	nd	0.01	23.40	0.02	1.80	6.87	93.67	91.52	
	Phl_03	38.60	0.82	16.24	1.13	4.02	nd	bdl	23.20	0.05	1.86	6.99	93.19	91.15	
	Phl_05	39.51	1.20	16.47	0.03	3.99	nd	bdl	22.26	0.02	1.69	7.24	92.52	90.87	
	Phl_05	38.74	1.02	15.98	0.98	3.94	nd	0.01	23.00	0.06	1.81	7.11	92.90	91.24	
	Phl_06	38.82	0.91	15.95	0.70	3.91	nd	0.05	23.12	0.02	1.72	7.07	92.47	91.33	
	Phl_07	38.15	1.44	16.16	0.36	4.13	nd	0.03	23.03	0.05	1.61	7.15	92.47	90.85	
	Phl_08	38.55	1.15	16.22	0.87	3.85	nd	0.03	22.87	0.08	1.56	7.19	92.78	91.36	
	Phl_10	37.96	1.35	16.23	0.30	3.98	nd	0.02	22.91	0.03	1.57	7.31	92.02	91.11	
	Phl_12	39.12	1.05	16.46	0.06	4.08	nd	0.03	23.03	0.02	1.65	7.27	93.15	90.97	
	Phl_14	38.70	0.86	15.86	0.72	3.92	nd	0.02	22.84	0.02	1.74	7.01	91.98	91.21	
	Phl_15	38.51	0.75	16.08	0.83	4.11	nd	0.03	22.48	0.07	1.65	6.94	91.62	90.69	
SH98X-18	Phl_01	40.21	0.29	15.99	0.67	3.72	nd	0.04	23.70	bdl	1.42	7.35	93.50	91.90	
	Phl_03	39.04	0.05	17.71	0.62	3.31	nd	0.03	23.33	0.09	1.91	6.76	92.99	92.62	
	Phl_04	38.98	0.15	16.48	0.39	3.04	nd	0.01	23.77	0.07	1.81	6.66	91.73	93.30	

Abbreviations: Phl = phlogopite, bdl = below detection limit, nd = not determined. *Note:* all oxides are in wt %.

Table A21. *Continued*

Sample	Mineral ID	SiO_2	TiO_2	Al_2O_3	Cr_2O_3	FeO	NiO	MnO	MgO	CaO	Na_2O	K_2O	Total	Mg#	Comment
SH98X-18	Phl_05	38.88	0.04	17.78	0.44	3.24	nd	0.02	23.77	0.05	1.99	6.85	93.43	92.90	
	Phl_06	38.05	0.14	16.32	1.07	3.44	nd	0.04	23.40	0.16	1.48	7.02	91.28	92.38	
	Phl_07	40.18	0.24	15.77	0.84	3.69	nd	0.04	23.81	bdl	1.43	7.52	93.78	92.00	
	Phl_08	38.98	0.13	16.30	0.59	3.52	nd	0.03	23.74	0.07	1.52	7.56	92.69	92.32	
	Phl_09	39.43	0.13	16.92	0.53	3.36	nd	0.03	23.72	bdl	1.57	7.54	93.39	92.63	
	Phl_10	38.77	0.14	16.69	0.84	3.83	nd	0.02	23.57	bdl	1.45	7.57	93.02	91.65	
	Phl_11	40.11	0.17	15.92	0.70	3.26	nd	0.01	23.87	0.05	1.45	7.20	92.96	92.88	
	Phl_12	39.91	0.27	15.19	0.77	3.74	nd	0.05	23.62	0.03	1.44	7.31	92.64	91.85	
	Phl_13	39.55	0.29	15.96	0.90	3.83	nd	0.03	23.59	0.03	1.43	7.49	93.27	91.65	
	Phl_15	39.15	0.08	16.81	0.65	3.68	nd	0.03	23.39	0.02	1.70	7.15	92.99	91.88	
	Phl_16	39.30	0.30	16.43	0.79	3.70	nd	0.03	23.75	0.08	1.48	7.49	93.70	91.95	
	Phl_17	40.07	0.25	16.14	0.33	3.24	nd	0.03	23.99	0.03	1.72	7.06	93.24	92.95	
	Phl_19	38.20	0.16	18.00	0.44	3.93	nd	0.02	23.13	bdl	1.85	7.28	93.35	91.29	
	Phl_21	40.56	bdl	15.55	0.49	3.41	nd	0.03	24.09	0.01	1.15	7.83	93.37	92.64	
	Phl_22	38.43	0.03	17.37	0.05	3.63	nd	0.03	23.30	0.03	1.24	8.07	92.48	91.96	
	Phl_23	38.97	0.56	17.12	bdl	3.57	nd	0.02	23.42	bdl	1.33	7.92	92.96	92.11	
	Phl_24	39.00	0.64	17.14	bdl	3.48	nd	0.01	23.41	bdl	1.27	8.02	93.22	92.30	
	Phl_25	38.61	0.47	18.21	0.03	3.59	nd	0.01	23.18	0.04	1.33	8.11	93.71	92.00	
	Phl_26	38.95	0.64	17.05	0.07	3.73	nd	0.01	23.48	0.03	1.20	7.89	93.28	91.81	
	Phl_27	39.38	0.60	16.45	0.02	3.37	nd	bdl	23.76	bdl	1.22	7.99	93.00	92.63	
	Phl_28	40.58	0.57	15.25	0.01	3.60	nd	0.02	24.22	0.03	1.20	7.62	93.34	92.31	
	Phl_30	39.25	0.99	16.47	0.01	3.86	nd	0.01	23.29	0.01	1.32	7.87	93.34	91.49	
SHX03-04	Phl_01	38.91	0.60	15.29	bdl	5.50	0.37	0.03	25.28	0.21	0.78	7.72	94.98	89.12	
	Phl_03	38.02	0.86	15.35	bdl	5.62	0.45	0.04	21.42	0.26	0.82	7.03	90.34	87.18	
	Phl_04	40.04	0.52	14.96	0.01	4.93	0.46	0.03	25.17	0.37	0.57	6.70	94.22	90.10	
	Phl_05	39.06	0.42	15.89	0.01	4.76	0.35	0.05	26.03	0.21	0.75	7.66	95.53	90.69	
SHIV-16-12-06	Phl_01	39.36	0.37	16.62	nd	4.36	0.09	0.01	20.57	0.02	1.86	6.64	90.23	82.52	
	Phl_02	38.32	0.60	16.20	nd	4.39	0.11	0.02	21.64	0.01	1.94	6.59	90.02	83.14	

Abbreviations: Phl = phlogopite, bdl = below detection limit, nd = not determined. *Note:* all oxides are in wt %.

Table A21. *Continued*

Sample	Mineral ID	SiO_2	TiO_2	Al_2O_3	Cr_2O_3	FeO	NiO	MnO	MgO	CaO	Na_2O	K_2O	Total	Mg#	Comment
SHIV-16-12-06	Phl_03	37.66	0.75	17.29	nd	4.46	0.13	bdl	20.99	0.02	1.93	6.75	90.26	82.48	
	Phl_04	37.57	0.58	17.11	nd	4.58	0.12	0.03	21.33	0.09	1.99	5.90	89.39	82.34	
	Phl_05	37.95	0.57	16.78	nd	4.45	0.13	bdl	21.49	0.14	1.88	5.76	89.40	82.86	
	Phl_06	38.63	0.46	16.35	nd	4.29	0.12	0.07	21.47	0.02	2.32	6.12	89.97	83.36	
	Phl_07	37.20	0.79	17.20	nd	4.65	0.13	0.01	21.36	bdl	2.34	6.43	90.37	82.11	
	Phl_08	37.92	0.53	17.25	nd	4.44	0.10	bdl	21.31	0.05	2.25	6.02	89.96	82.75	
	Phl_09	38.72	0.62	17.03	nd	4.87	0.12	bdl	21.51	0.03	2.47	6.22	91.68	81.53	
	Phl_10	37.07	0.79	16.53	nd	4.54	0.13	0.03	21.55	0.01	2.32	6.22	89.35	82.61	
	Phl_11	39.10	0.59	17.53	nd	4.75	0.10	0.03	21.41	bdl	2.14	6.43	92.28	81.85	
	Phl_12	38.25	0.98	16.36	nd	4.73	0.14	0.02	21.05	0.04	2.08	6.28	90.05	81.65	
	Phl_13	37.71	0.84	16.72	nd	4.63	0.12	bdl	20.67	0.13	1.84	6.26	89.19	81.70	
	Phl_14	37.29	0.34	16.93	nd	4.07	0.14	0.05	21.70	0.02	2.25	6.80	89.88	84.21	
	Phl_15	37.30	0.56	17.30	nd	4.51	0.10	0.04	21.44	0.02	2.05	6.40	89.85	82.61	
	Phl_16	37.90	0.39	17.16	nd	4.55	0.11	bdl	21.75	0.11	1.94	5.96	89.98	82.71	
	Phl_17	37.32	0.48	16.83	nd	4.29	0.12	0.02	21.25	0.03	2.25	6.43	89.36	83.19	
	Phl_18	37.86	0.54	16.59	nd	4.66	0.13	0.02	21.36	0.01	2.19	6.54	90.02	82.08	
	Phl_19	37.58	0.41	17.30	nd	4.28	0.15	bdl	21.44	0.04	2.13	6.46	89.89	83.37	
	Phl_20	37.33	0.68	16.91	nd	4.49	0.13	0.02	21.01	0.04	2.08	6.54	89.32	82.40	
	Phl_21	38.22	0.75	16.97	nd	4.35	0.14	0.03	21.44	0.01	2.04	6.25	90.29	83.12	
	Phl_22	37.10	0.27	17.30	nd	4.79	0.11	bdl	21.95	0.01	2.30	6.43	90.55	82.08	
	Phl_23	38.16	0.61	17.03	nd	4.11	0.13	bdl	21.61	0.02	2.29	6.19	90.43	84.01	
	Phl_24	38.09	0.94	16.23	nd	4.51	0.13	0.06	21.05	0.02	2.18	6.38	89.69	82.37	
	Phl_25	37.60	0.79	17.08	nd	4.71	0.14	0.02	21.29	0.02	2.21	6.33	90.30	81.90	
	Phl_26	37.23	0.49	16.26	nd	4.42	0.14	0.01	20.32	0.15	1.45	5.09	85.62	82.14	
	Phl_27	37.27	0.79	16.92	nd	4.61	0.10	bdl	21.09	0.03	2.30	6.28	89.64	82.08	
	Phl_28	37.25	0.61	16.88	nd	4.45	0.12	0.01	21.22	0.01	2.18	6.31	89.31	82.65	
	Phl_29	37.53	0.68	17.04	nd	4.56	0.16	0.02	21.56	0.03	2.30	6.13	90.27	82.54	
	Phl_30	37.46	0.36	16.73	nd	4.78	0.14	bdl	21.56	0.05	1.91	6.26	89.45	81.84	

Abbreviations: Phl = phlogopite, bdl = below detection limit, nd = not determined. *Note:* all oxides are in wt %.

Table A21. *Continued*

Sample	Mineral ID	SiO_2	TiO_2	Al_2O_3	Cr_2O_3	FeO	NiO	MnO	MgO	CaO	Na_2O	K_2O	Total	Mg#	Comment
AVX-16-03-24	Phl_01	40.62	0.02	17.99	0.01	2.48	0.09	0.01	24.35	0.05	1.93	6.38	93.93	94.60	
	Phl_02	39.47	0.04	18.12	0.10	2.66	0.14	0.02	20.82	0.07	1.87	6.46	89.79	93.31	
	Phl_03	40.19	0.04	18.37	0.02	2.66	0.15	0.01	25.89	0.23	1.68	5.96	95.20	94.55	

Abbreviations: Phl = phlogopite. *Note:* all oxides are in wt %.

Appendix B
Mineral trace element compositions

Table B22. *Trace element compositions of amphibole in Shiveluch and Avachinsky mantle xenoliths*

Sample	SH98X-16							
Mineral ID	Am_01	Am_02	Am_03	Am_04	Am_05	Am_06	Am_10	Am_11
Li	4.83	3.25	4.31	4.53	3.72	2.99	4.57	4.96
Be	0.16	0.02	0.29	0.28	0.34	0.17	0.20	0.13
Ti	3891.40	661.30	3300.77	3394.05	1448.68	1309.98	5703.86	1832.67
V	273.38	89.28	255.19	223.70	158.54	150.63	413.24	194.96
Cr	26.59	bdl	7.49	47.08	823.77	776.15	127.80	77.74
Mn	1421.51	969.35	1133.83	1119.33	938.73	965.09	1132.70	1239.34
Co	45.99	38.63	47.02	43.29	39.86	36.04	43.61	45.05
Ni	577.65	379.71	211.34	614.66	607.01	621.27	423.83	656.53
Cu	2.71	2.93	1.94	2.00	5.52	1.44	8.19	1.84
Zn	45.09	35.21	38.04	37.01	36.49	29.50	34.37	34.49
Rb	0.32	0.27	0.48	0.35	0.33	0.32	0.70	0.31
Sr	89.38	58.15	94.98	132.38	101.40	103.38	110.05	100.19
Y	26.84	4.66	21.32	17.32	5.57	5.62	25.52	27.52
Zr	29.63	13.62	28.57	26.65	12.81	12.18	46.62	37.55
Nb	1.04	0.35	1.11	0.85	0.46	0.26	1.24	0.87
Mo	0.04	0.08	bdl	0.04	bdl	bdl	0.04	bdl
Cs	bdl	bdl	bdl	bdl	bdl	bdl	bdl	bdl
Ba	11.92	3.91	14.03	10.69	9.33	4.62	41.21	9.24
La	3.94	2.57	3.23	4.86	3.46	2.24	4.21	7.07
Ce	16.23	7.65	13.73	15.23	10.16	7.13	17.75	24.55
Pr	3.05	1.11	2.75	2.24	1.31	1.15	3.33	3.69
Nd	16.12	4.47	14.05	10.78	5.06	5.22	17.29	18.41
Sm	4.32	1.09	4.13	2.88	0.98	1.09	4.40	4.83
Eu	1.22	0.47	1.05	0.97	0.62	0.44	1.35	1.32
Gd	4.80	0.90	3.96	3.11	0.91	1.15	5.05	5.07
Tb	0.81	0.12	0.64	0.52	0.15	0.17	0.84	0.84
Dy	4.60	0.76	3.66	3.00	0.83	0.92	4.69	5.11
Ho	1.06	0.17	0.81	0.70	0.23	0.23	1.02	1.15
Er	3.03	0.60	2.31	1.97	0.62	0.68	2.94	3.04
Tm	0.47	0.10	0.33	0.29	0.11	0.11	0.42	0.45
Yb	2.79	0.53	2.04	2.05	0.73	0.58	3.00	2.50
Lu	0.39	0.09	0.38	0.33	0.13	0.11	0.43	0.42
Hf	1.79	0.55	1.67	1.85	0.56	0.55	2.39	2.69
Ta	0.05	0.05	0.06	0.07	0.05	0.04	0.05	0.04
Pb	0.58	0.32	0.52	0.63	0.41	0.36	0.92	0.59
Th	0.20	0.20	0.22	0.39	0.29	0.20	0.20	0.47
U	0.10	0.07	0.11	0.11	0.11	0.06	0.17	0.18

Abbreviations: Am = amphibole, bdl = below detection limit. *Note:* all trace element concentrations are in μg g^{-1}.

Table B22. *Continued*

Sample	SH98X-16							
Mineral ID	Am_12	Am_13	Am_14	Am_15	Am_16	Am_17	Am_18	Am_19
Li	4.82	3.80	4.62	4.33	3.54	3.30	4.51	3.75
Be	0.15	0.13	0.34	0.17	bdl	0.04	0.16	0.24
Ti	3537.46	2084.08	3801.57	3113.77	1444.42	1499.41	4188.29	3447.55
V	250.76	219.75	230.30	232.56	175.88	143.47	370.50	252.17
Cr	111.21	2526.48	63.80	5.84	427.59	1.27	8.51	136.62
Mn	1315.65	1037.64	1141.47	1055.64	842.70	877.87	1258.14	933.98
Co	44.98	43.37	43.62	43.31	37.69	37.00	49.38	38.04
Ni	673.56	747.22	634.47	461.25	578.24	384.51	219.21	554.14
Cu	2.19	12.08	3.78	2.57	2.59	1.85	3.58	3.89
Zn	39.39	42.50	39.03	40.08	28.02	26.70	32.40	28.91
Rb	0.23	26.54	0.24	0.31	0.39	0.36	0.57	0.40
Sr	138.05	129.49	165.46	53.03	101.87	64.71	98.47	147.89
Y	17.21	7.65	6.66	21.52	6.54	15.43	28.74	15.77
Zr	27.36	35.61	12.91	26.86	17.77	29.66	30.98	27.61
Nb	0.88	0.42	0.71	0.87	0.27	1.41	0.99	0.68
Mo	bdl	0.06	0.04	bdl	bdl	bdl	0.07	0.05
Cs	bdl	1.23	bdl	bdl	bdl	bdl	bdl	bdl
Ba	7.72	68.08	10.11	11.13	4.55	7.22	14.56	8.33
La	6.23	2.25	4.82	3.41	2.24	5.32	3.78	4.28
Ce	17.50	6.53	11.58	14.14	6.77	21.11	15.79	13.08
Pr	2.50	0.90	1.41	2.86	1.06	3.67	3.13	2.10
Nd	11.98	3.91	4.75	13.83	4.55	17.81	16.96	10.05
Sm	3.02	0.98	1.07	4.04	1.10	4.12	5.04	2.47
Eu	1.15	0.38	0.68	1.02	0.39	0.82	1.37	0.70
Gd	2.80	0.99	0.90	3.69	1.12	3.48	5.22	2.49
Tb	0.48	0.17	0.16	0.66	0.19	0.52	0.87	0.45
Dy	2.93	0.97	1.21	3.72	1.07	2.84	5.17	2.71
Ho	0.67	0.28	0.24	0.79	0.23	0.58	1.10	0.66
Er	2.00	0.89	0.82	2.23	0.71	1.65	3.35	1.84
Tm	0.26	0.19	0.16	0.28	0.11	0.18	0.41	0.32
Yb	2.00	1.24	1.04	2.20	0.84	1.37	3.15	2.10
Lu	0.30	0.19	0.20	0.33	0.15	0.20	0.48	0.35
Hf	1.61	1.90	0.61	1.68	0.89	2.63	2.00	1.61
Ta	0.06	0.07	0.08	0.05	0.04	0.17	0.06	0.09
Pb	0.66	0.50	0.68	0.40	0.38	0.32	0.51	0.57
Th	0.46	0.36	0.40	0.11	0.28	0.32	0.40	0.57
U	0.16	0.10	0.10	0.06	0.07	0.08	0.13	0.10

Abbreviations: Am = amphibole, bdl = below detection limit. *Note:* all trace element concentrations are in $\mu g\ g^{-1}$.

Table B22. *Continued*

Sample	SH98X-16			SHX03-18				
Mineral ID	Am_20	Am_21	Am_22	Am_01	Am_02	Am_03	Am_04	Am_05
Li	3.59	3.89	3.22	6.39	5.84	6.24	6.44	6.81
Be	0.25	0.20	0.08	0.58	0.51	0.38	0.62	0.37
Ti	4312.58	3958.82	1159.93	6093.43	5344.27	4464.40	6176.43	3892.07
V	180.57	189.99	107.04	325.70	298.94	316.50	374.77	148.66
Cr	3.51	3.38	1.67	29.43	48.26	33.21	39.21	8.39
Mn	970.98	1120.52	1037.53	1298.49	1125.63	1505.00	1460.06	1279.37
Co	38.45	41.12	38.92	54.02	52.73	54.94	53.90	48.79
Ni	458.15	400.24	477.80	379.82	566.61	324.94	371.86	699.92
Cu	3.78	1.71	1.81	4.01	2.67	3.28	3.85	3.02
Zn	29.04	30.30	31.04	86.59	72.43	99.54	81.70	69.02
Rb	1.08	0.25	0.18	0.89	1.25	0.63	0.71	1.32
Sr	64.39	64.70	59.73	83.69	47.25	58.49	70.27	76.07
Y	8.01	9.43	2.76	31.95	33.95	30.54	32.02	24.58
Zr	29.23	34.06	7.41	49.26	52.78	36.00	44.53	64.19
Nb	0.54	0.65	0.41	1.50	1.87	1.34	1.49	1.10
Mo	0.08	0.05	bdl	0.10	0.06	bdl	bdl	0.10
Cs	bdl	bdl	bdl	bdl	0.03	bdl	bdl	bdl
Ba	17.25	8.68	2.53	37.02	49.97	21.20	28.70	28.87
La	7.21	8.29	2.35	4.83	6.30	6.21	4.43	4.44
Ce	23.71	26.46	5.86	20.89	27.17	24.23	19.41	18.84
Pr	3.12	3.51	0.76	3.74	4.88	3.97	3.59	3.40
Nd	12.19	14.10	3.23	21.26	24.82	20.61	19.81	17.63
Sm	2.15	2.75	0.65	6.02	7.13	5.71	5.46	4.60
Eu	1.00	1.16	0.45	1.80	1.89	1.74	1.64	1.53
Gd	1.72	2.14	0.47	6.58	6.95	6.24	6.05	4.16
Tb	0.26	0.29	0.05	1.06	1.09	0.95	1.00	0.71
Dy	1.53	1.70	0.42	6.06	6.43	6.07	6.03	4.14
Ho	0.31	0.33	0.09	1.40	1.38	1.19	1.27	0.92
Er	0.94	0.92	0.31	3.99	3.90	3.67	3.76	2.82
Tm	0.11	0.14	0.06	0.52	0.54	0.50	0.50	0.38
Yb	0.82	0.89	0.39	3.22	3.24	2.88	3.29	2.88
Lu	0.14	0.15	0.07	0.49	0.50	0.45	0.47	0.44
Hf	1.84	2.18	0.25	2.44	2.77	2.39	2.24	3.07
Ta	0.25	0.08	0.04	0.08	0.11	0.10	0.07	0.04
Pb	0.44	0.47	0.27	0.72	0.43	0.46	0.54	0.62
Th	0.46	0.52	0.19	0.13	0.11	0.13	0.08	0.16
U	0.18	0.12	0.07	0.06	0.03	0.03	0.05	0.08

Abbreviations: Am = amphibole, bdl = below detection limit. *Note:* all trace element concentrations are in µg g^{-1}.

Table B22. *Continued*

Sample	SHX03-18							
Mineral ID	Am_06	Am_07	Am_08	Am_09	Am_10	Am_11	Am_12	Am_13
Li	6.44	6.08	7.21	6.75	6.00	6.69	6.31	5.83
Be	0.73	0.82	0.53	0.28	0.51	0.54	0.36	0.40
Ti	7447.37	6186.48	7355.30	6186.06	4924.31	6462.87	7870.37	3755.03
V	387.56	349.40	371.95	382.63	303.02	377.51	399.12	258.73
Cr	43.13	41.05	48.69	69.08	50.74	47.36	31.85	26.32
Mn	1299.74	1248.16	1551.77	1710.94	1325.00	1737.25	1451.72	899.01
Co	51.98	52.71	52.56	53.37	54.43	53.18	52.28	48.88
Ni	423.24	353.51	298.65	298.84	294.80	271.36	326.55	759.78
Cu	3.51	5.15	7.27	5.34	1.92	8.84	4.39	2.17
Zn	78.89	84.77	107.23	112.79	88.96	118.84	94.62	55.54
Rb	0.88	0.65	0.84	0.64	0.36	0.76	0.96	0.84
Sr	125.54	71.86	112.19	69.65	31.68	75.87	132.60	34.45
Y	35.09	34.11	34.46	30.03	32.73	32.06	34.43	28.10
Zr	45.65	46.81	44.52	42.47	33.90	44.10	50.02	44.44
Nb	1.28	1.66	1.59	1.51	1.24	1.63	1.48	1.80
Mo	0.06	bdl	bdl	bdl	bdl	bdl	bdl	0.07
Cs	bdl	bdl	bdl	bdl	bdl	bdl	bdl	0.04
Ba	49.61	32.99	50.19	27.23	15.50	33.03	50.40	24.75
La	4.31	5.34	5.42	4.33	5.74	4.35	4.01	7.64
Ce	18.54	23.15	22.69	19.36	24.02	19.32	18.75	29.70
Pr	3.55	4.29	3.98	3.52	4.27	3.72	3.60	4.69
Nd	19.55	23.85	22.55	19.70	21.35	20.12	20.38	23.95
Sm	5.89	6.32	6.52	5.40	6.55	6.10	6.47	6.52
Eu	1.88	1.93	2.03	1.71	1.86	1.54	1.81	1.66
Gd	6.67	6.88	6.73	6.12	6.49	6.42	6.26	5.75
Tb	1.12	1.03	1.10	0.94	1.04	1.00	1.16	0.92
Dy	6.70	6.54	6.59	6.13	6.09	6.41	7.01	5.77
Ho	1.42	1.30	1.45	1.14	1.35	1.33	1.40	1.14
Er	4.17	4.10	3.97	3.35	3.71	3.65	4.13	3.20
Tm	0.60	0.55	0.52	0.45	0.55	0.57	0.56	0.43
Yb	3.55	3.31	3.26	3.03	3.11	3.15	3.53	2.36
Lu	0.54	0.58	0.52	0.46	0.48	0.50	0.51	0.36
Hf	2.49	2.45	2.64	2.20	2.22	2.43	2.36	2.54
Ta	0.06	0.08	0.11	0.08	0.07	0.07	0.11	0.16
Pb	0.80	0.61	0.84	0.51	0.51	0.63	0.85	0.48
Th	0.13	0.13	0.09	0.08	0.12	0.16	0.45	0.50
U	0.09	0.06	0.08	0.05	0.04	0.08	0.09	0.12

Abbreviations: Am = amphibole, bdl = below detection limit. *Note:* all trace element concentrations are in $\mu g\ g^{-1}$.

Table B22. *Continued*

Sample	SHX03-18							
Mineral ID	Am_14	Am_15	Am_16	Am_17	Am_18	Am_19	Am_20	Am_21
Li	6.80	6.65	6.29	6.98	6.75	6.90	6.49	6.10
Be	0.32	0.57	0.63	0.50	0.78	0.81	0.66	0.43
Ti	5758.48	6579.76	5258.51	6380.55	6367.03	6370.14	4052.48	3588.19
V	276.34	370.26	304.64	396.85	295.76	385.21	330.74	271.34
Cr	9.36	11.09	38.99	41.93	11.95	42.75	22.91	17.52
Mn	1424.95	1279.93	1356.37	1737.76	1345.82	1651.72	1509.42	1328.89
Co	54.44	55.81	52.95	53.78	53.85	55.12	51.94	52.01
Ni	396.73	552.32	254.95	284.06	371.66	288.61	250.98	269.02
Cu	2.54	2.47	1.81	4.08	2.59	7.05	2.28	2.94
Zn	83.22	77.38	89.56	106.70	78.96	103.47	92.85	83.26
Rb	1.37	0.90	0.52	0.73	0.90	0.72	0.43	0.32
Sr	52.54	74.49	45.58	66.52	89.74	67.13	35.07	29.58
Y	32.36	39.58	29.80	29.57	32.67	31.33	31.99	27.98
Zr	45.06	56.06	42.60	41.57	60.16	46.77	32.26	27.88
Nb	1.55	1.52	1.38	1.36	1.27	1.52	0.94	1.05
Mo	0.06	bdl	bdl	bdl	0.05	0.10	bdl	bdl
Cs	0.03	bdl	bdl	bdl	bdl	bdl	bdl	bdl
Ba	34.35	33.67	18.11	27.85	32.96	30.87	18.57	10.69
La	5.13	5.04	6.43	4.05	4.80	4.76	4.69	5.12
Ce	21.65	22.85	23.95	16.67	18.25	19.33	17.67	18.85
Pr	3.83	4.23	3.97	3.43	3.55	3.79	3.35	3.57
Nd	20.34	24.09	20.93	18.61	19.63	21.02	18.47	19.46
Sm	6.33	7.20	6.18	5.77	5.39	6.00	6.02	5.87
Eu	1.87	1.85	1.72	1.50	1.80	1.60	1.73	1.78
Gd	5.86	7.79	6.45	6.02	5.94	6.21	6.00	5.85
Tb	1.06	1.29	0.99	0.95	0.95	1.01	1.06	0.94
Dy	5.97	7.81	5.66	5.60	6.23	6.17	6.54	5.18
Ho	1.32	1.69	1.25	1.25	1.30	1.33	1.37	1.07
Er	3.71	4.57	3.44	3.45	3.62	3.69	3.87	3.25
Tm	0.50	0.65	0.56	0.44	0.53	0.52	0.50	0.43
Yb	3.44	4.09	3.06	2.91	3.41	3.11	3.42	2.86
Lu	0.49	0.61	0.48	0.47	0.58	0.51	0.52	0.39
Hf	2.46	2.91	2.45	2.09	3.01	2.46	2.20	1.75
Ta	0.06	0.09	0.10	0.07	0.06	0.09	0.07	0.07
Pb	0.61	0.68	0.54	0.57	0.77	0.60	0.37	0.36
Th	0.23	0.28	0.32	0.08	0.30	0.21	0.22	0.23
U	0.10	0.10	0.10	0.05	0.15	0.09	0.06	0.06

Abbreviations: Am = amphibole, bdl = below detection limit. *Note:* all trace element concentrations are in μg g^{-1}.

Table B22. *Continued*

Sample	SHX03-18				SHX03-04		
Mineral ID	Am_22	Am_23	Am_24	Am_25	Am_01	Am_02	Am_05
Li	6.16	5.84	6.12	6.82	4.57	4.01	3.21
Be	0.46	0.44	0.61	1.06	0.26	0.33	0.11
Ti	5253.82	4435.91	4829.77	6793.00	4710.17	5698.73	1570.07
V	270.08	329.80	350.82	283.75	224.09	220.34	92.71
Cr	29.46	28.80	60.41	14.08	335.10	93.87	80.74
Mn	983.28	1368.98	1316.98	1118.35	1656.83	1345.64	1236.82
Co	52.92	53.31	53.87	54.88	57.97	52.60	59.60
Ni	592.86	271.35	256.74	413.11	1089.26	992.40	1214.46
Cu	2.64	1.89	2.91	3.08	2.15	3.14	3.63
Zn	61.77	83.34	82.50	70.07	115.56	75.72	76.71
Rb	0.59	0.41	0.55	0.84	1.06	0.88	1.36
Sr	76.80	27.74	51.04	110.58	140.77	142.18	81.41
Y	35.58	32.91	35.25	35.54	20.57	27.91	12.83
Zr	56.45	28.77	40.18	59.16	53.34	57.28	75.37
Nb	1.28	1.25	1.36	1.29	1.55	1.38	2.46
Mo	0.10	bdl	bdl	bdl	bdl	0.06	0.17
Cs	bdl	bdl	bdl	bdl	bdl	bdl	bdl
Ba	29.66	13.39	23.30	39.68	54.31	46.94	55.13
La	4.81	6.31	7.11	4.72	2.85	2.67	4.32
Ce	19.70	23.43	25.58	19.32	11.80	11.39	16.80
Pr	3.89	4.33	4.53	3.87	2.38	2.43	3.13
Nd	21.85	23.84	23.71	22.85	13.54	15.03	13.69
Sm	6.41	6.63	6.63	6.78	4.16	4.83	2.95
Eu	1.87	1.91	2.00	2.07	1.17	1.42	1.66
Gd	6.44	6.99	7.08	6.95	4.28	5.11	2.64
Tb	1.10	1.10	1.15	1.08	0.67	0.82	0.36
Dy	6.73	6.17	6.90	6.41	3.98	4.99	2.35
Ho	1.40	1.21	1.51	1.45	0.73	1.04	0.43
Er	4.07	3.63	4.21	4.07	2.37	3.00	1.27
Tm	0.59	0.46	0.58	0.61	0.29	0.46	0.16
Yb	4.06	3.16	3.46	3.86	2.01	2.92	1.31
Lu	0.59	0.46	0.51	0.62	0.32	0.41	0.15
Hf	2.99	2.15	2.57	2.74	2.52	2.26	3.31
Ta	0.08	0.13	0.15	0.07	0.12	0.08	0.28
Pb	0.63	0.39	0.52	0.85	0.49	0.49	0.53
Th	0.30	0.22	0.33	0.23	0.05	0.06	0.45
U	0.14	0.07	0.14	0.11	0.03	0.07	0.17

Abbreviations: Am = amphibole, bdl = below detection limit. *Note:* all trace element concentrations are in $\mu g\ g^{-1}$.

Table B22. *Continued*

Sample	AVX-16-03-24							
Mineral ID	Am_01	Am_02	Am_03	Am_04	Am_05	Am_06	Am_07	Am_08
Li	1.11	1.34	1.65	1.36	1.41	1.34	1.27	0.94
Be	bdl	bdl	bdl	0.08	bdl	bdl	bdl	bdl
Ti	217.74	174.21	248.80	235.24	285.02	269.39	281.38	286.55
V	270.55	253.24	340.67	311.46	313.24	307.28	303.20	262.71
Cr	376.99	341.25	30.49	323.29	588.41	455.45	517.45	37.94
Mn	553.18	569.75	544.14	478.94	465.92	478.43	462.40	455.74
Co	36.94	44.42	44.54	46.06	46.41	47.00	45.52	37.47
Ni	463.00	465.54	384.12	419.53	475.07	454.49	481.26	469.16
Cu	0.89	0.97	0.87	1.15	2.61	1.75	1.05	0.60
Zn	13.71	18.86	17.70	22.64	21.75	23.21	21.33	17.79
Rb	0.88	0.91	1.12	1.03	1.07	1.10	1.02	0.69
Sr	40.15	19.37	31.73	45.49	42.98	41.35	40.18	35.56
Y	0.82	0.51	0.94	1.28	1.98	1.74	1.94	2.07
Zr	1.22	0.98	1.45	1.48	1.66	1.95	1.79	2.27
Nb	bdl	bdl	bdl	0.01	0.01	bdl	bdl	0.01
Mo	bdl	bdl	bdl	bdl	bdl	bdl	bdl	bdl
Cs	bdl	bdl	bdl	bdl	bdl	bdl	bdl	bdl
Ba	24.58	9.64	15.25	30.21	29.64	27.49	27.55	15.06
La	0.12	0.12	0.18	0.16	0.15	0.13	0.14	0.15
Ce	0.25	0.25	0.35	0.35	0.31	0.30	0.28	0.28
Pr	0.03	0.03	0.04	0.05	0.06	0.05	0.04	0.04
Nd	0.15	0.19	0.24	0.24	0.29	0.34	0.36	0.27
Sm	0.04	0.05	0.08	0.12	0.12	0.11	0.12	0.12
Eu	0.06	0.11	0.15	0.12	0.10	0.09	0.08	0.08
Gd	0.16	bdl	bdl	bdl	0.23	0.27	0.26	0.16
Tb	0.02	0.01	0.02	0.03	0.05	0.04	0.04	0.04
Dy	0.17	0.06	0.15	0.21	0.26	0.23	0.36	0.32
Ho	0.02	0.01	0.04	0.04	0.08	0.10	0.06	0.10
Er	0.12	0.06	0.12	0.17	0.26	0.23	0.27	0.28
Tm	0.01	0.01	0.02	0.03	0.06	0.05	0.04	0.04
Yb	0.13	0.09	0.15	0.19	0.34	0.28	0.28	0.37
Lu	0.04	0.02	0.02	0.04	0.04	0.05	0.06	0.07
Hf	0.04	0.01	0.03	0.05	0.09	0.08	0.07	0.11
Ta	bdl	bdl	bdl	bdl	bdl	bdl	bdl	bdl
Pb	0.47	0.13	0.30	0.26	0.26	0.24	0.23	0.19
Th	bdl	bdl	bdl	bdl	bdl	bdl	bdl	bdl
U	0.01	bdl	0.01	bdl	bdl	bdl	bdl	bdl

Abbreviations: Am = amphibole, bdl = below detection limit. *Note:* all trace element concentrations are in µg g^{-1}.

Table B22. *Continued*

Sample	AVX-16-03-24							
Mineral ID	Am_09	Am_10	Am_11	Am_12	Am_13	Am_14	Am_15	Am_17
Li	0.86	0.88	1.12	1.17	1.03	1.31	1.09	1.02
Be	bdl	bdl	0.05	bdl	bdl	bdl	bdl	0.01
Ti	231.84	219.93	241.13	243.07	1008.57	176.13	147.31	1616.38
V	258.09	264.14	263.15	265.61	635.29	245.12	256.73	799.81
Cr	361.35	282.36	81.63	308.06	1259.85	75.49	27.55	2265.04
Mn	421.16	422.78	443.18	419.35	571.92	421.90	479.86	426.29
Co	33.23	36.43	31.38	44.60	46.99	41.66	40.84	40.37
Ni	686.24	570.61	431.59	531.42	1002.36	420.29	349.26	934.11
Cu	0.60	1.22	1.00	1.85	0.82	1.04	1.53	1.50
Zn	10.00	14.49	9.11	21.67	18.24	19.22	17.12	14.19
Rb	0.64	0.68	0.43	0.93	2.13	0.80	1.07	4.58
Sr	31.44	17.96	63.05	42.57	15.86	40.42	32.26	23.00
Y	0.97	0.75	0.75	1.43	5.02	0.80	0.48	8.46
Zr	1.35	1.25	1.42	1.63	5.83	1.11	0.69	17.04
Nb	bdl	0.01	0.01	0.02	0.02	0.02	0.03	0.75
Mo	bdl	bdl	bdl	bdl	0.21	bdl	0.01	0.25
Cs	bdl	bdl	bdl	bdl	bdl	bdl	bdl	bdl
Ba	4.97	8.26	3.34	26.16	13.91	19.10	13.05	21.38
La	0.11	0.12	0.08	0.14	0.28	0.12	0.14	0.42
Ce	0.17	0.22	0.20	0.25	0.79	0.21	0.23	1.24
Pr	0.03	0.02	0.02	0.05	0.12	0.02	0.03	0.22
Nd	0.12	0.07	0.16	0.22	0.85	0.13	0.08	1.26
Sm	0.10	0.07	0.07	0.04	0.37	0.05	0.05	0.52
Eu	0.03	0.08	0.05	0.09	0.18	0.09	0.12	0.16
Gd	bdl	0.08	0.16	0.23	0.51	bdl	bdl	0.98
Tb	0.01	bdl	0.01	0.03	0.12	bdl	bdl	0.17
Dy	0.14	0.07	0.10	0.28	0.89	0.02	0.04	1.42
Ho	0.04	0.02	0.03	0.05	0.17	0.02	0.01	0.31
Er	0.10	0.12	0.07	0.19	0.58	0.15	0.06	1.23
Tm	0.02	0.03	0.02	0.02	0.10	0.01	0.01	0.18
Yb	0.25	0.15	0.13	0.27	0.66	0.04	0.07	1.09
Lu	0.03	0.02	0.02	0.04	0.10	0.04	0.02	0.19
Hf	0.06	0.05	0.04	0.04	0.26	0.04	bdl	0.57
Ta	bdl	bdl	bdl	bdl	bdl	bdl	bdl	0.05
Pb	0.30	0.10	0.63	0.33	0.16	0.30	0.41	0.24
Th	0.01	bdl	bdl	bdl	bdl	bdl	bdl	0.01
U	bdl	bdl	0.01	bdl	0.01	bdl	bdl	0.01

Abbreviations: Am = amphibole, bdl = below detection limit. *Note:* all trace element concentrations are in $\mu g\ g^{-1}$.

Table B22. *Continued*

Sample	AVX-16-03-24			AVX-16-03-10				
Mineral ID	Am_20	Am_21	Am_22	Am_01	Am_03	Am_04	Am_05	Am_06
Li	0.82	0.98	0.94	1.49	0.99	1.05	1.18	0.90
Be	bdl	bdl	bdl	0.09	0.07	bdl	0.24	bdl
Ti	153.67	242.18	310.36	5907.56	5449.61	5046.62	4506.23	5925.88
V	228.88	287.06	290.63	356.06	310.77	299.64	268.18	342.80
Cr	320.48	473.20	423.85	543.94	461.61	159.11	235.89	260.68
Mn	594.26	459.71	441.94	851.33	1206.60	901.41	816.37	969.44
Co	37.32	45.56	46.08	42.48	39.20	41.13	40.26	42.09
Ni	327.33	459.56	551.63	616.56	762.28	690.91	729.57	610.62
Cu	0.56	1.60	0.70	0.60	0.44	0.47	1.36	0.57
Zn	9.96	20.85	19.83	36.05	50.47	40.98	32.54	45.92
Rb	0.67	0.78	0.84	0.63	0.45	0.52	0.63	0.44
Sr	42.35	30.36	28.17	228.18	128.86	218.89	265.04	138.05
Y	0.32	1.50	1.92	20.83	31.40	19.05	17.65	21.84
Zr	0.50	1.51	2.39	23.52	25.53	28.26	32.35	17.70
Nb	0.01	bdl	0.02	0.45	0.34	0.44	0.61	0.28
Mo	bdl	bdl	0.04	bdl	bdl	bdl	0.05	0.03
Cs	bdl	bdl	bdl	bdl	bdl	bdl	bdl	bdl
Ba	29.01	16.03	17.78	76.47	31.06	92.04	136.98	31.24
La	0.14	0.14	0.12	1.49	0.82	1.85	2.44	0.60
Ce	0.20	0.25	0.33	5.18	3.98	5.80	6.98	3.13
Pr	0.02	0.05	0.04	1.05	1.07	0.99	1.19	0.87
Nd	0.11	0.26	0.32	6.54	7.99	6.34	6.88	6.52
Sm	0.02	0.13	0.13	2.52	3.64	2.31	2.28	2.91
Eu	0.10	0.07	0.11	0.94	1.18	0.75	0.81	1.02
Gd	bdl	0.13	0.14	3.40	4.87	3.12	2.97	3.37
Tb	bdl	0.03	0.04	0.60	0.85	0.52	0.47	0.65
Dy	0.03	0.26	0.25	3.78	5.62	3.89	3.06	4.05
Ho	bdl	0.04	0.07	0.90	1.20	0.82	0.65	0.84
Er	0.07	0.18	0.26	2.38	3.89	2.44	1.63	2.64
Tm	bdl	0.02	0.04	0.33	0.52	0.28	0.28	0.36
Yb	0.02	0.17	0.34	2.06	2.92	1.63	2.00	2.27
Lu	0.01	0.02	0.05	0.27	0.46	0.29	0.19	0.30
Hf	0.02	0.07	0.07	0.95	1.32	1.06	1.09	0.92
Ta	bdl	bdl	bdl	0.03	0.02	0.03	0.02	0.02
Pb	0.46	0.17	0.17	0.39	0.21	0.31	0.41	0.20
Th	bdl	bdl	bdl	0.05	0.01	0.05	0.14	bdl
U	bdl	bdl	0.01	0.02	bdl	0.04	0.06	bdl

Abbreviations: Am = amphibole, bdl = below detection limit. *Note:* all trace element concentrations are in $\mu g\ g^{-1}$.

Table B22. *Continued*

Sample	AVX-16-03-10				AVX-16-03-20		
Mineral ID	Am_08	Am_10	Am_11	Am_13	Am_01	Am_02	Am_03
Li	1.05	1.24	0.95	0.92	1.10	1.03	1.02
Be	0.15	0.05	0.12	0.12	bdl	bdl	0.13
Ti	5989.99	1742.04	6466.26	6869.26	5564.65	5899.36	6069.62
V	335.83	122.43	353.25	396.80	223.54	239.07	240.80
Cr	34.78	182.79	32.19	32.65	301.92	30.56	378.47
Mn	879.68	959.04	940.15	1032.74	1759.20	1960.21	1936.71
Co	43.54	43.45	41.42	44.31	27.99	28.13	28.12
Ni	682.98	1266.83	614.58	611.61	542.02	488.76	521.62
Cu	0.50	0.36	0.30	0.31	0.37	0.48	0.25
Zn	37.28	35.57	47.05	51.51	84.41	91.98	97.18
Rb	0.33	0.68	0.48	0.43	0.37	0.34	0.38
Sr	143.69	216.61	160.88	135.88	88.82	68.47	99.53
Y	24.95	15.31	24.71	25.29	44.91	56.57	46.56
Zr	16.57	56.41	18.08	15.38	24.00	30.55	23.07
Nb	0.33	1.01	0.34	0.23	0.40	0.66	0.54
Mo	bdl	bdl	bdl	bdl	bdl	bdl	bdl
Cs	bdl	bdl	bdl	bdl	bdl	bdl	bdl
Ba	31.24	61.45	46.35	28.15	22.71	20.94	24.93
La	0.77	2.77	0.78	0.56	0.89	1.26	0.80
Ce	3.22	13.29	3.43	2.84	4.70	7.26	4.70
Pr	0.89	2.64	0.84	0.78	1.37	2.07	1.43
Nd	6.16	14.63	6.48	6.37	10.45	14.94	11.22
Sm	3.01	3.26	2.77	2.98	5.21	6.56	5.54
Eu	1.15	0.91	1.06	0.99	1.57	1.82	1.74
Gd	4.55	2.70	4.16	4.49	7.04	8.53	7.20
Tb	0.77	0.42	0.73	0.74	1.32	1.67	1.36
Dy	4.36	2.41	4.78	4.70	8.51	10.42	8.69
Ho	1.00	0.52	1.00	1.05	1.74	2.11	1.82
Er	3.14	1.72	2.92	3.06	5.12	6.75	5.76
Tm	0.38	0.25	0.35	0.38	0.74	0.96	0.69
Yb	2.10	2.10	2.18	2.34	4.15	5.56	4.53
Lu	0.30	0.30	0.26	0.35	0.57	0.85	0.60
Hf	0.89	2.26	0.90	0.83	1.26	1.62	1.26
Ta	0.02	0.06	0.02	0.01	0.04	0.04	0.03
Pb	0.23	0.46	0.29	0.17	0.17	0.18	0.18
Th	0.01	0.03	bdl	bdl	0.01	bdl	bdl
U	0.03	0.02	0.01	bdl	bdl	bdl	bdl

Abbreviations: Am = amphibole, bdl = below detection limit. *Note:* all trace element concentrations are in $\mu g\ g^{-1}$.

Table B22. *Continued*

Sample	AVX-16-03-20							
Mineral ID	Am_04	Am_05	Am_06	Am_08	Am_09	Am_10	Am_11	Am_12
Li	1.10	1.05	0.92	0.98	1.06	1.17	1.02	1.07
Be	bdl	0.08	0.09	bdl	0.08	0.05	0.10	0.10
Ti	5952.92	6474.25	6356.12	6062.29	6289.42	6243.80	6622.71	7191.89
V	237.31	270.33	258.85	251.42	252.18	250.50	271.83	311.25
Cr	26.78	29.85	23.80	12.40	26.02	22.72	31.44	615.00
Mn	1804.63	1892.23	1897.27	1950.07	1509.77	2045.04	1610.44	2134.41
Co	28.37	28.80	28.08	28.21	28.99	27.11	29.12	29.42
Ni	489.88	496.78	499.11	461.19	469.44	488.88	531.43	779.38
Cu	0.37	bdl	0.22	0.32	0.19	0.30	0.27	0.30
Zn	84.86	92.70	93.03	88.12	79.61	100.83	78.98	90.80
Rb	0.31	0.37	0.34	0.25	0.24	0.22	0.39	0.24
Sr	88.60	96.56	93.51	71.33	98.47	96.57	112.80	75.66
Y	49.71	48.66	45.17	52.31	48.51	48.66	47.43	66.57
Zr	27.46	23.09	23.34	30.66	26.20	21.98	24.24	33.50
Nb	0.62	0.46	0.45	0.68	0.53	0.45	0.54	0.71
Mo	bdl	bdl	bdl	bdl	bdl	bdl	0.04	bdl
Cs	bdl	bdl	bdl	bdl	bdl	bdl	bdl	bdl
Ba	24.35	23.94	24.90	22.00	25.24	21.15	25.88	26.46
La	1.05	0.82	0.87	1.38	0.79	0.81	0.75	1.51
Ce	6.06	5.12	4.96	7.74	4.81	4.89	4.76	8.80
Pr	1.70	1.51	1.37	2.12	1.50	1.48	1.38	2.29
Nd	12.44	11.60	10.66	13.86	11.87	12.09	10.94	17.76
Sm	6.23	5.99	5.21	6.33	5.63	6.02	5.72	7.87
Eu	1.71	1.72	1.52	1.98	1.85	1.83	1.63	2.29
Gd	7.84	7.88	7.25	8.40	7.56	7.36	7.42	10.37
Tb	1.41	1.38	1.35	1.37	1.39	1.47	1.45	1.88
Dy	9.07	8.99	8.41	9.03	8.68	8.98	8.52	12.14
Ho	1.98	1.94	1.77	2.06	1.85	2.06	1.77	2.71
Er	6.04	5.96	5.17	6.00	5.68	5.56	5.85	8.26
Tm	0.81	0.72	0.66	0.82	0.75	0.79	0.81	1.08
Yb	4.67	4.93	4.58	5.21	4.33	4.60	4.57	6.81
Lu	0.72	0.66	0.55	0.78	0.67	0.65	0.66	0.88
Hf	1.49	1.32	1.38	1.54	1.46	1.36	1.30	1.72
Ta	0.04	0.04	0.02	0.02	0.04	0.03	0.02	0.02
Pb	0.17	0.16	0.20	0.14	0.15	0.18	0.14	0.25
Th	bdl	0.01	bdl	bdl	0.01	bdl	bdl	0.01
U	bdl	bdl	bdl	bdl	bdl	bdl	bdl	0.01

Abbreviations: Am = amphibole, bdl = below detection limit. *Note:* all trace element concentrations are in µg g^{-1}.

Table B22. *Continued*

Sample	AVX-16-03-20							
Mineral ID	Am_14	Am_15	Am_16	Am_19	Am_20	Am_21	Am_22	Am_23
Li	0.99	1.06	1.07	1.00	1.08	0.89	1.03	1.12
Be	bdl	0.02	0.08	0.14	0.07	0.34	0.12	0.31
Ti	6889.97	6619.69	7179.47	6381.19	6736.33	6930.28	7037.79	6695.06
V	280.20	271.81	302.49	276.24	288.17	285.32	292.27	267.39
Cr	19.45	35.01	92.76	127.98	135.32	118.10	89.29	73.88
Mn	1812.38	1604.55	1814.04	1542.28	1562.90	1575.52	1607.99	2359.31
Co	27.16	28.44	26.54	28.23	28.19	28.27	28.69	28.80
Ni	460.15	462.99	390.09	408.28	448.73	430.71	441.93	571.55
Cu	0.25	0.90	0.45	0.27	0.26	0.29	0.31	0.25
Zn	92.23	76.97	90.59	79.16	71.12	73.86	78.46	99.99
Rb	0.40	0.32	0.41	0.44	0.38	0.33	0.41	0.27
Sr	103.00	97.88	106.95	109.98	116.01	108.87	114.15	61.50
Y	41.30	49.61	43.31	42.87	46.08	48.29	47.06	69.82
Zr	19.25	24.32	22.17	24.96	22.94	24.57	22.03	39.20
Nb	0.43	0.57	0.42	0.52	0.47	0.50	0.47	0.94
Mo	bdl	bdl	bdl	bdl	bdl	bdl	bdl	bdl
Cs	bdl	bdl	bdl	bdl	bdl	bdl	bdl	bdl
Ba	28.21	24.27	29.40	27.24	28.44	25.75	27.33	23.07
La	0.74	0.88	0.79	0.79	0.77	0.80	0.74	2.01
Ce	4.00	5.07	4.54	4.68	4.53	4.80	4.67	9.91
Pr	1.16	1.47	1.31	1.36	1.31	1.41	1.46	2.75
Nd	9.89	11.73	9.79	10.82	10.81	11.35	11.37	19.28
Sm	4.70	6.04	5.18	5.14	5.55	5.29	5.55	9.16
Eu	1.62	1.88	1.56	1.57	1.65	1.79	1.79	2.38
Gd	6.91	7.98	7.45	7.11	7.96	8.09	7.95	10.83
Tb	1.30	1.42	1.17	1.24	1.28	1.40	1.34	1.79
Dy	7.82	9.22	8.57	8.28	8.60	9.38	9.29	13.18
Ho	1.73	2.04	1.65	1.76	1.83	1.91	1.98	2.65
Er	4.77	5.62	5.07	5.40	5.19	5.86	5.41	8.44
Tm	0.60	0.79	0.69	0.70	0.75	0.81	0.78	1.17
Yb	3.87	4.72	4.18	4.55	4.17	4.43	4.70	7.17
Lu	0.50	0.67	0.59	0.60	0.57	0.67	0.60	0.91
Hf	1.06	1.48	1.10	1.33	1.30	1.46	1.22	2.10
Ta	0.02	0.03	0.02	0.04	0.03	0.02	0.02	0.03
Pb	0.18	0.20	0.18	0.17	0.17	0.17	0.26	0.19
Th	0.01	0.01	0.01	bdl	bdl	bdl	bdl	0.01
U	bdl	bdl	bdl	bdl	bdl	bdl	bdl	bdl

Abbreviations: Am = amphibole, bdl = below detection limit. *Note:* all trace element concentrations are in $\mu g\ g^{-1}$.

Table B23*. Trace element compositions of phlogopite in Shiveluch and Avachinsky mantle xenoliths*

Sample	SH98X-16							
Mineral ID	Phl_01	Phl_02	Phl_03	Phl_04	Phl_05	Phl_06	Phl_07	Phl_08
Li	4.69	4.51	4.55	5.71	4.49	4.62	4.58	4.26
Be	bdl	bdl	bdl	bdl	bdl	bdl	bdl	bdl
Ti	2750.85	2623.04	2255.50	1066.49	2530.50	2578.97	2652.13	2522.15
V	160.54	165.38	230.66	111.74	150.57	154.20	158.12	151.40
Cr	bdl	396.82	6225.64	2535.37	bdl	bdl	bdl	0.90
Mn	238.04	212.31	208.16	1042.17	227.25	228.26	248.28	231.78
Co	55.02	55.70	56.33	95.20	54.84	54.81	55.21	55.01
Ni	885.80	1193.66	973.37	1250.81	887.64	889.49	857.23	867.62
Cu	40.31	26.08	46.47	15.61	39.21	17.26	105.61	18.43
Zn	39.85	37.17	42.80	65.40	41.37	38.42	39.94	37.95
Rb	224.27	217.51	202.82	101.85	216.33	219.76	213.00	220.38
Sr	23.90	26.52	33.21	14.92	24.11	23.26	27.96	22.30
Y	0.04	bdl	bdl	bdl	0.05	bdl	0.25	bdl
Zr	2.40	3.26	2.06	1.08	2.13	1.98	2.66	2.16
Nb	0.71	0.69	0.49	0.24	0.68	0.67	0.64	0.64
Mo	0.13	0.17	0.14	0.06	0.11	0.13	0.13	0.09
Cs	10.47	8.74	7.38	3.89	9.89	9.99	9.76	5.65
Ba	1030.30	935.57	682.06	313.06	916.63	919.33	951.81	860.24
La	0.05	0.01	0.01	0.01	0.01	0.01	0.12	bdl
Ce	0.13	0.01	0.02	0.02	0.03	0.01	0.30	0.02
Pr	0.01	bdl	bdl	bdl	bdl	bdl	0.05	bdl
Nd	0.05	bdl	bdl	bdl	bdl	bdl	0.23	0.01
Sm	bdl	bdl	bdl	bdl	bdl	bdl	0.03	bdl
Eu	0.02	bdl	bdl	bdl	bdl	bdl	0.02	bdl
Gd	bdl	bdl	bdl	bdl	bdl	bdl	bdl	bdl
Tb	bdl	bdl	bdl	bdl	bdl	bdl	0.01	bdl
Dy	bdl	bdl	bdl	bdl	bdl	bdl	0.04	bdl
Ho	bdl	bdl	bdl	bdl	bdl	bdl	bdl	bdl
Er	bdl	bdl	bdl	bdl	bdl	bdl	0.01	bdl
Tm	bdl	bdl	bdl	bdl	bdl	bdl	bdl	bdl
Yb	bdl	bdl	bdl	bdl	bdl	bdl	0.02	bdl
Lu	bdl	bdl	bdl	bdl	bdl	bdl	bdl	bdl
Hf	0.07	0.10	0.03	0.02	0.06	0.04	0.08	0.07
Ta	0.07	0.07	0.04	0.01	0.06	0.07	0.06	0.06
Pb	0.87	0.92	1.09	0.48	0.91	0.88	0.88	0.80
Th	bdl	bdl	0.01	0.05	bdl	bdl	bdl	0.01
U	0.02	0.03	0.01	0.03	0.02	0.02	0.02	0.02

Abbreviations: Phl = phlogopite, bdl = below detection limit. *Note:* all trace element concentrations are in μg g^{-1}.

***Table B23**. Continued*

Sample	SH98X-16							
Mineral ID	Phl_09	Phl_10	Phl_11	Phl_12	Phl_13	Phl_14	Phl_15	Phl_16
Li	4.67	4.53	4.43	4.41	3.49	4.60	4.99	4.72
Be	bdl	bdl	bdl	bdl	bdl	bdl	bdl	bdl
Ti	1873.85	1785.72	2257.26	2285.47	1835.95	2822.67	3945.64	2419.44
V	151.41	155.60	152.90	155.51	155.51	225.16	259.06	185.87
Cr	480.01	382.56	3.51	7.58	453.84	2321.07	4644.60	1232.50
Mn	199.03	288.67	224.30	226.79	265.71	249.82	273.06	240.62
Co	52.88	54.18	55.74	55.12	60.63	59.99	62.51	57.64
Ni	897.78	946.64	924.51	938.34	1089.51	1177.22	1192.30	1155.87
Cu	63.09	29.39	58.04	77.97	1147.92	142.78	13.15	7.23
Zn	36.72	36.18	38.60	38.60	39.58	53.94	58.87	50.57
Rb	212.51	206.25	214.96	219.27	135.83	216.73	229.19	220.94
Sr	24.46	25.69	25.09	26.11	46.47	30.71	29.66	31.45
Y	0.03	0.03	bdl	0.03	0.52	0.07	bdl	0.10
Zr	2.16	2.23	1.93	2.07	1.79	1.61	1.54	1.87
Nb	0.50	0.52	0.62	0.60	0.47	0.45	0.53	0.51
Mo	0.13	0.14	0.14	0.13	0.13	0.07	0.10	bdl
Cs	8.76	9.81	9.66	7.68	6.04	8.17	8.61	14.76
Ba	716.34	820.09	836.33	864.30	433.50	1045.67	1090.06	955.42
La	0.03	0.01	0.03	0.03	1.18	0.09	bdl	0.01
Ce	0.05	0.03	0.03	0.05	1.97	0.12	bdl	0.07
Pr	bdl	bdl	bdl	bdl	0.18	0.01	bdl	0.02
Nd	0.02	bdl	bdl	bdl	0.79	0.06	bdl	0.07
Sm	bdl	bdl	bdl	bdl	0.06	bdl	bdl	0.02
Eu	bdl	bdl	0.01	bdl	0.03	bdl	0.01	bdl
Gd	bdl	bdl	bdl	bdl	0.15	bdl	bdl	bdl
Tb	bdl	bdl	bdl	bdl	bdl	bdl	bdl	bdl
Dy	bdl	bdl	bdl	bdl	0.02	bdl	bdl	bdl
Ho	bdl	bdl	bdl	bdl	bdl	bdl	bdl	bdl
Er	bdl	bdl	bdl	bdl	0.02	bdl	bdl	bdl
Tm	bdl	bdl	bdl	bdl	bdl	bdl	bdl	bdl
Yb	bdl	bdl	bdl	bdl	bdl	bdl	bdl	bdl
Lu	bdl	bdl	bdl	bdl	0.01	bdl	bdl	bdl
Hf	0.11	0.09	0.07	0.07	0.08	0.04	0.02	0.09
Ta	0.04	0.05	0.05	0.05	0.04	0.04	0.04	0.05
Pb	0.93	1.05	0.96	0.91	3.27	1.71	1.28	1.24
Th	bdl	0.01	bdl	bdl	bdl	bdl	bdl	bdl
U	0.02	0.03	0.02	0.03	0.03	0.02	0.01	0.01

Abbreviations: Phl = phlogopite, bdl = below detection limit. *Note:* all trace element concentrations are in $\mu g\ g^{-1}$.

Table B23. *Continued*

Sample	SH98X-16						
Mineral ID	Phl_17	Phl_18	Phl_19	Phl_20	Phl_21	Phl_22	Phl_23
Li	5.03	4.45	5.35	5.51	3.97	4.18	3.65
Be	bdl	0.02	bdl	bdl	bdl	0.02	bdl
Ti	2300.45	2027.22	2327.78	2355.10	2981.77	2494.36	1329.15
V	163.89	163.89	165.57	172.27	250.58	191.27	107.37
Cr	4.39	5.86	bdl	bdl	6137.22	2079.72	918.51
Mn	236.66	249.29	255.01	232.23	196.91	249.94	841.11
Co	56.61	58.48	58.95	59.14	56.33	58.76	67.36
Ni	956.77	975.21	824.04	817.59	989.96	1023.14	918.06
Cu	9.19	270.72	73.28	7.49	103.68	172.65	99.36
Zn	43.06	53.25	49.85	49.76	37.52	35.92	47.44
Rb	224.95	198.80	212.61	218.88	214.86	212.12	105.57
Sr	27.08	33.05	23.34	19.27	34.21	31.17	15.57
Y	bdl	0.15	0.09	bdl	0.05	0.05	0.10
Zr	1.88	1.69	1.68	1.84	1.29	1.21	0.69
Nb	0.55	0.58	0.55	0.68	0.51	0.45	0.25
Mo	0.13	0.06	0.15	0.14	0.12	0.18	0.09
Cs	12.29	12.84	9.89	7.96	5.41	3.51	1.68
Ba	955.42	757.84	1220.67	1409.22	750.62	666.72	334.71
La	bdl	0.34	0.10	bdl	0.05	0.04	0.06
Ce	bdl	0.80	0.13	0.01	0.06	0.06	0.11
Pr	bdl	0.04	0.02	bdl	0.01	bdl	0.01
Nd	bdl	0.14	0.07	bdl	0.03	0.01	0.04
Sm	bdl	bdl	0.03	bdl	bdl	bdl	bdl
Eu	0.01	0.02	0.02	bdl	bdl	0.01	bdl
Gd	bdl	bdl	bdl	bdl	bdl	bdl	bdl
Tb	bdl	bdl	bdl	bdl	bdl	bdl	bdl
Dy	bdl	bdl	bdl	bdl	bdl	bdl	bdl
Ho	bdl	bdl	bdl	bdl	bdl	bdl	bdl
Er	bdl	bdl	bdl	bdl	bdl	bdl	bdl
Tm	bdl	bdl	bdl	bdl	bdl	bdl	bdl
Yb	bdl	bdl	bdl	bdl	bdl	bdl	bdl
Lu	bdl	bdl	bdl	bdl	bdl	bdl	bdl
Hf	0.03	0.03	0.04	0.03	0.02	0.04	0.01
Ta	0.04	0.04	0.06	0.07	0.03	0.02	0.02
Pb	1.08	1.15	1.21	1.25	1.08	0.92	0.53
Th	bdl	bdl	bdl	bdl	bdl	0.01	0.02
U	0.01	0.01	0.02	0.02	0.03	0.03	0.02

Abbreviations: Phl = phlogopite, bdl = below detection limit. *Note:* all trace element concentrations are in µg g^{-1}.

Table B23. *Continued*

Sample	SHIV-16-12-06							
Mineral ID	Phl_01	Phl_02	Phl_03	Phl_04	Phl_05	Phl_06	Phl_07	Phl_08
Li	2.58	2.56	3.18	2.22	3.57	2.09	2.25	2.64
Be	0.13	bdl	bdl	0.53	bdl	bdl	0.43	0.19
Ti	3121.36	3563.48	3622.55	3234.74	2024.39	3693.06	3296.43	3009.02
V	56.14	58.11	53.26	51.59	27.13	54.29	51.31	56.58
Cr	189.72	157.50	118.20	630.68	24.56	178.65	330.23	299.43
Mn	169.97	160.07	145.63	112.15	769.86	140.83	250.86	155.35
Co	56.14	59.23	56.33	49.61	119.10	60.44	55.77	62.57
Ni	836.87	871.08	803.76	756.76	1315.01	919.90	836.95	950.96
Cu	98.12	90.93	62.45	40.50	6.23	2.93	17.17	7.59
Zn	35.58	31.19	28.32	23.94	54.33	24.48	26.98	24.10
Rb	85.97	85.28	88.63	81.77	44.59	103.61	77.56	99.86
Sr	92.87	101.77	94.55	262.59	41.67	107.68	159.63	108.91
Y	0.29	0.26	0.23	0.17	0.05	bdl	0.11	bdl
Zr	23.62	17.26	24.99	23.36	8.70	27.34	24.54	33.50
Nb	12.03	11.90	10.32	9.01	3.26	10.52	9.17	13.00
Mo	0.48	0.97	0.38	0.71	0.42	0.28	1.27	0.82
Cs	2.39	2.69	2.09	1.96	0.71	2.24	1.99	2.92
Ba	1345.88	1603.83	1676.27	1828.74	821.56	2116.54	1596.88	1555.83
La	1.37	1.74	1.04	1.52	0.15	0.02	0.81	0.17
Ce	1.39	2.07	1.26	1.97	0.17	bdl	0.83	0.11
Pr	0.11	0.16	0.09	0.12	bdl	bdl	0.07	0.01
Nd	0.26	0.50	0.42	0.34	bdl	bdl	0.05	0.05
Sm	bdl	bdl	0.03	bdl	bdl	bdl	0.15	bdl
Eu	bdl	0.11	0.08	0.12	0.04	0.05	0.05	bdl
Gd	bdl	bdl	bdl	bdl	bdl	bdl	bdl	bdl
Tb	bdl	0.01	0.01	bdl	bdl	bdl	bdl	bdl
Dy	bdl	bdl	bdl	bdl	bdl	bdl	bdl	bdl
Ho	0.01	bdl	bdl	bdl	bdl	bdl	bdl	bdl
Er	bdl	0.01	bdl	bdl	bdl	bdl	0.01	bdl
Tm	0.01	bdl	bdl	bdl	bdl	bdl	bdl	bdl
Yb	bdl	bdl	bdl	0.03	bdl	bdl	bdl	bdl
Lu	bdl	bdl	0.02	bdl	bdl	bdl	bdl	bdl
Hf	0.37	0.31	0.46	0.39	0.09	0.35	0.42	0.55
Ta	0.60	0.63	0.50	0.41	0.18	0.51	0.51	0.78
Pb	6.25	6.16	6.15	6.56	2.59	7.15	6.03	6.72
Th	0.01	bdl	bdl	bdl	0.04	bdl	0.04	bdl
U	0.04	0.07	0.04	0.05	0.04	0.06	0.08	0.08

Abbreviations: Phl = phlogopite, bdl = below detection limit. *Note:* all trace element concentrations are in $\mu g\ g^{-1}$.

Table B23. *Continued*

Sample	SHIV-16-12-06			SHX03-17				
Mineral ID	Phl_09	Phl_10	Phl_11	Phl_01	Phl_02	Phl_03	Phl_04	Phl_05
Li	2.77	2.99	3.99	3.59	5.03	5.63	6.15	5.59
Be	0.33	0.15	0.32	84600.00	0.08	0.02	bdl	bdl
Ti	3093.71	3628.88	4177.83	41.47	501.52	434.53	485.65	497.99
V	60.43	59.67	61.09	9.10	27.45	21.73	25.13	26.24
Cr	2010.25	345.65	195.79	0.21	966.33	95.28	29.77	775.95
Mn	196.44	147.88	163.52	9.64	245.69	379.05	182.89	172.56
Co	61.47	61.71	63.71	0.59	71.56	71.37	75.86	74.18
Ni	926.36	954.67	918.06	3.38	1451.75	1331.93	1502.45	1531.95
Cu	8.72	3.08	16.53	7.37	8.63	3.84	5.79	13.96
Zn	26.00	22.14	23.32	25.04	52.62	50.12	43.78	39.67
Rb	96.37	107.33	105.18	20.64	159.24	164.23	171.28	184.80
Sr	103.81	121.15	138.19	1.21	26.73	10.45	26.73	27.80
Y	bdl	0.04	0.07	0.29	2.65	0.05	0.06	bdl
Zr	34.41	33.97	35.85	0.30	10.33	5.77	8.04	7.98
Nb	14.36	11.41	11.48	0.11	2.31	2.19	2.52	2.58
Mo	2.73	0.44	0.60	0.11	0.15	0.12	0.20	0.13
Cs	3.89	2.29	2.34	0.13	1.63	2.19	1.72	2.33
Ba	1700.63	2072.81	2232.92	bdl	1068.19	1055.56	1045.64	1116.01
La	0.09	0.04	0.25	bdl	1.04	0.03	0.05	0.07
Ce	0.09	0.02	0.21	bdl	4.62	0.05	0.11	0.06
Pr	0.02	bdl	0.01	bdl	0.90	bdl	0.02	0.01
Nd	bdl	bdl	0.05	bdl	4.19	bdl	0.11	0.01
Sm	bdl	bdl	0.07	bdl	0.97	bdl	bdl	bdl
Eu	0.05	0.05	0.09	bdl	0.21	0.02	0.03	0.03
Gd	bdl	bdl	bdl	bdl	0.56	bdl	bdl	bdl
Tb	bdl	bdl	bdl	bdl	0.08	bdl	bdl	bdl
Dy	bdl	bdl	bdl	bdl	0.44	bdl	0.01	bdl
Ho	bdl	bdl	bdl	bdl	0.11	bdl	bdl	bdl
Er	bdl	bdl	bdl	bdl	0.19	bdl	bdl	bdl
Tm	bdl	bdl	bdl	bdl	0.04	bdl	bdl	bdl
Yb	bdl	bdl	bdl	bdl	0.19	bdl	0.01	bdl
Lu	bdl	bdl	bdl	bdl	0.03	bdl	bdl	0.01
Hf	0.85	0.52	0.57	bdl	0.58	0.32	0.50	0.41
Ta	0.98	0.59	0.66	bdl	0.23	0.18	0.24	0.23
Pb	7.03	7.28	7.91	bdl	0.66	0.53	0.69	0.70
Th	0.01	bdl	0.02	bdl	0.09	0.04	0.01	0.01
U	0.07	0.07	0.08	bdl	0.03	0.03	0.03	0.03

Abbreviations: Phl = phlogopite, bdl = below detection limit. *Note:* all trace element concentrations are in $\mu g\ g^{-1}$.

Table B23. *Continued*

Sample	SHX03-17							
Mineral ID	Phl_06	Phl_07	Phl_08	Phl_09	Phl_10	Phl_11	Phl_12	Phl_13
Li	5.78	6.06	6.27	5.48	6.42	5.60	5.66	6.25
Be	bdl	bdl	bdl	0.04	0.07	0.18	0.10	0.05
Ti	517.38	458.57	496.15	557.04	587.89	536.77	529.72	584.37
V	28.57	25.19	25.78	30.10	29.03	27.15	26.86	30.02
Cr	1576.26	28.95	214.79	110.71	3774.18	103.22	298.20	71.10
Mn	172.10	170.00	216.39	166.93	168.04	296.97	225.03	174.59
Co	76.79	72.62	74.41	75.11	75.67	80.44	71.28	76.98
Ni	1648.09	1574.90	1578.86	1705.23	1726.43	1704.31	1541.16	1652.69
Cu	14.79	4.55	4.15	13.77	8.26	23.51	2.64	3.54
Zn	30.56	44.49	44.53	26.18	39.94	28.14	46.46	48.51
Rb	158.06	187.25	185.60	159.53	185.00	147.49	180.00	192.63
Sr	36.65	13.04	12.55	36.46	22.58	37.71	9.75	14.47
Y	bdl	0.03	bdl	bdl	bdl	0.02	0.92	bdl
Zr	8.09	8.01	8.54	10.50	9.38	9.19	7.24	6.37
Nb	2.75	2.73	2.67	2.78	2.73	2.51	2.40	2.64
Mo	0.17	0.15	0.12	0.21	0.18	0.15	0.17	0.15
Cs	2.03	1.77	1.86	2.20	1.98	1.87	1.76	1.83
Ba	1091.65	1102.24	1080.21	997.82	1160.22	950.01	1063.68	1108.79
La	0.07	0.04	0.01	0.08	0.02	0.09	0.20	0.01
Ce	0.05	0.05	0.01	0.07	0.03	0.25	0.94	0.01
Pr	0.01	bdl	0.01	0.01	bdl	0.03	0.20	bdl
Nd	0.06	0.02	0.02	bdl	0.02	0.02	1.02	0.03
Sm	bdl	0.01	bdl	bdl	bdl	bdl	0.25	bdl
Eu	bdl	0.03	0.02	bdl	0.03	0.03	0.07	bdl
Gd	bdl	bdl	bdl	bdl	bdl	bdl	bdl	bdl
Tb	bdl	bdl	bdl	bdl	bdl	bdl	0.03	bdl
Dy	bdl	bdl	bdl	bdl	bdl	0.01	0.18	bdl
Ho	bdl	bdl	bdl	bdl	bdl	bdl	0.03	bdl
Er	bdl	bdl	bdl	bdl	bdl	bdl	0.07	bdl
Tm	bdl	bdl	bdl	bdl	bdl	bdl	bdl	bdl
Yb	bdl	bdl	bdl	bdl	bdl	bdl	0.05	bdl
Lu	bdl	bdl	bdl	bdl	bdl	bdl	0.01	bdl
Hf	0.41	0.57	0.56	0.69	0.60	0.63	0.57	0.48
Ta	0.25	0.27	0.25	0.23	0.23	0.21	0.25	0.26
Pb	0.68	0.61	0.64	0.54	0.68	1.29	0.61	0.67
Th	0.03	0.01	0.01	0.02	0.02	0.02	0.03	0.01
U	0.03	0.03	0.04	0.04	0.03	0.06	0.04	0.04

Abbreviations: Phl = phlogopite, bdl = below detection limit. *Note:* all trace element concentrations are in $\mu g\ g^{-1}$.

Table B23. *Continued*

Sample	SHX03-17			SHX03-18				
Mineral ID	Phl_14	Phl_15	Phl_16	Phl_01	Phl_02	Phl_03	Phl_04	Phl_05
Li	5.55	5.13	5.42	8.12	9.39	9.54	9.02	10.15
Be	0.16	0.04	0.15	bdl	0.02	bdl	0.07	0.02
Ti	545.36	475.96	515.62	6716.38	7368.50	6829.96	7685.24	6960.85
V	30.24	25.79	27.38	256.79	260.92	263.34	291.58	252.40
Cr	56.73	65.50	67.40	37.40	49.35	42.77	23.21	32.72
Mn	172.03	413.18	249.38	204.68	223.65	214.61	213.54	234.72
Co	73.33	72.59	70.53	78.61	76.70	75.95	74.94	74.45
Ni	1648.21	1423.18	1518.12	617.05	544.75	543.00	554.81	485.93
Cu	3.82	4.45	5.99	27.54	22.68	21.40	9.94	18.86
Zn	44.72	55.84	45.92	79.09	89.25	86.39	88.08	103.05
Rb	184.53	153.75	159.43	147.07	189.60	195.67	200.78	209.82
Sr	15.71	9.61	13.20	84.30	40.05	33.95	37.15	53.56
Y	bdl	0.40	5.51	0.65	0.25	0.25	0.25	0.21
Zr	6.51	6.17	13.40	8.32	7.80	8.62	9.05	7.55
Nb	2.55	2.19	2.37	2.45	2.59	2.49	2.59	2.45
Mo	0.25	0.16	0.20	0.28	0.21	0.24	0.24	0.18
Cs	1.84	1.68	1.72	3.24	4.52	3.44	3.78	3.34
Ba	1075.80	1013.16	914.82	3438.82	2138.19	2133.68	2307.69	2833.43
La	0.06	0.01	1.50	2.95	0.68	0.37	0.29	0.66
Ce	0.10	0.03	7.35	5.47	1.78	1.02	0.80	1.20
Pr	0.01	bdl	1.53	0.71	0.28	0.16	0.13	0.16
Nd	bdl	0.02	7.39	3.26	1.48	0.86	0.71	0.73
Sm	bdl	bdl	1.79	0.44	0.24	0.10	0.07	0.07
Eu	0.03	0.03	0.42	0.16	0.08	0.07	0.10	0.07
Gd	bdl	bdl	1.13	0.27	0.12	bdl	0.11	bdl
Tb	bdl	0.01	0.16	0.03	0.01	0.01	bdl	bdl
Dy	bdl	0.07	0.89	0.08	0.02	0.01	0.05	0.03
Ho	bdl	bdl	0.21	0.04	bdl	0.01	0.01	bdl
Er	0.01	0.05	0.48	0.06	bdl	0.03	0.03	0.01
Tm	bdl	0.01	0.08	0.02	bdl	bdl	bdl	bdl
Yb	bdl	0.08	0.35	0.05	bdl	bdl	0.02	bdl
Lu	bdl	0.01	0.08	0.01	bdl	bdl	bdl	bdl
Hf	0.57	0.42	0.94	0.35	0.37	0.40	0.52	0.31
Ta	0.22	0.20	0.20	0.21	0.22	0.22	0.23	0.24
Pb	0.70	0.59	0.65	2.26	1.54	1.48	1.69	2.23
Th	0.01	0.02	0.10	0.01	0.01	0.01	bdl	bdl
U	0.03	0.02	0.06	0.01	0.01	0.01	0.01	0.01

Abbreviations: Phl = phlogopite, bdl = below detection limit. *Note:* all trace element concentrations are in μg g^{-1}.

Table B23. *Continued*

Sample	SHX03-18							
Mineral ID	Phl_06	Phl_07	Phl_08	Phl_09	Phl_10	Phl_11	Phl_12	Phl_13
Li	11.52	8.97	9.26	9.68	11.30	9.51	8.83	8.31
Be	bdl	bdl	bdl	0.08	bdl	bdl	bdl	0.05
Ti	8239.42	7342.06	8616.46	7474.27	6222.68	6602.85	8364.48	9757.09
V	307.57	220.13	311.05	304.68	250.49	259.15	312.32	321.73
Cr	15.53	12.00	26.70	13.99	9.38	6.30	37.35	44.12
Mn	201.35	259.25	226.55	240.34	229.74	280.15	276.22	250.67
Co	74.02	73.43	74.29	70.91	71.37	76.52	76.23	78.29
Ni	1064.08	425.11	515.12	415.34	525.58	420.62	513.14	888.57
Cu	66.41	2.62	6.31	25.16	60.06	16.70	5.43	17.32
Zn	83.87	110.70	92.86	102.03	99.80	132.08	123.38	94.35
Rb	203.64	187.05	221.24	203.60	208.50	207.21	205.76	204.09
Sr	28.81	34.50	37.43	54.79	31.13	48.40	47.89	35.42
Y	0.91	0.05	0.05	0.60	0.64	0.12	0.21	0.15
Zr	8.60	4.51	9.97	10.61	7.50	13.47	8.58	5.00
Nb	2.94	2.28	2.75	2.73	2.33	2.79	2.86	3.23
Mo	0.18	0.24	0.26	0.16	0.22	0.14	0.18	0.18
Cs	3.78	2.59	3.71	3.53	3.31	4.75	3.07	4.10
Ba	2238.30	2489.15	2281.80	2054.29	2010.08	2467.15	2349.31	2612.75
La	2.22	0.04	0.04	1.51	0.97	0.24	0.08	0.33
Ce	6.62	0.09	0.14	3.86	2.76	0.71	0.28	0.82
Pr	1.05	0.02	0.02	0.64	0.43	0.11	0.06	0.11
Nd	5.05	0.07	0.14	3.11	2.13	0.52	0.21	0.77
Sm	0.92	bdl	0.02	0.57	0.45	0.10	0.05	0.13
Eu	0.22	0.06	0.05	0.14	0.13	0.06	0.05	0.06
Gd	0.64	bdl	bdl	0.40	0.27	bdl	bdl	bdl
Tb	0.04	bdl	bdl	0.03	0.04	0.01	0.01	0.01
Dy	0.22	bdl	bdl	0.12	0.13	0.02	0.03	0.03
Ho	0.03	bdl	bdl	0.03	0.02	bdl	bdl	0.01
Er	0.10	0.01	bdl	0.07	0.07	0.01	0.02	0.01
Tm	0.01	bdl	bdl	0.01	0.01	bdl	bdl	bdl
Yb	0.05	bdl	bdl	0.08	0.04	bdl	0.02	bdl
Lu	0.01	0.01	bdl	0.01	0.01	bdl	bdl	0.01
Hf	0.41	0.15	0.52	0.55	0.32	0.52	0.39	0.22
Ta	0.20	0.18	0.26	0.23	0.19	0.20	0.26	0.21
Pb	1.36	1.42	1.62	1.53	1.32	1.95	1.88	1.64
Th	bdl	bdl	0.01	0.01	0.01	bdl	0.01	bdl
U	0.01	0.02	0.02	0.03	0.02	0.02	0.02	0.01

Abbreviations: Phl = phlogopite, bdl = below detection limit. *Note:* all trace element concentrations are in $\mu g\ g^{-1}$.

Table B23. *Continued*

Sample	SHX03-18	
Mineral ID	Phl_14	Phl_15
Li	8.95	7.85
Be	bdl	bdl
Ti	8197.01	7201.03
V	268.18	323.12
Cr	34.29	24.45
Mn	241.73	171.36
Co	71.00	70.81
Ni	560.42	906.08
Cu	11.26	9.46
Zn	93.27	64.51
Rb	190.19	188.13
Sr	53.94	55.73
Y	0.14	0.08
Zr	8.29	9.22
Nb	2.48	2.84
Mo	0.23	0.27
Cs	4.42	3.42
Ba	1977.60	2227.51
La	0.32	0.35
Ce	0.79	0.82
Pr	0.08	0.10
Nd	0.45	0.38
Sm	0.12	0.05
Eu	0.07	0.06
Gd	bdl	bdl
Tb	bdl	bdl
Dy	0.04	bdl
Ho	0.01	bdl
Er	0.04	0.01
Tm	bdl	bdl
Yb	0.01	bdl
Lu	bdl	bdl
Hf	0.35	0.36
Ta	0.22	0.23
Pb	1.52	1.40
Th	0.02	0.01
U	0.01	0.01

Abbreviations: Phl = phlogopite, bdl = below detection limit. *Note:* all trace element concentrations are in µg g^{-1}.

Table B24. *Trace element compositions of clinopyroxene in Shiveluch and Avachinsky mantle xenoliths*

Sample	AVX-16-03-24							
Mineral ID	Cpx_01	Cpx_02	Cpx_03	Cpx_04	Cpx_05	Cpx_06	Cpx_07	Cpx_08
Li	1.36	1.17	1.84	1.77	1.08	1.13	1.35	1.17
Be	bdl	bdl	bdl	bdl	bdl	bdl	bdl	bdl
Ti	69.28	213.47	231.19	333.73	51.75	74.00	220.55	108.99
V	121.33	261.38	292.86	340.09	118.75	139.56	319.48	209.05
Cr	278.62	397.90	450.23	489.86	339.50	341.35	443.11	557.81
Mn	700.93	776.55	761.80	752.00	681.25	610.39	857.00	557.47
Co	22.09	27.76	28.96	28.17	23.71	23.34	31.55	25.39
Ni	329.06	362.25	416.63	430.26	344.56	423.17	485.72	503.56
Cu	0.77	1.53	1.08	0.61	0.73	0.60	1.14	3.23
Zn	9.47	11.17	12.33	10.83	9.96	10.19	12.87	11.48
Rb	bdl	bdl	bdl	bdl	bdl	bdl	bdl	0.09
Sr	17.26	11.02	8.58	8.80	26.84	22.38	8.93	26.33
Y	0.70	1.54	2.16	2.86	0.75	1.03	2.21	1.39
Zr	0.51	1.58	2.14	3.73	0.73	0.49	1.79	1.09
Nb	bdl	bdl	bdl	bdl	bdl	bdl	bdl	bdl
Mo	bdl	bdl	bdl	bdl	bdl	bdl	bdl	bdl
Cs	bdl	bdl	bdl	bdl	bdl	bdl	bdl	bdl
Ba	0.17	0.85	0.04	0.04	0.24	0.18	0.08	2.11
La	0.05	0.07	0.09	0.13	0.06	0.04	0.09	0.06
Ce	0.10	0.23	0.26	0.42	0.16	0.10	0.27	0.19
Pr	0.01	0.04	0.07	0.07	0.02	0.01	0.06	0.02
Nd	0.04	0.29	0.41	0.44	0.09	0.10	0.31	0.30
Sm	bdl	0.11	0.09	0.19	bdl	0.07	0.15	0.12
Eu	0.02	0.04	0.06	0.06	0.02	0.04	0.06	0.02
Gd	bdl	0.21	0.27	0.36	bdl	0.10	0.26	0.21
Tb	0.01	0.04	0.05	0.06	0.02	0.03	0.06	0.03
Dy	0.12	0.30	0.40	0.46	0.10	0.18	0.33	0.26
Ho	0.03	0.07	0.09	0.12	0.02	0.04	0.10	0.06
Er	0.11	0.23	0.28	0.29	0.10	0.15	0.30	0.20
Tm	0.02	0.03	0.05	0.06	0.02	0.02	0.04	0.03
Yb	0.16	0.23	0.30	0.40	0.08	0.16	0.31	0.18
Lu	0.03	0.04	0.05	0.06	0.02	0.02	0.04	0.03
Hf	0.02	0.06	0.08	0.18	0.03	0.02	0.08	0.06
Ta	bdl	bdl	bdl	bdl	bdl	bdl	bdl	bdl
Pb	0.07	0.12	0.07	0.06	0.11	0.08	0.08	0.10
Th	bdl	bdl	bdl	bdl	bdl	bdl	0.02	bdl
U	bdl	bdl	bdl	bdl	bdl	bdl	0.01	bdl

Abbreviations: Cpx = clinopyroxene, bdl = below detection limit. *Note:* all trace element concentrations are in μg g^{-1}.

Table B24. *Continued*

Sample	AVX-16-03-24	AVX-16-03-20	BAK-16-22-04				
Mineral ID	Cpx_09	Cpx	Cpx_01	Cpx_02	Cpx_03	Cpx_05	Cpx_06
Li	1.11	1.18	6.13	6.98	13.30	14.12	30.86
Be	bdl	0.05	0.32	0.21	0.10	0.26	0.41
Ti	69.79	1357.37	1829.97	1900.50	1807.99	1691.67	1816.23
V	178.85	113.33	226.08	215.53	214.85	202.27	207.11
Cr	537.46	17.21	6799.23	5032.35	5670.65	3996.28	5050.85
Mn	565.03	2227.06	875.90	855.11	845.66	835.27	839.99
Co	21.21	16.80	34.37	28.09	28.00	25.12	24.55
Ni	369.54	200.43	317.20	279.54	282.51	258.52	256.64
Cu	0.64	0.14	4.97	6.52	10.85	3.00	4.47
Zn	8.96	42.69	48.00	23.34	28.84	10.95	12.24
Rb	bdl	bdl	bdl	0.07	bdl	bdl	bdl
Sr	26.03	21.88	42.79	53.26	47.61	46.94	49.51
Y	1.37	17.69	7.90	8.51	8.25	8.14	8.67
Zr	0.99	9.25	7.52	7.85	9.42	7.94	9.08
Nb	bdl	bdl	0.05	0.19	0.07	0.05	0.06
Mo	bdl	bdl	0.03	bdl	bdl	bdl	bdl
Cs	bdl	bdl	bdl	bdl	bdl	bdl	bdl
Ba	bdl	bdl	0.07	2.65	0.29	bdl	bdl
La	0.07	0.33	2.87	3.32	3.02	3.02	3.73
Ce	0.13	2.15	5.19	5.87	5.73	5.87	6.56
Pr	0.03	0.64	0.68	0.70	0.72	0.64	0.75
Nd	0.16	5.14	2.67	3.02	2.97	3.11	3.12
Sm	0.06	2.29	0.90	1.20	0.94	1.12	1.07
Eu	0.03	0.71	0.33	0.37	0.40	0.37	0.38
Gd	0.15	2.82	1.40	1.36	1.36	1.31	1.34
Tb	0.03	0.56	0.23	0.26	0.25	0.21	0.25
Dy	0.23	3.53	1.48	1.60	1.32	1.51	1.64
Ho	0.05	0.78	0.30	0.34	0.34	0.33	0.37
Er	0.19	2.03	1.09	1.10	0.87	0.98	1.09
Tm	0.03	0.31	0.14	0.12	0.16	0.14	0.15
Yb	0.18	1.96	1.01	0.96	0.97	0.95	0.92
Lu	0.02	0.26	0.16	0.15	0.15	0.16	0.15
Hf	0.04	0.53	0.35	0.34	0.38	0.32	0.42
Ta	bdl	bdl	bdl	0.01	0.01	bdl	0.01
Pb	0.10	0.03	0.13	0.17	0.14	0.13	0.18
Th	bdl	bdl	0.34	0.44	0.35	0.32	0.46
U	bdl	bdl	0.15	0.16	0.16	0.15	0.20

Abbreviations: Cpx = clinopyroxene, bdl = below detection limit. *Note:* all trace element concentrations are in $\mu g\ g^{-1}$.

Table B24. *Continued*

Sample	BAK-16-22-04				BAK-16-22-03			
Mineral ID	Cpx_07	Cpx_08	Cpx_09	Cpx_10	Cpx_01	Cpx_02	Cpx_03	Cpx_04
Li	38.57	19.38	15.95	27.77	10.43	20.27	41.47	36.71
Be	0.50	0.42	0.56	0.49	bdl	0.07	bdl	bdl
Ti	1865.69	1597.33	1745.71	1684.34	1359.32	1495.70	1623.16	1606.23
V	221.05	204.60	204.69	209.05	252.14	277.60	296.06	297.34
Cr	4838.09	3802.02	4013.86	3552.25	6908.72	4806.45	5147.85	3782.28
Mn	850.38	816.37	843.77	837.16	bdl	bdl	bdl	bdl
Co	26.06	24.91	24.46	24.14	28.09	31.87	27.62	28.10
Ni	263.48	259.61	257.03	253.96	258.12	259.26	235.33	245.30
Cu	5.82	3.25	5.50	4.40	4.40	8.16	4.17	17.71
Zn	15.29	11.75	12.57	11.84	14.47	24.05	15.45	14.56
Rb	bdl	bdl	bdl	bdl	bdl	bdl	bdl	bdl
Sr	46.15	58.21	59.89	61.76	38.39	45.36	53.51	54.99
Y	8.83	7.97	9.16	8.73	6.89	8.52	11.41	11.03
Zr	10.59	8.87	11.95	13.49	5.02	10.36	36.82	32.79
Nb	0.10	0.07	0.10	0.08	0.03	0.07	0.15	0.12
Mo	bdl	bdl	bdl	bdl	bdl	bdl	bdl	bdl
Cs	bdl	bdl	bdl	bdl	bdl	bdl	bdl	bdl
Ba	bdl	bdl	0.05	bdl	bdl	bdl	0.44	0.20
La	3.82	3.75	4.69	4.33	0.54	1.39	2.12	2.13
Ce	6.81	6.55	7.98	7.93	1.60	4.25	7.60	7.36
Pr	0.73	0.70	0.90	0.98	0.31	0.76	1.55	1.46
Nd	3.38	3.39	3.92	3.89	1.96	3.80	8.75	8.17
Sm	1.10	0.97	1.34	0.90	0.86	1.19	2.53	2.27
Eu	0.36	0.35	0.38	0.40	0.38	0.47	0.85	0.75
Gd	1.32	1.30	1.46	1.40	1.47	1.48	2.43	2.38
Tb	0.28	0.27	0.29	0.26	0.21	0.24	0.39	0.35
Dy	1.69	1.58	1.66	1.72	1.44	1.57	2.41	2.27
Ho	0.36	0.36	0.38	0.36	0.30	0.33	0.47	0.47
Er	1.02	0.98	1.17	1.10	0.87	0.93	1.28	1.20
Tm	0.15	0.14	0.15	0.14	0.09	0.13	0.19	0.15
Yb	1.08	1.02	1.05	1.17	0.78	0.90	1.16	0.94
Lu	0.13	0.13	0.16	0.14	0.10	0.10	0.14	0.17
Hf	0.37	0.39	0.42	0.40	0.23	0.33	0.49	0.62
Ta	0.01	bdl	0.01	0.01	0.01	0.01	0.02	0.02
Pb	0.19	0.18	0.17	0.17	0.05	0.07	0.09	0.11
Th	0.47	0.43	0.57	0.46	0.04	0.10	0.15	0.19
U	0.22	0.16	0.22	0.16	0.03	0.03	0.04	0.04

Abbreviations: Cpx = clinopyroxene, bdl = below detection limit. *Note:* all trace element concentrations are in µg g^{-1}.

Table B24. *Continued*

Sample	BAK-16-22-03							
Mineral ID	Cpx_05	Cpx_06	Cpx_07	Cpx_08	Cpx_09	Cpx_10	Cpx_11	Cpx_12
Li	63.49	45.40	43.74	53.88	46.64	45.91	35.99	45.19
Be	0.09	0.15	0.14	0.10	0.09	0.14	0.13	0.20
Ti	1983.27	2176.70	1834.42	1772.91	1932.47	1866.51	1591.97	1943.16
V	325.37	352.31	300.79	308.79	337.50	323.69	278.69	342.44
Cr	5246.67	4887.31	4905.28	4662.71	4465.06	3970.94	5147.85	5632.98
Mn	bdl	bdl	bdl	bdl	bdl	bdl	bdl	bdl
Co	26.85	27.45	28.87	27.86	26.75	28.78	29.65	28.49
Ni	227.92	230.77	244.25	238.37	234.57	238.56	239.22	238.37
Cu	10.70	13.11	11.59	5.45	11.01	8.65	8.31	6.10
Zn	15.05	14.62	15.91	14.74	15.11	14.74	14.83	15.11
Rb	bdl	bdl	bdl	bdl	bdl	bdl	bdl	bdl
Sr	50.47	41.44	50.86	44.58	37.90	36.72	46.64	44.38
Y	11.92	11.22	12.29	10.55	10.13	9.67	9.81	10.45
Zr	30.72	16.18	34.90	22.06	10.25	11.53	19.61	18.86
Nb	0.19	0.13	0.15	0.09	0.07	0.06	0.11	0.14
Mo	0.07	bdl	bdl	bdl	bdl	bdl	bdl	bdl
Cs	bdl	bdl	bdl	bdl	bdl	bdl	bdl	bdl
Ba	0.09	bdl	bdl	bdl	bdl	bdl	bdl	bdl
La	2.22	1.55	1.77	1.43	1.16	1.23	1.50	1.45
Ce	7.52	5.82	6.89	5.64	3.88	3.86	6.04	5.75
Pr	1.48	1.09	1.40	1.03	0.65	0.72	1.09	1.08
Nd	8.28	5.53	8.44	5.36	3.92	3.67	6.47	5.79
Sm	2.30	1.77	2.54	1.60	1.37	1.25	1.71	1.70
Eu	0.83	0.56	0.84	0.61	0.45	0.52	0.59	0.63
Gd	2.64	2.05	2.63	2.04	1.69	1.65	1.96	2.20
Tb	0.41	0.36	0.41	0.36	0.30	0.27	0.30	0.30
Dy	2.48	2.26	2.40	2.06	2.13	1.80	1.82	2.07
Ho	0.44	0.46	0.48	0.44	0.39	0.38	0.40	0.43
Er	1.28	1.30	1.35	1.19	1.24	1.09	1.06	1.16
Tm	0.20	0.13	0.18	0.17	0.17	0.14	0.14	0.17
Yb	1.10	1.14	1.04	1.19	0.97	1.02	0.99	1.16
Lu	0.17	0.18	0.15	0.15	0.16	0.15	0.14	0.16
Hf	0.70	0.52	0.78	0.47	0.50	0.40	0.45	0.34
Ta	0.03	0.02	0.03	0.02	bdl	0.01	0.01	0.01
Pb	0.07	0.07	0.07	0.07	0.07	0.04	0.06	0.07
Th	0.19	0.11	0.09	0.07	0.07	0.06	0.05	0.05
U	0.05	0.03	0.04	0.04	0.03	0.03	0.02	0.03

Abbreviations: Cpx = clinopyroxene, bdl = below detection limit. *Note:* all trace element concentrations are in µg g^{-1}.

Table B24. *Continued*

Sample	BAK-16-22-03	BAK-16-22-05						
Mineral ID	Cpx_13	Cpx_01	Cpx_02	Cpx_03	Cpx_04	Cpx_05	Cpx_06	Cpx_07
Li	28.23	27.00	68.97	4.97	5.93	3.83	3.32	46.64
Be	bdl	0.33	0.34	bdl	0.08	0.06	bdl	0.29
Ti	1549.18	2075.08	2158.87	2072.41	1921.77	2320.21	2063.50	2008.23
V	289.15	367.50	369.08	364.54	363.36	380.93	377.97	373.03
Cr	6432.56	2546.07	2514.63	2519.12	2493.97	2428.38	2533.50	2529.90
Mn	bdl	bdl	bdl	bdl	bdl	bdl	bdl	bdl
Co	29.74	32.09	26.02	38.43	36.31	34.57	35.15	33.22
Ni	245.87	171.32	144.16	188.03	178.06	174.45	174.45	171.60
Cu	8.02	9.34	3.69	1.38	4.44	1.69	2.35	1.44
Zn	15.57	25.06	50.59	18.24	17.94	17.72	17.88	27.27
Rb	bdl	bdl	bdl	bdl	bdl	bdl	bdl	bdl
Sr	39.67	52.24	87.78	43.40	44.09	47.23	48.70	62.84
Y	8.54	11.01	13.97	10.69	10.54	11.38	10.87	10.54
Zr	8.77	9.87	20.77	9.59	8.68	9.90	10.53	9.73
Nb	0.07	0.26	0.55	0.10	0.08	0.12	0.11	0.17
Mo	0.06	bdl	bdl	bdl	bdl	bdl	bdl	bdl
Cs	bdl	bdl	bdl	bdl	bdl	bdl	bdl	bdl
Ba	bdl	bdl	bdl	bdl	bdl	bdl	bdl	bdl
La	1.13	1.72	4.43	0.63	0.64	0.83	0.89	2.20
Ce	3.55	4.53	13.03	2.27	2.23	2.83	2.93	5.74
Pr	0.64	0.66	2.06	0.47	0.46	0.57	0.55	0.85
Nd	3.25	3.55	9.20	2.71	2.78	3.46	3.44	4.41
Sm	1.05	1.36	2.37	1.41	1.26	1.20	1.53	1.42
Eu	0.33	0.47	0.87	0.49	0.49	0.49	0.53	0.47
Gd	1.36	1.85	2.54	1.62	1.80	1.96	1.81	1.84
Tb	0.24	0.30	0.43	0.33	0.29	0.33	0.34	0.31
Dy	1.52	2.08	2.66	2.21	2.09	2.45	2.04	1.92
Ho	0.36	0.44	0.53	0.51	0.42	0.43	0.47	0.46
Er	0.95	1.33	1.47	1.28	1.24	1.40	1.29	1.12
Tm	0.10	0.17	0.22	0.18	0.15	0.20	0.17	0.17
Yb	0.84	1.23	1.54	1.14	1.03	1.27	1.18	1.09
Lu	0.13	0.18	0.18	0.14	0.14	0.16	0.17	0.15
Hf	0.28	0.44	0.59	0.48	0.35	0.52	0.47	0.54
Ta	bdl	0.02	0.06	0.01	bdl	0.02	0.01	0.02
Pb	0.06	0.05	0.08	0.05	0.03	0.04	0.05	0.07
Th	0.05	0.07	0.04	0.03	0.02	0.03	0.03	0.05
U	0.02	0.02	0.01	0.02	0.01	0.01	0.02	0.02

Abbreviations: Cpx = clinopyroxene, bdl = below detection limit. *Note:* all trace element concentrations are in $\mu g\ g^{-1}$.

Table B24. *Continued*

Sample	BAK-16-22-05							BAK-16-22-32
Mineral ID	Cpx_08	Cpx_09	Cpx_10	Cpx_11	Cpx_12	Cpx_13	Cpx_14	Cpx_01
Li	11.78	12.13	8.54	12.92	14.11	8.02	6.01	38.05
Be	0.07	bdl	bdl	0.12	bdl	0.07	0.13	bdl
Ti	2002.88	2042.99	2062.60	2028.73	2144.61	1964.55	1769.35	3279.31
V	377.47	387.83	381.91	358.13	380.93	362.08	358.23	400.66
Cr	2565.84	2525.41	2486.78	2509.24	2493.07	2401.43	2601.77	881.33
Mn	bdl	bdl	bdl	bdl	bdl	bdl	bdl	bdl
Co	35.00	34.96	35.83	35.36	34.76	35.10	34.47	34.28
Ni	180.72	173.22	176.16	183.57	178.63	174.17	174.07	201.61
Cu	10.19	1.74	3.72	3.65	2.75	2.25	7.17	6.77
Zn	20.18	19.63	19.07	18.89	18.80	20.09	21.28	13.76
Rb	bdl	bdl	bdl	bdl	bdl	bdl	bdl	bdl
Sr	47.82	48.51	48.90	47.52	49.49	50.77	53.02	36.33
Y	10.94	10.83	10.83	11.17	11.01	10.57	10.09	15.82
Zr	8.76	9.40	9.25	9.61	9.75	11.28	10.71	12.62
Nb	0.10	0.10	0.12	0.12	0.11	0.14	0.11	0.02
Mo	bdl	bdl	bdl	bdl	bdl	bdl	bdl	bdl
Cs	bdl	bdl	bdl	bdl	bdl	bdl	bdl	bdl
Ba	bdl	bdl	bdl	bdl	bdl	bdl	bdl	bdl
La	0.92	0.93	0.82	0.89	0.82	0.99	0.99	0.52
Ce	2.94	2.83	2.65	2.92	2.81	3.33	3.15	2.32
Pr	0.52	0.55	0.55	0.55	0.54	0.65	0.58	0.57
Nd	3.47	3.31	3.28	3.78	3.23	3.58	3.41	3.68
Sm	1.26	1.41	1.42	1.44	1.35	1.13	1.33	2.00
Eu	0.41	0.46	0.54	0.51	0.43	0.46	0.53	0.74
Gd	1.85	1.76	1.63	1.80	1.78	1.63	1.82	2.80
Tb	0.29	0.31	0.29	0.31	0.34	0.31	0.32	0.41
Dy	2.18	1.91	2.02	2.09	2.21	2.08	2.01	3.01
Ho	0.44	0.39	0.40	0.53	0.44	0.46	0.40	0.62
Er	1.22	1.10	1.14	1.31	1.22	1.19	1.23	1.83
Tm	0.20	0.14	0.16	0.15	0.18	0.15	0.15	0.22
Yb	1.15	0.99	1.14	1.01	0.90	0.99	0.90	1.53
Lu	0.18	0.17	0.14	0.15	0.16	0.18	0.14	0.23
Hf	0.39	0.47	0.45	0.40	0.38	0.41	0.46	0.59
Ta	0.01	0.02	0.01	0.01	0.01	0.02	0.02	bdl
Pb	0.06	0.03	0.03	0.06	0.03	0.03	0.03	0.05
Th	0.03	0.03	0.03	0.04	0.03	0.03	0.02	0.01
U	0.01	bdl	0.01	0.01	0.02	0.02	bdl	0.01

Abbreviations: Cpx = clinopyroxene, bdl = below detection limit. *Note:* all trace element concentrations are in $\mu g\ g^{-1}$.

Table B24. *Continued*

Sample	BAK-16-22-32							
Mineral ID	Cpx_02	Cpx_03	Cpx_04	Cpx_05	Cpx_06	Cpx_07	Cpx_08	Cpx_09
Li	49.95	29.99	60.70	22.19	16.90	49.12	51.39	12.68
Be	bdl	0.12	bdl	bdl	bdl	bdl	0.10	bdl
Ti	3378.25	3027.05	22952.49	3431.73	3418.36	3569.00	3333.68	3511.95
V	408.56	365.14	5180.98	399.68	415.47	417.44	408.56	401.65
Cr	908.29	946.92	14868.56	1540.76	640.56	692.67	656.73	701.65
Mn	bdl	bdl	bdl	bdl	bdl	bdl	bdl	bdl
Co	33.31	34.18	2386.11	34.18	33.68	32.93	34.18	33.22
Ni	194.97	210.45	10797.70	189.74	188.79	183.48	188.60	186.32
Cu	3.14	0.81	5.67	1.38	2.49	8.68	5.22	0.55
Zn	13.36	13.82	1456.75	13.14	13.21	13.82	13.98	14.64
Rb	bdl	bdl	bdl	bdl	bdl	bdl	bdl	bdl
Sr	37.41	37.90	1.50	38.59	36.63	36.43	39.37	37.80
Y	15.30	15.45	32.83	16.05	16.01	15.35	16.03	15.58
Zr	12.96	12.61	29.73	13.39	12.85	13.93	12.99	13.55
Nb	bdl	0.03	bdl	0.03	0.01	bdl	0.02	0.03
Mo	bdl	bdl	bdl	bdl	bdl	bdl	bdl	bdl
Cs	bdl	bdl	bdl	bdl	bdl	bdl	bdl	bdl
Ba	bdl	bdl	bdl	bdl	bdl	bdl	bdl	bdl
La	0.47	0.52	0.13	0.54	0.48	0.55	0.55	0.55
Ce	2.32	2.34	0.34	2.35	2.23	2.43	2.41	2.40
Pr	0.57	0.57	bdl	0.55	0.60	0.52	0.57	0.55
Nd	4.06	4.13	bdl	4.02	4.07	3.87	4.05	4.29
Sm	1.85	1.86	bdl	1.84	2.04	1.85	1.94	2.06
Eu	0.64	0.68	bdl	0.65	0.67	0.73	0.72	0.74
Gd	2.50	2.47	bdl	2.51	2.66	2.54	2.64	2.63
Tb	0.44	0.45	0.53	0.48	0.47	0.43	0.40	0.44
Dy	2.87	2.82	3.40	2.95	3.20	3.00	2.86	3.24
Ho	0.65	0.62	1.60	0.61	0.67	0.67	0.70	0.67
Er	1.71	1.62	5.76	1.96	1.82	1.77	1.81	1.82
Tm	0.25	0.24	0.98	0.29	0.22	0.25	0.27	0.25
Yb	1.54	1.35	9.05	1.62	1.52	1.55	1.74	1.62
Lu	0.22	0.18	1.17	0.23	0.23	0.20	0.23	0.20
Hf	0.57	0.63	2.25	0.84	0.69	0.69	0.76	0.62
Ta	0.01	bdl	bdl	bdl	bdl	bdl	bdl	0.01
Pb	0.03	0.03	bdl	0.05	0.03	0.03	0.03	0.03
Th	0.01	0.01	bdl	0.01	0.01	0.01	0.01	0.01
U	bdl	bdl	bdl	bdl	bdl	0.01	bdl	bdl

Abbreviations: Cpx = clinopyroxene, bdl = below detection limit. *Note:* all trace element concentrations are in µg g^{-1}.

Table B24. *Continued*

Sample	BAK-16-22-32	BAK-16-22-09						
Mineral ID	Cpx_10	Cpx_01	Cpx_02	Cpx_03	Cpx_04	Cpx_05	Cpx_06	Cpx_07
Li	26.70	15.93	29.99	31.13	28.18	22.03	30.92	35.26
Be	0.05	0.07	0.08	0.07	0.03	bdl	0.06	bdl
Ti	3467.39	1613.36	1615.14	1573.25	1567.90	1400.32	1656.14	1648.12
V	402.64	241.29	240.30	252.73	243.95	222.24	255.89	249.48
Cr	852.58	5049.02	5803.68	6405.61	6225.93	5884.54	6279.83	5947.43
Mn	bdl	bdl	bdl	bdl	bdl	bdl	bdl	bdl
Co	34.57	29.21	28.29	27.91	28.00	31.38	29.45	29.45
Ni	198.86	298.20	288.41	285.85	274.93	332.38	290.60	297.25
Cu	1.88	3.95	7.91	1.50	8.36	1.36	2.40	5.70
Zn	13.64	15.76	14.04	13.64	12.56	14.83	12.30	13.18
Rb	bdl	bdl	bdl	bdl	bdl	bdl	bdl	bdl
Sr	38.29	47.62	48.80	46.94	48.80	49.88	43.01	46.74
Y	15.64	7.87	8.13	8.09	7.73	7.55	7.82	8.21
Zr	12.79	6.70	7.25	6.82	6.55	9.20	7.01	7.26
Nb	0.02	0.10	0.10	0.12	0.11	0.12	0.09	0.10
Mo	bdl	bdl	bdl	bdl	bdl	bdl	bdl	bdl
Cs	bdl	bdl	bdl	bdl	bdl	bdl	bdl	bdl
Ba	bdl	bdl	bdl	bdl	bdl	bdl	bdl	bdl
La	0.55	0.71	0.70	0.77	0.80	0.84	0.54	0.68
Ce	2.31	2.37	2.40	2.33	2.31	2.40	1.90	2.28
Pr	0.52	0.46	0.44	0.43	0.42	0.44	0.39	0.39
Nd	4.04	2.72	2.45	2.66	2.43	2.95	2.73	2.45
Sm	1.92	1.13	1.08	1.30	1.19	0.99	0.98	1.16
Eu	0.68	0.36	0.42	0.38	0.36	0.37	0.35	0.40
Gd	2.59	1.54	1.48	1.47	1.29	1.44	1.28	1.38
Tb	0.45	0.23	0.23	0.24	0.24	0.22	0.22	0.25
Dy	3.16	1.54	1.69	1.53	1.62	1.49	1.65	1.62
Ho	0.66	0.34	0.34	0.29	0.28	0.28	0.35	0.33
Er	1.95	0.81	0.84	0.95	0.86	0.93	0.81	0.89
Tm	0.22	0.11	0.11	0.11	0.13	0.15	0.11	0.12
Yb	1.43	0.80	0.80	0.73	0.76	0.68	0.74	0.80
Lu	0.22	0.13	0.15	0.13	0.14	0.11	0.12	0.15
Hf	0.54	0.27	0.34	0.39	0.29	0.34	0.30	0.39
Ta	bdl	0.01	0.01	0.01	0.01	0.03	bdl	0.01
Pb	0.02	0.05	0.06	0.04	0.06	0.03	0.05	0.04
Th	bdl	0.04	0.04	0.04	0.03	0.04	0.03	0.05
U	bdl	0.02	0.01	0.02	0.02	0.02	0.02	0.01

Abbreviations: Cpx = clinopyroxene, bdl = below detection limit. *Note:* all trace element concentrations are in $\mu g\ g^{-1}$.

Table B24. *Continued*

Sample	BAK-16-22-09							
Mineral ID	Cpx_08	Cpx_09	Cpx_10	Cpx_11	Cpx_12	Cpx_13	Cpx_14	Cpx_15
Li	20.61	25.68	18.30	29.37	60.08	43.54	37.02	40.64
Be	bdl	0.07	bdl	0.07	0.08	0.06	bdl	0.02
Ti	1552.75	1643.67	1553.64	1584.84	1566.12	1547.40	1644.56	1508.18
V	242.27	236.25	233.49	239.21	233.39	234.38	243.06	233.98
Cr	6504.44	6522.40	5803.68	6854.81	6055.23	6630.21	6980.59	6522.40
Mn	bdl	bdl	bdl	bdl	bdl	bdl	bdl	bdl
Co	30.71	29.45	29.16	29.36	30.32	29.65	29.07	29.07
Ni	299.14	295.25	296.30	292.59	312.44	301.52	309.59	297.25
Cu	3.53	5.57	1.91	6.68	8.04	8.93	1.58	6.64
Zn	12.88	12.66	12.44	13.08	13.54	12.33	12.72	12.78
Rb	bdl	bdl	bdl	bdl	bdl	bdl	bdl	bdl
Sr	42.71	45.46	44.97	45.56	49.39	50.27	50.96	48.31
Y	8.36	7.93	8.10	7.73	7.88	8.27	8.23	7.80
Zr	6.54	6.37	6.52	6.61	8.37	8.45	7.77	7.33
Nb	0.08	0.07	0.09	0.10	0.12	0.12	0.11	0.11
Mo	bdl	bdl	bdl	bdl	bdl	bdl	bdl	bdl
Cs	bdl	bdl	bdl	bdl	bdl	bdl	bdl	bdl
Ba	bdl	bdl	bdl	bdl	bdl	bdl	bdl	bdl
La	0.44	0.56	0.57	0.70	0.85	0.73	0.83	0.71
Ce	1.88	1.97	2.03	2.28	2.60	2.43	2.66	2.40
Pr	0.40	0.43	0.37	0.42	0.48	0.46	0.52	0.45
Nd	2.53	2.62	2.76	2.63	3.11	2.79	3.09	2.76
Sm	1.13	1.05	0.93	1.15	1.26	1.16	1.20	1.16
Eu	0.41	0.38	0.34	0.29	0.41	0.42	0.41	0.36
Gd	1.15	1.54	1.38	1.46	1.25	1.33	1.43	1.28
Tb	0.23	0.25	0.25	0.24	0.21	0.20	0.24	0.20
Dy	1.54	1.53	1.44	1.48	1.49	1.74	1.68	1.61
Ho	0.31	0.33	0.34	0.33	0.34	0.30	0.32	0.30
Er	0.93	0.89	0.90	0.78	0.90	0.94	0.98	0.86
Tm	0.13	0.11	0.13	0.13	0.12	0.12	0.12	0.12
Yb	0.75	0.74	0.56	0.67	0.75	0.70	0.66	0.72
Lu	0.11	0.12	0.11	0.13	0.10	0.12	0.12	0.11
Hf	0.33	0.32	0.29	0.26	0.34	0.42	0.40	0.39
Ta	0.01	bdl	bdl	0.01	0.01	0.01	0.02	0.01
Pb	0.03	0.04	0.05	0.07	0.07	0.05	0.06	0.05
Th	0.02	0.03	0.02	0.02	0.03	0.03	0.04	0.02
U	0.02	0.02	0.01	0.02	0.02	0.02	0.01	0.01

Abbreviations: Cpx = clinopyroxene, bdl = below detection limit. *Note:* all trace element concentrations are in $\mu g\ g^{-1}$.

Table B24. *Continued*

Sample	BAK-16-22-09					BAK-16-22-42		
Mineral ID	Cpx_16	Cpx_17	Cpx_18	Cpx_19	Cpx_20	Cpx_01	Cpx_02	Cpx_03
Li	63.60	41.82	43.02	33.40	31.64	9.55	10.99	13.82
Be	0.03	bdl	bdl	bdl	0.10	bdl	0.02	bdl
Ti	1579.49	1538.49	1529.57	1614.25	1666.84	2007.43	1973.18	2023.66
V	244.15	242.86	241.09	240.20	246.42	308.19	304.76	303.29
Cr	6450.53	6522.40	6594.28	6693.10	6513.42	3175.93	3217.62	3335.45
Mn	bdl	bdl	bdl	bdl	bdl	bdl	bdl	bdl
Co	28.83	28.81	29.14	28.68	29.55	33.16	31.43	32.58
Ni	289.65	281.67	289.46	284.90	283.00	295.80	291.59	298.28
Cu	5.44	8.34	4.08	6.24	6.21	4.30	4.26	5.54
Zn	12.31	12.72	13.39	13.27	14.01	18.79	18.43	19.06
Rb	bdl	bdl	bdl	bdl	bdl	bdl	bdl	bdl
Sr	45.17	46.64	45.76	45.46	47.82	41.35	41.05	42.03
Y	8.08	8.12	7.68	8.18	8.40	10.01	10.17	10.29
Zr	6.62	6.52	6.88	7.05	8.05	8.30	8.06	7.91
Nb	0.14	0.11	0.10	0.12	0.11	0.05	0.04	0.04
Mo	bdl	bdl	bdl	0.04	bdl	bdl	bdl	bdl
Cs	bdl	bdl	bdl	bdl	bdl	bdl	bdl	bdl
Ba	bdl	bdl	bdl	bdl	bdl	bdl	bdl	bdl
La	0.59	0.72	0.67	0.75	0.75	0.46	0.49	0.50
Ce	1.96	2.11	2.13	2.20	2.45	1.93	1.97	2.03
Pr	0.39	0.42	0.39	0.42	0.42	0.46	0.45	0.43
Nd	2.63	2.63	2.88	2.59	3.03	3.06	2.96	3.25
Sm	0.90	1.09	1.07	1.07	1.13	1.24	1.13	1.15
Eu	0.39	0.40	0.36	0.39	0.37	0.39	0.45	0.48
Gd	1.55	1.21	1.42	1.20	1.65	2.01	1.69	1.77
Tb	0.22	0.25	0.23	0.25	0.25	0.28	0.28	0.29
Dy	1.74	1.58	1.50	1.63	1.52	1.90	1.92	2.12
Ho	0.32	0.33	0.34	0.32	0.35	0.45	0.46	0.40
Er	1.08	0.96	0.89	0.78	0.96	1.33	1.22	1.24
Tm	0.15	0.12	0.10	0.12	0.13	0.16	0.16	0.18
Yb	0.84	0.68	0.76	0.89	0.70	0.94	1.10	1.10
Lu	0.14	0.11	0.10	0.11	0.12	0.15	0.13	0.18
Hf	0.33	0.33	0.29	0.34	0.35	0.35	0.36	0.35
Ta	0.01	0.01	0.01	0.01	0.01	bdl	bdl	bdl
Pb	0.04	0.05	0.04	0.05	0.05	0.04	0.02	0.03
Th	0.04	0.04	0.04	0.03	0.04	0.02	0.02	0.01
U	0.02	0.02	0.01	0.01	0.01	0.01	0.01	bdl

Abbreviations: Cpx = clinopyroxene, bdl = below detection limit. *Note:* all trace element concentrations are in $\mu g\ g^{-1}$.

***Table B24**. Continued*

Sample	BAK-16-22-42							
Mineral ID	Cpx_04	Cpx_05	Cpx_06	Cpx_07	Cpx_08	Cpx_09	Cpx_10	Cpx_11
Li	12.25	4.92	5.28	9.86	11.55	8.30	8.13	49.18
Be	0.06	bdl	0.02	bdl	0.03	0.05	bdl	bdl
Ti	1942.53	1890.25	1883.94	2027.26	2036.28	2066.02	1965.07	1863.21
V	295.47	306.23	306.23	316.01	317.97	308.19	300.36	285.00
Cr	3398.90	2972.90	3199.49	3235.75	3244.81	3344.51	3308.26	3290.13
Mn	bdl	bdl	bdl	bdl	bdl	bdl	bdl	bdl
Co	31.43	33.74	32.49	32.30	33.45	32.97	33.07	32.49
Ni	288.05	311.67	291.59	290.63	306.89	296.37	286.81	286.81
Cu	5.83	2.22	3.66	3.23	4.32	3.86	6.21	9.10
Zn	19.15	21.13	19.24	18.61	18.79	17.26	18.88	18.61
Rb	bdl	bdl	bdl	bdl	bdl	bdl	bdl	bdl
Sr	41.44	42.22	41.05	44.27	43.10	42.22	41.35	41.93
Y	10.20	10.20	10.05	10.18	10.55	10.91	10.75	10.63
Zr	8.02	7.72	8.01	9.77	8.66	8.62	8.18	8.14
Nb	0.04	0.05	0.06	0.12	0.07	0.06	0.05	0.04
Mo	bdl	bdl	bdl	bdl	bdl	bdl	bdl	bdl
Cs	bdl	bdl	bdl	bdl	bdl	bdl	bdl	bdl
Ba	bdl	bdl	bdl	bdl	bdl	bdl	bdl	bdl
La	0.46	0.46	0.43	0.60	0.58	0.51	0.47	0.45
Ce	2.03	2.06	1.96	2.21	2.18	2.08	2.14	1.92
Pr	0.45	0.49	0.47	0.49	0.50	0.44	0.47	0.39
Nd	3.13	2.93	2.85	3.15	3.17	3.14	3.22	2.68
Sm	1.23	1.14	1.29	1.21	1.26	1.25	1.25	1.20
Eu	0.43	0.51	0.46	0.45	0.45	0.49	0.49	0.40
Gd	1.60	1.50	1.67	1.71	1.88	1.75	1.67	1.69
Tb	0.30	0.25	0.29	0.26	0.32	0.31	0.32	0.33
Dy	2.08	1.81	2.09	1.98	1.87	2.06	1.90	1.93
Ho	0.37	0.43	0.36	0.44	0.41	0.46	0.39	0.44
Er	1.22	1.28	1.22	1.20	1.30	1.33	1.20	1.18
Tm	0.14	0.18	0.15	0.17	0.18	0.16	0.16	0.17
Yb	1.13	0.89	1.04	1.04	0.93	1.10	1.03	1.08
Lu	0.14	0.16	0.14	0.13	0.13	0.16	0.13	0.15
Hf	0.38	0.45	0.23	0.53	0.50	0.42	0.47	0.40
Ta	bdl	bdl	0.01	0.01	0.02	0.01	bdl	bdl
Pb	0.04	0.03	0.03	0.06	0.03	0.03	0.03	0.01
Th	0.01	0.02	0.01	0.02	0.01	0.01	0.01	0.01
U	0.01	bdl	bdl	bdl	bdl	0.01	bdl	0.01

Abbreviations: Cpx = clinopyroxene, bdl = below detection limit. *Note:* all trace element concentrations are in µg g^{-1}.

Table B24. *Continued*

Sample	BAK-16-22-42						BAK-16-22-01B	
Mineral ID	Cpx_12	Cpx_13	Cpx_14	Cpx_15	Cpx_16	Cpx_17	Cpx_01	Cpx_02
Li	41.43	21.04	38.92	8.89	12.64	11.27	50.33	6.59
Be	bdl	bdl	0.07	bdl	bdl	0.03	0.04	bdl
Ti	1971.38	1956.95	1934.42	1940.73	1931.71	1839.77	1819.04	429.07
V	307.21	297.42	302.32	299.38	296.44	303.29	307.21	148.71
Cr	3317.32	3244.81	3362.64	3235.75	3217.62	3126.98	6970.00	2420.01
Mn	bdl	bdl	bdl	bdl	bdl	bdl	bdl	bdl
Co	33.26	31.14	32.20	32.01	32.49	31.82	26.72	62.19
Ni	290.63	282.99	295.41	301.15	288.72	295.41	233.94	424.48
Cu	4.91	6.13	8.18	64.00	4.93	5.79	15.29	1.31
Zn	18.43	18.16	17.53	19.15	17.71	17.71	13.48	47.92
Rb	bdl	bdl	bdl	bdl	bdl	bdl	bdl	bdl
Sr	42.03	40.86	42.22	40.76	41.25	39.79	33.94	0.15
Y	10.73	10.46	10.49	10.32	10.62	10.58	9.19	0.64
Zr	8.62	8.19	8.56	9.01	7.95	8.17	6.82	0.63
Nb	0.05	0.05	0.06	0.13	0.07	0.09	0.03	bdl
Mo	bdl	bdl	bdl	bdl	bdl	bdl	bdl	bdl
Cs	bdl	bdl	bdl	bdl	bdl	bdl	bdl	bdl
Ba	bdl	bdl	bdl	2.83	bdl	bdl	bdl	bdl
La	0.50	0.46	0.51	0.53	0.56	0.48	0.48	bdl
Ce	2.06	1.99	2.13	2.08	2.18	2.02	1.73	0.02
Pr	0.48	0.47	0.47	0.47	0.45	0.44	0.38	bdl
Nd	3.11	2.74	3.00	3.17	3.08	2.99	2.31	0.04
Sm	1.41	1.27	1.11	1.05	1.18	1.24	1.15	bdl
Eu	0.49	0.51	0.46	0.51	0.50	0.43	0.33	bdl
Gd	1.97	1.61	1.72	1.56	1.49	1.57	1.27	bdl
Tb	0.33	0.31	0.29	0.30	0.27	0.28	0.25	bdl
Dy	2.20	2.02	1.90	2.01	2.07	2.12	1.77	0.09
Ho	0.46	0.41	0.46	0.41	0.42	0.40	0.38	0.03
Er	1.25	1.12	1.21	1.23	1.25	1.18	0.97	0.10
Tm	0.16	0.14	0.15	0.17	0.17	0.16	0.15	0.02
Yb	1.04	1.07	1.07	1.01	0.89	0.95	0.93	0.15
Lu	0.17	0.15	0.14	0.15	0.17	0.14	0.14	0.03
Hf	0.35	0.33	0.43	0.46	0.41	0.39	0.30	0.01
Ta	bdl	bdl	bdl	0.01	0.01	0.01	bdl	bdl
Pb	0.01	0.02	0.04	0.03	0.03	0.03	0.04	bdl
Th	0.01	bdl	0.01	0.02	0.01	0.01	0.03	bdl
U	0.01	bdl	0.01	0.01	0.01	bdl	0.02	bdl

Abbreviations: Cpx = clinopyroxene, bdl = below detection limit. *Note:* all trace element concentrations are in µg g^{-1}.

***Table B24**. Continued*

Sample	BAK-16-22-01B						BAK-16-22-01A	
Mineral ID	Cpx_03	Cpx_04	Cpx_05	Cpx_06	Cpx_07	Cpx_08	Cpx_09	Cpx_10
Li	30.21	50.22	47.71	15.79	25.99	15.67	17.27	39.55
Be	bdl	bdl	0.20	bdl	0.05	bdl	0.13	0.22
Ti	1474.70	1409.80	1928.11	1704.56	1941.63	1570.25	1805.52	2168.78
V	251.34	271.99	324.82	285.68	319.93	268.07	373.74	374.71
Cr	8003.27	6108.95	5710.15	6834.05	6661.84	5411.04	2628.48	2565.03
Mn	bdl	bdl	bdl	bdl	bdl	bdl	bdl	bdl
Co	27.30	28.36	27.49	27.01	26.72	28.16	34.80	33.07
Ni	234.99	250.48	241.88	234.23	233.75	245.70	180.31	167.59
Cu	7.36	5.98	11.53	9.24	10.40	7.69	5.39	3.24
Zn	13.84	14.74	12.77	11.91	12.81	13.84	23.64	21.04
Rb	bdl	bdl	bdl	bdl	bdl	bdl	bdl	bdl
Sr	38.71	57.83	44.18	33.94	35.79	35.11	39.79	45.35
Y	8.57	8.35	8.95	8.25	8.25	7.43	8.85	10.00
Zr	5.95	13.83	7.91	6.49	7.12	5.91	7.28	9.23
Nb	0.06	0.10	0.09	0.02	0.05	0.04	0.07	0.15
Mo	bdl	0.03	bdl	bdl	0.05	bdl	bdl	bdl
Cs	bdl	bdl	bdl	bdl	bdl	bdl	bdl	bdl
Ba	bdl	bdl	bdl	bdl	bdl	bdl	bdl	bdl
La	0.82	2.04	1.49	0.42	0.80	0.59	0.50	1.08
Ce	1.92	5.55	3.68	1.56	2.02	1.70	1.99	2.96
Pr	0.38	0.88	0.52	0.32	0.37	0.33	0.40	0.58
Nd	2.08	3.85	2.66	2.15	2.32	2.26	2.92	3.55
Sm	0.91	1.03	1.14	0.90	0.87	0.73	1.13	1.26
Eu	0.36	0.36	0.42	0.40	0.37	0.37	0.46	0.49
Gd	1.21	1.32	1.42	1.59	1.64	1.27	1.56	2.03
Tb	0.21	0.21	0.27	0.26	0.24	0.21	0.26	0.32
Dy	1.57	1.42	1.63	1.64	1.70	1.48	1.73	2.29
Ho	0.31	0.36	0.37	0.32	0.37	0.33	0.43	0.46
Er	0.91	0.90	1.03	0.93	1.02	1.09	1.18	1.30
Tm	0.14	0.13	0.16	0.14	0.14	0.13	0.15	0.18
Yb	0.87	0.85	0.94	0.92	1.12	0.80	0.88	1.05
Lu	0.13	0.12	0.14	0.16	0.14	0.11	0.13	0.16
Hf	0.14	0.22	0.39	0.25	0.30	0.27	0.38	0.47
Ta	bdl	0.01	bdl	bdl	bdl	bdl	bdl	bdl
Pb	0.07	0.12	0.09	0.04	0.07	0.06	0.06	0.06
Th	0.06	0.09	0.09	0.03	0.06	0.04	0.01	0.04
U	0.04	0.04	0.04	0.03	0.03	0.02	0.02	0.02

Abbreviations: Cpx = clinopyroxene, bdl = below detection limit. *Note:* all trace element concentrations are in $\mu g\ g^{-1}$.

Table B24. *Continued*

Sample	BAK-16-22-01A			
Mineral ID	Cpx_11	Cpx_12	Cpx_13	Cpx_14
Li	51.90	23.91	12.11	19.03
Be	0.22	0.20	0.10	0.16
Ti	2031.77	2094.87	2024.56	2113.80
V	350.26	361.02	362.97	366.89
Cr	2301.28	2429.98	2555.97	2500.68
Mn	bdl	bdl	bdl	bdl
Co	31.82	32.96	33.64	35.47
Ni	167.40	175.43	174.29	188.82
Cu	9.21	6.94	3.17	5.52
Zn	23.64	18.97	18.52	20.50
Rb	bdl	bdl	bdl	bdl
Sr	50.51	45.54	44.86	46.22
Y	9.37	9.67	9.60	10.00
Zr	8.67	8.42	8.68	9.13
Nb	0.21	0.13	0.14	0.13
Mo	bdl	bdl	bdl	bdl
Cs	bdl	bdl	bdl	bdl
Ba	bdl	0.06	bdl	bdl
La	1.35	1.08	0.90	1.03
Ce	3.51	2.88	2.57	3.06
Pr	0.60	0.52	0.49	0.56
Nd	3.30	3.32	3.08	3.34
Sm	1.31	1.26	1.20	1.35
Eu	0.45	0.50	0.46	0.44
Gd	1.65	1.69	1.71	1.77
Tb	0.30	0.30	0.30	0.33
Dy	2.01	2.03	2.01	2.13
Ho	0.39	0.41	0.42	0.43
Er	1.23	1.18	1.25	1.33
Tm	0.17	0.16	0.18	0.18
Yb	1.11	1.12	1.01	1.12
Lu	0.14	0.16	0.15	0.14
Hf	0.44	0.50	0.35	0.44
Ta	0.01	0.01	bdl	0.01
Pb	0.07	0.06	0.05	0.06
Th	0.07	0.05	0.06	0.04
U	0.02	0.01	0.02	0.02

Abbreviations: Cpx = clinopyroxene, bdl = below detection limit. *Note:* all trace element concentrations are in µg g^{-1}.

Table B25. *Trace element compositions of orthopyroxene in Shiveluch and Avachinsky mantle xenoliths*

Sample	AVX-16-03-10						BAK-16-22-05	
Mineral ID	Opx_01	Opx_02	Opx_03	Opx_04	Opx_05	Opx_06	Opx_01	Opx_02
Li	0.86	0.81	0.54	0.80	0.91	0.82	0.78	1.00
Be	bdl	bdl	bdl	bdl	0.08	bdl	bdl	0.03
Ti	390.17	149.48	54.31	270.19	250.04	370.94	434.97	441.11
V	80.72	37.26	34.09	52.07	37.45	77.43	157.72	159.36
Cr	129.51	289.18	436.35	134.04	104.44	107.03	1367.88	1407.56
Mn	2220.45	1377.62	1002.51	1300.14	1806.60	1974.78	nd	nd
Co	66.04	60.92	53.29	57.93	62.75	61.69	74.01	75.53
Ni	1099.31	942.69	563.04	800.94	975.40	948.63	289.59	304.82
Cu	0.31	0.25	0.44	1.09	0.27	0.45	0.61	0.32
Zn	99.80	56.92	41.93	48.00	81.49	83.01	60.38	59.66
Rb	bdl	bdl	bdl	bdl	bdl	bdl	bdl	bdl
Sr	0.18	0.20	0.05	0.09	0.08	0.10	0.08	0.07
Y	0.77	0.38	0.17	0.47	0.72	0.66	0.70	0.67
Zr	1.53	3.11	0.51	2.31	3.59	2.03	0.82	0.70
Nb	bdl	bdl	bdl	bdl	bdl	bdl	0.01	0.01
Mo	bdl	bdl	bdl	bdl	bdl	bdl	bdl	bdl
Cs	bdl	bdl	bdl	bdl	bdl	bdl	bdl	bdl
Ba	0.18	0.03	bdl	0.14	0.08	bdl	bdl	bdl
La	bdl	bdl	0.01	bdl	bdl	bdl	bdl	bdl
Ce	0.02	0.02	0.01	0.03	0.02	0.01	bdl	0.01
Pr	bdl	bdl	bdl	bdl	bdl	0.01	bdl	bdl
Nd	0.03	0.05	0.01	0.05	0.02	0.01	bdl	0.03
Sm	bdl	bdl	bdl	bdl	bdl	bdl	bdl	bdl
Eu	bdl	bdl	bdl	bdl	0.01	bdl	bdl	bdl
Gd	bdl	bdl	bdl	bdl	bdl	bdl	bdl	bdl
Tb	0.01	bdl	bdl	0.01	0.01	0.01	0.01	bdl
Dy	0.10	0.04	bdl	0.05	0.07	0.09	0.08	0.07
Ho	0.03	0.01	bdl	0.03	0.02	0.02	0.03	0.02
Er	0.10	0.05	0.01	0.05	0.10	0.11	0.11	0.12
Tm	0.02	0.02	bdl	0.01	0.01	0.01	0.02	0.01
Yb	0.21	0.11	0.09	0.15	0.18	0.22	0.14	0.13
Lu	0.03	0.01	0.01	0.02	0.05	0.03	0.03	0.04
Hf	0.06	0.08	bdl	0.06	0.15	0.07	bdl	0.01
Ta	bdl	bdl	bdl	bdl	bdl	bdl	bdl	bdl
Pb	bdl	bdl	bdl	0.01	bdl	bdl	bdl	bdl
Th	0.01	bdl	0.04	0.00	bdl	0.01	bdl	bdl
U	bdl	bdl	0.02	bdl	bdl	bdl	bdl	bdl

Abbreviations: Opx = orthopyroxene, bdl = below detection limit, nd = not determined. *Note:* all trace element concentrations are in μg g^{-1}.

Table B25. *Continued*

Sample	BAK-16-22-05			BAK-16-22-32				
Mineral ID	Opx_03	Opx_04	Opx_05	Opx_01	Opx_02	Opx_03	Opx_04	Opx_05
Li	7.84	12.40	8.28	4.32	2.11	2.90	3.24	6.44
Be	bdl	0.09	bdl	bdl	bdl	bdl	bdl	bdl
Ti	463.91	501.62	494.60	722.61	677.01	690.16	686.65	766.46
V	160.42	158.59	158.01	181.63	151.45	159.65	153.09	174.69
Cr	1457.83	1402.27	1427.85	478.89	531.80	439.20	519.46	489.47
Mn	nd	nd	nd	nd	nd	nd	nd	nd
Co	76.09	72.88	77.13	77.42	74.01	74.11	72.31	73.07
Ni	314.81	297.06	316.49	363.39	355.91	357.78	340.03	337.23
Cu	2.61	2.51	2.01	0.20	0.17	0.13	0.28	0.28
Zn	63.26	91.20	67.05	47.04	46.05	46.86	48.30	44.61
Rb	bdl	bdl	bdl	bdl	bdl	bdl	bdl	bdl
Sr	0.05	0.13	0.08	0.04	0.08	0.06	0.08	0.05
Y	0.71	0.75	0.72	1.13	1.05	1.03	0.99	1.14
Zr	0.70	0.94	0.74	1.09	0.92	0.98	0.98	1.17
Nb	bdl	bdl	bdl	bdl	bdl	bdl	bdl	bdl
Mo	bdl	bdl	bdl	bdl	bdl	bdl	bdl	bdl
Cs	bdl	bdl	bdl	bdl	bdl	bdl	bdl	bdl
Ba	bdl	bdl	bdl	bdl	bdl	bdl	bdl	bdl
La	0.01	bdl	bdl	bdl	bdl	bdl	bdl	bdl
Ce	bdl	0.02	0.02	bdl	0.02	0.01	0.01	0.01
Pr	bdl	0.01	bdl	bdl	bdl	bdl	bdl	bdl
Nd	bdl	0.03	0.05	0.01	bdl	bdl	bdl	0.03
Sm	bdl	bdl	bdl	bdl	bdl	bdl	bdl	bdl
Eu	0.04	bdl	bdl	bdl	bdl	bdl	bdl	bdl
Gd	bdl	bdl	bdl	bdl	bdl	bdl	bdl	bdl
Tb	0.01	0.01	0.01	0.02	0.02	0.01	0.01	0.01
Dy	0.12	0.11	0.11	0.14	0.14	0.11	0.14	0.14
Ho	0.02	0.02	0.02	0.05	0.04	0.05	0.04	0.04
Er	0.09	0.10	0.06	0.15	0.15	0.22	0.12	0.14
Tm	0.02	0.02	0.02	0.04	0.04	0.02	0.03	0.03
Yb	0.20	0.22	0.17	0.24	0.30	0.17	0.25	0.29
Lu	0.04	0.03	0.03	0.05	0.05	0.05	0.05	0.06
Hf	0.05	0.05	bdl	0.08	0.06	0.07	0.06	0.04
Ta	bdl	bdl	bdl	bdl	bdl	bdl	bdl	bdl
Pb	bdl	bdl	bdl	bdl	bdl	bdl	bdl	bdl
Th	bdl	bdl	bdl	bdl	bdl	bdl	bdl	bdl
U	bdl	bdl	bdl	bdl	bdl	bdl	bdl	bdl

Abbreviations: Opx = orthopyroxene, bdl = below detection limit, nd = not determined. *Note:* all trace element concentrations are in $\mu g\ g^{-1}$.

***Table B25**. Continued*

Sample	BAK-16-22-32							
Mineral ID	Opx_06	Opx_07	Opx_08	Opx_09	Opx_10	Opx_11	Opx_12	Opx_13
Li	3.49	6.10	4.88	2.92	5.06	4.84	2.26	2.35
Be	bdl	0.05	0.03	0.06	bdl	bdl	bdl	0.04
Ti	712.09	689.29	692.79	703.32	714.72	674.38	695.42	740.15
V	157.05	157.43	169.39	167.84	174.59	162.73	167.55	181.82
Cr	520.34	622.64	650.87	580.31	397.75	481.53	497.41	505.35
Mn	nd	nd	nd	nd	nd	nd	nd	nd
Co	75.62	75.62	72.88	74.20	74.77	72.60	73.16	73.54
Ni	334.43	340.97	312.94	331.63	325.09	313.88	329.76	326.02
Cu	0.21	1.72	0.42	0.16	0.19	bdl	0.11	bdl
Zn	46.59	45.87	46.05	45.60	45.78	44.97	45.42	45.24
Rb	bdl	bdl	bdl	bdl	bdl	bdl	bdl	bdl
Sr	0.05	0.03	0.05	0.07	0.08	0.06	0.05	0.05
Y	1.05	1.02	1.00	1.05	1.11	1.03	1.02	1.01
Zr	0.89	0.81	1.12	1.07	1.10	0.99	0.96	1.13
Nb	bdl	bdl	bdl	bdl	bdl	bdl	bdl	bdl
Mo	bdl	bdl	bdl	bdl	bdl	bdl	bdl	bdl
Cs	bdl	bdl	bdl	bdl	bdl	bdl	bdl	bdl
Ba	bdl	bdl	bdl	bdl	bdl	bdl	bdl	bdl
La	bdl	bdl	bdl	bdl	bdl	bdl	bdl	bdl
Ce	bdl	0.01	bdl	0.01	bdl	0.01	0.01	bdl
Pr	bdl	bdl	bdl	bdl	bdl	bdl	bdl	bdl
Nd	bdl	0.04	bdl	bdl	bdl	bdl	0.05	bdl
Sm	bdl	bdl	bdl	bdl	bdl	bdl	bdl	bdl
Eu	bdl	bdl	bdl	bdl	bdl	bdl	bdl	bdl
Gd	bdl	bdl	bdl	bdl	bdl	bdl	bdl	bdl
Tb	0.01	0.01	0.02	0.01	0.01	0.01	0.01	0.01
Dy	0.16	0.15	0.14	0.12	0.14	0.13	0.12	0.09
Ho	0.04	0.03	0.06	0.04	0.05	0.04	0.04	0.05
Er	0.17	0.14	0.14	0.16	0.12	0.11	0.13	0.19
Tm	0.04	0.03	0.03	0.02	0.03	0.03	0.03	0.03
Yb	0.27	0.25	0.24	0.24	0.22	0.23	0.21	0.24
Lu	0.04	0.03	0.05	0.03	0.05	0.04	0.04	0.05
Hf	0.03	bdl	0.08	0.03	0.02	0.01	0.02	bdl
Ta	bdl	bdl	bdl	bdl	bdl	bdl	bdl	bdl
Pb	bdl	bdl	bdl	bdl	bdl	bdl	bdl	bdl
Th	bdl	bdl	bdl	bdl	bdl	bdl	bdl	bdl
U	bdl	bdl	bdl	bdl	bdl	bdl	bdl	bdl

Abbreviations: Opx = orthopyroxene, bdl = below detection limit, nd = not determined. *Note:* all trace element concentrations are in $\mu g\ g^{-1}$.

Table B25. *Continued*

Sample	BAK-16-22-32				BAK-16-22-09		BAK-16-22-42	
Mineral ID	Opx_14	Opx_15	Opx_16	Opx_17	Opx_01	Opx_02	Opx_01	Opx_02
Li	3.24	2.29	3.99	2.46	2.70	9.08	1.42	1.68
Be	bdl	bdl	bdl	bdl	bdl	bdl	bdl	bdl
Ti	825.21	726.12	760.32	742.78	413.04	1349.63	428.58	458.68
V	183.08	177.00	172.76	159.36	86.28	204.77	121.55	132.60
Cr	436.56	652.63	507.11	476.24	2089.30	4577.23	1867.76	1982.43
Mn	nd	nd	nd	nd	nd	nd	nd	nd
Co	74.58	74.96	73.82	73.82	64.56	25.75	70.13	74.00
Ni	338.16	336.30	341.90	337.23	535.27	265.30	490.10	504.95
Cu	0.46	0.14	0.18	0.23	3.11	0.58	0.95	0.18
Zn	43.62	44.16	45.15	45.87	46.41	11.81	62.25	68.71
Rb	bdl	bdl	bdl	bdl	bdl	bdl	bdl	bdl
Sr	0.11	0.05	0.05	bdl	0.05	41.33	0.19	0.08
Y	1.09	1.14	0.99	1.01	0.53	7.17	0.67	0.76
Zr	1.24	1.06	0.93	0.99	0.65	6.00	0.66	0.57
Nb	bdl	bdl	0.01	bdl	bdl	0.08	0.02	0.01
Mo	bdl	bdl	bdl	bdl	bdl	bdl	bdl	bdl
Cs	bdl	bdl	bdl	bdl	bdl	bdl	bdl	bdl
Ba	bdl	bdl	bdl	bdl	bdl	bdl	0.27	0.02
La	bdl	bdl	bdl	bdl	bdl	0.56	bdl	bdl
Ce	0.01	0.01	0.01	bdl	bdl	1.81	0.01	0.01
Pr	bdl	bdl	bdl	bdl	0.01	0.36	bdl	bdl
Nd	bdl	0.04	bdl	bdl	bdl	2.21	bdl	bdl
Sm	bdl	bdl	0.03	bdl	bdl	0.95	bdl	bdl
Eu	bdl	bdl	bdl	bdl	bdl	0.31	bdl	bdl
Gd	bdl	bdl	bdl	bdl	bdl	1.34	bdl	bdl
Tb	0.02	0.01	0.02	0.01	bdl	0.22	bdl	0.01
Dy	0.17	0.14	0.14	0.15	0.04	1.33	0.05	0.11
Ho	0.04	0.04	0.03	0.03	0.02	0.28	0.01	0.02
Er	0.16	0.14	0.12	0.14	0.07	0.87	0.10	0.12
Tm	0.04	0.02	0.03	0.02	0.02	0.11	0.02	0.03
Yb	0.24	0.24	0.22	0.26	0.14	0.68	0.14	0.26
Lu	0.06	0.05	0.04	0.05	0.03	0.09	0.04	0.05
Hf	0.08	bdl	0.07	0.04	0.03	0.25	bdl	0.01
Ta	bdl	bdl	bdl	bdl	bdl	0.01	bdl	bdl
Pb	bdl	bdl	bdl	bdl	bdl	0.05	bdl	bdl
Th	bdl	bdl	bdl	bdl	bdl	0.04	0.01	bdl
U	bdl	bdl	bdl	bdl	bdl	0.01	bdl	bdl

Abbreviations: Opx = orthopyroxene, bdl = below detection limit, nd = not determined. *Note:* all trace element concentrations are in μg g^{-1}.

Table B25. *Continued*

Sample	BAK-16-22-42					
Mineral ID	Opx_03	Opx_04	Opx_05	Opx_06	Opx_07	Opx_08
Li	2.00	1.56	0.95	5.42	0.65	6.16
Be	bdl	bdl	bdl	bdl	bdl	0.08
Ti	519.78	504.73	567.60	576.45	445.40	1916.20
V	125.78	122.42	139.52	128.08	126.16	282.50
Cr	1822.42	1814.42	2009.10	1992.21	1965.54	2960.32
Mn	nd	nd	nd	nd	nd	nd
Co	70.79	71.26	68.81	71.73	76.07	30.30
Ni	487.31	489.17	481.74	480.82	521.66	264.54
Cu	1.26	1.33	0.44	1.69	0.26	1.55
Zn	63.22	64.11	62.87	63.13	64.82	17.62
Rb	bdl	bdl	bdl	bdl	bdl	bdl
Sr	0.13	0.08	3.40	2.25	0.07	36.55
Y	0.67	0.66	1.46	1.12	0.76	10.08
Zr	0.59	0.62	1.25	1.32	0.71	7.72
Nb	bdl	bdl	bdl	0.01	0.01	0.05
Mo	bdl	bdl	bdl	bdl	bdl	bdl
Cs	bdl	bdl	bdl	bdl	bdl	bdl
Ba	bdl	bdl	bdl	bdl	bdl	bdl
La	bdl	bdl	0.05	0.02	bdl	0.47
Ce	0.01	bdl	0.15	0.09	bdl	1.93
Pr	bdl	bdl	0.05	0.02	bdl	0.44
Nd	0.03	0.05	0.28	0.09	0.02	2.85
Sm	0.01	0.06	0.18	0.06	bdl	1.23
Eu	bdl	bdl	0.05	0.03	bdl	0.44
Gd	bdl	bdl	bdl	bdl	bdl	1.69
Tb	0.01	0.01	0.02	0.02	0.02	0.31
Dy	0.06	0.05	0.28	0.18	0.11	1.93
Ho	0.02	0.02	0.05	0.04	0.03	0.36
Er	0.09	0.10	0.16	0.18	0.10	1.24
Tm	0.02	0.03	0.03	0.02	0.02	0.16
Yb	0.17	0.19	0.33	0.21	0.15	1.16
Lu	0.03	0.03	0.03	0.04	0.04	0.13
Hf	0.04	bdl	bdl	bdl	0.05	0.45
Ta	bdl	bdl	bdl	bdl	bdl	bdl
Pb	bdl	bdl	0.02	bdl	bdl	0.04
Th	bdl	bdl	bdl	bdl	bdl	0.01
U	bdl	bdl	bdl	bdl	bdl	bdl

Abbreviations: Opx = orthopyroxene, bdl = below detection limit, nd = not determined. *Note:* all trace element concentrations are in $\mu g\ g^{-1}$.